UNIVERSIDADE FEDERAL FLUMINENSE

INSTITUTO DE GEOCIÊNCIAS

DEPARTAMENTO DE GEOLOGIA - LAGEMAR

PROGRAMA DE PÓS-GRADUAÇÃO EM DINÂMICA DOS OCEANOS E DA TERRA

FABRICIO FERREIRA

Planktonic foraminifera biostratigraphy and paleoceanographic reconstructions of western equatorial Atlantic for the last ~1.93 Ma

Niterói

2020

FABRICIO FERREIRA

Planktonic foraminifera biostratigraphy and paleoceanographic reconstructions of western equatorial Atlantic for the last ~1.93 Ma

Tese apresentada ao programa de Pós-Graduação em Dinâmica dos Oceanos e da Terra da Universidade Federal Fluminense, como requisito parcial para obtenção do grau de Doutor em Ciências, área de concentração: Geologia e Geofísica Marinha.

Orientador: Prof. Dr.CLEVERSON G. SILVA

Niterói

2020

FABRICIO FERREIRA

Planktonic foraminifera biostratigraphy and paleoceanographic reconstructions of western equatorial Atlantic for the last ~1.93 Ma

Tese apresentada ao programa de Pós-Graduação em Dinâmica dos Oceanos e da Terra da Universidade Federal Fluminense, como requisito parcial para obtenção do grau de Doutorem Ciências, área de concentração: Geologia e Geofísica Marinha.

Aprovado em Março de 2020

BANCA EXAMINADORA:

Prof. Dr. Cleverson G. Silva

Prof. Dr. Paul A. Baker

Prof. Dr. Gary Dwyer

Profa. Dra. Catherine A. Rigsby

Prof. Dr. Cristiano M. Chiess

Dr. Rodrigo Portilho-Ramos

Niterói-RJ

2020

Ficha catalográfica automática - SDC/BIG
Gerada com informações fornecidas pelo autor

F383p Ferreira, Fabricio
Planktonic foraminifera biostratigraphy and paleoceanographic reconstructions of western equatorial Atlantic for the last ~1.93 Ma / Fabricio Ferreira ; Cleverson Guizan Silva, orientador ; Paul Baker, coorientador. Niterói, 2020.
170 f. : il.

Tese (doutorado)-Universidade Federal Fluminense, Niterói, 2020.

DOI: http://dx.doi.org/10.22409/PPGDOT .2020.d.96142685068

1. Geociências. 2. Bioestratigrafia. 3. Geoquímica. 4. Paleoceanografia. 5. Produção intelectual. I. Silva, Cleverson Guizan, orientador. II. Baker, Paul, coorientador. III. Universidade Federal Fluminense. Instituto de Geociências. IV. Título.

CDD -

Bibliotecário responsável: Sandra Lopes Coelho - CRB7/3389

Dedico essa obra à minha família, pelo carinho, atenção e apoio incondicional.

Acknowledgments

I would first and foremost like to acknowledge my advisers Professors Cleverson G. Silva, Paul Baker, and Gary Dwyer for continuous support and encouragement, and all the scientific support. I also thank to introducing me in this field of study and for expanding my knowledge and interest by including different analysis into my project. I would especially like to thank Gary Dwyer for all the scientific support and helpful advice during the lab process.

I would like to thank Cristiano Chiessi for all the discussions and comments that improve this work in many different ways.

I would like to especially thank a new family that I was lucky enough to meet and that welcomed me throughout this journey, Paul A. Baker, Catherine Rigsby, Nate Baker, and Scarllet, for all the personal and professional support, constant encouragement, and friendship, making my days better.

I also would like to thank all members of IGEO-UFF, especially the members of 304 room for all friendship, laughs, hard work, and scientific discussions. To Allan S. Oliveira, Rafael Cuelar, Rodrigo Abuchacra, Paula Falheiro, Gustavo Melo, João Regis, José Dutra, Valquíria, and many others, for the exchange of knowledge and good times together.

Finally, I would like to acknowledge the Programa de Pós-graduação em Dinâmica dos Oceanos e da Terra do Universidade Federal Fluminense (DOT-UFF) and the Division of Earth and Ocean Sciences Nicholas School of the Environment at Duke University for providing all the necessary support during the development of this work. I also had the support of the Brazilian agency CAPES [grant numbers 99999.000623/2016-04, 88882.151083/2017-01, 88881.185132/2018-01], which allowed the development of this study.

To all others who, directly or indirectly, contributed to this work.

Abstract

The western Equatorial Atlantic is considered the main route for cross-equatorial transport of heat and salt to the North Atlantic, and a key component of the climate system. Planktonic foraminifera is an important biochronostratigraphic tool applied to Pleistocene and older sediments, and one of the main proxies in paleoceanographic studies. Conversely, few quantitative studies are coupling the biostratigraphic events with the paleoceanographic records on long sections of the western equatorial Atlantic. Here we present the integration of quantitative analyses of planktonic foraminifera biostratigraphy, planktonic and benthic foraminifera oxygen isotopic records, and planktonic foraminifera radiocarbon ages to construct a biochronostratigraphic framework for the last 1.93 Ma. In addition, we present the integration of independent proxies for sea surface temperature (SST), and seawater oxygen isotopic records ($\delta^{18}O_{sw}$) based on planktonic foraminifera species (census-based) and trace elements (Mg/Ca in *Globigerinoides ruber*), applied for sea surface reconstructions. The ages of the biostratigraphic events derived from our records are consistent with previous works except for the highest occurrences of *Globigerinoides fistulosus* (~1.82 Ma; MIS 66; all ages refer to our records), *Globoturborotalia obliquus* (~1.48 Ma; MIS 49), and *Globorotalia tosaensis* (~1.07 Ma; MIS 31). The largest age difference (~460 kyr) was found for the highest occurrence of *G. tosaensis*. In addition, we describe for the first time in the equatorial and western South Atlantic the oldest Pleistocene *Globorotalia menardii* disappearance (D) and reappearance (R) events D5 (~1.79 Ma; MIS 64), R5 (~1.68 Ma; MIS 60), D4 (~1.05 Ma; MIS 30) and R4 (~0.96 Ma; MIS 26). Our records present a systematic difference in the ages of *G. menardii* D and R events compared to the North and South Atlantic. While the onset of D events occurs initially at high latitudes and later in the equatorial region, the timing of R events exhibit the opposite behavior. The oscillations in abundance of the complexes *Pulleniatina* and *Globorotalia crassaformis* together with the species *Globorotalia truncatulinoides* and *Globoconella inflata* allowed the subdivision of the last 1.93 Ma into 20 subzones, substantially improving the biochronostratigraphic resolution for the western equatorial Atlantic. Our reconstruction of Pleistocene paleoceanographic conditions support the applications of the abundance events of the *G. menardii* complex as a proxy for the warm and salty waters transported from the Southern Hemisphere to the Equator, in particular during the events R4 (~0.96 Ma; MIS 26; boundary T/S); R3 (~0.54 Ma; MIS 12/14; boundary U/V) and R2 (~0.13 Ma; MIS 5/6; boundary W/X) and the subzonal boundaries R2/R1 (~1.31 Ma; MIS 41) and T2/T1 (~0.68; MIS 16). The disappearance events of the taxon are related to synchronous decreases or interruptions of the Agulhas leakage and slowdown AMOC (due to North Atlantic stadial events). Over the Mid-

Pleistocene Transition (~0.88 Ma and ~0.63 Ma), we record for the first time two large scale events, for which the upper water column is characterized by cold and low-salinity layer (>50 m). Our results suggest a large freshwater influx (large river influx and heavy precipitation) and strongest NBCR system. Our results also provide the first record of salt and heat accumulation events (~1.26-1.12 Ma and ~0.33 Ma), here related to the coupling between North Atlantic stadial events and increased Agulhas leakage. We also addressed the influence of the NBCR strength system as an important inter-hemisphere heat and salt transport regulator, and the oscillations impact over millennial time scale for the global and local climate.

RESUMO

O Atlântico equatorial ocidental é considerado a principal rota para o transporte de calor e salinidade para o Atlântico Norte, e um componente essencial do sistema climático. Os foraminíferos planctônicos são uma importante ferramenta biocronoestratigráfica aplicada aos sedimentos do pleistoceno e uma das principais proxies em estudos paleoceanográficos. Por outro lado, existem poucos estudos quantitativos que associam os eventos bioestratigráficos e paleoceanográficos em seções do Atlântico equatorial ocidental. Apresento aqui a integração de análises quantitativas da bioestratigrafia (foraminíferos planctônicos), isótopos estáveis de oxigênio de foraminíferos planctônicos e bentônicos, e idades radiocarbônicas em uma estrutura biocronostratigráfica para os últimos 1,93 Ma. Além disso, apresento a integração de proxies independentes como temperatura superficial do mar (SST), salinidade superficial do mar (SSS) e a reconstrução dos isotópicos estáveis de oxigênio da água do mar (δ^{18}Osw) e elementos traços (Mg/Ca em *G. ruber*), aplicados às reconstruções da condições da superfície da coluna d´água. As idades dos eventos bioestratigráficos derivados de nossos registros são consistentes com trabalhos anteriores, com exceção de *Globigerinoides fistulosus* (~1,82 Ma; MIS 66; todas as idades se referem aos nossos registros), *Globoturborotalia obliquus* (~1,48 Ma; MIS 49) e *Globorotalia tosaensis* (~1,07 Ma; MIS 31). A maior diferença entre idades (~460 kyr) foi encontrada na ocorrência de *G. tosaensis.* Além disso, descrevo pela primeira vez no Atlântico Sul equatorial e ocidental os eventos mais antigo de desaparecimento (D) e reaparecimento (R) do plexo *Globorotalia menardii*, sendo eles D5 (~1,79 Ma; MIS 64), R5 (~1,68 Ma; MIS 60) , D4 (~1,05 Ma; MIS 30) e R4 (~0,96 Ma; MIS 26). Nossos registros apresentam uma diferença sistemática na idade dos eventos de *G. menardii* D e R em comparação ao Atlântico Norte e Sul. Enquanto o início dos eventos D ocorre inicialmente em altas latitudes e mais tarde ocorre na região equatorial, enquanto as idades dos eventos R exibem o comportamento oposto. As oscilações em abundância dos complexos *Pulleniatina* e *Globorotalia crassaformis*, juntamente com as espécies *Globorotalia truncatulinoides* e *Globoconella inflata,* permitiram a subdivisão dos últimos 1,93 Ma em 20 subzonas, melhorando substancialmente a resolução biocronoestratigráfica do Atlântico equatorial ocidental. A reconstrução das condições paleoceanográficas do Pleistoceno suporta a sugestão da aplicação dos eventos de abundância do complexo *G. menardii* como proxy para traçar as ocorrência de águas quentes e salinas transportadas do hemisfério sul para o Equador, especialmente durante os eventos R4 (~ 0,96 Ma; MIS 26; limite T / S); R3 (~ 0,54 Ma; MIS 12/14; limite U / V) e R2 (~ 0,13 Ma; MIS 5/6; limite W / X) e os limites subzonais R2 / R1 (~ 1,31 Ma; MIS 41) e T2 / T1 (~ 0,68; MIS 16). Enquanto os eventos de desaparecimento do

táxon estão relacionados à ação síncrona de diminuição ou interrupção do vazamento de Agulhas e desaceleração do AMOC (devido a eventos estaduais do Atlântico Norte). Durante a transição do Pleistoceno Médio (~0,88 Ma e ~0,63 Ma), foram registrados pela primeira vez dois eventos climáticos, onde a coluna d´água superficial é caracterizada por ima camada fria e de baixa salinidade (> 50 m), resultado do acoplamento entre o grande fluxo de água doce (grande fluxo de rio e forte precipitação) e o aumento NBCR. Nossos resultados também fornecem o primeiro registro de eventos de acumulação de águas salgadas e quentes (~1,26-1,12 Ma e ~0,33 Ma), aqui relacionados ao acoplamento entre eventos de resfriamento do Atlântico Norte e aumento do vazamento de Agulhas. Também abordamos a influência do sistema de força NBCR como um importante regulador inter-hemisférico de transporte de calor e sal e os impactos das suas oscilações ao longo para o clima global e local.

Figures List

Figure 1. Location of marine sediment core CDH-79 (green star) with (a.) long-term mean annual sea surface temperature (color scale) (Locarnini et al., 2018) and (b) long-term mean annual sea surface salinity (color scale) (Zweng et al., 2018), and the surface ocean currents of interest for this study (black arrows). The white dashed rectangle indicates the area used to estimate the long term mean sea surface temperature and salinity for the study area. BC - Brazil Current; NBC-North Brazil Current; NECC- North Equatorial Countercurrent; SEC - South Equatorial Current (Peterson and Stramma, 1991).....20

Figure 2. Piston core CDH-79 retrieved during a Cruise on the RV Knorr (KNR197-4) on the Brazilian continental slope of Pará-Maranhão basin in February 2010.....23

Figure 3. Age model of core CDH-79 based on calibrated AMS ^{14}C ages (blue triangles) and tie-points (green triangles) based on the alignment of our stable oxygen isotopic ($\delta^{18}O$) records to the reference $\delta^{18}O$ stack LR04 (Lisiecki and Raymo, 2005). Black dotted lines indicate the uncertainty of the median age (solid red line) at (a.) 5 cm, and (b.) 1 cm resolution. Note that between 50 -60 cm core depth, there is a hiatus.....27

Figure 4. Stable oxygen isotopic ($\delta^{18}O$) records from (a.) LR04 stack (Lisiecki and Raymo, 2005); revised isotope stratigraphy of Ceara Rise ODP Leg 154 (b.) smooth; (c.) Site 925; (d.) Site 927 (Wilkens et al., 2017); (e) equatorial Pacific ODP Leg 130 Site 806b (de Garidel-Thoron et al.,2005); and western equatorial Atlantic core CDH-79 (f.) *Globigerinoides ruber* (white); (g.) benthic foraminifera (this study). Marine isotopic stages according to the LR04 stack (Lisiecki and Raymo, 2005), and substages according to Railsback et al. (2015).....28

Tables List

Table 1. Raw ^{14}C AMS data and calibrated ages for core CDH-79.....28

Table of Contents

Acknowledgements ..... **vi**

Abstract ..... **vii**

RESUMO ..... **ix**

Figures List ..... **xi**

Tables List ..... **xii**

1. Introduction **14**

2. Study Area **19**

2.1. Ocean Circulation 19

2.2. Climate and hydrography 21

3. Material and Methods **23**

3.1. Preparation and analysis of planktonic foraminifera 23

3.2. Planktonic foraminifera biostratigraphy 24

3.3. Stable oxygen isotopic analyses and radiocarbon dating 25

3.4. Chronology and age model 26

3.5. Planktonic foraminifera census-based paleoceanography 28

3.6. Sea surface reconstruction by Modern Analogue Technique (MAT) 30

3.7. Trace Elements Analysis: Mg/Ca ratio and derived temperature estimation 30

4. Results **35**

4.1. Chapter 1: Biochronostratigraphy of the western equatorial Atlantic for the last 1.93 Ma 35

4.2. Chapter 2: Paleoceanographic reconstructions of western equatorial Atlantic for the last ~1.93 Ma 105

5. Conclusion **157**

6. References **160**

1. Introduction

The Quaternary Period has been punctuated by a series of global climatic oscillations, between warmer and cooler conditions controlled by cyclic variations in the Earth's orbital parameters (Imbrie et al., 1989; Lisiecki and Raymo, 2005). These shifts led to the expansion and retreat of continental ice sheets changing the ocean circulation and the position of oceanic fronts (Niebler and Gersonde, 1998; Ruddiman, 2003; Kemp et al., 2010). This variability in ocean circulation changed the vertical distribution of carbon and nutrients affecting, in turn, the primary productivity into the deep ocean as well as in the surface waters (Bröecker and Peng, 1989; Sarnthein and Winn, 1990). Two major climatic changes, the Mid-Pleistocene Transition (MPT) and the Mid-Brunhes Event (MBE) characterized the Quaternary (Becquey and Gersonde, 2002). These periods were marked by intense climate change and are a subject of great scientific interest because contain the keys to better understanding the climate system.

Over the MPT (~1.2-0.6 Ma), glacial-interglacial contrasts became more severe with long climate cooling phases interrupted by relatively rapid climate warming phases associated with ice decay (Becquey and Gersonde, 2002). Throughout this period the dominant periodicity of the glacial-interglacial cycles changed from symmetrical low-amplitude, high-frequency (41 kyr) ice volume variations to high-amplitude, low-frequency (100 kyr) asymmetrical saw-toothed ice volume variations that indicate a gradual ice build-up terminated by rapid deglaciation events (Broecker and Van Donk, 1970; Durham et al., 2001; Maslin et al., 2001; Ruddiman, 2003). The world´s oceans benthic foraminifera $\delta^{18}O$ records documented a general increase in global ice volume and the onset of weak 100 kyr cycles between 1.2 and 0.95 Ma (Diekmann and Kuhn, 2002), a dramatic increase in the size of the northern hemisphere ice cap between 0.95 and 0.9 Ma and the establishment of strong 100 kyr cycles by 0.64 Ma (Ruddiman et al., 1989; Imbrie et al., 1993; Berger et al., 1994; Chen et al., 1995; Mudelsee and Schulz, 1997; Rutherford and D'Hondt, 2000). A significant strengthening of glacial deep-water ventilation in the Pacific sector of the Southern Ocean occurred near the start of the MPT at 1.1 Ma as part of subsequent glacially enhances the production of deep Southern Component Water (SCW; Sexton and Barker, 2012). Planktonic foraminifera isotope and census-based sea surface temperature (SST) estimates document northwards movement of the Polar fronts in the Southern Ocean after 1.2 Ma (Becquey and Gersonde, 2002; Diekmann and Kuhn, 2002). During the latter half of the MPT (MIS 22-12),

glacial periods were the coldest during the Pleistocene and interglacials close to present temperatures (Hayward et al., 2012).

Following the MPT, the Earth´s climate system had lower mean global temperatures, increased global ice volume, lower mean SST, and increasingly severe glacial temperatures (Shackleton et al., 1990). Poor preservation of carbonates in the South Atlantic between ~0.92 Ma (marine isotopic stage- MIS 24) and ~0.53 Ma (MIS 13) is the result of reduction of North Atlantic Deep Water (NADW) production and an increased influence of more corrosive water from SCW (Schmieder et al., 2000). Significant changes in the thermohaline circulation took place during this climate transition causing a reduction of NADW input to the Antarctic Circumpolar Current (ACC), a weakening of the surface waters from the Indian Ocean to the South Atlantic via the Agulhas Current, and an increase in biological activity was documented during glacial stages of the last ~0.6 Ma (Schmieder et al., 2000; Sigman and Boyle, 2000; Kuhn and Diekmann, 2002).

The MBE (~0.6-0.2 Ma) represents a major climatic decoupling of climate conditions in different latitudes with glacial-to-interglacial contrasts up to 8°C (Kunz et al., 2002; Holden et al., 2011). In South Hemisphere, climate shows a transition to "interglacial-like" conditions, related to an intensified atmospheric and ocean circulations, which could lead to a shallower nutricline and enhanced productivity in this interval. On the other hand, in North Hemisphere, the conditions became more "glacial" during the MBE (Leonhardt et al., 2015). The MBE marks the onset of the Late Quaternary regime of glacial cycles enhanced by larger continental ice sheets, lower sea level, cooler temperatures in Antarctica, and lower atmospheric CO^2 concentration. It is also marked by a strong increase in the accumulation of carbonate in the oceans that might have been caused by the proliferation of phytoplankton (Flores et al., 2003, Barker et al., 2006). The Mid-Brunhes event has been a focus for paleoclimatological studies because of the culmination of global climate deterioration from 3 to 2.7 Ma (Mix et al., 1995), a prominent deglacial event termed Termination V between MIS 12 and MIS 11 (McManus et al., 1999) and possible long-term climate shift concerning dominant orbital parameters (Jansen et al., 1986). Moreover, insolation variations with a 400-kyr periodicity (Berger and Loutre, 1991) position MIS 11 as the most recent climate analog for the present interglaciation (Berger and Loutre, 2003). Attempts at a high-resolution analysis of the Mid-Brunhes by deep-sea cores (Oppo et al., 1998) and lacustrine sediment archives (Tzedakis et al., 2003) suggest that millennial-scale variations in the Late Pleistocene may have persisted over a longer timescale. In addition, the earliest Brunhes chron at 0.7-0.8 Ma is known for the Mid-Pleistocene climate

revolution shifting from the 41-kyr obliquity cycle to the 100-kyr eccentricity cycle (Ruddiman, 2003).

Planktonic foraminifera group has been shown one of the most important tools in the biostratigraphic and paleoceanographic investigations around the world ocean basins (e.g. Wade et al., 2011; Toledo et al., 2016; Schiebel and Hemleben, 2017). They are an organism that shows high sensitivity to environmental variations, in particular to changes in SST, sea-surface salinity (SSS), upper ocean stratification, and productivity (e.g. Bé et al., 1976; Portilho-Ramos et al., 2014). They also have the principal characteristics to be considered an ideal biostratigraphic index fossil - been a diverse morphologically distinct group that presents globally distribution and rapidly-evolution throughout the Mesozoic and Cenozoic, as well as a high preservation potential (Wade et al., 2011). Throughout the Cenozoic, the planktonic foraminifera has been an abundant and diverse group in the tropics and subtropics, showing an average of 1.5 new appearance and 1.3 disappearance events per million years (Thunell, 1984). These evolutionary events are used as criteria to settle biozones boundaries and other stratigraphic units, allowing the construction of detailed zonal schemes for the last 65 Ma (Blow, 1969; Bolli and Premoli Silva, 1973; Stainforth et al., 1975; Kennett and Srinivasan, 1983; Thunell, 1984; Bolli and Saunders, 1985), and the most detailed zonal schemes for the tropical and subtropical latitudes (Wade et al., 2011). Even though there are almost no extinctions or appearances of planktonic foraminifera species in the Quaternary (last 2.58 Ma, Gibbard et al., 2010), the records of the climatic oscillations that characterize this Period (glacial-interglacial periods) can be observed in the marine sediments by the control of changes in the abundance of planktonic foraminifera assemblages and/or species (*e.g.* Ericson and Wollin, 1968). During the Quaternary, the group showed significant expansions and contractions in the geographic distribution of certain assemblages and/or species, due to migratory events with non-evolutionary characteristics in response to climatic variations (Kennett and Huddlestun, 1972; Bé et al., 1976; Thunnel, 1984; Calley et al., 2012). In addition, the group also enables census-based proxies and the recovery of geochemical records based on its calcareous shells, as stable isotopic (i.e. oxygen and carbon), trace elements (i.e. Mg/Ca ratio), and radiocarbons (^{14}C AMS) reconstructions (e.g. Kucera et al., 2005b; Ferreira et al., 2014; Portilho-Ramos et al., 2014, 2017; Schiebel and Hemleben, 2017). Thus, control of the relative abundance of assemblages and/or species of planktonic foraminifera sensitive to climatic oscillations coupling which geochemical analysis on its calcite shell can provide a robust age model and a complete record of the paleoceanographic and paleoclimatic oscillations with good resolution for the Quaternary sections in both local and global scale (e.g.

Ericson and Wollin, 1968; Kennett and Huddlestun, 1972; Bé et al., 1976; Thunnel, 1984; Martin et al., 1990, 1993; Ferreira et al., 2012; Calley et al., 2012; Portilho-Ramos et al., 2014; Nace et al., 2014; Toledo et al., 2016).

The western equatorial Atlantic margin is an ideal region to study the variability in the tropical atmospheric circulation, and ocean currents of South America, and the global climate system as well (e.g. Wilson et al., 2011; Nace et al., 2014; Zhang et al., 2017; Crivellari et al., 2018). The sediments deposited in this area provide a complete record of past changes on the North Brazil Current (NBC) system, that associated with the Atlantic Meridional Overturning Circulation (AMOC), promote the main pathway for the cross-equatorial transport of warm and salty surface waters into high latitudes of the North Atlantic (e.g. Nace et al., 2014; Zhang et al., 2015), and one of the most important components of the thermohaline circulation and Earth's climate (e.g. Arz et al., 1998; Zhang et al., 2017; Crivellari et al., 2018). The accumulation of excess salt in this region ultimately impacts the density of high latitude surface waters which drive the formation of NADW affecting both local and global climate systems (Johns et al., 1998; Wilson et al., 2011). It is also suggested that a freshwater influence from the equatorial Atlantic leads to a weakening of the AMOC, which results in surface air temperatures over the North Atlantic cool, and temperatures over the South Atlantic warm (Barker et al., 2009). However, just a few long sequences with sufficient continuity and homogeneity that enables integrated biostratigraphic, paleoceanographic, and paleoclimatological studies for the Late to Middle Pleistocene are available in the western equatorial Atlantic.

To improve the biochronostratigraphic framework and the long-term paleoceanographic fluctuations in Pleistocene sections (core CDH-79) from the western equatorial Atlantic, the main proposes of this study are: (1) construct a biocrhonostratigraphic framework based on planktonic biostratigraphic events calibrated with the oxygen isotopic records and radiocarbon dating; (2) reconstruction of the superficial ocean conditions based on planktonic foraminifera census-based and geochemical proxies for sea surface temperature, salinity, and seawater oxygen isotopic records. For achieving these goals, this thesis is divided into two articles manuscripts to be submitted in a peer-reviewed international journal. The manuscripts are included as result chapters and presented as:

- **Chapter 1:** Biochronostratigraphy of the western equatorial Atlantic for the last 1.93 Ma.
- **Chapter 2:** Paleoceanographic reconstructions of western equatorial Atlantic for the last ~1.93 Ma.

In Chapter 1, I present the integration of quantitative analyses of planktonic foraminifera biostratigraphy, planktonic and benthic foraminifera oxygen isotopic records, and planktonic foraminifera radiocarbon ages in a biochronostratigraphic framework for the last ~1.93 Ma of the western equatorial Atlantic. The oscillations in the abundance of 14 species allowed the recognition of 16 biostratigraphic events, and the subdivision of the Pleistocene in 12 zones and 20 subzones, substantially improving the biochronostratigraphic resolution for the Quaternary of the western equatorial Atlantic. The ages of the biostratigraphic events derived from our records are consistent with previous works with few exceptions of specie highest occurrences. In addition, I present the first record in the equatorial and western South Atlantic of the oldest Pleistocene *Globorotalia menardii* disappearance (D) and reappearance (R) events and highlight the systematic difference in the ages of the *G. menardii* events when compared which the North and South Atlantic events.

In Chapter 2, I present the integration of independent proxies based on planktonic foraminifera species (census-based and geochemistry proxies) applied for the reconstruction of Gelasian to early Pleistocene (~1.93-0.01 Ma) paleoceanographic conditions. The results support the applications of the *G. menardii* complex disappearance (D) and reappearance (R) events, and abundance oscillation of the taxon as a proxy for the heat and salty waters transported from the southern hemisphere to the Equator. I also present the first record of two large scale events characterized by cool and low-salinity waters that marks the onset and the middle Mid-Pleistocene Transition, and the first record of salty and warm accumulation events. Both large-scale events here are related to the influence of the NBCR strength system that can impact over millennial time scale the global and local climate over.

Together, these two chapters provide a complete overview of the main biostratigraphic and paleoceanographic events for the longest continuous record in the Brazilian equatorial margin, addressing the influence of the NBCR strength system as an important inter-hemisphere heat and salt transport regulator, and the impact of the millennial-scale current oscillations in the global and local climate.

2. Study Area

We investigated core CDH-79 (Figure 1), retrieved during RV Knorr cruise KNR 197-4 in February 2010 in the western equatorial Atlantic. The coring site is located on the top of a sea mountain (2345 m water depth) in the continental slope of Pará-Maranhão Basin, 320 km from the modern coastline of Maranhão Gulf, northeastern Brazil. In the region of our record (core CDH-79; Figure 1), long-term annual mean sea surface temperature is 27.5°C (between 27.3°C and 28.2°C) (Locarnini et al., 2018), while sea surface salinity is 35.7 (between 28.2 and 36.2) (Zweng et al., 2018).

2.1. Ocean Circulation

The modern surface ocean circulation in the western equatorial Atlantic is controlled by the North Brazil Current (NBC) and the North Equatorial Countercurrent (NECC). The NBC results from the bifurcation of the South Equatorial Current (SEC) at 10-15°S and flows northwestwards along the continental margin of northeastern Brazil (Figure 1; Peterson and Stramma, 1991; Schott et al., 1995; Stramma et al., 1995). At the bifurcation, the Brazil Current is also originated and flows southwards along the continental margin of eastern Brazil. With its large anticyclonic rings, the NBC is the main pathway for the cross-equatorial transport of warm and salty surface waters that balances the southward export of North Atlantic Deep Water (Johns et al., 1998; Goni and Johns, 2001; Haarsma et al., 2011). NBC extends from the surface to intermediate water depths (approximately 800 m water depth) where it merges with northward advected Antarctic Intermediate Water (Talley et al., 2011). The deepwater circulation in the area is dominated by interactions between the southward flowing NADW and the northward-flowing Circumpolar Deep Water (Bickert et al., 1997). As a result of the importance of inter-hemispheric heat and salinity exchange through thermohaline circulation, variations in the relative flux of the NADW to the Southern Ocean are thought to be a major driving force in the growth and decay of continental ice sheets (Harris et al., 2008).

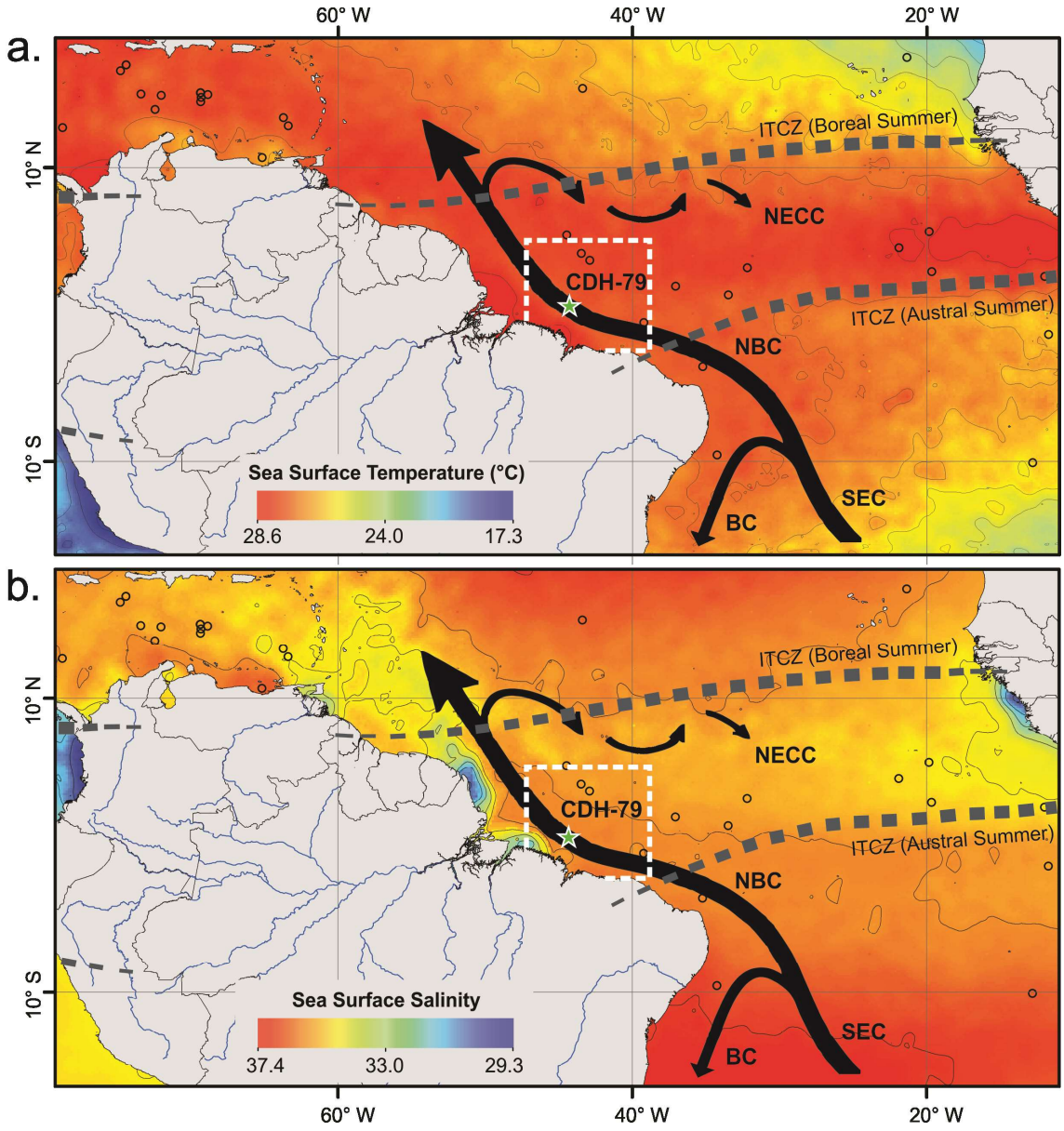

Figure 1. Location of marine sediment core CDH-79 (green star) with (a.) long-term mean annual sea surface temperature (color scale) (Locarnini et al., 2018) and (b) long-term mean annual sea surface salinity (color scale) (Zweng et al., 2018), and the surface ocean currents of interest for this study (black arrows). The white dashed rectangle indicates the area used to estimate the long term mean sea surface temperature and salinity for the study area. BC - Brazil Current; NBC-North Brazil Current; NECC- North Equatorial Countercurrent; SEC - South Equatorial Current (Peterson and Stramma, 1991).

The transport variability of NBC is also observed in different timescale, showing a positive correlation with the decrease of the strength of Atlantic Meridional Overturning Circulation (AMOC) on decadal timescales (Zhang et al., 2011). Reconstructed δ^{18}Osw values

from the Early Holocene and core-top samples demonstrated a similar surface current such that the freshwater plume lows northwestwards with the NBC (Wilson et al., 2011). That variability is also observed on the millennial-scale, where the NBC presented a marked decrease in the strength during AMOC slowdown events of the last deglaciation, such as the Younger Dryas (i.e. YD, 13–11.5ka) and Heinrich Stadial 1 (i.e. H1, 18–15ka) (Arz et al., 1999; Wilson et al., 2011). Those millennial-scale abrupt changes in AMOC strength during the last deglaciation greatly influenced the South American Monsoon System (SAMS) and the mean position of the ITCZ (Zhang et al., 2015).

The NBC is also responsible for the northwestward transport of freshwater and terrigenous sediment from important fluvial sources of Northeast region of Brazil delivered to the ocean by Parnaíba River (Zhang et al., 2015), with an annual average discharge rate of the 1272 m^3/s (Marques et al., 2004), and Amazon River with average around 2 $\times 10^6 m^3/s$ (Lentz, 1995; Allison et al., 2000). The large increase in terrigenous sediments offshore was interpreted as the product of massive fluvial input from the adjacent continent (Arz et al., 1998; Jennerjahn et al., 2004; Dupont et al., 2010; Zhang et al. 2015). However, the role of the NBC (in particular its potential reversal) in the redistribution and deposition of terrigenous sediments on the NE South American continental margin remains inconclusive.

2.2. Climate and hydrography

Northeast Brazil is located close to the equator, has semi-arid characteristics, with low rainfall and rainy seasons restricted to a few months. A frontal system and the ITCZ (a convective belt of increased cloud and precipitation in tropical latitudes) are responsible for about 80% of the total amount of rain over Northeast Brazil and meso- micro-scale mechanisms supplement the total amount of observed rain. The Atlantic ITCZ is a branch of the Hadley cell, who marks a dynamic boundary between the southeast and northeast Atlantic trade winds and is associated with a band of low pressure and high precipitation that occurs predominantly over the ocean basin (e.g. Molion and Bernardo 2000). Associated with the expansion and contraction of subtropical anticyclones over the North and South Atlantic Ocean, the seasonal migration of the ITCZ plays a major role in controlling the patterns of rainfall over the adjacent continent, imposing distinctive wet and dry season across northern South America (Hastenrath and Heller 1977).

Over the Atlantic, the ITCZ migrates from a further north position about 14°N in August-September to the further south position at about 4°S during March-April (Schneider et al, 2014). Due to its influence on ocean current dynamics, the migration of the ITCZ has a more

marked effect on the climate of coastal regions, being the main mechanism responsible for the rainy season (February to May) in northern Northeast Brazil. Convection and wind direction patterns, controlled largely by insolation changes, are associated with the equatorial low-pressure trough and the South American Summer Monsoon (SASM), which influences the timing of the onset of the wet season across South America (Wilson et al., 2011). The variations of the northeast and southeast trade winds seem to be one of the causes of changes in intensity and positioning of the ITCZ, where the predominance of southeast trade winds are recorded in November, which changes in direction from northeast to the southeast in June (Silva et al., 2005). Some models show that the strength of northeast trade winds is associated with the seasonal southward displacement of the ITCZ (Wang et al., 2004).

According to Hastenrath (2006), the inter-annual variability of rainfall in Northeast Brazil is associated with variations of sea surface temperature patterns (SST) over the tropical oceans, affecting the position and intensity of the ITCZ. Cruz et al. (2009) suggested that the fluctuations in rainfall over Northeast Brazil follow the precession cycle, occurring in a coordinated stage with paleoclimatic records in the northern hemisphere and reverse with the records of South speleothems and southeastern Brazil (Cruz et al. 2005, Cruz et al. 2006). The southerly position of the ITCZ during the winter is associated with stronger northeast trade winds that favor a large influx of South Atlantic water and a stronger Caribbean Current. However, the magnitudes of Amazon and Northeast precipitation and ecosystems changes in the orbital time scale are almost totally unknown, by the limited paleoclimatic record (Baker and Fritz, 2015).

Changes in the ITCZ position in the millennial time scale were recorded by Peterson et al. (2000) in the sediments of the Cariaco Basin (Caribbean Sea). The authors suggested that the ITCZ maintained a southern position during the glacial periods and stadials stages, resulting in an increased sedimentation yield from the river draining into the Caribbean basin, while during interglacial periods and interstadials stages the ITCZ maintained a northern position, resulting in a decrease in the sedimentation yield from the river drains (Peterson et al., 2000). During glacial stages, an increased latitudinal thermal gradient is thought to have led to reduced penetration of the ITCZ into the northern hemisphere, which greatly alters the dynamics of regional climate causing a decrease in the cross-equatorial transport of heat and salinity by upper-level ocean currents (Berger and Wefer, 1996; Maslin et al., 1997; Vink et al., 2002), changing the vegetation, continental runoff and river outflow patterns in the Amazon Basin (Wilson et al., 2011).

3. Material and Methods

I investigated the core CDH-79 (00° 39.6853' N, 44° 20.7723' W; 32.12 m core length; 2345 m water depth; Figure 1), retrieved during RV Knorr cruise KNR 197-4 in February 2010. The coring site is located on the top of a sea mountain in the western equatorial Atlantic (Pará-Maranhão Basin), 320 km from the modern coastline of northeastern Brazil 20 km from the modern coastline of Maranhão Gulf. The Core CDH-79 was collected from a conformable sediment sequence as verified by a high-resolution 3.5.kHz seismic reflection survey. The core was refrigerated and shipped to Wood Hole Oceanographic Institute (WHOI) for storage and subsequent splitting, core description, sampling, and analysis. The sedimentological visual description was performed on a 1:20 scale, including color, granulometry, facies, and primary structures by Oliveira (2016). The CDH-79 sample showed a fine sediment domain, gray to brown muds, with different carbonate contents (Figure 2).

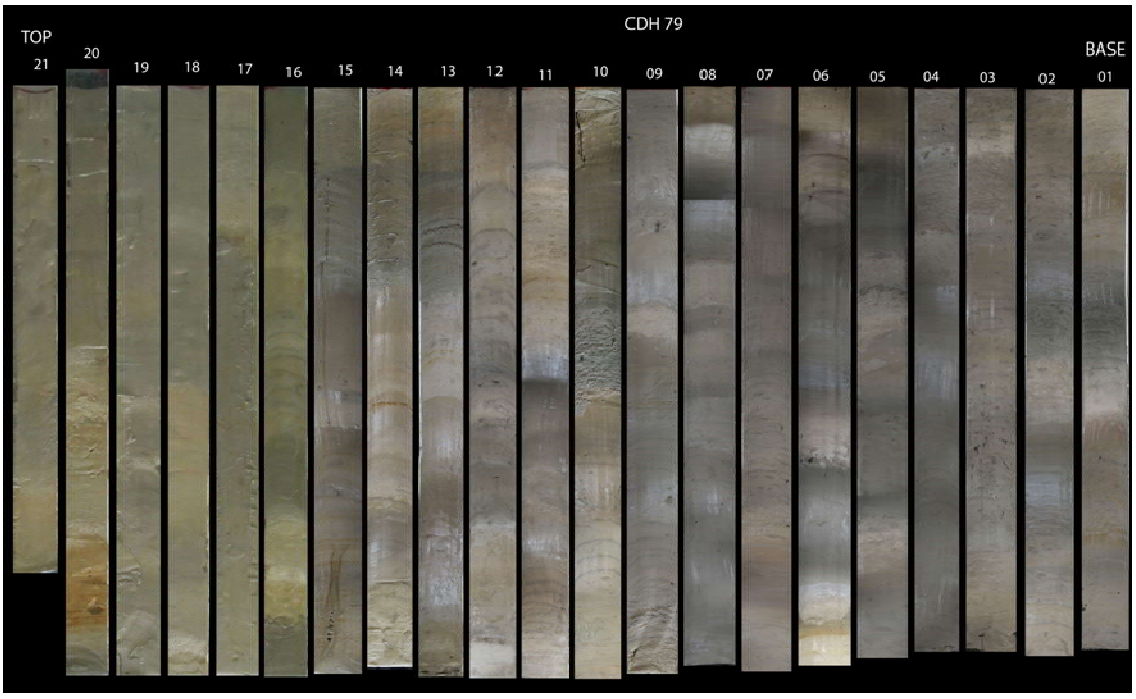

Figure 2. Piston core CDH-79 was retrieved during a Cruise on the RV Knorr (KNR197-4) on the Brazilian continental slope of the Pará-Maranhão basin in February 2010.

3.1. Preparation and analysis of planktonic foraminifera

The unlithified sediment samples were washed through a sieve of 62 μm mesh size (keeping the retained material) and dried at 50°C (Leipnitz et al., 2005). Dry residues were

weighed and stored in glass vials. Planktonic foraminifera was dry picked from the >150 µm fraction in subsample splits (if necessary) containing 300–600 specimens. This results in a 95% level of confidence for species with at least 1% of abundance (Patterson and Fishbein, 1989). The subsamples were stored in micropaleontological slides and all specimens were identified and counted. The specimen preservation was qualitatively estimated and the Le and Shackleton (1992) fragmentation index (FRAG) was calculated for each sample. The taxonomic concepts for Neogene taxa were adopted from Stainforth et al. (1975), Kennett and Srinivasan (1983), and Bolli and Saunders (1985) and revised based on Hayward et al. (2019). The used taxonomic terms are available in Chapter 1, Table S1.

3.2. Planktonic foraminifera biostratigraphy

Only species significant for Quaternary biostratigraphy were considered for the construction of the biostratigraphic framework (e.g. Ericson and Wollin, 1968; Berggren et al., 1985a, 1995a, 1995b; Wade et al. 2011*;* Toledo et al., 2016). The biostratigraphic zonal scheme for the Neogene followed Blow (1969), modified by Kennett and Srinivasan (1983). The Quaternary biostratigraphic zonal scheme followed Bolli and Premili Silva (1973), with the modifications from Bolli and Saunders (1985), Berggren et al. (1995a; 1995b) and the revision of the Cenozoic topical biostratigraphy presented by Wade et al. (2011). The nomenclature adopted for evolutionary events, new appearance, and disappearance of the taxon, following Wade et al. (2011), where lowest occurrence (LO) is used with the same meaning of first appearance datum and/or the first occurrence. Similarly, the highest occurrence (HO) is used with the same mean of last appearance datum and/or last occurrence. Following Wade et al. (2011), we also applied the letter B (base) in the same meaning of LO, and T (top) in the same meaning of (HO).

In addition, the *Globorotalia menardii* complex abundance events (*G. menardii* zonation) from Ericson and Wollin (1968) were employed and referred to as EW68 zones/subzones. *G. menardii* complex refers to the assemblage which combines *G. menardii* spp., *Globorotalia tumida,* and *Globorotalia flexuosa* without distinction of the different morphotypes or subspecies. The same was applied for *Globorotalia crassaformis* (*G. crassaformis*, *G. crassaformis hessi*, *G. crassaformis ronda*, *G. crassaformis viola,* and *G. crassaformis imbricata*) and the *Pulleniatina* (*P. obliquiloculata* and *P. primalis*) genera. However, when the abundance of *G. flexuosa*, *G. crassaformis imbricata*, *G. crassaformis hessi,* and *G. crassaformis viola* are considered, their individual relative abundance, rather than those of the complexes are presented. The EW68 zonation is extensively used in biostratigraphic,

paleoclimatic, and paleoceanographic studies in tropical (e.g. Martin et al., 1990, 1993; Kohl et al., 2004) and subtropical areas (e.g. Vicalvi, 1997; Ferreira et al., 2012, 2014; Portilho-Ramos et al., 2014; Toledo et al., 2016), providing a more detailed biostratigraphic zonation for the Quaternary. For this study, the virtual disappearance of the *G. menardii* complex is defined when its relative abundance drops to <1%. Following Toledo et al. (2016), the disappearance events were numbered top-down by *G. menardii* D1, D2, D3, D4, and D5, and were associated with the base of the EW68 zones Y, W, U, S, and Q, respectively. The reappearance events were numbered top-down by *G. menardii* R2, R3, R4, and R5 and were associated with the base of EW68 zones X, V, T, and R, respectively.

3.3. Stable oxygen isotopic analyses and radiocarbon dating

Five specimens of the planktonic foraminifer *Globigerinoides ruber* (white) within the size fraction 250-350 μm, and at least two specimens of the benthic foraminifer *Uvigerina peregrine* and *Cibicidoides wuellerstorfi* within the size fraction >125 μm were hand-picked for stable oxygen isotopic analyses ($\delta^{18}O$). The tests of foraminifera were soaked in 15% H_2O_2 for 30 min to remove organic matter, and then rinsed with methanol and sonically cleaned to remove fine-grained particles. The methanol was removed with a syringe, and samples were dried at 50°C for 24h. The clean foraminifera tests were crushed, and between 20 to 60 mg of calcite was loaded into glass reaction vessels. Benthic foraminifera tests were directly loaded into glass reaction vessels. Both planktonic and benthic foraminifera were reacted with three drops of H_3PO_4 (specific gravity = 1.92) using a Finnigan MAT Kiel III carbonate preparation device. Isotope ratios were measured by a Finnigan MAT 252 mass spectrometer. The standard deviation of the international standard NBS19 is <0.07‰ during the measurement periods. Planktonic foraminifera was analyzed at the Light Stable Isotope Mass Spectrometer Laboratory, Department of Geological Sciences, University of Florida USA. Benthic foraminifera was analyzed at the State Key Laboratory of Marine Geology, Tongji University, China. The results of benthic foraminifera were corrected following Marchitto et al. (2014).

Five samples composed of mixed well-preserved specimens of planktonic foraminifera from the size range 250-350 μm were used for radiocarbon (^{14}C) dating (Table 1). The samples were hand-picked and analyzed by accelerator mass spectrometry (AMS) at the National Ocean Sciences Accelerators Mass Spectrometry - USA. The radiocarbon ages were calibrated with the software PaleoDataView version 0.9.2 (Langner and Mulitza, 2019) using the IntCal13 calibration curve (Reimer et al., 2013) and a variable reservoir effect (Butzin et al., 2017).

The chronology adopted for this study follows Gibbard et al. (2009) and Gibbard and Head (2010), where the base of the Quaternary Period, that coincides with the base of the Pleistocene Epoch, has an estimated age of 2.58 Ma. The Pleistocene Epoch is divided into the Gelasian (2.58–1.80 Ma), Calabrian (1.80 – 0.781 Ma), Middle Pleistocene (0.781–0.126 Ma), and Late Pleistocene (0.126–0.012 Ma) (Cohen and Gibbard, 2019).

Table 1. Raw ^{14}C AMS data and calibrated ages for core CDH-79.

Depth (cm)	Lab ID	Radiocarbon age (yr BP)	Age error (yr)	Reservoir age (yr)	Reservoir age error (yr)	Calibrated age means [95%] (cal a BP)	Calibrated age min [95%] (cal a BP)	Calibrated age max [95%] (cal a BP)
10	OS122410	13900	290	559	55	16054	15225	16942
20	OS122411	17950	510	675	46	20930	19738	22202
30	OS122412	22800	940	781	62	26347	24438	28115
40	OS122413	22900	960	793	63	26437	24506	28272
50	OS122414	25700	1400	740	92	29355	26973	32361

3.4. Chronology and age model

The age model for core CDH-79 is based on five calibrated AMS ^{14}C ages (Table 1) and 114 $\delta^{18}O$ tie-points (Chapter 1; Table S3). The tie-points were derived from the alignment of our $\delta^{18}O$ records to the reference $\delta^{18}O$ stack LR04 (Lisiecki and Raymo, 2005). According to Govin et al. (2015), we estimated the age uncertainty for each tie-point (Chapter 1; Table S3) by taking into account (i) the mean resolution and dating uncertainty of the reference curve LR04 (resolution 1 kyr; uncertainty 6 kyr from 2-1 Ma and 4 kyr from 1-0 Ma; Lisiecki and Raymo, 2005), and (ii) an estimated relative alignment uncertainty (~1.04 kyr).

The age model and associated uncertainties were calculated by using the BACON algorithm version 2.2 (Blaauw and Christen, 2011) within the PaleoDataView software version 0.9.2 (Langner and Mulitza, 2019). A total of 10000 age-depth realizations have been used to calculate the median age and the 2σ uncertainty at 1 cm resolution for the interval 10-50 cm core depth (Figure 3b), and 5 cm resolution for the interval 60-3212 cm (Figure 3a). We assume the presence of a depositional unconformity (hiatus) between 50-60 cm, as shown in section 4.4.

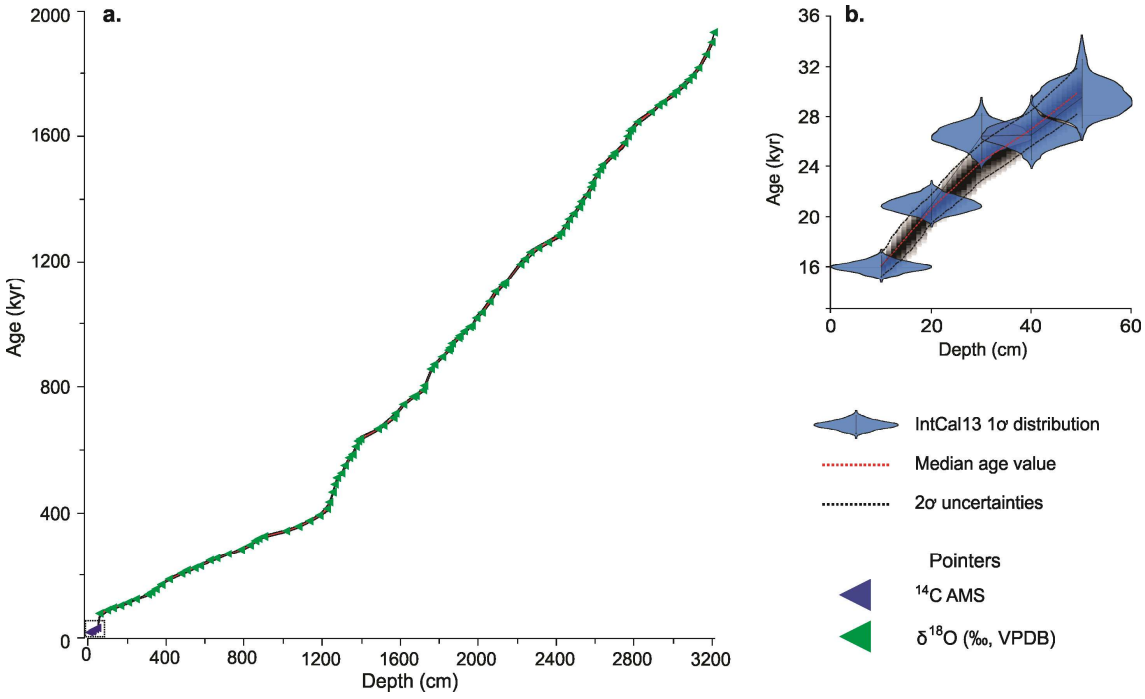

Figure 3. Age model of core CDH-79 based on calibrated AMS ^{14}C ages (blue triangles) and tie-points (green triangles) based on the alignment of our stable oxygen isotopic ($\delta^{18}O$) records to the reference $\delta^{18}O$ stack LR04 (Lisiecki and Raymo, 2005). Black dotted lines indicate the uncertainty of the median age (solid red line) at (a.) 5 cm, and (b.) 1 cm resolution. Note that between 50 -60 cm core depth, there is a hiatus.

The biochronostatrigraphic model built for core CDH-79 indicates an average accumulation rate of 3.35 cm/kyr, showing a good correlation with the LR04 stack (Lisiecki and Raymo, 2005) and the revised isotopic stratigraphies of ODP Leg 154 (Ceara Rise - Sites 925, 927, and benthic smooth; Wilkens et al, 2017), and ODP Site 806b (equatorial Pacific; de Garidel-Thoron et al., 2005) (Figure 4). CDH-79 reaches an estimated age of 1.93 Ma at the base (i.e., 32.12 m core depth) of the core and records marine isotopes stages (MIS) 1-73, thus covering most of the Quaternary (Figure 4).

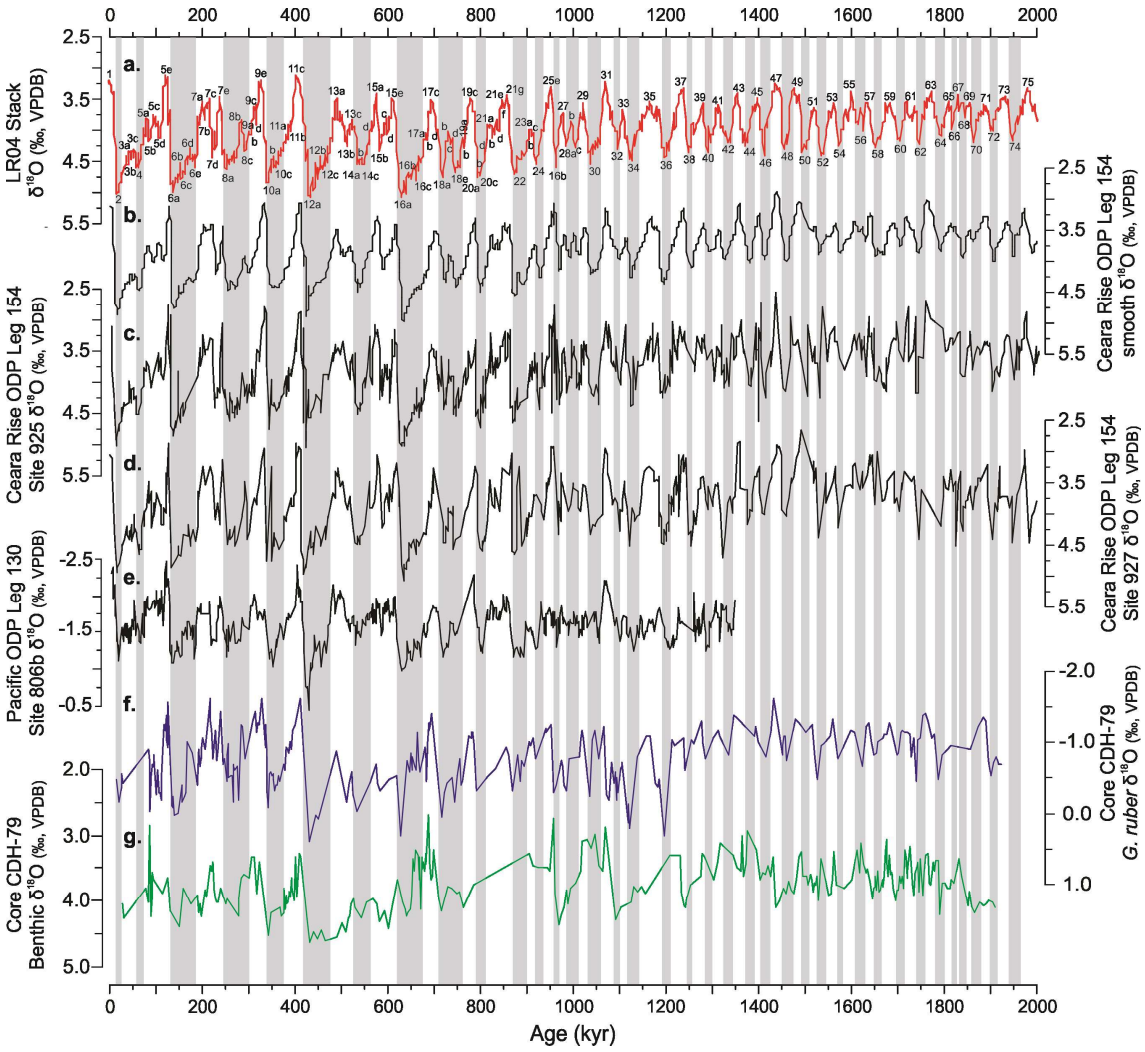

Figure 4. Stable oxygen isotopic ($\delta^{18}O$) records from (a.) LR04 stack (Lisiecki and Raymo, 2005); revised isotope stratigraphy of Ceara Rise ODP Leg 154 (b.) smooth; (c.) Site 925; (d.) Site 927 (Wilkens et al., 2017); (e) equatorial Pacific ODP Leg 130 Site 806b (de Garidel-Thoron et al.,2005); and western equatorial Atlantic core CDH-79 (f.) *Globigerinoides ruber* (white); (g.) benthic foraminifera (this study). Marine isotopic stages according to the LR04 stack (Lisiecki and Raymo, 2005), and substages according to Railsback et al. (2015).

3.5. Planktonic foraminifera census-based paleoceanography

For each sample, species richness (S), Shannon-Weaver diversity (H´), and equitability (J) were calculated (Buzas and Gibson, 1969). Species richness is the number of species in each sample, whereas the Shannon-Weaver index describes diversity, taking into account the relative population of each species within a sample ($H = -\Sigma Pi \ lnPi$; where Pi is the proportion of each species). Equitability is a measure of the evenness of the species distribution within a

sample (E=H/S). Equitability equals one if all species are present in the same population and approaches zero when one species dominate the fauna. The planktonic foraminifera diversity is controlled by the structure of the upper water column (e.g., Rutherford et al., 1999), presenting a diversity decreases from the central gyres of the ocean towards continental margins and/or eutrophic regions (e.g. Martinez et al., 2007). The lower diversity values also were related to a deep thermocline in the Caribbean Sea (Martinez et al., 2007).

For paleoceanographic reconstruction and interpretations, we considered only the abundance of significant species for the paleoceanographic and paleoclimatic reconstructions of the Quaternary (e.g. Nishi et al., 2000; Caley et al., 2012; Portilho-Ramos et al., 2017). The species *Globigerinoides ruber* and *G. sacculifer*, are applied as indicators of the oligotrophic conditions with stable deep-mixed layers (e.g. Nishi et al., 2000; Martinez et al., 2007). While the opportunistic species as *G. glutinata*, *G. bulloides,* and *N. dutertrei* are applied as indicators of eutrophic conditions and used to track the past variability and intensity of surface authorization (Schiebel et al. 2004; Kucera et al., 2005a; Mohtadi et al., 2005; Lessa et al., 2014). The dwelling species as *Globorotalia truncatulinoides e Globorotalia inflata* are used in the recognization of the water column conditions stratification conditions. The specie *G. inflata* are used as indicators of cold subtropical water (Kipp, 1976), and related to low SST (~15-20°C), reduced salinity seasonality, and well-oxygenated waters, that characterizing times when the surface-water stratification decreased (e.g. Nishi et al., 2000).

We also apply the abundance events of *G. menardii* complex (disappearance events *G. menardii* D5, D4, D3, D2 and D1; and reappearance events *G. menardii* R5, R4, R3, R2; Ferreira et al., A) as a track the past inter-ocean exchange from Indian to the Atlantic Ocean (eg. Peeters et al., 2004; Caley et al., 2011). We assume that the Quaternary taxon reseeding of the Atlantic Ocean was related to an increase in the Agulhas leakage (Agulhas current; Caley et al., 2012) as discussed in Chapter 2, item 5.1. In this study, *G. menardii* refers to the complex assemblage who combines *G. menardii* spp. and *Globorotalia tumida* without distinction of the different morphotypes or subspecies.

As a proxy for the mixed layer depth, we applied the *Neogloboquadrina* sp./*G. glutinata* ratio ($R_{N/Gg}$ ratio) from Portilho-Ramos et al. (2017). This proxy considers the opposite abundance patters of *Neogloboquadrina* species (*N. dutertrei and N. imcopta*) and *G. glutinata* in the equatorial Atlantic Ocean as a proxy to track significant changes in the hydrographic and trophic structure of the upper ocean associated with the shallowest mixed layer related to the ITCZ (Portilho-Ramos et al., 2017).

$$R_{N/Gg} = \%Neogloboquadrina/(\%Neogloboquadrina + \%G.\ glutinata) \quad (1)$$

3.6. Sea surface reconstruction by Modern Analogue Technique (MAT)

Mean sea surface temperature was estimated from planktonic foraminifera assemblage data (>150µm size fraction) using the Modern Analog Technique (MAT) performed on the software Past 3.25 (Hammer et al., 2001). The planktonic foraminiferal calibration data set used here composed of a compilation of 430 surface samples from the Atlantic Ocean (predominantly South Atlantic), between 10°N and 30°S from the MARGO Project (Kucera et al., 2005a) that is available at PANGAEA DATABASE (http://epic.awi.de/30068/). For the MAT transfer function, the squared chord distance was applied as a similarity measure. Additionally, when reconstruction results were evaluated, the weighted mean of the best ten modern analogs was used (Kucera et al., 2005b). We estimate the annual mean SST and the temperature of the warmest and coolest months. The SST reconstruction presented a correlation (P>95%; Chapter 2 - Figure S2) and an average standard deviation of R^2= 0.992 and 0.26°C for the annual mean temperature, and R^2=0.984 and 0.17°C for warmest (summer) and R^2=0.980 and 0.32°C for the coolest months (winter).

3.7. Trace Elements Analysis: Mg/Ca ratio and derived temperature estimation

Since the discovery of the temperature dependency relation between the Mg/Ca in foraminiferal calcite and the calcification temperature (e.g. Lea et al., 1999; Mashiotta et al.,1999; Nürnberg et al., 1996; Rosenthal et al., 2000), the Mg/Ca thermometry has become an increasingly useful proxy for the temperature reconstruction of surface water conditions (*e.g.* Nürnberg et al., 2000; Elderfield and Gannssen., 2000; Lea et al., 2000; Dekens et al., 2002); during the Cenozoic paleoceanography and paleoclimatic studies (Barker and Elderfield, 2002; Rosenthal and Lohman, 2002; Anand et al., 2003; de Villiers, 2003; Barker et al., 2005; Fehrenbacher et al., 2006; Martyn et al., 2011; Nace et al., 2014; Herztberg, et al., 2016; Scheiner et al., 2018).

The Ca and Mg oceanic residence times are relatively long (106 and 107 years, respectively), and the Mg/Ca ratio of seawater is considered to be constant over glacial/interglacial timescales (Barker et al., 2005). These characteristics reduce considerable uncertainty when reconstructing paleotemperatures using foraminiferal Mg/Ca ratios. The incorporation of divalent cation Mg^{2+} during the precipitation of foraminiferal shell (formation of biogenic calcium carbonate), is influenced by the temperature of the surrounding seawater

during growth (e.g. Nürnberg et al., 1996; Barker et al., 2005). The Mg^{2+} substitution for Ca^{2+} is exponentially increased as seawater temperatures rise, presented an Mg/Ca ratio (in mmol/mol) increases by 9.0±0.3% at each 1 °C temperature increase (Anand et al. al., 2003). The temperature dependence of planktonic foraminiferal Mg uptake has been well established with culture experiments (e.g., Nürnberg et al., 1996; Lea et al., 1999) and core top calibration studies (Mashiotta et al., 1999; Elderfield and Ganssen, 2000; Dekens er al., 2002; Anand et al., 2003; Friedrich et al., 2012). The secondary factors that can affect Mg/Ca include shell growth rate, pH and salinity, and species-specific effects (Rosenthal et al., 1997; Lea et al., 1999; Elderfield et al 2002).

As an independent temperature proxy, the advantage that Mg/Ca-derived temperature shows its potential to record changes in calcification temperature (e.g. McConnell and Thunell, 2005) and to distinguish the temperature component of the $\delta^{18}O$ signal recorded in calcite from salinity and ice-volume effects through paired measurements of Mg/Ca and $\delta^{18}O$ (e.g., Mashiotta et al., 1999; Elderfield and Ganssen, 2000; Dekens et al. 2002). In this context, only the Mg/Ca ratio coupled with $\delta^{18}O$ (same specie and size fraction) can guarantee a common source of the signal, averaging the same environmental conditions (temporal and spatial habitat; Barker et al., 2005). However, it is well documented that the relationship between decreases in foraminiferal Mg/Ca and the partial dissolution of planktic foraminiferal tests results in a reduction of Mg/Ca ratios (Rosenthal et al., 2000; Dekens et al.,2002). A loss of Mg due to partial dissolution results in an underestimation of seawater paleotemperatures and can lead to imprecise inferences about past climates (Lea et al., 2000; Dekens et al., 2002; Rosenthal and Lohmann, 2002; Regenberg et al., 2014; Rongstad et al. 2017).

We use the planktonic foraminifera *Globigerinoides ruber* (white) for the magnesium (Mg) and calcium (Ca) analysis. Typically around 40-50 specimens of *G. ruber* (white) from 250-350 µm size fractions (233 samples) were selected. The specie *G. ruber* is ideally suited for this study because a) it is cosmopolitan nature, high abundance, and continuously abundant throughout the core; b) the specie is the most widely applied proxy for tropical and sub-tropical SST (Gray et al., 2018). The highest Mg/Ca ratio observed in *G. ruber* white indicates that it inhabits the shallowest habitat, calcifying at or close to the sea surface in warm temperatures (Dekens et al. 2002), living and representing mixed layer temperature (Bé, 1977; Fairbanks et al., 1982). Measured calcification temperature for this specie is in good agreement with predicted $\delta^{18}O$ at 25–50 m water depth (Anand et al. 2003). Its restricted migration through the water column makes *G. ruber* white thought to be the most accurate recorder of SST (Dekens et al., 2002; Lea et al., 2000).

For sample preparation, the picked shells were gently crushed using glass plates, to open chambers, homogenized, and then were chemically cleaned following modified Barker et al. (2003), with adding a reductive step to remove oxide contamination before analysis. The clay removal step consisted of three sonication steps alternating between methanol and ultrapure water. Following the clay removal, a 100 µl of reduction agent (375 µl of hydrazine in 10 ml of 1:1 ammonium hydroxide and citric acid) was applied to each sample. The covered samples were placed in a hot water bath (70-80°C) for 30 minutes, with 10 seconds of sonication every 2 min. After the hot bath, the reduction agent was siphoned and the sample rinsed with ultrapure water. For the oxidation step, a 250 µl of oxidation agent (600 µl of H_2O_2 in 60 ml 1N NaOH) was applied to each sample, and after covered the samples were placed in a hot water bath (80-90°C) for 10 minutes with 10 seconds of sonication after 5 min. After the hot bath, the oxidation agent was siphoned and the sample rinsed with ultrapure water. The following Barker step consists of removing residual coarse-grained silicates of the dry samples with a single hairbrush. After the Barker step, the samples were transferred to new acid-washed vials for the weak acid leaching and sample dissolution (digestion). For the leaching step, a 250 µl of a weak acid (0.002N of HNO_3) was applied two times to each sample, following by 30 seconds of sonication, acid siphon, and rinse with ultrapure water, respectively. The sample solution was transferred for a new acid-washed vial for the dissolution (digestion) step. For this, a 500 µl of 0.05N HNO_3 was added to each sample and placed in a sonicator for about one hour or the time required for the complete dissolution of the sample. After the final dissolution, the sample was centrifuged for 10 minutes at 11.000 rpm and transfer for acid washed 5 ml analysis vial.

The Ca concentration of the cleaned sample was analyzed before the final dilution and DCP analysis, seeking the establishment of a standard Ca concentration of approximately 30 ppm for each sample. For Ca concentration evaluation, 25 µl of cleaned sample solution was transferred to a new 5 ml analysis vial, diluted in 1.5 ml of 0.05N HNO_3, and analyzed. The results are used to calculate the final dilution of the samples and the volume needed to make 4.5 ml of the final sample solution that reaches the desired target of Ca concentration. The samples were analyzed by a direct current plasma atomic emission spectrometer Spectraspan 7, in the Earth and Ocean Sciences Division of the Duke University. Analytical precision on internal standards throughout this study was <0.75%. A total of ten whole sample replicates for each size fraction were performed and yielded a mean of Mg/Ca concentration with relative standard deviation (RSD) of 2.17% from size fraction 250-350 µm, suggesting that digenetic alternation and detrital contamination are minimal.

For Mg/Ca derived temperature calibrations we applied the Dekens et al. (2002) equation for specie *G. ruber,* based on core-tops samples from the Ceara Rise:

$$Mg/Ca=0.38\ exp(0.09*T) \quad (2)$$

Where T is in °C and Mg/Ca is a mole ratio. The SST reconstruction presented a correlation (P>95%; Figure S2) of R^2= 0.997, and a standard error of an estimate is 1.2°C, 95% confidence interval for the preexponential constant is ±0.05, and 95% confidence interval for the exponential constant is ±0.015 (Dekens et al., 2002). Other equatorial Atlantic calibrations for *G. ruber* (white) presented similar pre-exponential and exponential constants (e.g. Kısakürek et al., 2008; Regenberg et al., 2009).

1.1. Seawater oxygen stable isotope record ($\delta^{18}O_{SW}$) and ice volume correction

To reconstruct the patterns of freshwater discharge over the area, we applied the Mg/Ca derived temperature (°C) to estimate the ancient seawater $\delta^{18}O$ ($\delta^{18}O_{SW}$), using the temperature and $\delta^{18}O$ relation from Bemis et al. (1998), which applied to *G. ruber* (Thunell et al., 1999):

$$SST=14.9-4.8(\delta^{18}O_{Ca}-\delta^{18}O_{SW}) \quad (3)$$

Where SST is at °C and $\delta^{18}O_{Ca}$ is $\delta^{18}O$ of the *G. ruber* white. The $\delta^{18}O_{SW}$ is reported in per mil relative to the Vienna Standard Mean Ocean Water (VSMOW) by adding 0.27‰ from the calculated $\delta^{18}O_{SW}$ (Bemis et al., 1998). We correct the ice-volume using the sea level estimates of Elderfield et al. (2012), and a linear conversion from the relative sea-level of 0.012‰/m sea-level fall, by assuming linear sequestration of $\delta^{16}O$ by continental ice sheets through the time (Shackleton, 1987).

$$\delta^{18}O_{SW\text{-}IVC} = \delta^{18}O_{SW}-(ESL*0.012) \quad (4)$$

Where $\delta^{18}O_{SW\text{-}IVC}$ is the seawater oxygen isotopic values corrected for ice volume changes and ESL is the estimated sea level difference in meters. The $\delta^{18}O_{SW\text{-}IVC}$ is a first-order approximation of SSS. For the reconstruction of the SSS, we applied the relationship presented by Weldeab et al. (2006). The estimated uncertainty of $\delta^{18}O_{SW\text{-}IVC}$ values was calculated taking into account the (i) standard error of the Mg/Ca-SST calibration (±1.2°C that corresponds to

~0.2‰; Dekens et al., 2002), and (ii) analytical error in the oxygen isotope (~0.07‰) analyses, resulting in cumulative error estimation of $\delta^{18}O_{SW}$ of ±0.27‰. This is close to the error estimation of $\delta^{18}O_{SW}$ (±0.22‰) reported by Schimidt et al. (2004), and ±0.25‰ reported by Weldeab et al. (2006). The uncertainties typically result in a 1σ error of about 0.3 -0.4 ‰ for d18Osw-ivc (Schmidt, 1999; Mohtadi et al., 2014).

4. Results

4.1. Chapter 1: Biochronostratigraphy of the western equatorial Atlantic for the last 1.93 Ma

Biochronostratigraphy of the western equatorial Atlantic for the last 1.93 Ma

Fabricio Ferreira[1,2]; Cleverson G. Silva[2]; Allan S.Oliveira[2]; Cristiano M. Chiessi[3]; Andrea K. Kern[4]; Paul A. Baker[5], Gary Dwyer[5]; Catherine A. Rigsby[6]; Enqing Huang[7]; Jun Tian[7]

[1]Postgraduate Program in Ocean and Earth Dynamics, Institute of Geosciences, Universidade Federal Fluminense, Av. Gal. Milton Tavares de Souza s/n, CEP: 24210-346 Niterói RJ, Brazil – *ferreira_paleo@hotmail.com*

[2]Marine Geology Laboratory (LAGEMAR), Institute of Geosciences, Universidade Federal Fluminense, Av. Gal. Milton Tavares de Souza s/n, CEP: 24210-346 Niterói RJ, Brazil

[3]School of Arts, Sciences and Humanities, University of São Paulo, Av. ArlindoBettio 1000, CEP: 03828-000 São Paulo SP, Brazil

[4]Department of Sedimentary and Environmental Geology, Institute of Geosciences, University of São Paulo, Rua do Lago 562, CEP: 05508-080 São Paulo SP, Brazil

[5]Division of Earth and Ocean Sciences, Duke University, NC 27708 Durham, USA

[6]Department of Geological Sciences, East Carolina University, NC 27858-4353Greenville, USA

[7]State Key Laboratory of Marine Geology, Tongji University, 1239 Siping Road, 200092 Shanghai, China

Abstract

Planktonic foraminiferas are an important biochronostratigraphic tool and one of the main proxies used in paleoceanographic studies. Here we present the integration of quantitative analyses of planktonic foraminifera biostratigraphy, planktonic and benthic foraminifera oxygen isotopic data, and planktonic foraminifera radiocarbon ages in a biochronostratigraphic framework for the last 1.93 Ma of the western equatorial Atlantic. The ages of the biostratigraphic events derived from our records are consistent with previous works except for the highest occurrences of *Globigerinoides fistulosus* (~1.82 Ma; MIS 66), *Globoturborotalia obliquus* (~1.48 Ma; MIS 49), and *Globorotalia tosaensis* (~1.05 Ma; MIS 31). The largest age difference (~460 kyr) was found for the highest occurrence of *G. tosaensis*. In addition, we describe for the first time in the equatorial and western South Atlantic the oldest Pleistocene *Globorotalia menardii* disappearance (D) and reappearance (R) events D5 (~1.79 Ma; MIS 64), R5 (~1.68 Ma; MIS 60), D4 (~1.05 Ma; MIS 30) and R4 (~0.96 Ma; MIS 26). Our records present a consistent difference in the ages of *G. menardii* D and R events compared to the North and South Atlantic. While the onset of D events occurs initially at high latitudes and later in the

equatorial region, the timing of R events exhibit the opposite trend. The oscillations in abundance of the complexes *Pulleniatina* and *Globorotalia crassaformis* together with the species *Globorotalia truncatulinoides* and *Globoconella inflata* allowed the subdivision of the last 1.93 Ma into 20 subzones, substantially improving the biochronostratigraphic resolution for the western equatorial Atlantic.

Keywords:
Planktonic foraminifera; biostratigraphy; equatorial western Atlantic; Brazilian Equatorial Margin; Pará-Maranhão Basin.

1. Introduction

Robust stratigraphic correlations within and between different oceanic basins are essential to deciphering the evolution of various components of the Earth system (Wade et al., 2011). Due to their high sensitivity to environmental conditions, high morphological diversity, global distributions, rapid evolution throughout the Mesozoic and Cenozoic, and high preservation potential, planktonic foraminifera are ideal biostratigraphic index fossils (Wade et al., 2011). Throughout the Cenozoic, planktonic foraminifera was an abundant and diverse microfossil group in the tropics and subtropics, and the evolutionary events of this group are used to set biozone boundaries, allowing the construction of detailed zonal schemes for the last 65 Ma (Blow, 1969; Bolli and Premoli Silva, 1973; Kennett and Srinivasan, 1983; Bolli and Saunders, 1985; Wade et al., 2011).

In addition to few first and last occurrence of planktonic foraminifera species (ten new appearances and seven disappearances of taxons; Wade et al., 2011) described for the Quaternary (last 2.58 Ma, Gibbard et al., 2010), glacial/interglacial climatic oscillations caused significant expansions and contractions in the geographic distribution of certain assemblages and/or species due to migration events with non-evolutionary characteristics (Kennett and Huddlestun, 1972; Bé et al., 1976; Thunnel, 1984; Caley et al., 2012). These changes in the relative abundance of assemblages and/or species of planktonic foraminifera themselves can provide an increased resolution of stratigraphic zoning during the Quaternary (Ericson and Wollin, 1968; Kennett and Huddlestun, 1972; Martin et al., 1993; Kohl et al., 2004; Ferreira et al., 2012; Toledo et al., 2016).

Yet, Quaternary biochronostratigraphical studies are scarce in the western equatorial Atlantic (e.g., Chaisson and Pearson, 1997), despite the great relevance of the region as an archive of climate variability of tropical South America (Arz et al., 1998; Nace et al., 2014;

Zhang et al., 2017; Crivellari et al., 2018). Here, we present the integration of quantitative analyses of planktonic foraminifera biostratigraphy, calibrated with planktonic and benthic foraminifera oxygen isotopic records and radiocarbon ages for the last 1.93 Ma in a core with an average accumulation rate around 3.35 cm/kyr.

2. Study Area

The modern surface ocean circulation in the western equatorial Atlantic is dominated by the North Brazil Current (NBC) and the North Equatorial Countercurrent. The NBC results from the bifurcation of the South Equatorial Current at 10-15°S. The NBC flows northwestwards along the continental margin of northeastern Brazil (Figure 1; Peterson and Stramma, 1991; Schott et al., 1995; Stramma et al., 1995). The southward flowing Brazil Current also originates at the bifurcation and subsequently moves southward along the continental margin of eastern Brazil. With its large anticyclonic rings, the NBC is the main pathway for the cross-equatorial transport of warm and salty surface waters that balances the southward export of North Atlantic Deep Water (Johns et al., 1998; Goni and Johns, 2001; Haarsma et al., 2011). The NBC extends from the surface to intermediate water depths (approximately 800 m water depth) where it merges with northward advected Antarctic Intermediate Water (Talley et al., 2011). In the region of core CDH-79, long-term annual mean sea surface temperature is 27.5°C (between 27.3°C and 28.2°C) (Locarnini et al., 2018), while sea surface salinity is 35.7 (varying widely between 28.2 and 36.2) (Zweng et al., 2018).

The NBC transport is highly variable, with maximum and minimum measured transport of approximately 36 Sv during the austral winter and 13 Sv during the austral fall (Johns et al., 1998). This variability in NBC transport is associated with the north-south migration of the Intertropical Convergence Zone and with changes in wind stress curl (Richardson et al., 1994; Talley et al., 2011). Between July and February, the NBC detaches from the continental margin at approximately 8°N feeding the North Equatorial Countercurrent in a process known as the NBC retroflection (Fonseca et al., 2004). Between March and June, the NBC flow continues farther northwestward along the continental slope of South America, entering the Caribbean Sea and eventually feeding the Gulf Stream (Johns et al., 1998; Lux et al., 2001).

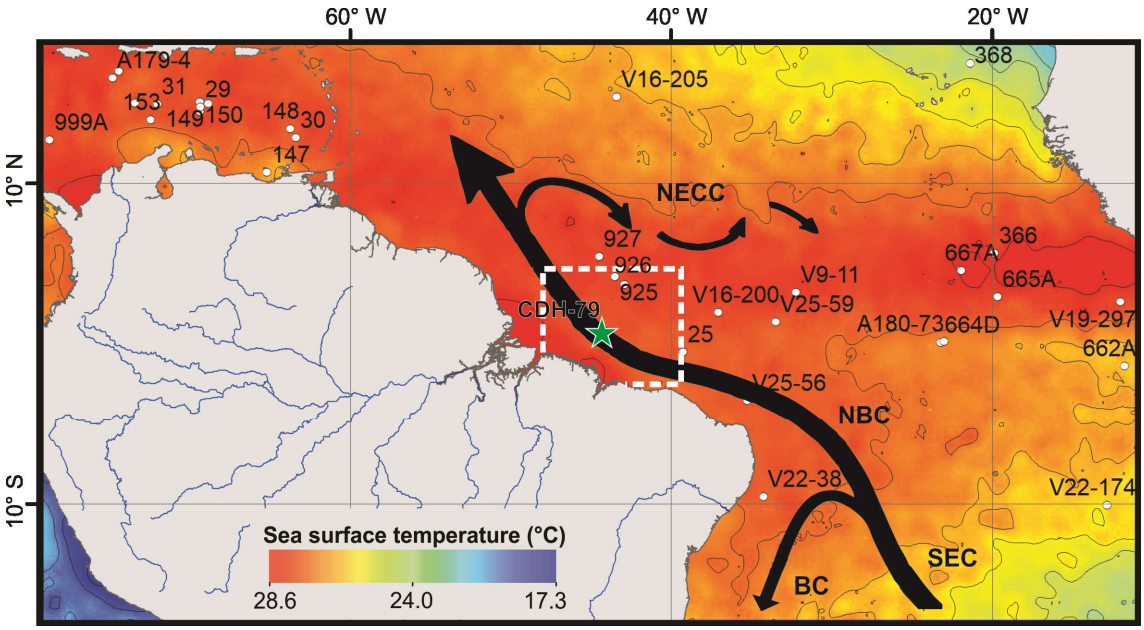

Figure 1. Location of marine sediment core CDH-79 (green star) with long-term mean annual sea surface temperature (color scale) (Locarnini et al., 2018) and surface ocean currents of interest for this study (black arrows). The white dashed rectangle indicates the area used to estimate the long term mean sea surface temperature for the study area. The black circles represent sites discussed in the text (see Table S1 and Figure S1 for details). BC - Brazil Current; NBC - North Brazil Current; NECC - North Equatorial Countercurrent; SEC - South Equatorial Current (Peterson and Stramma, 1991).

The NBC transport variability is also observed on different timescales and correlates positively with the strength of Atlantic meridional overturning circulation (AMOC) on decadal timescale (Zhang et al., 2011). On millennial timescales, decreases in NBC strength coincided with northern Hemisphere cold events like the Heinrich stadials and the Younger Dryas (Arz et al., 1999; Wilson et al., 2011; Nace et al., 2014; Zhang et al., 2015).

3. Material and Methods

We investigated core CDH-79 (00° 39.6853' N, 44° 20.7723' W; 32.12 m core length; 2345 m water depth; Figure 1), retrieved during RV Knorr cruise KNR 197-4 in February 2010. The coring site is located on the top of a seamount in the western equatorial Atlantic (Pará-Maranhão Basin), 320 km from the modern coastline of northeastern Brazil. Core CDH-79 was shipped to Woods Hole Oceanographic Institution for storage at 4°C. The working halves of the split cores were visually described and sampled (10 cm^3) every 10 cm for a total of 322 samples.

3.1. Preparation of planktonic foraminifera

The unlithified sediment samples were washed through a sieve of 62 µm mesh size (retaining the coarse fraction) and dried at 50°C (Leipnitz et al., 2005). Dry residues were weighed and stored in glass vials. Planktonic foraminifera were dry picked from the >150 µm fraction in subsample splits (if necessary) containing 300 – 600 specimens. This results in a 95% level of confidence for species with at least 1% of abundance (Patterson and Fishbein, 1989). The subsamples were stored in micropaleontological slides and all specimens were identified and counted. The specimen preservation was qualitatively estimated and the Le and Shackleton (1992) fragmentation index (FRAG) was calculated for each sample. The taxonomic concepts for Neogene taxa were adopted from Stainforth et al. (1975), Kennett and Srinivasan (1983), and Bolli and Saunders (1985) and revised based on Hayward et al. (2019). The taxonomic terms that were utilized are available in Table S2.

3.2. Planktonic foraminifera biostratigraphy

Only species significant for Quaternary biostratigraphy were considered for the construction of the biostratigraphic framework (e.g., Ericson and Wollin, 1968; Berggren et al., 1985a, 1995a, 1995b; Wade et al. 2011*;* Toledo et al., 2016). The biostratigraphic zonal scheme for the Neogene followed Blow (1969), modified by Kennett and Srinivasan (1983). The Quaternary biostratigraphic zonal scheme followed Bolli and Premili Silva (1973), with the modifications from Bolli and Saunders (1985), Berggren et al. (1995a; 1995b) and the revision of the Cenozoic tropical biostratigraphy presented by Wade et al. (2011). The nomenclature adopted for evolutionary events, new appearance, and disappearance of the taxon, follow Wade et al. (2011), where lowest occurrence (LO) is used with the same meaning as first appearance datum and/or first occurrence. Similarly, the highest occurrence (HO) is used with the same meaning as the last appearance datum and/or the last occurrence. Following Wade et al. (2011), we also applied the letter B (base) in the same meaning of LO, and T (top) in the same meaning of (HO).

In addition, the *Globorotalia menardii* complex abundance events (*G. menardii* zonation) from Ericson and Wollin (1968) were employed and referred to as EW68 zones/subzones. *G. menardii* complex refers to the assemblage which combines *G. menardii* spp., *Globorotalia tumida,* and *Globorotalia flexuosa* without distinction between the different morphotypes or subspecies. The same nomenclature was applied for *Globorotalia crassaformis* (*G. crassaformis*, *G. crassaformis hessi*, *G. crassaformis ronda*, *G. crassaformis viola,* and *G.*

crassaformis imbricata) and the *Pulleniatina* (*P. obliquiloculata* and *P. primalis*) genera. However, when the abundance of *G. flexuosa*, *G. crassaformis imbricata*, *G. crassaformis hessi,* and *G. crassaformis viola* are considered, their individual relative abundance, rather than those of the complexes are presented. The EW68 zonation is extensively used in biostratigraphic, paleoclimatic and paleoceanographic studies in tropical (e.g., Martin et al., 1990, 1993; Kohl et al., 2004) and subtropical areas (e.g., Vicalvi, 1997; Ferreira et al., 2012, 2014; Portilho-Ramos et al., 2014; Toledo et al., 2016), providing a more detailed biostratigraphic zonation for the Quaternary. For this study, the virtual disappearance of the *G. menardii* complex is defined when its relative abundance drops to <1%. Following Toledo et al. (2016), the disappearance events were numbered top-down by *G. menardii* D1, D2, D3, D4, and D5, and were respectively associated with the base of the EW68 zones Y, W, U, S, and Q. The reappearance events were numbered top-down by *G. menardii* R2, R3, R4, and R5 and were respectively associated with the base of EW68 zones X, V, T, and R.

3.3. Stable oxygen isotopic analyses and radiocarbon dating

Five specimens of the planktonic foraminifer *Globigerinoides ruber* (white) within the size fraction 250-350 μm, and at least two specimens of the benthic foraminifer *Uvigerina peregrine* and *Cibicidoides wuellerstorfi* within the size fraction >125 μm were hand-picked for stable oxygen isotopic analyses ($\delta^{18}O$). The tests of planktonic foraminifera were soaked in 15% H_2O_2 for 30 min to remove organic matter, and then rinsed with methanol and ultra-sonically cleaned to remove fine-grained particles. The methanol was removed with a syringe, and samples were dried at 50°C for 24h. The clean foraminifera tests were crushed, and between 20 to 60 mg of calcite was loaded into glass reaction vessels. Benthic foraminifera crushed tests were rinsed with alcohol, dried, and directly loaded into glass reaction vessels. Both planktonic and benthic foraminifera were reacted with three drops of H_3PO_4 (specific gravity = 1.92) using a Finnigan MAT Kiel III carbonate preparation device. Isotope ratios were measured by a Finnigan MAT 252 mass spectrometer. The standard deviation of the international standard NBS19 is <0.07‰ during the measurement periods. Planktonic foraminifera were analyzed at the Light Stable Isotope Mass Spectrometer Laboratory, Department of Geological Sciences, University of Florida USA. Benthic foraminifera were analyzed at the State Key Laboratory of Marine Geology, Tongji University, China. The results of benthic foraminifera were corrected following Machitto et al. (2014).

Five samples composed of mixed well-preserved specimens of planktonic foraminifera from the size range 250-350 μm were used for radiocarbon (^{14}C) dating (Table 1). The samples

were hand-picked and analyzed by accelerator mass spectrometry (AMS) at the National Ocean Sciences Accelerators Mass Spectrometry - USA. The radiocarbon ages were calibrated with the software PaleoDataView version 0.9.2 (Langner and Mulitza, 2019) using the IntCal13 calibration curve (Reimer et al., 2013) and a variable reservoir effect (Butzin et al., 2017).

Table 1. Raw ^{14}C AMS data and calibrated ages for core CDH-79.

Depth (cm)	Lab ID	Radiocarbon age (yr BP)	Age error (yr)	Reservoir age (yr)	Reservoir age error (yr)	Calibrated age median [95%] (cal a BP)	Calibrated age min [95%] (cal a BP)	Calibrated age max [95%] (cal a BP)
10	OS122410	13900	290	559	55	16054	15225	16942
20	OS122411	17950	510	675	46	20930	19738	22202
30	OS122412	22800	940	781	62	26347	24438	28115
40	OS122413	22900	960	793	63	26437	24506	28272
50	OS122414	25700	1400	740	92	29355	26973	32361

The chronology adopted for this study follows Gibbard et al. (2009) and Gibbard and Head (2010), where the base of the Quaternary Period, that coincides with the base of the Pleistocene Epoch, has an estimated age of 2.58 Ma. The Pleistocene Epoch is divided into the Gelasian (2.58–1.80 Ma), Calabrian (1.80 – 0.781 Ma), Middle Pleistocene (0.781–0.126 Ma) and Late Pleistocene (0.126–0.012 Ma) (Cohen and Gibbard, 2019).

4. RESULTS

4.1. Stable oxygen isotopes

The planktonic foraminifera $\delta^{18}O$ values range between -1.64 and 0.38‰ with a maximum amplitude of ~2.02‰ (310 samples; 3210-10 cm core depth; Figure S2). Lower variability was found near the base of the core (3210 - 2330 cm core depth), with values oscillating between -1.63 and-0.46‰ (average amplitude of -1.03‰; Figure S2). Above this interval, from 2310 to 1240 cm core depth, the record shows the highest average values -0.63‰, oscillating between-1.41 and 0.38‰, with average amplitudeof~1.79‰. The depth interval 1240-1228 cm showed the highest change between two adjacent samples 2‰ (from 0.38 to -1.62‰; Figure S2). In the uppermost depth interval 1228-10 cm core depth, the $\delta^{18}O$

values oscillate between-1.64 and 0.02‰ (average amplitude ~1.66‰ and an average value of -0.74‰).

The benthic foraminifera $\delta^{18}O$ record varies from2.70 to 4.63‰ (average 3.74‰), with a maximum amplitude of ~1.93‰ (288 samples; 3210 - 40 cm core depth; Figure S2). The lowest variability (amplitude average of ~1.27‰) was found in the base of core (3210 - 2330 cm), with values oscillating between 2.93 and 4.20‰ (mean value of 3.64‰; Figure S2). Above this interval, from 2310 to 1236 cm core depth, the record shows average values of 3.81‰ (ranging from 2.70 to 4.63‰), with an average amplitude of ~1.93‰. In the uppermost depth interval, 1228 - 40 cm core depth, the $\delta^{18}O$ values oscillate between 2.85 to 4.52‰ (average amplitude~1.67‰ and the average value of 3.87‰).

4.2. Chronology and age model

The age model for core CDH-79 is based on five calibrated AMS ^{14}C ages (Table 1) and 118 $\delta^{18}O$ tie-points (Table S3). The tie-points were derived from the alignment of our $\delta^{18}O$ records to the reference $\delta^{18}O$ stack LR04 (Lisiecki and Raymo, 2005). According to Govin et al. (2015), we estimated the age uncertainty for each tie-point (Table S3) by taking into account (i) the mean resolution and dating uncertainty of the reference curve LR04 (resolution 1 kyr; uncertainty 6 kyr from 2 - 1 Ma and 4 kyr from 1 - 0 Ma; Lisiecki and Raymo, 2005), and (ii) an estimated relative alignment uncertainty (~1.04 kyr).

The age model and associated uncertainties were calculated by using the BACON algorithm version 2.2 (Blaauw and Christen, 2011) within the PaleoDataView software version 0.9.2 (Langner and Mulitza, 2019). A total of 10,000 age depth realizations have been used to calculate the median age and the 2σ uncertainty at 1 cm resolution for the interval 10-50 cm core depth (Figure 2b), and 5 cm resolution for the interval 60 - 3212 cm (Figure 2a). We assume the presence of a depositional unconformity (hiatus) between 50 - 60 cm, as discussed in section 4.4.

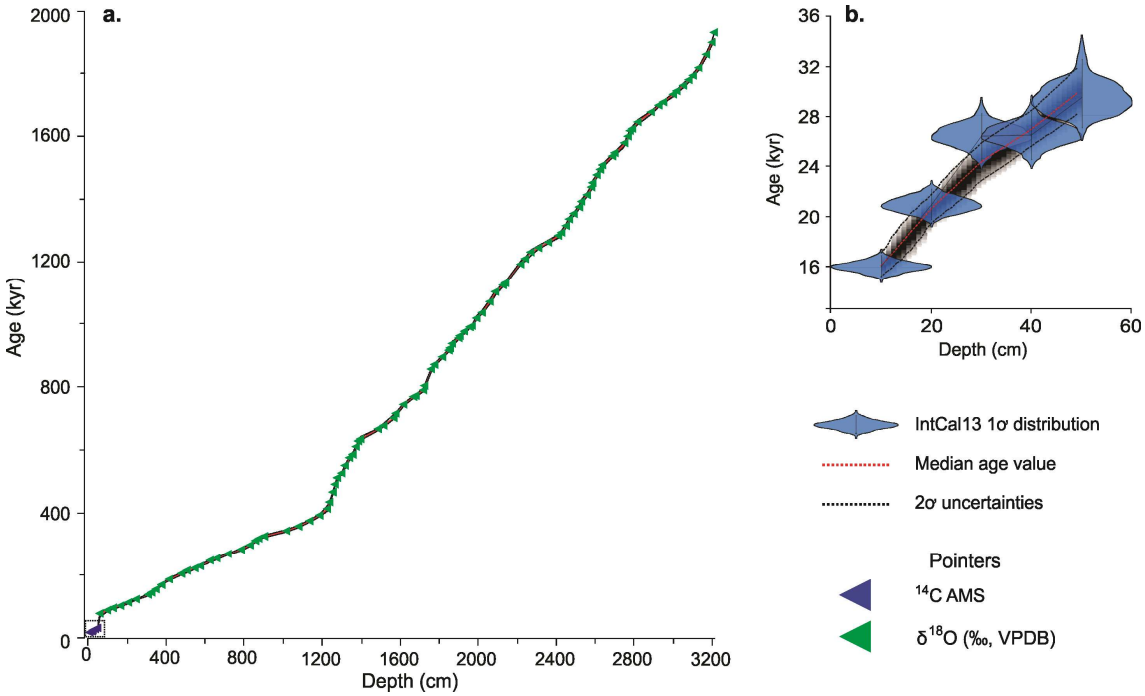

Figure 2. Age model of core CDH-79 based on calibrated AMS ^{14}C ages (blue triangles) and tie-points (green triangles) based on the alignment of our stable oxygen isotopic ($\delta^{18}O$) records to the reference $\delta^{18}O$ stack LR04 (Lisiecki and Raymo, 2005). Black dotted lines indicate the uncertainty of the median age (solid red line) at (a.) 5 cm, and (b.) 1 cm resolution. Note that between 50 - 60 cm core depth, there is a hiatus.

The biochronostatrigraphic model built for core CDH-79 indicates an average accumulation rate of 3.35 cm/kyr, showing a good correlation with the LR04 stack (Lisiecki and Raymo, 2005) and the revised isotopic stratigraphies of ODP Leg 154 (Ceara Rise - Sites 925, 927, and benthic smooth; Wilkens et al, 2017), and ODP Site 806b (equatorial Pacific; de Garidel-Thoron et al., 2005) (Figure 3). CDH-79 reaches an estimated age of 1.93 Ma at the base (i.e., 3212 cm core depth) of the core and records marine isotopes stages (MIS) 1 - 73, thus continuously covering most of the Quaternary (Figure 3).

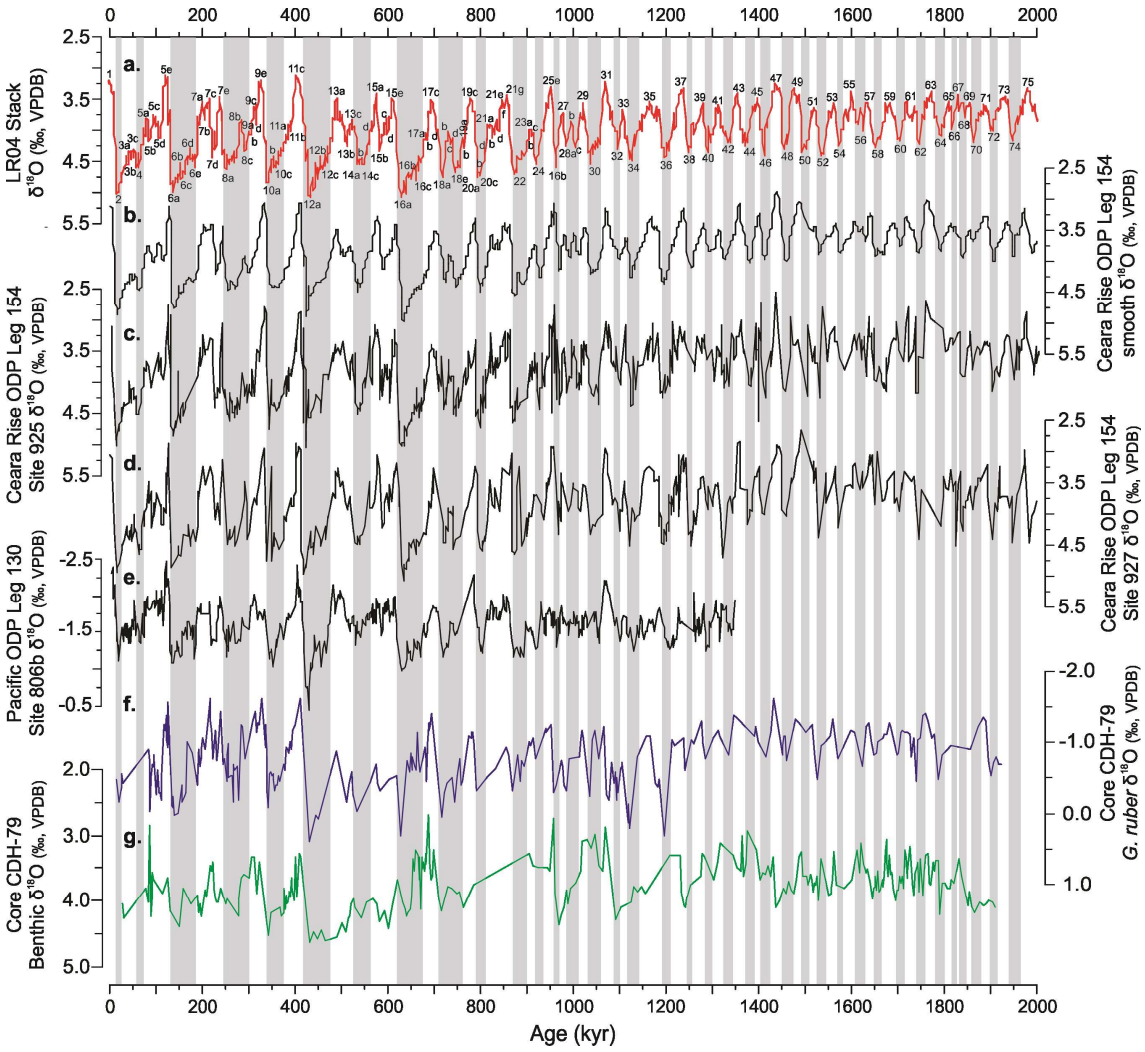

Figure 3. Stable oxygen isotopic ($\delta^{18}O$) records from (a.) LR04 stack (Lisiecki and Raymo, 2005); revised isotope stratigraphy of Ceara Rise ODP Leg 154 (b.) smooth; (c.) Site 925; (d.) Site 927 (Wilkens et al., 2017); (e) equatorial Pacific ODP Leg 130 - Site 806b (de Garidel-Thoron et al., 2005); and western equatorial Atlantic core CDH-79 (f.) *Globigerinoides ruber* (white); (g.) benthic foraminifera (this study). Marine isotopic stages according to the LR04 stack (Lisiecki and Raymo, 2005), and substages according to Railsback et al. (2015).

4.3. Planktonic foraminifera and biostratigraphy

A total of 111,749 foraminifera (planktonic and benthic forms) were recovered, of which 99.24% (110,913 specimens) are planktonic forms. In general, the foraminifera presented an excellent state of preservation, which allowed the classification at the species level. Among the 24 recovered species (a taxonomic list is presented at Table S2), 14 can be used for the biostratigraphic approach, resulting in the recognition of 17 biostratigraphic events (see details in the supplementary material section Text S1) in the Quaternary of the

Pará-Maranhão Basin (Table 2). The events range from the Gelasian to the Late Pleistocene, with estimated ages of ~1.93 and 0.016 Ma (MIS 73 and MIS 2, respectively).

Table 2. Quaternary planktonic foraminifera events calibrated ages and marine isotopic stages (MIS) for core CDH-79 and references.

Bioevents (Datum)	Depth (cm)	CDH-79 Age (interval) (Ma)	MIS	Age - Referecens (Ma)	MIS	Location	References
				2.58		South Pacific	Srinivasan and Sinha (1992)
B *Globorotalia truncatulinoides*				1.93		Ceara Rise	Chaisson and Pearson (1997); Lourens et al. (2004)
				1.93		Revision	Wade et al. (2011)
	3200	**1.90** (1.89-1.91)	**72**			**Pará-Maranhão Basin**	**This work**
				1.77		Panama Basin	Shackleton et al, 1990
T *Globigerinoides fistulosus*				1.88		Ceara Rise	Chaisson and Pearson (1997); Lourens et al. (2004)
	3130	**1.82** (1.81-1.82)	**66**			**Pará-Maranhão Basin**	**This work**
Globorotalia menardii **D5** Base of EW68 Zone **Q**				1.80		Gulf of Mexico	Martin et al. (1990, 1993)
	3092	**1.79** (1.78-1.79)	**64**			**Pará-Maranhão Basin**	**This work**
				1.99		Revision	Wade et al. (2011)
				1.98		Ceara Rise	Chaisson and Pearson (1997); Lourens et al. (2004)
T *Globigerinoides extremus*				0.78-1.8		Lau Basin and Tonga Platform	Chaproniere et al. (1994)
				1.77		Revision	Berggren et al. (1985b); Berggren et al. (1995b)
	3070	**1.77** (1.77-1.78)	**63**			**Pará-Maranhão Basin**	**This work**
Globorotalia menardii **R5** Base of EW68 Zone **R**				1.50		Gulf of Mexico	Martin et al. (1990, 1993)
	2890	**1.68** (1.67-1.68)	**59**			**Pará-Maranhão Basin**	**This work**
				1.30		Ceara Rise	Chaisson and Pearson (1997); Lourens et al. (2004)
T *Globoturborotalia obliquus*				1.30		Revision	Wade et al. (2011)
	2610	**1.48** (1.47-1.48)	**49**			**Pará-Maranhão Basin**	**This work**

Table 2. Continued

				0.61			Mix et al. (1995); Lourens et al. (2004)
T *Globorotalia tosaensis*	**2052**	**1.07** (1.06-1.07)	**31**			**Pará-Maranhão Basin**	**This work**
*Globorotalia menardii***D4**				1.20		Gulf of Mexico	Martin et al. (1990, 1993)
Base of EW68 Zone **S**	**2032**	**1.05** (1.04-1.06)	**30**			**Pará-Maranhão Basin**	**This work**
Globorotalia menardii **R4**				1.00	24/25	Gulf of Mexico	Martin et al. (1990, 1993)
				0.99	27/28		Nishi et al. (2000)
Base of EW68 Zone**T**	**1912**	**0.96** (0.96-0.97)	**26**			**Pará-Maranhão Basin**	**This work**
				0.75		Equatorial to Subarctic regions	Bylinskaya (2004)
B *Globorotalia crassaformis hessi*				0.75	17	Lau Basin and Tonga Platform/Revision	Chaproniere et al. (1994)/ Wade et al. (2011)
				0.77		Santos Basin	Toledo et al. (2016)
	1692	**0.78** (0.77-0.78)	**19**			**Pará-Maranhão Basin**	**This work**
				0.62-0.52	16	Gulf of Mexico	Martin et al. (1993)
Globorotalia menardii **D3**				0.61		Gulf of Mexico / Santos Basin	Kohl et al. (2004)/ Ferreira et al. (2012)
Base of EW68 Zone				0.63	16	Santos Basin	Toledo et al. (2016)
U	**1362**	**0.59** (0.58-0.59)	**15**			**Pará-Maranhão Basin**	**This work**
				0.48		Gulf of Mexico / Santos Basin	Kohl et al. (2004)/ Ferreira et al. (2012)
Globorotalia menardii **R3**					13	Caribbean Sea	Matin et al. (1990); Martinez et al. (2007)
Base of EW68 Zone				0.49	13	Santos Basin	Toledo et al. (2016)
V	**1312**	**0.54** (0.53-0.55)	**13/14**			**Pará-Maranhão Basin**	**This work**
				0.10-0.20		Equatorial to Subarctic regions	Bylinskaya (2004)
T *Globorotalia crassaformis hessi*				0.058	4	Santos Basin	Toledo et al. (2016)
	920	**0.33** (0.32-0.33)	**9/10**			**Pará-Maranhão Basin**	**This work**
				0.20-0.18	7	Gulf of Mexico	Martin et al. (1993) / Kohl et al. (2004)
Globorotalia menardii **D2**					7/6	Caribbean Sea	Martin et al. (1990)
Base of EW68 Zone					6	Caribbean Sea	Martinez et al. (2007)
W				0.142	6b	Santos Basin	Toledo et al. (2016)
	352	**0.16** (0.15-0.16)	**8**			**Pará-Maranhão Basin**	**This work**

Table 2. Continued

				4.70		Revision	Kennett and Srinivasan (1983)
				0.220		Pacific Ocean	Chaproniere et al. (1994); Wade et al. (2011)
B *Globigerinella calida calida*				0.140		Equatorial Atlantic	Bolli and Premoli Silva (1973)
				0.135	6a	Santos Basin	Toledo et al. (2016)
	320	**0.14** (0.14-0.15)	**6**			**Pará-Maranhão Basin**	**This work**
				0.13		Gulf of Mexico	Kohl et al. (2004); Martinez et al. (2007)
Globorotalia menardii **R2**				0.12	5	Santos Basin	Toledo et al. (2016)
Base of EW68 Zone **X**				0.12		Campos Basin	Vicalvi (1997)
	290	**0.13** (0.13-0.14)	**5/6**			**Pará-Maranhão Basin**	**This work**
				0.068		Florida Continental slope	Joyce et al. (1990)
				0.084		Santos Basin	Vicalvi (1997), Ferreira et al. (2012)
T *Globorotalia flexuosa*				0.077		Revision	Berrgren et al. (1995a, b)/Wade et al. (2011)
				0.088	5	Santos Basin	Toledo et al. (2016)
	70	**0.085** (0.080-0.085)	**5**			**Pará-Maranhão Basin**	**This work**
				0.090-0.084		Gulf of Mexico	Martin et al. (1993)/ Kohl et al. (2004)
Globorotalia menardii **D1**				0.084		Campos Basin	Vicalvi (1997); Portilho Ramos et al. (2006)
Base of EW68 Zone **Y**				0.084		Santos Basin	Ferreira et al. (2012); Toledo et al. (2016)
	62	**0.077** (0.069-0.083)	**5**			**Pará-Maranhão Basin**	**This work**
G. crassaformis Optimum Event *Gc*OE	**	**	**	0.084-0.071		Campos Basin / Santos Basin	Portilho-Ramos et al. (2014)
HCO *G. crassaformis*	**	**	**	0.082.9	5	Santos Basin	Toledo et al. (2016)
G. crassaformis Transition Event *Gc*TE	**	**	**	0.072	5/4	Santos Basin	Toledo et al. (2016)
LCO *G. crassaformis*	**	**	**	0.068.8	4	Santos Basin	Toledo et al. (2016)
*Globorotalia menardii **R1***	**	**	**	0.012		Gulf of Mexico	Kohl et al. (2004)
*Base of **Z** Zone (EW68)*				0.012		Campos Basin	Vicalvi (1997); Portilho Ramos et al. (2006)
B *Globorotalia fimbriata*						Santos Basin	Ferreira et al. (2012); Toledo et al. (2016)
	**	**	**	11		Equatorial Atlantic	Bolli and Premoli Silva (1973)

The LO of *Globorotalia truncatulinodes* (~1.90 Ma; MIS 73), *G. crassaformis hessi* (~0.78 Ma; MIS 19), and *Globigerinella calida calida* (~0.140 Ma; MIS 6), as well as the HO of

Globigerinoides fistulosus (~1.82 Ma; MIS 66), *Globigerinoides extremus* (~1.77 Ma; MIS 63), *Globigerinoides obliquus* (~1.48 Ma; MIS 49), *Globorotalia tosaensis* (~1.05 Ma; MIS 30/31), and *G. flexuosa* (~0.85 Ma; MIS 5) were used as the main bioevents for the establishment of the biostratigraphy of the area (Table 2; Figure 4a, b). Also, the relative abundance of the complexes of *G. menardii*, *Pulleniatina*, and *Globorotalia crassaformis*), together with the relative abundance of the species *G. truncatulinoides* and *Globoconella inflata*, were used to define the EW68 zones/subzones.

The bioevents include *G. menardii* D5 (3092 cm; MIS 63/64; ~1.79 Ma), R5 (2892 cm; MIS 59; ~1.68 Ma), D4 (2032 cm; MIS 30; ~1.05 Ma), R4 (1912 cm, MIS 26/27, ~0.96 Ma), D3 (1362 cm, MIS 15, ~0.59 Ma), R3 (1310 cm; MIS 13/14; ~0.54 Ma), D2 (352 cm, MIS 6, ~0.16 Ma), R2 (292 cm, MIS 5/6; ~ 0.14 Ma) and D1 (62 cm; MIS 5; ~0.08 Ma) and respectively mark the base of EW68 zones Q, R, S, T, U, V, W , X and Y (Figure 4a, b; Table 2). The oscillations in abundance are controlled by the entire genus *Pulleniatina,* the *G. crassaformis* complex*,* as well as the *G. truncatulinoides* and *G. inflata* species, which allowed the division of recognized zones into 20 subzones (Q2, Q1, R3, R2, R1, S2, S1, T4, T3, T2, T1, V3, V2, V1, W2, W1, X3, X2, X1 e Y1A; Figure 4a, b; Table 3) with a subzonal average resolution of ∼85 kyr. The detailed descriptions of the EW68 zones and subzones are presented in the supplementary materials (see details in the supplementary material section Text S2).

Figure 4a. *Relative abundance of selected planktonic foraminifera species, bioevents and zonal schemes for core CDH-79. Planktonic (blue) and benthic (green) stable oxygen isotopic($\delta^{18}O$) records, and marine isotope stages (MIS; gray and white horizontal bands) are also shown. The red line indicates the position of the identified lowermost hiatus.*

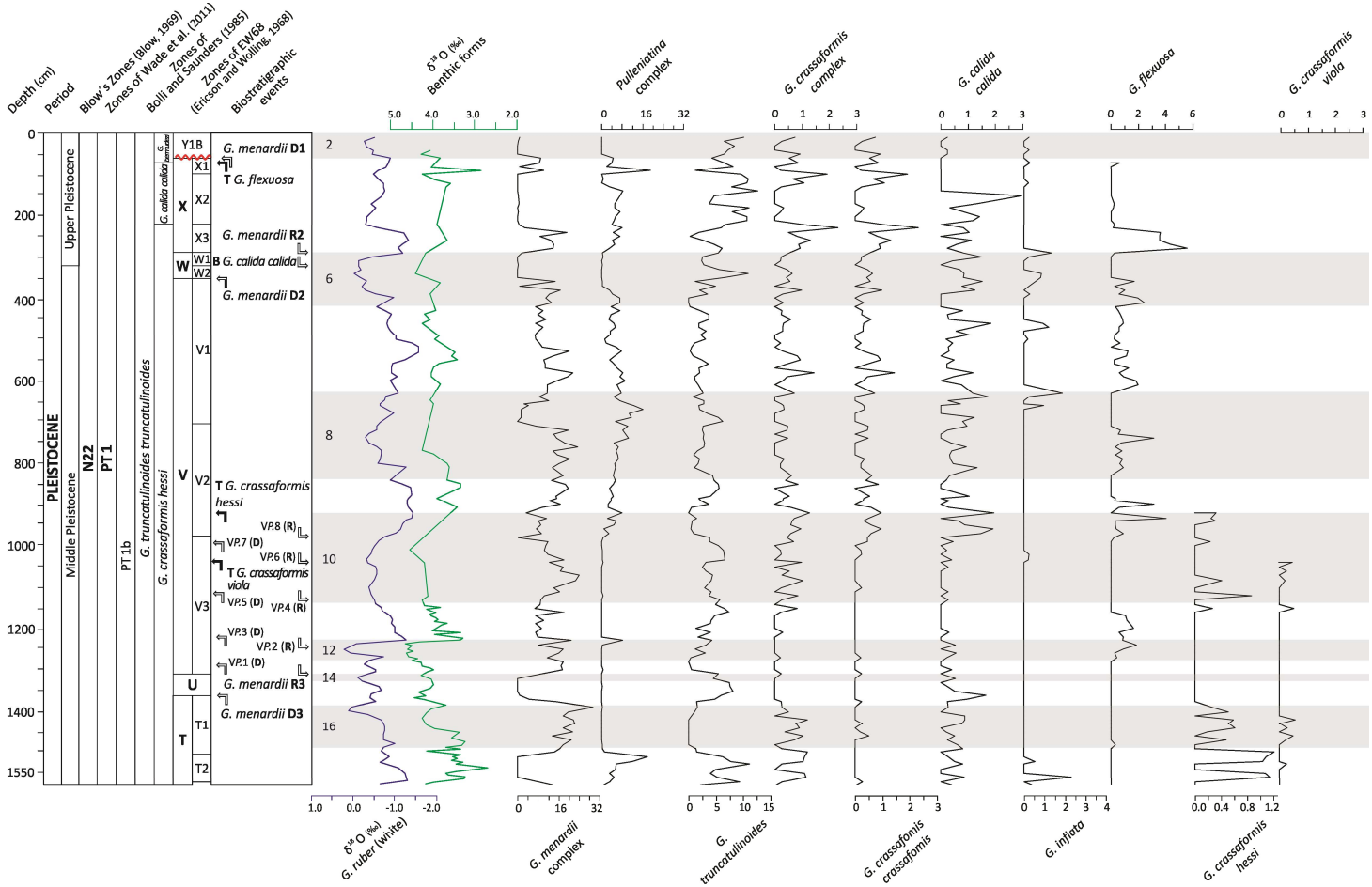

Figure 4b. *Continued.*

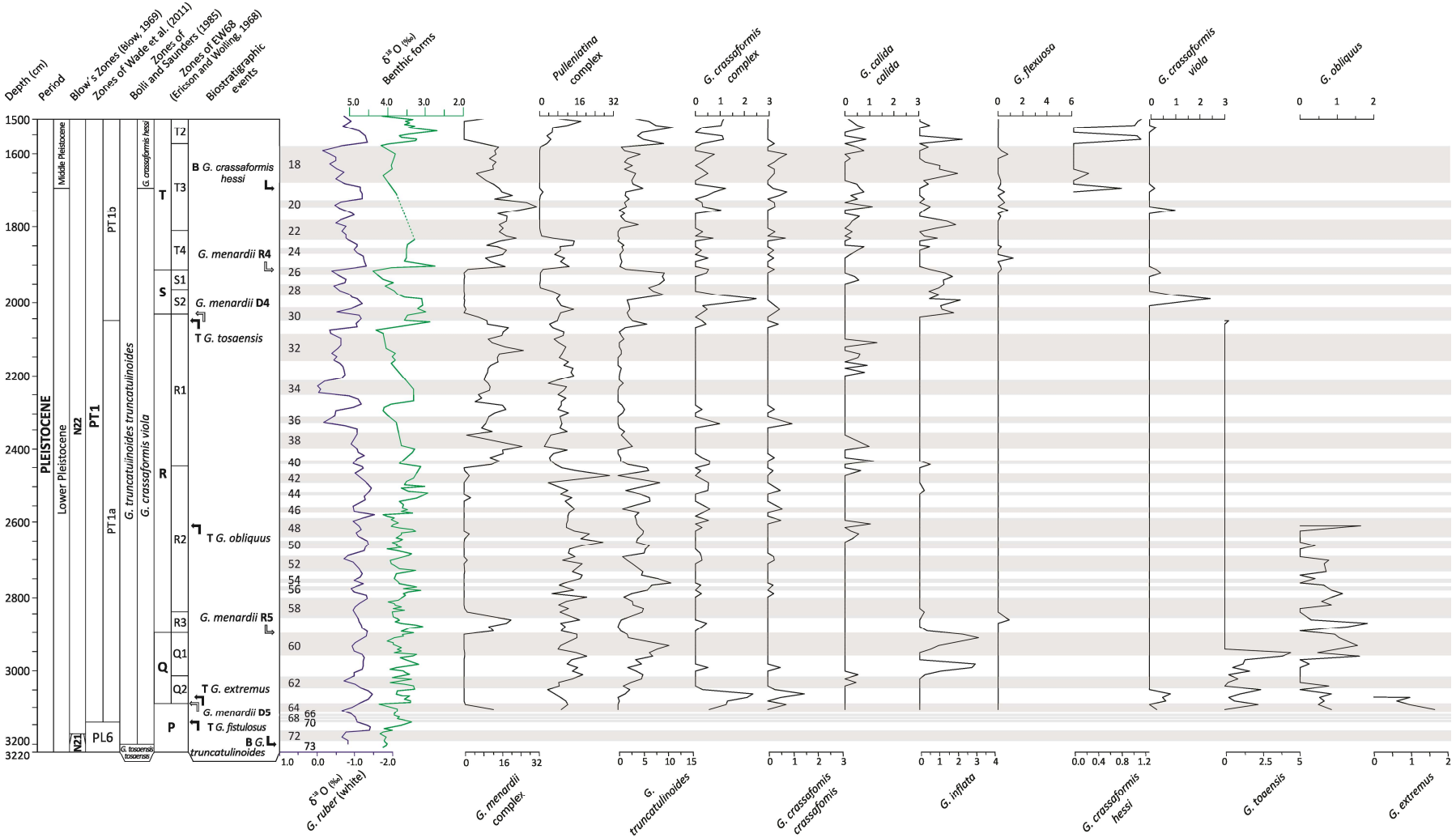

Table 3. Ericson and Wollin (1968) zones and subzones, calibrated ages, marine isotope stages (MIS), and accumulation rate in core CDH-79. The MIS identifications were based on the reference $\delta^{18}O$ stack LR04 (Lisiecki and Raymo, 2005).

EW68		Depth(cm)		Age (Ma)		MIS (LR04)		Accumulation
Zones	/ Subzones	Top	Base	Top	Base	Top	Base	rate (cm/kyr)
Y		10	52	0.02	0.03	2	2	3.18
	X1	60	92	0.08	0.09	5	5	3.28
X	X2	100	222	0.09	0.12	5	5	4.66
	X3	230	292	0.12	0.13	5	5/6	4.11
W	W1	300	322	0.13	0.14	6	6	2.87
	W2	330	352	0.15	0.16	6	6	2.12
	V1	360	702	0.16	0.26	6	8	3.34
V	V2	710	982	0.26	0.34	8	9	3.75
	V3	990	1312	0.34	0.54	9	13/14	1.60
U		1320	1362	0.55	0.59	14	15	1.06
	T1	1370	1500	0.60	0.67	15	16	1.85
T	T2	1510	1562	0.68	0.70	16	17	2.19
	T3	1570	1802	0.70	0.89	17	22	1.27
	T4	1810	1912	0.89	0.96	22	26	1.41
S	S1	1920	1962	0.97	0.99	26/27	28	1.92
	S2	1970	2032	1.00	1.05	28	30	1.18
	R1	2040	2442	1.06	1.31	30/31	41	1.60
R	R2	2450	2832	1.32	1.65	41	58	1.13
	R3	2840	2892	1.66	1.68	58	59	2.41
Q	Q1	2900	3002	1.68	1.74	59	61	1.97
	Q2	3010	3092	1.74	1.79	61	64	1.67
P		3102	3212	1.80	1.93	64	73	0.94

4.4. Unconformity (hiatus)

Based on the combination of the radiocarbon ages, biostratigraphic events, and MIS identification, two unconformities were detected and confirmed by examination of the core lithology. The lower unconformity was recorded within the interval 60-50 cm core depth (Figure 5), above the HO of *G. flexuosa* (~0.085 Ma; 70 cm) and *G. menardii* D1 event (~0.08

Ma; 62 cm), both recorded during MIS 5 within EW68 Zone X (Subzone X1), and below the AMS ^{14}C age (Table 1) obtained at 50 cm core depth (~0.03 Ma; MIS 2; EW68 Zone Y). In the visual core description, a thin bed (~2 cm) of sand was observed within the interval 60-50 cm, while the planktonic foraminifera fragmentation rate showed a slight increase. Thus, we suggest the presence of a stratigraphic unconformity (hiatus) close to the top of core CDH-79. This unconformity spans from the top of MIS 5 (~0.08 Ma based on *G. menardii* D1 event) to the base of MIS 2 (~0.03 Ma based on a calibrated AMS ^{14}C age) and is represented by a no depositional/erosional gap covering MIS 4-3 (approximately 50 kyr).

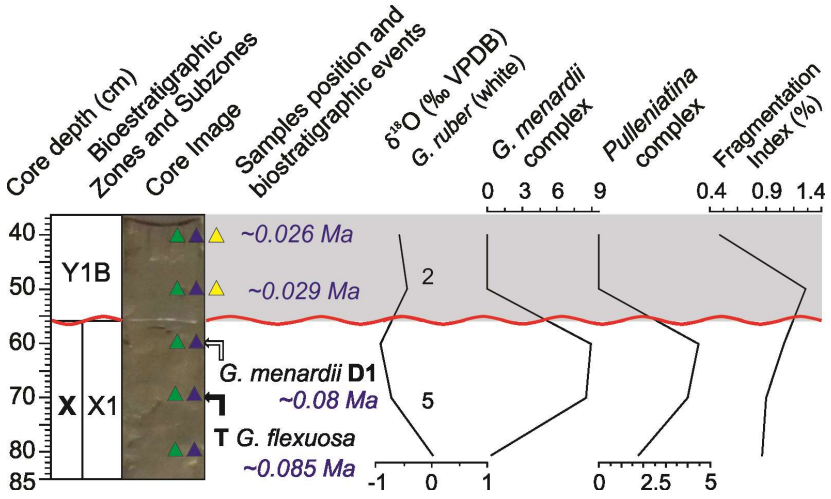

Figure 5: Position of the lower unconformity recorded between 60 and 50 cm of core CDH-79 (red line). From left to right: Ericson and Wollin (1968) zones/subzones; core image and location of samples used for planktonic foraminifera faunal analyses (green triangles), stable oxygen isotopic (δ^{18}O) analysis (blue triangles), AMS ^{14}C analyses (yellow triangles; the blue values denote calibrated AMS ^{14}C ages); Oxygen isotope (δ^{18}O) of *G. ruber* white (‰ VPDB) and marine isotopic stages (MIS); Planktonic foraminifera abundance of *G. menardii* and *Pulleniatina* complexes; and Fragmentation index.

The interval 50-10 cm contains no specimens of the *G. menardii* complex. The *G. menardii* R1 event (~0.012 Ma) of Toledo et al. (2016) represents the return of the *G. menardii* complex to the South Atlantic after a period of absence represented by the EW68 Zone Y. Event R1 records Holocene ages and establishes the base of EW68 Zone Z (Holocene) in the Gulf of Mexico and the tropical Atlantic (e.g., Ericson and Wollin, 1968; Martin et al., 1990, 1993; Kohl et al., 2004), as well as the southeastern Brazilian continental margin (e.g., Vicalvi, 1997; Ferreira et al., 2012; Portilho-Ramos et al., 2014; Toledo et al., 2016). The absence of

specimens from the *G. menardii* complex in the uppermost samples of core CDH-79 suggests the absence of the EW68 Zone Z and therefore sediments of Holocene age. This topmost hiatus is also supported by the only AMS ^{14}C results of CDH-79 obtained from the interval 10-12 cm (~0.016 Ma; Table 1).

5. Discussion

5.1. Biochronostratigraphic zonation of the western equatorial Atlantic for the last 1.93 Ma

Our data allow the establishment of a biochronostratigraphic framework for the longest Quaternary sediment core from the Pará-Maranhão Basin in the western equatorial Atlantic, spanning from the Gelasian (~1.93 Ma; MIS 73) to the Late Pleistocene (~0.016 Ma; MIS 2). The evolutionary events allowed the recognition and chronostratigraphic position of the Neogene zones N21 to N22 from Blow (1969), as well as the Cenozoic Zone PL6 and Zone PT1, and the subzones PT1a and PT1b from Berggren et al. (1995a, 1995b) and Wade et al. (2011). The Bolli and Saunders (1985) zones *G. tosaensis tosaensis* and *G. truncatulinoides truncatulinoides* and the subzones *G. crassaformis viola*, *G. crassaformis hessi*, *G. calida calida*, and *G. bermudezi* were further recorded. Appling the EW68 zonation increased the resolution in our record, with ten zones (from P to Y) and 20 subzones, with the first record and description of the zones P, Q, R, and S for the western equatorial Atlantic.

The described stratigraphic unconformities (hiatus; section 4.4) could have been triggered by at least two processes: (i) major changes in sea level at the EW68 zonal boundary X/Y (from the exceptionally warm interglacial MIS 5 to the succeeding glacial MIS 4) and later to the Last Glacial Maximum (Grant et al., 2012) may have triggered mass transport deposits (Martin et al., 1993); or (ii) piston coring may have disturbed the uppermost soft sediments of the sedimentary column (Stow and Aksu, 1978).

5.1.1. Gelasian - Calabrian (~1.93-0.781 Ma – MIS 73-19)

The occurrence of the *G. menardii* complex at the base of the core (between ~5 to 12%; 3212 - 3102 cm; Figure 4b), followed by the first disappearance event *G. menardii* D5 (~1.79 Ma; MIS 64; Table 2), support the EW68 Zone P as recorded in the Northwest Gulf of Mexico (ODP 625B), Caribbean Sea (DSDP 502B), and Tropical Atlantic (V16-205) by Martin et al. (1990, 1993). Both occurrence and disappearance events are recorded for the first time in the western equatorial Atlantic, and Brazilian basins as well. Within Zone P, two evolutionary events have been used to define zone and subzone boundaries, the LO of *G. truncatulinoides,*

and HO of *G. fistulosus* (B *G. truncatulinoides*, ~1.90 Ma; T *G. fistulosus*, ~1.82 Ma; Table 2). The absence of *G. truncatulinoides* associated with the occurrence of *G. tosaensis* recorded between the base of core CDH-79 and the LO of *G. truncatulinoides* (3200 cm, MIS 72; Table 2) points towards the Neogene Zone N21 of Blow (1969). Bolli and Saunders (1985) associated the upper part of Blow´s Zone N21 with the Zone *G. tosaensis tosaensis* (Bolli and Premoli Silva, 1973), as recorded in core CDH-79. The LO of *G. truncatulinoides* has been used to define the boundary of the Neogene zones N21/N22 (Blow, 1969), and between the Bolli and Saunders (1985) Zone *G. tosaensis tosaensis* and Quaternary Zone *G. truncatulinoides truncatulinoides* as well. The HO of *G. fistulosus* (3130 cm, MIS 66; Table 2) defined the boundary between the basal Zone PL6 – *Globigerinoides fistulosus* Highest-occurrence Zone and Zone PT1 – *Globigerinoides ruber* Partial-range Zone, and the boundary between Zone PL6 and Subzone PT1a - *Globorotalia tosaensis* Highest-occurrence Subzone as well (Berggren et al., 1995a, 1995b; Wade et al., 2011). The evolutionary events place the base of the core in the Neogene Zone N21 (Blow, 1969), and in the Cenozoic Zones PL6 (Berggren et al., 1995a, b; Wade et al., 2011) and *G. tosaensis tosaensis* (Bolli and Saunders, 1985), while the abundance event *G. menardii* D5 position it in EW68 Zone P. Taken together, we place the base of core CDH-79 within the Olduvai Subchron (C2n) supporting an estimated age between 1.90 - 1.93 Ma (median age 1.92 Ma; MIS 73), as indicated by our $\delta^{18}O$ records (Figures 2, 3).

The LO of *G. truncatulinoides* is recorded for the first time in the Pará-Maranhão Basin, and its upward constant presence placed the interval 3200 - 10 cm of core CDH-79 within both zones, Blow (1969) Neogene Zone N22, and Quaternary Zone *G. truncatulinoides truncatulinoides* of Bolli and Saunders (1985). The HO of *G. fistulosus* marks the base of Zone PT1, which extends from the HO of *G. fistulosus* to the Recent, further characterized by the base of Subzone PT1a, which ranges the HO of *G. fistulosus* to the HO of *G. tosaensis*(Berggren et al.,1995a, b; Wade et al., 2011). These events differ slightly in chronostratigraphic position from the ages reported in the literature (e.g., Shackleton et al, 1990; Srinivasan and Sinha, 1992; Table 2). However, in the tropical Atlantic (Site 925; Chaisson and Pearson, 1997) they appeared isochronously (e.g., Lourens et al., 2004; Wade et al., 2011). An exception occurs with the event HO of *G. tosaensis* (usually record above the HO of *G. crassaformis hessi,* Wade et al., 2011), which is located earlier in CDH-79 within MIS 31 (2050 cm; Table 2). This inserts the top of Subzone PT1a, as well as the subzonal boundary PT1b/PT1a, within the Calabrian in the Pará-Maranhão Basin (between 1.06-1.07 Ma).

The evolutionary HO events of *G. extremus* (T *G. extremus* – median age 1.77 Ma; MIS 63) and *G. obliquus* (T *G. obliquus* - 1.48 Ma; MIS 49), are in accordance with a Calabrian age

(older than ~1.40 Ma) for the interval below 2610 cm core depth (Table 2; Figure 4b). The abundance events *G. menardii* R5 (1.78-1.79 Ma, MIS 64), *G. menardii* D4 (1.04-1.06 Ma, MIS 30), and *G. menardii* R4 (0.96-0.97 Ma, MIS 26) mark the base and the first record of EW68 zones R, S, and T, for this area. These *G. menardii* events further support Calabrian ages for the interval 2890 - 1910 cm core depth (Table 2; Figure 4b). The event HO of *G. extremus* can be correlated with the top of the Olduvai Subchron (~1.77 Ma; Lourens et al., 2004; Ogg et al., 2012) in our core, and are considered to be isochronous as previously observed in the southwest Pacific (DSDP Legs 22, 23, 24 and 90) by Srinivasan and Shina (1992) and in the Lau Basin (ODP Leg 135, Sites 834, 835, 837, and 839) and Tongan Platform (ODP Leg 135, Sites 840 and 841) by Chaproniere et al. (1994). The events *G. menardii* R5 and HO *G. obliquus* appear older (around 180 kyr) than previously published (e.g., Martin et al., 1990, 1993; Wade et al., 2011; Table 2), while *G. menardii* D4 (boundary S/R) and *G. menardii* R4 (boundary T/S) present lower records in the Gulf of Mexico (Martin et al., 1990, 1993; Table 2). In our record, however, the *G. menardii* complex events D4 and R4 showed slight differences in both ages, base (MIS 31; ~1.07 Ma) and top (MIS 28; ~0.99 Ma) of Jaramillo Subchron (C1r.1n). Yet, these abundance events can be used to estimate the position of the Subchron in the Brazilian Equatorial Margin, as diachronism presumably is related to the changes in the climatic system of the Mid-Pleistocene Transition (Berger et al., 1993; Berger and Loutre, 1994). The Mid-Pleistocene Transition marks the change from an earlier 41-kyr dominant oscillation to the higher-amplitude100-kyr eccentricity-dominated periodicity present in the Late Pleistocene. These higher amplitude and longer duration glacial/interglacial cycles mark the reorganization of ice sheets and ocean currents around 0.9 Ma (MIS 25-22; Berger et al., 1993; Nishi et al., 2000), which might contribute to higher uncertainties in the transitions of S/R and T/S zones (Caley et al., 2012).

The LO of *G. crassaformis hessi* (0.77-0.78 Ma; Table 2) occurs within the lower $\delta^{18}O$ values of MIS 19 (Subzone T3) and has been used as a marker for the top of Calabrian Subzone *G. crassaformis viola* (Bolli and Premoli Silva, 1973). The occurrence of *G. crassaformis viola* between evolutionary events LO of *G. truncatulinoides* and LO of *G. crassaformis hessi* (Table 2) supports a Gelasian to Calabrian age, spanning from ~1.93 - 0.781 Ma (MIS 73-19) and the Subzone *G. crassaformis viola* to this interval. This event is synchronous to the one recorded by Toledo et al. (2016) in the Santos Basin and is used in our records to define the boundary between the Calabrian and the Middle Pleistocene.

5.1.2. Middle Pleistocene (~0.781-0.126 Ma – MIS19-6)

The Middle Pleistocene is characterized by the Subzone *G. crassaformis hessi* (Bolli and Premoli Silva, 1973) indicated at the base by the LO of *G. crassaformis hessi* (B *G. crassaformis hessi* - 0.78 Ma; MIS 19; Table 2) and at the top by the LO of *G. calida calida* (0.14 - 0.15 Ma; Table 2). This Subzone covers almost the entire Middle Pleistocene. In addition to these zonal marker events, three abundance events of the *G. menardii* complex (D3, R3, and D2) were recorded within this subzone in the Pará-Maranhão Basin, supporting the Middle Pleistocene age estimate (Figure 4a, b; Table 2). The evolutionary event HO of *G. crassaformis hessi* is usually associated with the Subzone *G. calida calida* (Late Pleistocene), however, this event appears to be older in our record, within Subzone V2 in the Middle Pleistocene, showing a wider range in comparison with the tropical Atlantic (0.20 - 0.10 Ma; Bylinskaya, 2005) and southeastern Brazilian continental margin (Cores GL-852 and GL-854; Toledo et al., 2016;).

The event *G. menardii* D3 had been recorded in the Santos Basin around 0.63 Ma (MIS 16; Toledo et al., 2016), while in the Gulf of Mexico it was registered at ~0.61 Ma (Kohl et al., 2004) and between 0.62 - 0.52 Ma (MIS 16 - MIS 15; Martin et al., 1990, 1993) suggesting that this event occurred first in the South Atlantic and later in the North Atlantic. In the Pará-Maranhão Basin, the third disappearance of the *G. menardii* complex (*G. menardii* D3; 0.58 - 0.59 Ma) occurs within a small increase in $\delta^{18}O$ values during MIS 15 (Figure 4a, b). Our records show a younger age than reported in the North and South Atlantic (Table 2), suggesting that the *G. menardii* complex D3 spread from the South and North Atlantic to the equatorial Atlantic. The third reappearance event of *G. menardii* complex (R3), in turn, occurred first in the equatorial Atlantic, spreading later to the southeastern Brazilian continental margin (Toledo et al. 2016), the Caribbean Sea and North Atlantic (Gulf of Mexico; Martin et al. 1993). This is an opposite trend than that of the *G. menardii* D3.

As described by Ferreira et al. (2012) for the southeastern Brazilian continental margin, a set of disappearance and reappearance events of the *Pulleniatina* complex (Table 4) has been recorded in the base of EW68 Zone V (Subzone V3). In general, these events appear to be older in the southeastern Brazilian continental margin (Cores BS-C and BS-D; Santos Basin), spreading later to the equatorial Atlantic (core CDH-79; Pará-Maranhão Basin). An exception is event V*P*.1, which occurs first in the equatorial margin. Prell and Damuth (1978) in the Gulf of Mexico, the Caribbean Sea, and equatorial Atlantic recorded a set of disappearance and reappearance events of the *Pulleniatina* complex, especially from *Pulleniatina obliquiloculata,* during the last 0.175 Ma (EW68 zones V to Z; Middle Pleistocene to Holocene), named as biohorizon Y*P.* Those authors used these events for regional correlation during EW68 Zone Y.

4. Position, ages, and marine isotope stages (MIS) of *Pulleniatina* complex disappearance (D) and reappearance (R) events in the Ericson and Wollin (1968) Zone V (Subzone V3) of core CDH-79, western equatorial Atlantic (text in bold; this study). Events ages from the Santos Basin cores BS-C and BS-D, southeastern Brazilian continental margin (normal text), are from Ferreira et al. (2012).

***Pulleniatina* complex events**	**Zone / Subzone**	**Age (Ma) BS-C**	**BS-D**	**CDH-79**	**MIS CDH-79**	**Depth (cm) CDH-79**
	V2	0.357	0.379			
V*P.*8 **(R)**				**0.337**		
	V3			**(0.332-0.340)**	**9**	**980**
	V3	0.399	0.400			
V*P.* 7 **(D)**				**0.342**		
	V3			**(0.338-0.345)**	**10**	**1010**
	V3	0.410	0.407			
V*P.* 6 **(R)**				**0.348**		
	V3			**(0.344-0.351)**	**10**	**1040**
	V3	0.416	0.428			
V*P.* 5 **(D)**				**0.367**		
	V3			**(0.364-0.372)**	**10**	**1120**
	V3	0.446	0.450			
V*P.* 4 **(R)**				**0.368**		
	V3			**(0.364-0.372)**	**10**	**1122**
	V3	**	0.462			
V*P.* 3 **(D)**				**0.411**		
	V3			**(0.406 - 0.422)**	**11**	**1228**
	V3	**	0.471			
V*P.* 2 **(R)**				**0.436**		
	V3			**(0.430-0.441)**	**12**	**1242**
	V3	0.481	0.480			
V*P.* 1 **(D)**				**0.525**		
	V3			**(0.522-0.530)**	**13**	**1300**

These events presented diachronic ages, ranging from ~0.60 Ma in the Gulf of Mexico to ~0.50 Ma in the Caribbean Sea and ~0.35 Ma in the equatorial Atlantic. These events showed older ages in the North Atlantic, and later spread to the equatorial Atlantic (Prell and Damuth, 1978), an opposite behavior from that observed for the proposed events of Zone V in the equatorial Atlantic (Pará-Maranhão Basin). Although the *Pulleniatina* complex disappearance and reappearance events can be established as biostratigraphic markers, their local and regional correlation to the EW68 Zone V needs further investigation.

The diachronism recorded for *G. menardii* D2 event at the base of EW68 Zone W (Subzone W2), supports the conclusion of Toledo et al. (2016) of the disappearance of *G. menardii* complex initially in the Northern Hemisphere, in the Gulf of Mexico and the Caribbean Sea (0.20 - 0.18 Ma - MIS7/6 to 7; Martin et al., 1993 and Kohl et al., 2004), spreading to the equatorial Atlantic (0.15 - 0.16 Ma – MIS 6; Table 2), and later to the southeastern Brazilian continental margin (~0.14 Ma – MIS6b; Toledo et al., 2016). Recorded within EW68 Zone W (Subzone W1; Table 2), the LO of *G. calida calida* (~0.14 Ma; MIS 6; Table 2) marks the top of the Bolli and Premoli Silva (1973) Pleistocene Subzone *G. crassaformis hessi*, and upper Middle Pleistocene, close to the boundary between Middle and Late Pleistocene in our core.

The HO of *G. tosaensis,* recorded during the Lower Pleistocene in the Pará-Maranhão Basin, marks the base of Wade et al. (2011) Subzone PT1b. According to Berggren et al. (1995a, b) and Wade et al. (2011) this Subzone (PT1b) spans the last 0.61 Ma (from 0.61 Ma to the Recent), and support the interval covered by the Bolli and Premoli Silva (1973) Subzone *G. crassaformis hessi* and Subzone *G. calida calida* were represented by sediments deposited during the Middle Pleistocene (between 0.781 – 0.126 Ma).

5.1.3. Late Pleistocene (0.126 - 0.016 Ma)

The LO of *G. calida calida* marks the boundary between the Middle Pleistocene Subzone *G. crassaformis hessi* and the Bolli and Premoli Silva (1973) Upper Pleistocene Subzone *G. calida calida*. This Subzone extends from the LO of *G. calida calida* to the HO of *G. flexuosa* (0.080 - 0.085 Ma; Table 2). In addition to the zonal markers, one abundance event has been recorded within this Subzone, namely the fourth reappearance event of the *G. menardii* complex (R2). The *G. menardii* R2 event (0.13 - 0.14 Ma; Table 2) from Toledo et al. (2016), marks the base of the EW68 Zone X. This zone was recorded in many basins from the North and South Atlantic during the last ~0.13 Ma (e.g., Ericson and Wollin, 1968; Martin et al., 1990, 1993; Vicalvi, 1997; Kohl et al. 2014; Ferreira et al., 2012; Portilho-Ramos et al., 2014;

Toledo et al. 2016), supporting the suggestion that the interval represents the Late Pleistocene. The HO of *G. flexuosa* has been recorded in the Pará-Maranhão Basin with an estimated median age of 0.085 Ma (Table 2), representing the top of Subzone *G. calida calida*, and the boundary between the subzones *G. calida calida* and *G. bermudezi*, subzone from Bolli and Premoli Silva (1973).

The Late Pleistocene Subzone *G. bermudezi* has been recorded in the top of core CDH-79 (62 – 0 cm; Figure 4a). During this Subzone, the abundance *G. menardii* D1 event (0.069 - 0.083 Ma; Table 2) has been recorded, marking the boundary between EW68 zones X/Y. The records in core CDH-79 suggest the occurrence of a hiatus (around 50 kyr), during the Subzone *G. bermudezi*, located above the *G. menardii* D1 event, and below to the AMS ^{14}C sample at 50 cm (median age 0.030 Ma; Table 1; Figure 5). The absence of the abundance events based on the *G. crassaformis* complex recorded by Portilho-Ramos et al. (2014) and Toledo et al. (2016) above the *G. menardii* D1 event confirms the presence of a hiatus in core CDH-79. The top of our core has a calibrated AMS ^{14}C age ~0.016 Ma (10 cm; Table 1), within the Subzone *G. bermudezi*. The absence of the evolutionary event LO *G. fimbriata* (~0.011 Ma; Bolli and Premoli Silva, 1973), which characterizes the top of Subzone *G. bermudezi*, as well as the boundary between the subzones *G. bermudezi* and *G. fimbriata* from Bolli and Saunders (1985), explains the complete absence of Subzone *G. fimbriata* from core CDH-79. The absence of Subzone *G. fimbriata* in addition to the calibrated AMS ^{14}C ages supports the lack of Holocene sediments in our core from the Pará-Maranhão Basin.

5.2. Summary of the main biostratigraphic events from Gelasian to Late Pleistocene in the western equatorial Atlantic

During the Gelasian to Late Pleistocene (last 1.93 Ma), six species became extinct (HO), and three species appeared (LO) in the Brazilian Equatorial Margin (Table 2; Figure 4a, b). Biostratigraphic events of highest occurrence (T *G. fistulosus*; T *G. extremus*; Table 2) observed in the base of our core during the Gelasian - Calabrian (~1.93–1.70 Ma) in agreement with previous findings (e.g., Berggren et al., 1985b, 1995b; Chaisson and Pearson, 1997; Lourens et al., 2004). However, the event T *G. obliquus* occurs earlier in our record (1.47 - 1.48 Ma) than in previous studies (~1.30 Ma; Chaisson and Pearson, 1997; Wade et al., 2011), while the T *G. tosaensis* (1.06 - 1.07 Ma) and T *G. crassaformis hessi*(0.32 - 0.33 Ma) events occurred with a large age difference between records from the tropical Pacific Site 846 (~0.61 Ma; ODP Leg 138; Mix et al., 1995) and southeastern Brazilian continental margin (~0.58 Ma; Toledo et al., 2016). Most of these HO events were recorded during interglacial MIS or deglaciations (Table

2). The most notable exceptions are the HO of *G. fistulosus*, recorded during the glacial MIS 66, and the HO of *G. crassaformis hessi*, recorded during the MIS 9/10 glacial inception. The LO biostratigraphic events observed in our record (B *G. truncatulinoides*; B *G. crassaformis hessi*, and B *G. calida calida*; Table 2), on the other hand, agree with previous observations (e.g., Chaisson and Pearson, 1997; Wade et al., 2011; Toledo et al., 2016). These events were associated with glacials, except for the B *G.crassaformis hessi* that occurred during MIS 19.

In addition to the LO and HO events, the abundance events of the *G. menardii* complex allowed the recognition of ten EW68 zones (from P to Y). We report the oldest *G. menardii* complex Quaternary abundance events in the Brazilian basins. These events are represented by the disappearance of the complex during *G. menardii* D5 (1.78-1.79 Ma) and D4 (1.04-1.05 Ma), while the reappearance events were recorded as R5 (1.67-1.68 Ma) and R4 (0.96-0.97 Ma). The disappearances events *G. menardii* D5 and D4 took place first in the North Atlantic (Gulf of Mexico; Martin et al., 1990, 1993), spreading transgressively to the equatorial Atlantic. The same behavior was observed with the events *G. menardii* D3 and D2, while *G. menardii* D1 was isochronous throughout (Martin et al., 1993; Kohl et al., 2004; Martinez et al., 2007; Table 2). In contrast, *G. menardii* complex reappearances events occurred first in the equatorial Atlantic, spreading later to the North and South Atlantic.

Our data suggest a small diachronism between the disappearance/reappearance events of the *G. menardii* complex compared to the records of North and South Atlantic. The average difference in the age of the *G. menardii* D events (D5, D4, D3, D2, and D1) between the North Atlantic and the equatorial Atlantic (our core CDH-79) is ~0.067±0.022 Ma, while the difference in the age of the *G. menardii* D events (D3, D2, and D1) between the South Atlantic and the equatorial Atlantic is ~0.022±0.010 Ma. However, the average age differences of the *G. menardii* R (events R5, R4, R3, and R2) events between the North Atlantic and equatorial Atlantic ~0.065±0.040 Ma, while the average difference in the age of the *G. menardii* R events (R3 and R2) between the South Atlantic and the equatorial Atlantic is ~0.030±0.020 Ma. These systematic differences in age may be related to the mechanism responsible for inter-ocean exchange of surface and central waters from the Indian Ocean to the South Atlantic via the Agulhas leakage (Peter et al., 2004; Caley et al., 2012). Caley et al. (2012) demonstrated that the reseeding of *G. menardii* in the Atlantic over the last 1.35 Ma is related to extreme leakage events, associated with the southward migration of the subtropical front. These conditions produced strong peaks in the accumulation rate of *G. menardii* at ODP Site 1087 (southern Benguela region). On the other hand, periods of reduced Indian-to-Atlantic transfer and

northward migration of the subtropical front, are marked by minimum abundance, if not complete absence, of the taxon.

6. Conclusions

Based on the identification of planktonic foraminifera from the ~32 m-long core CDH-79 and the calibration of the biostratigraphic events with oxygen isotope records and radiocarbon ages, a biochronostratigraphic framework was established for this, the longest continuous record (~1.93 - 0.01 Ma) in the Brazilian equatorial margin. We present 17 calibrated biostratigraphic events and their associated uncertainties, providing the first recognition and description of the taxon appearance, such as the earliest occurrence of *G. truncatulinoides* (1.89-1.91 Ma) and taxon disappearance, as *G. fistulosus* (1.81-1.82 Ma) for the Pará-Maranhão Basin. Evolutionary events in deeper time, such as last occurrences of *G. fistulosus* appear to be younger in our record, while *G. obliquus* and *G.tosaensis* presented older ages than in previously published records. The explanation for these differences is not known, demonstrating the need for more biostratigraphic studies for the lower Pleistocene, particularly in the tropical Atlantic.

Oscillations in the abundance of the *G. menardii* complex showed the oldest Pleistocene disappearance and reappearance events of the complex (*G. menardii* D5, R5, D4, and R4) in the western Atlantic and Brazilian basins in this study. These new events allowed the first determination of the biostratigraphic zones P, Q, R and S and subzones Q2, Q1, R3, R2, R1, S2, and S1 in the Brazilian basins, improving the resolution of lower Pleistocene events for the area. Our data presented a small diachronism of *G. menardii* events compared to other sites in the North and South Atlantic, possible related to the reseeding mechanism of the taxon due to latitudinal migration of the subtropical front, which appears to be directly connected to the strength of warm waters entering the South Atlantic from the Indian Ocean through the Agulhas leakage.

The integration of observations of the bioevents *G. menardii* R2 (reappearance) and T *G. flexuosa* (disappearance), a radiocarbon age, and lithologic observation, suggests the occurrence of an unconformity (hiatus) of approximately 50 kyr close to the top of our core (i.e., 50-62 cm core depth) between MIS 5 and MIS 2. Furthermore, the absence of *G. menardii* R1 event and *G. fimbriata* specimens, corroborated by the uppermost radiocarbon age (10 cm core depth), demonstrate the absence of sediments deposited during the Holocene. Both unconformities were recognized in the upper section of our records (uppermost 60 cm) and may relate to changes in sea level and/or coring disturbance.

This record greatly improves the resolution of the biostratigraphic events from the Gelasian to the Late Pleistocene, thus forms an important basis for improved temporal resolution for all future paleoenvironmental reconstructions in the tropical western Atlantic.

7. Acknowledgments and Funding

Fabricio Ferreira has the support of the Brazilian agency CAPES [grants 88882.151083/2017-01, 88881.185132/2018-01], which allowed the development of this study. C. M. Chiessi acknowledges the financial support from FAPESP [grant 2018/15123-4], CAPES [grants 564/2015 and 88881.313535/2019-01], CNPq [grants 302607/2016-1, 422255/2016-5] and the State Key Laboratory of Marine Geology, Tongji University, China [grant MGK1602]. A. K. Kern received funding from FAPESP [grants2014/05582-0 and 2015/18314-7] and CAPES [grant 88887.370034/2019-00].

8. Data Availability

Datasets related to this article can be found at https://doi.pangaea.de/10.1594/PANGAEA.917897, an open-source online data repository hosted at PANGAEA (Ferreira et al., 2020 (DOI registration in progress)).

9. References

Arz, H. W., Pätzold, J., Wefer, G., 1998. Correlated millennial-scale changes in surface hydrography and terrigenous sediment yield inferred from last-glacial marine deposits off northeastern Brazil. Quaternary Research, 50(2), 157-166.

Arz, H.W., Patzold, J., Wefer, G., 1999. The deglacial history of thewestern tropical Atlantic as inferred from high-resolution stable isotope records off northeastern Brazil. Earth and Planetary Science Letters, 167, 105–117.

Bé, A.W.H., Damuth, J.E., Lott, L., Free, R., 1976. Late Quaternary Climatic Record in Western Equatorial Atlantic Sediment. In: Geological Society of America. Investigations of Late Quaternary Paleoceanography and Paleoclimatology. Geological Society of America Memoir, 145, 162-200.

Berger, W.H., Bickert, T., Schmidt, H., Wefer, G., 1993. Quaternary oxygen isotope record of pelagic foraminifers: Site 806, Ontong Java Plateau. In: Berger, W.H., Kroenke, L.W., Mayer, L.A., et al., ODP Proceedings Scientific Results, 130 (College Station, TX), pp. 381–395.

Berger, W.H., Loutre, M.F., 1994. Precession, eccentricity, obliquity, insolation and paleoclimates. In: Duplessy, J.-C., Spyridakis, M.T. (Eds.), Long-Term Climatic Variations: Data and Modeling. NATO Science Series, 22, 107–152.

Berggren, W. A., Kent, D. V., van Couvering, J. A., 1985a. Neogene geochronology and chronostratigraphy. In: Snelling, N. J., (Ed.), The chronology of the geological record. Geological Society of London Memoir, 10, 211–250.

Berggren, W. A., Kent, D. V., Flynn, J. J., van Couvering, J. A., 1985b. Cenozoic geochronology. Geological Society of America Bulletin, 96, 1407–1418.

Berggren, W.A., Hilgen, F.J., Langereis, C.G., Kent, D.V., Obradovich, J.D., Raffi, I., Raymo, M.E., Shackleton, N.J., 1995a. Late Neogene chronology: new perspectives in high-resolution stratigraphy. Geological Society of America Bulletin, 107, 1272-1287.

Berggren, W.A., Kent, D.V., van Couvering, J. A., 1995b. Neogene geochronology and chronostratigraphy. Geological Society Memoirs, 10, 211-260. DOI: 10.1144/GSL.MEM.1985. 010. 01.18

Blaauw, M., Christen, J.A., 2011. Flexible paleoclimate age-depth models using an autoregressive gamma process. Bayesian Analysis, 6(3), 457-474.

Blow, W.H., 1969. Late middle Eocene to Recent planktonic foraminiferal biostratigraphy. *In:* P. Bronnimann, H.H. Renz (Eds.), Proceedings of the First International Conference on Planktonic Microfossils, Geneva, pp. 199-422.

Bolli, H.M., Premoli Silva, I., 1973. Oligocene to Recent Planktonic Foraminífera and Stratigraphy of Leg 15 sites in the Caribean Sea. Initial Reports of the Deep Sea Drilling Project, 15, 475-497.

Bolli, H.M., Saunders, J.B., 1985. Oligocene to Holocene low latitude planktic foraminifera. In: Bolli, H.M., Saunders, J.B., Perch-Nielsen, K. (Eds.), Plankton Stratigraphy. Cambridge University Press, New York, pp. 156-262.

Butzin, M., Köhler, P., Lohmann, G., 2017. Marine radiocarbon reservoir age simulations for the past 50,000 years. Geophysical Research Letters, 44, 8473-8480, DOI:10.1002/2017 GL074688

Bylinskaya, M.E., 2005. Range and stratigraphic significance of the *Globorotalia crassaformis* plexus. Journal of Iberian Geology, 31(1), 51–63.

Caley, T., Giraudeau, J., Malaizé, B., Rossignol, L., Pierre, C. 2012. Agulhas leakage as a key process in the modes of Quaternary climate change. Proceedings of the National Academy of Sciences, 109 (18), 6835-6839. DOI: 10.1073/pnas.1115545109.

Chaisson, W.P., Pearson, P.N. 1997. Planktonic foraminifer Biostratigraphy at Site 925: Middle Miocene-Pleistocene. In: Shackleton, N.J., Curry, W.B., Richter, C., Bralower, T.J. (Eds.) Proceedings of the Ocean Drilling Program, Scientific Results, Vol. 154.

Chaproniere, G.C.H., Styzen, M.J., Sager, W.W., Nishi, H., Quinterno, P.J., Abrahamsen, N., 1994. Late Neogene biostratigraphic and magnetostratigraphic synthesis, Leg 135. In: Hawkins, J; Parson, L; Allan, J; et al. (Eds.), Proceedings of the Ocean Drilling Program, Scientific Results, College Station, TX (Ocean Drilling Program), 135, 857-877, https://doi.org/10.2973/odp.proc.sr.135.116.1994.

Cohen, K.M. Gibbard, P.L., 2019. Global chronostratigraphical correlation table for the last 2.7 million years, version 2019 QI-500. Quaternary International, 500, 20-31.

Crivellaria, S., Chiessi, C.M., Kuhnert, H., Häggi, C., Portilho-Ramos, R.C., Zeng, J.Y., Zhang, Y., Schefuß, E., Mollenhauer, G., Hefter, J., Alexandre, F., Sampaio, G., Mulitza, S., 2017. Increased Amazon freshwater discharge during late Heinrich Stadial 1. Quaternary Science Reviews, 181, 144-155. doi.org/10.1016/j.quascirev.2017.12.005.

de Garidel-Thoron, T., Rosenthal, Y., Bassinot, F., Beaufort, L., 2005. Stable sea surface temperatures in the western Pacific warm pool over the past 1.75 million years. Nature, 433(7023), 294-298.

Ericson, D.B., Wollin, G., 1968. Pleistocene climates and chronology in deep-sea sediments. Science, 162, 1227-1243.

Ferreira, F., Frontalini, F., Leão, C.J., Leipnitz, I.I., 2014. Changes in the water column structure and paleoproductivity in the western South Atlantic Ocean since the middle Pleistocene: Evidence from benthic and planktonic foraminífera. Quaternary International, 352, 111-123.

Ferreira, F., Leipnitz, I.I., Vicalvi, M.A., Sanjinés, A.E.S., 2012. Zoneamento Paleoclimático do Quaternário da Bacia de Santos com base em foraminíferos planctônicos. Revista Brasileira de Paleontologia. 15(2), 173–188.

Fonseca, C.A., Goni, G.J., Johns, W.E., Campos, E.J.D., 2004. Investigation of the North Brazil Current retroflection and North Equatorial Countercurrent variability. Geophysical Research Letters, 31(21), 1–5. http://dx.doi.org/10.1029/2004GL020054.

Gibbard, P. L., Head, M. J., Walker, M. J. C., Subcommission on Quaternary Stratigraphy, 2009. Formal ratification of the Quaternary System/Period and the Pleistocene Series/Epoch with a base at 2.58 Ma. Journal of Quaternary Science, 25, 96-102.

Gibbard, P.L., Head, M.J., 2010 The newly-ratified definition of the Quaternary System/Period and redefinition of the Pleistocene Series/Epoch, and comparison of proposals advanced prior to formal ratification. Episodes, 33, 152-158.

Gibbard, P.L; Head, M.J.; Walker, M.J.C., The Subcommission on Quaternary Stratigraphy. 2010. Formal ratification of the Quaternary System/Period and the Pleistocene Series/Epoch with a base at 2.58 Ma. Journal of Quaternary Science, 25, 96-102.

Goni, G.J., Johns, W.E., 2001. A census of North Brazil Current Rings observed from TOPEX/POSEIDON altimetry: 1992–1998. Geophysical Research Letters, 28(1), 1–4.

Govin, A., Capron, E., Tzedakis, P.C., Verheyden, S., Ghaleb, B., Hillaire-Marcel, C., St-Onge, G., Stoner, J.S., Bassinot, F., Bazin, L., Blunier, T., Combourieu-Nebout, N., El Ouahabi, A., Genty, D., Gersonde, R., Jimenez-Amat, P., Landais, A., Martrat, B., Masson-Delmotte, V., Parrenin, F., Seidenkrantz, M.-S., Veres, D., Waelbroeck, C., Zahn, R. 2015. Sequence of events from the onset to the demise of the Last Interglacial: Evaluating strengths and limitations of chronologies used in climatic archives. Quaternary Science Reviews, 129, 1-36.

Grant, K.M, Rohling, E.J., Bar-Mathews, M., Aylon, A., Medina-Elizalde, M., Ramsey, C.B., Satow, C., Roberts, A.P. 2012. Rapid coupling between ice volume and polar temperature over past 150.000 years. Nature, 491, 744-747. DOI:10.1038/nature11593.

Haarsma, R.J., Campos, E.J.D., Drijfhout, S., Hazeleger, W., Severijns, C., 2011. Impacts of interruption of the Agulhas leakage on the tropical Atlantic in coupled ocean-atmosphere simulations. Climate Dynamics, 36(5–6), 989–1003. http://dx.doi.org/10.1007/00382-009-0692-7.

Hayward, B.W.; Le Coze, F.; Vachard, D.; Gross, O., 2019. World Foraminifera Database. Accessed at http://www.marinespecies.org/foraminifera on 2019-12-14. DOI:10.14284/305.

Johns, W.E., Lee, T.N., Beardsley, R., Candela, J., Castro, B., 1998. Annual cycle and variability of the North Brazil Current. Journal of Physical Oceanography, 28, 103–128.

Joyce, J.E., Tjalsma, L.R., Prutzman, J.M., 1990. High-resolution planktonic isotope record and spectral analysis for the last 5.35 Ma: Ocean Drilling Program Site 625 – Northeast Gulf of Mexico. Paleoceanography, 5(4), 507-529.

Kennett, J. P., Srinivasan, M. S., 1983. Neogene planktonic foraminifera. Stroudsburg: Hutchinson Ross Publishing Company, 265 pp.

Kennett, J.P., Huddlestun, P., 1972. Late Pleistocene paleoclimatology, foraminiferal biostratigraphy, and tephrochronology, Western Gulf of Mexico. Quaternary Research, 2, 38-69.

Kohl, B., Fillon, R.H., Roberts, H.H., 2004. Foraminiferal biostratigraphy and paleoenvironments of the Pleistocene Lagniappe Delta and related section, Northeastern Gulf of Mexico. In: B. Anderson, R.H. Fillon (Eds.), Late Quaternary Stratigraphic Evolution of the Northern Gulf of Mexico Margin. Society for Sedimentary Geology, 79, 190-216.

Langner, M., Mulitza, S., 2019. Technical Note: PaleoDataView – A software toolbox for the collection, homogenization, and visualization of marine proxy data. Climate of the Past, 15, 2067–2072. doi.org/10.5194/cp-15-2067-2019.

Le, J., Shackleton, N.J., 1992. Carbonate dissolution fluctuations in the western equatorial Pacific during the late Quaternary. Paleoceanography, 7(1), 21–42.

Leipnitz, I.I., Silva, J.L.L., Leipnitz, B., Aguiar, E.S., Leão, C.J., Giovanoni, L., Ferreira, F. 2005. Métodos para o trabalho com microfósseis e formas atuais. In: Timm, L.L., Cademartoti, C.V., (Eds.), Cadernos La Salle XI - Métodos de Estudo em Biologia, 2(1), 49-58.

Lisiecki, L., Raymo, M.E., 2005. A Pliocene-Pleistocene stack of 57 globally distributed benthic $\delta^{18}O$ records. Paleoceanography, 20, PA1003. DOI:10.1029/2004PA001071.

Locarnini, R. A., Mishonov, A.V., Baranova, O.K., Boyer, T.P., Zweng, M.M., Garcia, H.E., Reagan, J.R., Seidov, D., Weathers, K., Paver, C.R., Smolyar, I., 2018. World Ocean Atlas 2018, Volume 1: Temperature. A. Mishonov Technical Ed.; NOAA Atlas NESDIS 81, 52 pp.

Lourens, L.J., Hilgen, F.J., Shacketon, N.J., Laskar, J., Wilson, D., 2004. The Neogene Period. In: Gradstein, F.M., Ogg, J.G., Smith, A.G. (Eds.), Geological Time Scale 2004. Cambridge University Press, PP. 409-440.

Lux, M., Mercier, H., Arhan, M., 2001. Interhemispheric exchanges of mass and heat in the Atlantic Ocean in January–March 1993. Deep-Sea Research, 48, 605–638.

Marchito, T.M., Curry, W.B., Lynch-Stieglitz, J., Bryan, S.P., Cobb, K.M., Lund, D.C., 2014. Improved oxygen isotope temperature calibrations for cosmopolitan benthic foraminifera. Geochimica et Cosmochimica Acta, 130, 1-11.

Martin, R.E.; Johnson, G.W.; Neff, E.D., Krantz, D.E., 1990. Quaternary planktonic foraminiferal assemblage zones of the northeast Gulf of México, Colombia basin (Caribbean Sea), and tropical Atlantic Ocean: Graphic correlation of microfossil and oxygen isotope datums. Paleoceanography, 5(4), 531-555.

Martin, R.E.; Neff, E.D.; Johnson, G.W., Krantz, D.E., 1993. Biostratigraphic Expression of Pleistocene Sequence Boundaries, Gulf of Mexico. Palaios, 8, 155-171.

Martinez, J.I; Mora, G. & Barrows, T.T., 2007. Paleoceanographic conditions in the Western Caribbean Sea for the last 560 kyr as inferred from planktonic foraminifera. Marine Micropaleontology, 64, 177-188.

Mix, A.C., Le, J., Shackleton, N.J., 1995. Benthic foraminiferal stable isotopes stratigraphy of Site 846: 0-1.8 Ma. In: Pisias, N.G., Mayer, L.A., Janecek, T.R., Palmer-Julson, A., van Andel, T.H. (Eds.), Proceedings of the Ocean Drilling Program, Scientific Results, Vol. 138.

Nace, T. E., Baker, P.A., Dwyer, G.S., Silva, C.G., Rigsby, C.A., Burns, S.J., Giosan, L., Otto-Bliesner, B., Liu, Z., Zhu, J. 2014. The role of North Brazil Current transport in the paleoclimate of the Brazilian Nordeste margin and paleoceanography of the western tropical Atlantic during the late Quaternary. Palaeogeography, Palaeoclimatology, Palaeoecology, 415(0), 3-13.

Nishi, H., Norris, R.D., Okada, H., 2000. Paleoceanographic changes in the dynamics of subtropical surface conditions at Hole 997A. In: Paull, C.K., Matsumoto, R., Wallace, P.J., and Dillon, W.P. (Eds.), Proceedings of the Ocean Drilling Program, Scientific Results, Vol. 164.

Ogg, J.G., 2012. The geomagnetic polarity timescale. In: Gradstein, F., Ogg, J.G., Schmitz, M., Ogg, G. (Eds.), The Geologic Time Scale 2012. Elsevier, Amsterdam, pp. 85-128.

Patterson, R.T., Fishbein, E., 1989. Re-Examination of the statistical methods used to determine the number of point counts needed for micropaleontological quantitative research. Journal of Paleontology, 63, 245-248.

Peeters, F.J., Acheson, R., Brummer, G.-J.A., Rujiter, W.P.M., Schneider, R.R., Ganssen, G.M., Ufker, E., Kroon, D., 2004. Vigorous exchange between the Indian and Atlantic oceans at the end of the past five glacial periods. Nature, 430, 661-665.

Peterson, R.G., Stramma, L., 1991. Upper-Level circulation in the South Atlantic Ocean. Prog. Oceanog., 26, 1-73.

Portilho-Ramos, R.C., Barbosa, C.F., Rios-Netto, A.M., 2014. Planktonic foraminiferal variations in the southwestern Atlantic since the last glacial-interglacial cycle. PALAIOS 29, 38–44. http://dx.doi.org/10.2110/palo.2012.104.

Portilho-Ramos, R.C., Rios-Netto, A.M., Barbosa, C.F., 2006. Caracterização bioestratigráfica do Neógeno superior da Bacia de Santos com base em foraminíferos planctônicos. Revista Brasileira de Paleontologia, 9, 349–354.

Prell, W.L., Damuth, J.E., 1978. The climate-related diachronous disappearance of Pulleniatina obliquiloculata in Late Quaternary sediments of the Atlantic and Caribbean. Marine Micropaleontology, 3, 267-277.

Railsback, L.B., Gibbard, P.L., Head, M.J., Voaristsoa, N.R.G., Toucanne, S., 2015. Na optimized scheme of lettered marine isotopic stages for the last 1.0 million years, and the climatostratigraphic nature of isotope stage and substages. Quaternary Science Reviews, 111, 94-106.

Reimer, P. J., Bard, E., Bayliss, A., Beck, J.W., Blackwell, P.G., Ramsey, C.B., Buck, C.E., Edwards, R.L., Friedrich, M., Grootes, P.M., Guilderson, T.P., Haflidason, H., Hajdas, I., Hatté, C., Heaton, T.J., Hoffmann, D.L., Hogg, A.G., Hughen, K.A., Kaiser, K.F., Kromer, B., Manning, S.W. , Niu, M., Reimer, R.W., Richards, D.A., Scott, E.M., Southon, J.R., Staff, R.A., Turney, C.S.M., van der Plicht, J., 2013. INTCAL13 and MARINE13 Radiocarbon Age Calibration Curves 0–50,000 Years Cal BP. Radiocarbon, 55(4), 1869–1887.

Richardson, P.L., Hufford, G.E., Limeburner, R., Brown, W.S., 1994. North Brazil Current retroflection eddies. Journal of Geophysical Research, 99, 5081–5093.

Schott, F., Stramma, L., Fischer, J., 1995. The warm water inflow into the western tropical Atlantic boundary regime, spring 1994. Journal of Geophysical Research, 100, 24745–24760.

Shackleton, N.J., Berger, A., Peltier, W.R., 1990. An alternative astronomical calibration of the lower Pleistocene timescale based on ODP Site 677. Philosophical Transactions of the Royal Society of Edinburgh, Earth Sciences, 81, 251–261.

Srinivasan, M. S., Sinha, D. K., 1992. Late Neogene planktonic foraminiferal events of the southwest Pacific and Indian Ocean: A comparison, In: Tsuchi, R., Ingle, J. C., Jr.,(Eds.), Pacific Neogene environment, evolution and events: Tokyo, University of Tokyo Press, pp. 203–220.

Stainforth, R.M.; Lamb, J.L.; Luterbaqcher, H.; Beard, J.H., Jeffords, R.M., 1975. Cenozoic planktonic foraminiferal zonation and characteristics of index forms. Paleontological Contributions, 62. Lawrence: University of Kansas Press. 425 p.

Stow, D.A.V., Aksu, A.E., 1978. Disturbances in soft sediments due to piston coring. Marine Geology, 28, 135-144.

Stramma, L., Fischer, J., Reppin, J., 1995. The North Brazil undercurrent. Deep Sea Research, 42, 773–795.

Talley, L., Pickard, G., Emery, W., Swift, J., 2011. Descriptive physical oceanography: An introduction. Elsevier Academic, Boston, 560 pp.

Thunnell, R.C., 1984. Pleistocene planktonic foraminiferal biostratigraphy and paleoclimatology of the Gulf of México. In: N. Healy-Williams (Ed.), Principles of Pleistocene Stratigraphy

Applied to the Gulf of Mexico. Boston, International Human Resources Development Corporation, pp. 25-64.

Toledo, F.A.L., Quadros, J.P., Camilo Jr., E., Santarosa, A.C.A., Flores, J.A., Costa, K.B., 2016. Plankton biochronology for the last 772,000 years from the western South Atlantic Ocean. Marine Micropaleontology, 127, 50–62. http://dx.doi.org/10.1016/j.marmicro.2016.07.002.

Vicalvi, M.A., 1997. Zoneamento bioestratigráfico e paleoclimático dos sedimentos do Quaternário superior do talude da Bacia de Campos, RJ, Brasil. Boletim de Geociências da Petrobrás, 11(1), 132-165.

Wade, B. S., Pearson, P.N., Berggren, W.A., Pälike, H., 2011. Review and revision of Cenozoic tropical planktonic foraminífera biostratigraphy and calibration to the geomagnetic polarity and astronomical time scale. Earth-Science Reviews, 104, 111-142.

Wilkens, R.H., Westerhold, T., Drury, A.J., Lyle, M., Gorgas, T., and Tian, J., 2017. Revisiting the Ceara Rise, equatorial Atlantic Ocean: isotope stratigraphy of ODP Leg 154 from 0 to 5 Ma. Climate of the Past, 13, 779–793. DOI: https://doi.org/10.5194/cp-13-779-2017.

Wilson, K.E., Maslin, M.A., Burns, S.J., 2011. Evidence for a prolonged retroflection of the North Brazil Current during glacial stages. Palaeogeography, Palaeoclimatology, Palaeoecology, 301(1–4), 86–96. http://dx.doi.org/10.1016/j.palaeo.2011.01.003.

Zhang, D., Msadek, R., McPhaden, M.J., Delworth, T., 2011. Multidecadal variability of the North Brazil Current and its connection to the Atlantic meridional overturning circulation. Journal of Geophysical Research, 116, C04012. http://dx.doi.org/10.1029/2010JC006812.

Zhang, Y., Chiessi, C. M., Mulitza, S., Sawakuchic, A.O., Häggi, C.,.Zabel, M., Portilho-Ramos, R.C., Schefuß, E., Crivellari, S., Wefer, G., 2017. Different precipitation patterns across tropical South America during Heinrich and Dansgaard-Oeschger stadials. Quaternary Science Reviews, 177, 1-9. doi.org/10.1016/j.quascirev.2017.10.012.

Zhang, Y., Chiessi, C. M., Mulitza, S., Zabel, M., Trindade, R.I.F., Hollanda, M.H.B.M., Dantas, E.L., Govina, A., Tiedemann, R., Wefer, G. 2015. Origin of increased terrigenous supply to the NE SouthAmerican continental margin during Heinrich Stadial 1 and the Younger Dryas. Earth and Planetary Science Letters, 432:493-500. http://dx.doi.org/10.1016/j.epsl. 2015. 09.054.

Zweng, M. M., Reagan, J. R., Seidov, D., Boyer, T.P., Locarnini, R.A., Garcia, H.E., Mishonov, A.V., Baranova, O.K., Weathers, K., Paver, C.R., Smolyar, I., 2018. World Ocean Atlas 2018, Volume 2: Salinity. A. Mishonov Technical Ed.; NOAA Atlas NESDIS 82, 50 pp.

Biochronostratigraphy of the western equatorial Atlantic for the last 1.93 Ma

- SUPPLEMENTARY MATERIAL -

Fabricio Ferreira[1,2]; Cleverson G. Silva[2]; Allan S.Oliveira[2]; Cristiano M. Chiessi[3]; Andrea K. Kern[4]; Paul A. Baker[5], Gary Dwyer[5]; Catherine A. Rigsby[6]; Enqing Huang[7]; Jun Tian[7]

[1]Postgraduate Program in Ocean and Earth Dynamics, Institute of Geosciences, Universidade Federal Fluminense, Av. Gal. Milton Tavares de Souza s/n, CEP: 24210-346 Niterói RJ, Brazil – *ferreira_paleo@hotmail.com*

[2]Marine Geology Laboratory (LAGEMAR), Institute of Geosciences, Universidade Federal Fluminense, Av. Gal. Milton Tavares de Souza s/n, CEP: 24210-346 Niterói RJ, Brazil

[3]School of Arts, Sciences and Humanities, University of São Paulo, Av. ArlindoBettio 1000, CEP: 03828-000 São Paulo SP, Brazil

[4]Department of Sedimentary and Environmental Geology, Institute of Geosciences, University of São Paulo, Rua do Lago 562, CEP: 05508-080 São Paulo SP, Brazil

[5]Division of Earth and Ocean Sciences, Duke University, NC 27708 Durham, USA

[6]Department of Geological Sciences, East Carolina University, NC 27858-4353Greenville, USA

[7]State Key Laboratory of Marine Geology, Tongji University, 1239 Siping Road, 200092 Shanghai, China

Supplementary material:

It contains three supplementary tables, two figures, and two supplementary texts which include the description and characterization of the planktonic foraminifera biostratigraphic events and the Ericson and Wollin (1968) zones and subzones recorded in core CDH-79.

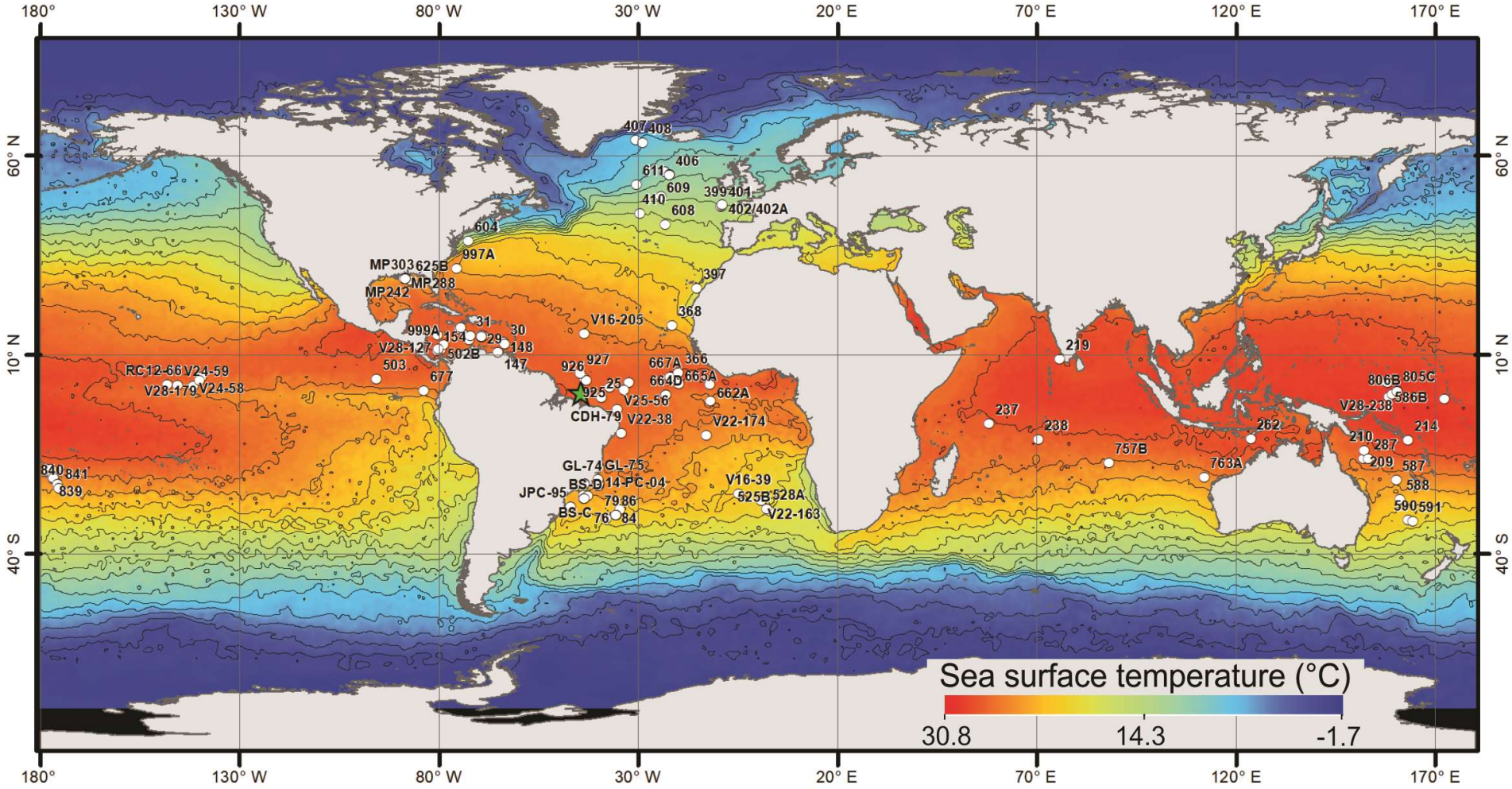

Supplementary Figure S1. Location of the marine sediment core CDH-79 (green star), and the black circle represent others studied sites (Table S1). Decadal annual mean sea surface temperature was interpolated from the WOA18 database (Locarnini et al., 2018).

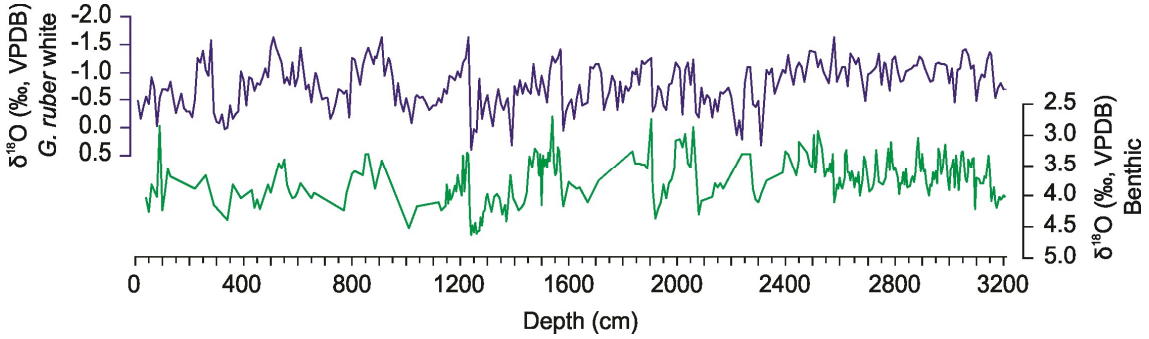

Supplementary Figure S2. Planktonic (blue) and benthonic (green) foraminifera stable oxygen isotopic ($\delta^{18}O$) records from core CDH-79.

Table S1. Coordinates and references of sites included in Figures 1 and S1.

Core		Latitude	Longitude	depth (m)	References
CDH-79		0.650190	-44.333548	2345	**Thiswork**
A172-6		14.983333	-68.850000	4160	Ericson and Wollin, 1968;
A179-4		16.600000	-74.800000	2965	Ericson and Wollin, 1968
V9-11		3.216667	-32.200000	4120	Ericson and Wollin, 1968
V12-18		-28.700000	-34.500000	2935	Ericson and Wollin, 1968
V12-122		17.000000	-74.400000	2730	Ericson and Wollin, 1968
V16-39		-24.716667	-4.750000	4510	Ericson and Wollin, 1968
V16-200		1.966667	-37.066667	4095	Ericson and Wollin, 1968
V16-205		15.400000	-43.400000	4045	Ericson and Wollin, 1968; Martin et al. 1990, 1993
V19-297		2.616667	-12.000000	4120	Ericson and Wollin, 1968
V22-163		-26.366667	0.933333	4440	Ericson and Wollin, 1968
ODP Leg 100	**625B**	28.816917	-87.150167	889	Martin et al. 1990; Martin et al. 1993
DSDP Leg 68	**502B**	11.483475	-79.366858	3051	Martin et al. 1990; Martin et al. 1993
DSDP Leg 90	**586B**	-0.483567	158.483581	2208	Srinivasan and Sinha, 1992
DSDP Leg 90	**587**	-21.183575	160.316942	1101	Srinivasan and Sinha, 1992; Spencer-Cervato et al., 1997
DSDP Leg 90	**588**	-26.100019	161.216683	1533	Srinivasan and Sinha, 1992; Spencer-Cervato et al., 1997
DSDP Leg 90	**590**	-31.166672	163.350142	1299	Srinivasan and Sinha, 1992
DSDP Leg 22	**214**	-11.333339	163.350142	1665	Srinivasan and Sinha, 1992
DSDP Leg 23	**219**	9.016875	75.866853	1764	Srinivasan and Sinha, 1992
DSDP Leg 24	**237**	-7.066942	58.116800	1640	Srinivasan and Sinha, 1992
DSDP Leg 24	**238**	-11.150058	70.516822	2844	Srinivasan and Sinha, 1992
DSDP Leg 15	**146**	15.100275	-69.366853	3949	Bolli and Premoli Silva (1973)
DSDP Leg 15	**147**	10.700133	-65.166800	892	Bolli and Premoli Silva (1973); Rögl and Bolli, 1973
DSDP Leg 15	**148**	13.416700	-63.716736	1232	Bolli and Premoli Silva (1973)
DSDP Leg 15	**149**	15.100069	-69.350236	3972	Bolli and Premoli Silva (1973)
DSDP Leg 15	**150**	14.500192	-69.350097	4545	Bolli and Premoli Silva (1973)
DSDP Leg 15	**151**	15.016672	-73.400161	2029	Bolli and Premoli Silva (1973)
DSDP Leg 15	**153**	13.966758	-72.433356	3932	Bolli and Premoli Silva (1973)
DSDP Leg 15	**154**	11.083364	-80.366875	3338	Bolli and Premoli Silva (1973)
DSDP Leg 4	**29**	14.783364	-69.316767	4247	Bolli and Premoli Silva (1973)
DSDP Leg 4	**30**	12.866922	-63.383333	1218	Bolli and Premoli Silva (1973)
DSDP Leg 4	**31**	14.933500	-72.016842	3369	Bolli and Premoli Silva (1973)
ODP Leg 135	**834**	-18.566683	-177.850204	2852.4	Chaproniere et al., 1994
ODP Leg 135	**835**	-18.500017	-177.300045	3076	Chaproniere et al., 1994
ODP Leg 135	**836**	-20.133471	-176.500002	2455.4	Chaproniere et al., 1994
ODP Leg 135	**837**	-20.216752	-176.816767	2847	Chaproniere et al., 1994
ODP Leg 135	**838**	-20.816838	-176.883445	2487	Chaproniere et al., 1994
ODP Leg 135	**839**	-20.683481	-176.766803	2846.7	Chaproniere et al., 1994
ODP Leg 135	**840**	-22.216736	-175.733588	759	Chaproniere et al., 1994
ODP Leg 135	**841**	-23.333541	-175.283575	5007.6	Chaproniere et al., 1994
ODP Leg 165	**999A**	12.733461	-78.733433	2827.9	Chaisson and D´Hondt, 2000; Martinez et al. 2007

Table S1. Continued.

ODP Leg 108	**658A**	20.733597	-18.566903	2274.1	Weaver and Raymo, 1989
ODP Leg 108	**662A**	-1.383447	-11.733431	4034.8	Weaver and Raymo, 1989
ODP Leg 108	**664D**	0.100122	-23.216847	4109	Weaver and Raymo, 1989; Spencer-Cervato et al., 1997
ODP Leg 108	**665A**	2.950019	-19.666686	4848.8	Weaver and Raymo, 1989
ODP Leg 108	**667A**	4.570833	-21.900189	3916.8	Weaver and Raymo, 1989
GL-852		-25.016667	-43.550000	1938	Toledo et al., 2016
GL-854		-25.200000	-42.616667	2220	Toledo et al., 2016
BS-C		-25.850139	-43.550222	2148	Ferreira et al., 2012
BS-D		-25.950250	-43.400028	2171	Ferreira et al., 2012
ODP Leg 154	**925**	4.200056	-43.483417	3040	Chaisson and Pearson, 1997; Bickert et al., 1997; Lourens et al., 2004; Wilkens et al., 2017
ODP Leg 154	**926**	3.716694	-42.900139	3598	Bickert et al., 1997; Wilkens et al., 2017
ODP Leg 154	**927**	5.450194	-44.466889	3326	Bickert et al., 1997; Wilkens et al., 2017
ODP Leg 130	**806B**	0.316697	159.350192	2520	Chaissom and Leckie, 1993; Berggren et al., 1995a; de Garidel-Thoron et al., 2005
ODP Leg 130	**805C**	1.216858	160.516881	3188	Berger et al., 1993
ODP Leg 122	**763A**	-20.583389	112.200139	1367.5	Sinha and Singh, 2008
DSDP Leg 90	**591**	-31.583350	164.433589	2131	Spencer-Cervato et al., 1997
DSDP Leg 72	**517**	-30.933558	-38.033464	2963	Spencer-Cervato et al., 1997
DSDP Leg 93	**604**	38.700219	-72.533597	2364	Spencer-Cervato et al., 1997
ODP Leg 121	**757B**	-17.016794	88.166916	1652.1	Spencer-Cervato et al., 1997
DSDP 68	**503**	4.066678	-95.633392	3672	Keigwin, 1982
ODP Leg 111	**677**	1.200038	-83.733394	3461.2	Shackleton et al., 1990
V19-96		-0.866667	172.483333	4252	Thompson and Sciarrillo, 1978
V24-58		2.266667	-141.666667	4490	Thompson and Sciarrillo, 1978
V24-59		2.566667	-145.533333	4662	Thompson and Sciarrillo, 1978
V28-179		4.616667	-139.600000	4502	Thompson and Sciarrillo, 1978
V28-238		1.016667	160.483333	3120	Thompson and Sciarrillo, 1978
V28-239		3.250000	158.183333	3490	Thompson and Sciarrillo, 1978
RC11-209		3.650000	-140.066667	4400	Thompson and Sciarrillo, 1978
RC12-66		2.616667	-148.216667	4755	Thompson and Sciarrillo, 1978
64		-30.000000	-35.550222	2100	Berggren, 1977
67		-29.950222	-35.550000	2195	Berggren, 1977
73		-29.983444	-35.550250	2150	Berggren, 1977
75		-29.966833	-35.533583	2260	Berggren, 1977
76		-29.933389	-35.550000	2315	Berggren, 1977
79		-29.950167	-35.550194	2214	Berggren, 1977
84		-29.983528	-35.550139	2210	Berggren, 1977
86		-30.000028	-35.550194	2090	Berggren, 1977
ODP Leg 164	**997A**	31.833497	-75.466699	2781.6	Nishi et al., 2000
DSDP Leg 27	**262**	-10.866719	123.833550	2298	Rögl, 1974
DSDP Leg 48	**399**	47.383444	-9.216750	4399	Krasheninnikov, 1979
DSDP Leg 48	**400/400A**	47.366917	-9.183583	4399	Krasheninnikov, 1979
DSDP Leg 48	**401**	47.416847	-8.800172	2495	Krasheninnikov, 1979
DSDP Leg 48	**402/402A**	47.866800	-8.833456	2339.5	Krasheninnikov, 1979

Table S1. Continued

DSDP Leg 48	**404**	56.050036	-23.233597	2306	Krasheninnikov, 1979
DSDP Leg 48	**405**	55.333383	-22.050136	2958	Krasheninnikov, 1979
DSDP Leg 48	**406**	55.250139	-22.083447	2911	Krasheninnikov, 1979
DSDP Leg 74	**525B**	-29.066733	2.986667	2467	Pflaumann, 1988
DSDP Leg 74	**528A**	-28.516711	2.300269	3815	Pflaumann, 1988
DSDP Leg 21	**209**	-15.933386	152.183408	1428	Chaproniere, 1991
DSDP Leg 21	**210**	-13.750275	152.250258	4643	Chaproniere, 1991
DSDP Leg 30	**287**	-15.900186	153.250258	4632	Chaproniere, 1991
DSDP Leg 4	**25**	-0.516667	-39.233444	1916	Bylinskaya, 2004
DSDP Leg 41	**366**	5.666861	-19.850028	2853	Bylinskaya, 2004
DSDP Leg 41	**368**	17.500111	-21.350056	3366	Bylinskaya, 2004
DSDP Leg 47	**397**	26.833419	-15.166889	2900	Bylinskaya, 2004
DSDP Leg 48	**403**	56.133419	-23.283511	2317	Bylinskaya, 2004
DSDP Leg 48	**404**	56.050036	-23.233597	2322	Bylinskaya, 2004
DSDP Leg 48	**405**	55.333383	-22.050136	2958	Bylinskaya, 2004
DSDP Leg 48	**406**	55.250139	-22.083447	2907	Bylinskaya, 2004
DSDP Leg 49	**407**	63.933422	-30.566822	2472	Bylinskaya, 2004
DSDP Leg 49	**408**	63.366842	-28.900197	1624	Bylinskaya, 2004
DSDP Leg 49	**410**	45.500142	-29.466822	2975	Bylinskaya, 2004
DSDP Leg 94	**608**	42.833390	-23.083403	3526	Bylinskaya, 2004
DSDP Leg 94	**609**	49.866852	-24.233413	3884	Bylinskaya, 2004
DSDP Leg 94	**611**	52.833464	-30.300161	3203	Bylinskaya, 2004
MP242		29.388089	-88.353547	56.1	Kohl et al., 2004
MP288		29.272769	-88.405483	77.1	Kohl et al., 2004
MP303		29.212278	-88.665192	71.9	Kohl et al., 2004
BLK774		29.196922	-88.383747	184.5	Kohl et al., 2004
JPC-95		-27.866869	-46.916736	1485	Portilho-Ramos et al., 2006
Bu-91/Gl-05		-22.136584	-39.914665	630	Vicalvi, 1997
Bu-91/Gl-07		-22.136916	-39.877200	955	Vicalvi, 1997
Bu-91/Gl-10		-22.380058	-40.113993	625	Vicalvi, 1997
14-PC-06		-22.484356	-40.184275	761	Vicalvi, 1997
14-PC-08		-22.686418	-40.051750	1557	Vicalvi, 1997
9-PC-05		-22.540898	-39.933448	1602	Vicalvi, 1997
5-PC-32		-22.477033	-40.027223	1024	Vicalvi, 1997
9-PC-01		-22.464693	-40.027366	990	Vicalvi, 1997
3-PC-01		-22.317139	-40.112154	247	Vicalvi, 1997
9-PC-06		-22.552626	-39.904526	1930	Vicalvi, 1997
5-PC-31		-22.502597	-40.002681	1141	Vicalvi, 1997
9-PC-04		-22.526754	-39.940966	1472	Vicalvi, 1997
10-PC-03		-22.405565	-40.123406	665	Vicalvi, 1997
14-PC-03		-22.330897	-39.953153	932	Vicalvi, 1997
14-PC-04		-22.375218	-39.838154	1482	Vicalvi, 1997
14-PC-09		-22.568593	-40.207489	915	Vicalvi, 1997
14-PC-05		-22.441053	-40.263039	554	Vicalvi, 1997

Table S1. Continued

14-PC-07	-22.595728	-43.485719	1254	Vicalvi, 1997
10-PC-01	-22.440977	-40.071054	850	Vicalvi, 1997
1-PC-02	-22.591888	-40.008375	1 436	Vicalvi, 1997
14-PC-10	-22.544586	-40.100217	1006	Vicalvi, 1997
6-PC-05	-22.436983	-40.095519	795	Vicalvi, 1997
5-PC-29	-22.044750	-39.850545	1 176	Vicalvi, 1997
9-PC-09	-22.091575	-40.014699	202	Vicalvi, 1997
14-PC-01	-22.079914	-39.979015	305	Vicalvi, 1997
5-PC-25	-22.067602	-39.910014	656	Vicalvi, 1997
14-PC-02	-22.075287	-43.449050	698	Vicalvi, 1997
5-PC-27	-22.091570	-39.879973	938	Vicalvi, 1997
7-PC-05	-22.196653	-43.459899	862	Vicalvi, 1997
V18-357	15.033333	-80.233333		Prell and Damuth, 1978
V28-127	11.650000	-80.133333		Prell and Damuth, 1978
V12-122	17.000000	-74.400000		Prell and Damuth, 1978
V25-59	1.366667	-33.483333		Prell and Damuth, 1978
V25-56	-3.550000	-35.233333		Prell and Damuth, 1978
V22-38	-9.550000	-34.250000		Prell and Damuth, 1978
A180-73	0.166667	-23.000000		Prell and Damuth, 1978
V22-174	-10.066667	-12.816667		Prell and Damuth, 1978
GL-74	-21.256250	-40.043389	1279	Portilho-Ramos et al., 2014
GL-75	-21.142222	-40.022800	1421	Portilho-Ramos et al., 2014

Table S2. Taxonomic list based in World Foraminifera Database -WoRMS (Hayward et al., 2019) of all species of planktonic foraminifera recovery from the last 1.93 Ma from core CDH-79, located in the western equatorial Atlantic (Pará-Maranhão Basin).

Kingdon: Chromista

Subkingdom: Harosa

Infrakingdom: Rhizaria

Phylum: Foraminifera

Class: Globothalamea

Subclass: Rotaliana

Order: Rotaliida

Suborder: Globigerinina

Superfamily: Globigerinitoidea

Family: Globigerinitidae

Subfamily: Globigerinitinae

Genus: *Globigerinita* Brönnimann, 1951

Specie: *Globigerinita glutinata* (Egger, 1893)

Globigerinita uvula (Ehrenberg, 1861)

Superfamily: Globigerinoidea

Family: Globigerinidae

Subfamily: Globigerininae

Genus: *Beella* Banner and Blow,1960

Beella digitata (Brady, 1879)

Genus: *Globigerina* d'Orbigny, 1826

Globigerina bulloides d'Orbigny, 1826

Globigerina falconensis Blow, 1959

Genus: *Globigerinella* Cushman, 1927

Globigerinella calida (Parker, 1962)

Globigerinella siphonifera (d'Orbigny, 1839)

Genus: *Globigerinoides* Cushman, 1927

Globigerinoides conglobatus (Brady, 1879)

Globigerinoides obliquus Bolli, 1957

Globigerinoides ruber (d'Orbigny, 1839)

Globigerinoides tenellus Parker, 1958

Genus: *Globoturborotalita* Hofker, 1976

Globoturborotalita rubescens (Hofker, 1956)

Genus: *Sphaeroidinella* Cushman, 1927

Sphaeroidinella dehiscens (Parker & Jones, 1865)

Genus: *Trilobatus* Spezzaferri et al., 2015

Trilobatus sacculifer (Brady, 1877)

Trilobatus trilobus(Reuss, 1850)

Genus: *Turborotalita* Blow& Banner, 1962

Turborotalita humilis (Brady, 1884)

Turborotalita quinqueloba (Natland, 1938)

Genus: *Globorotaloides* Bolli, 1957

Globorotaloides hexagonus (Natland, 1938)

Subfamily: Orbulininae

Genus: *Orbulina* d'Orbigny, 1839

Orbulina universa d'Orbigny, 1839

Family: Hastigerinidae

Genus: *Hastigerina* Thomson in Murray, 1876

Hastigerina pelagica (d'Orbigny, 1839)

Superfamily: Globorotalioidea

Family: Candeinidae

Subfamily: Candeininae

Genus: *Candeina* d'Orbigny, 1839

*Candeina nitida*d'Orbigny, 1839

Family: Globorotaliidae

Genus: *Globorotalia* Cushman, 1927

Globorotalia crassaformis (Galloway and Wissler, 1927)

Globorotalia hessi Bolli and Premoli Silva, 1973

Globorotalia crassaformis subsp. *imbricata* Krasheninnikov and Bylinskaya, 2002

Globorotalia ronda Blow, 1969

Globorotalia viola Blow, 1969

Globorotalia hirsuta (d'Orbigny, 1839)

Globorotalia menardii (d'Orbigny in Parker, Jones and Brady, 1865)

Globorotalia flexuosa (Koch, 1923)

Globorotalia scitula (Brady, 1882)

Globorotalia tumida (Brady, 1877)

Genus: *Globoconella* Bandy, 1975

Globoconella inflata (d'Orbigny, 1839)

Genus: *Neogloboquadrina* Bandy, Frerichs and Vincent, 1967

Neogloboquadrina dutertrei (d'Orbigny, 1839)

Neogloboquadrina incompta (Cifelli, 1961)

Neogloboquadrina pachyderma (Ehrenberg, 1861)

Family: Pulleniatinidae

Genus: *Pulleniatina* Cushman, 1927

Pulleniatina obliquiloculata (Parker and Jones, 1865)

Pulleniatina okinawaensis Natori, 1976

Table S3. List of tie-points and associated age and uncertainties. Tie-points were based on the alignments of $\delta^{18}O$ records measured in *G. ruber* (white) to the reference $\delta^{18}O$ stacks LR04 (Lisiecki and Raymo, 2005). The age uncertainty was derived from the quadratic sum of individual uncertainties, by taking into account (i) the mean resolution and dating uncertainty of the reference curve LR04 (resolution 1 kyr; uncertainty 6 kyr from 2-1 Ma and 4 kyr from 1-0 Ma; Lisiecki and Raymo, 2005), and (ii) an estimated relative alignment uncertainty (~1.04kyr) based on Govin et al. (2015).

Depth (cm)	Type	Cal yrs (ka BP)	Cal yrs min (95%)	Cal yrs max (95%)
10	AMS	16.05	15.23	16.94
20	AMS	20.93	19.74	22.20
30	AMS	26.35	24.44	28.12
40	AMS	26.44	24.51	28.27
50	AMS	29.36	26.97	32.36
60	LR04	84.00	79.87	88.13
100	LR04	93.00	88.87	97.13
130	LR04	95.52	91.39	99.65
150	LR04	98.00	93.87	102.13
170	LR04	102.00	97.87	106.13
210	LR04	109.00	104.87	113.13
230	LR04	119.00	114.87	123.13
250	LR04	123.00	118.87	127.13
278	LR04	125.96	121.83	130.09
310	LR04	135.97	131.84	140.10
330	LR04	145.00	140.87	149.13
350	LR04	154.99	150.86	159.12
360	LR04	160.00	155.87	164.13
380	LR04	171.00	166.87	175.13
390	LR04	174.00	169.87	178.13
410	LR04	185.00	180.87	189.13
420	LR04	192.00	187.87	196.13
480	LR04	200.23	196.10	204.36
510	LR04	216.97	212.84	221.10

Table S3. Continued.

550	LR04	223.00	218.87	227.13
580	LR04	229.00	224.87	233.13
610	LR04	239.27	235.14	243.40
630	LR04	245.55	241.42	249.68
650	LR04	252.00	247.87	256.13
662	LR04	255.03	250.90	259.16
720	LR04	266.47	262.34	270.60
790	LR04	277.00	272.87	281.13
800	LR04	285.42	281.29	289.55
810	LR04	288.11	283.98	292.24
830	LR04	295.00	290.87	299.13
860	LR04	315.34	311.21	319.47
878	LR04	317.00	312.87	321.13
908	LR04	329.21	325.08	333.34
1020	LR04	341.34	337.21	345.47
1083	LR04	355.00	350.87	359.13
1140	LR04	371.00	366.87	375.13
1188	LR04	389.00	384.87	393.13
1228	LR04	405.00	400.87	409.13
1240	LR04	432.90	428.77	437.03
1260	LR04	465.00	460.87	469.13
1270	LR04	491.04	486.91	495.17
1280	LR04	513.00	508.87	517.13
1300	LR04	524.00	519.87	528.13
1320	LR04	549.00	544.87	553.13
1340	LR04	575.00	570.87	579.13
1360	LR04	584.00	579.87	588.13
1376	LR04	610.00	605.87	614.13
1389	LR04	630.00	625.87	634.13
1400	LR04	644.00	639.87	648.13
1470	LR04	658.00	653.87	662.13
1490	LR04	668.00	663.87	672.13
1520	LR04	678.00	673.87	682.13

Table S3. Continued.

1570	LR04	696.42	692.29	700.55
1580	LR04	718.36	714.23	722.49
1620	LR04	746.00	741.87	750.13
1670	LR04	766.00	761.87	770.13
1680	LR04	774.00	769.87	778.13
1720	LR04	787.99	783.86	792.12
1730	LR04	802.00	797.87	806.13
1760	LR04	858.00	853.87	862.13
1780	LR04	872.87	868.74	877.00
1820	LR04	895.92	891.79	900.05
1850	LR04	915.74	911.61	919.87
1860	LR04	923.07	918.94	927.20
1870	LR04	944.00	939.87	948.13
1903	LR04	955.86	951.73	959.99
1910	LR04	961.43	957.30	965.56
1930	LR04	978.00	973.87	982.13
1960	LR04	988.00	983.87	992.13
1970	LR04	994.87	990.74	999.00
1995	LR04	1022.00	1015.91	1028.09
2020	LR04	1038.00	1031.91	1044.09
2060	LR04	1070.77	1064.68	1076.86
2090	LR04	1108.00	1101.91	1114.09
2130	LR04	1122.00	1115.91	1128.09
2140	LR04	1132.00	1125.91	1138.09
2220	LR04	1198.00	1191.91	1204.09
2240	LR04	1208.00	1201.91	1214.09
2269	LR04	1240.00	1233.91	1246.09
2310	LR04	1248.00	1241.91	1254.09
2360	LR04	1262.00	1255.91	1268.09
2410	LR04	1280.00	1273.91	1286.09
2430	LR04	1288.69	1282.60	1294.78
2450	LR04	1316.28	1310.19	1322.37
2470	LR04	1339.49	1333.40	1345.58

Table S3. Continued.

2490	LR04	1354.00	1347.91	1360.09
2520	LR04	1372.00	1365.91	1378.09
2530	LR04	1398.00	1391.91	1404.09
2560	LR04	1412.00	1405.91	1418.09
2580	LR04	1437.33	1431.24	1443.42
2590	LR04	1456.06	1449.97	1462.15
2610	LR04	1476.00	1469.91	1482.09
2628	LR04	1496.00	1489.91	1502.09
2640	LR04	1512.50	1506.41	1518.59
2690	LR04	1535.00	1528.91	1541.09
2700	LR04	1552.50	1546.41	1558.59
2740	LR04	1564.77	1558.68	1570.86
2750	LR04	1576.95	1570.86	1583.04
2767	LR04	1602.50	1596.41	1608.59
2780	LR04	1617.50	1611.41	1623.59
2790	LR04	1630.00	1623.91	1636.09
2820	LR04	1655.00	1648.91	1661.09
2890	LR04	1675.00	1668.91	1681.09
2930	LR04	1700.00	1693.91	1706.09
2950	LR04	1712.78	1706.69	1718.87
3000	LR04	1732.50	1726.41	1738.59
3020	LR04	1745.26	1739.17	1751.35
3050	LR04	1759.31	1759.31	1759.31
3080	LR04	1779.56	1773.47	1785.65
3102	LR04	1795.00	1788.91	1801.09
3132	LR04	1817.50	1811.42	1823.58
3172	LR04	1862.50	1856.41	1868.59
3202	LR04	1900.00	1893.92	1906.08

Text S1. Western equatorial Atlantic planktonic foraminifera biostratigraphic events and Biochronology

Lowest Occurrence (LO) of Globorotalia truncatulinoides (B G. truncatulinoides)

The LO of *Globorotalia truncatulinoides* (B *G. truncatulinoides;* Figure 4b) have been recorded for the first time in the Pará-Maranhã Basin at 3200 cm (presence in the residue) and had an estimated between 1.89-1.91 Ma (median age 1.90 Ma; MIS 73; Table 2). In the base of core CDH-79 (interval 3212–3070 cm), the presence of *G. truncatulinoides* is rare to absent (between zero to 0.22%) where only one individual was observed in the residue of samples 3200, 3157, 3150, 3130 and 3110 cm. The species increased in abundance in the interval above 3060 cm (1.49%; Figure 4b). The species *G. truncatulinoides* originated in the Northern Hemisphere (sub) tropical and transitional latitudes around the Chron C2n/C2r boundary (~2 Ma) and is a widespread element in Pleistocene faunas globally (Berggren et al., 1995a). Srinivasan and Sinha (1992) suggested that the first occurrence of this species coincides with the Matuyama-Gauss boundary (~2.58 Ma) in the southwest Pacific DSDP cores. But in most subtropical regions of the Atlantic and Indo-Pacific Oceans, the LO of *G. truncatulinoides* generally occurs just below the base of the Olduvai Subchron (~1.92 Ma; Channell et al., 2016) (Berggren et al., 1995b; Sinha and Singh, 2008). Although the LO of *G. truncatulinoides* has been shown diachronous between the subtropics and the tropics, wherein the tropics the species seems to have appeared isochronously (Spencer-Cervato et al., 1994, 1997; Chaisson and Pearson, 1997; Chaisson and d'Hondt, 2000). This event was recognized by different authors (e.g. Spencer-Cervato et al., 1997; Chaisson and Pearson, 1997; Lourens et al., 2004) and for the tropics has an estimated age of ~1.93 Ma confirmed by Wade et al. (2011). In records of the Gulf of Mexico, the LO of *G. truncatulinoides* occurs within the EW68 Zone P (Martin et al., 1990, 1993), which is characterized by the presence of the *G. menardii* complex, similar to the western equatorial Atlantic (CDH-79; Figure 4b.The LO of *G. truncatulinoides* was used by Blow (1969) to mark the base of Zone N22 and by Bolli and Saunders (1985) to establish the beginning of Zone *G. truncatulinoides*, both representatives of the Lower Pleistocene.

Highest Occurrence (HO) of Globigerinoides fistulosus (T G. fistulosus)

The HO of *Globigerinoides fistulosus* (T *G. fistulosus*; Figure 4b) has been recorded close to the base of the core (3130 cm) with an estimated age of 1.81-1.82 Ma (median age 1.82Ma; MIS 66; Table 2). The HO of *G. fistulosus* appears to be synchronous in the top of the Olduvai Subchron at SW Pacific and Indian Oceans (Srinivasan and Sinha, 1993; Sinha and

Singh, 2008), and consistent with its disappearance in the Atlantic (sub) tropical sites (Berggren et al. 1985b; Berggren et al. 1995b). For this reason, this event is used as a marker for the top of Zone PL6 (Berggren, 1973, 1977). This zone (PL6) was initially described from (sub) tropical-transitional areas of the Atlantic Ocean as representative of Pliocene sediments (Pleistocene according to ISC, 2019) with ages spanning from 2.30-1.77 Ma (Berggren, 1977). In our records, the species *G. fistulosus* is extremely rare, but overlapping with *G. truncatulinoides,* where the HO of *G. fistulosus* occurs above the LO *G. truncatulinoides* (Table 2), and within the EW68 Zone P (Figure 4b). A similar overlap with *G. truncatulinoides* has been demonstrated in the western equatorial Pacific in the ODP Site 806 (Chaisson and Leckie, 1993; Berggren et al., 1995a), in the eastern tropical Pacific, in the DSDP Site 503 (Keigwin, 1982), and Kennett and Srinivasan (1983) in *G. tosaensis-G. truncatulinoides* Interval (="*overlap*") Range Zone. On the other hand for Bolli and Premoli Silva (1973) the *G. fistulosus* taxon as *sensustricto* forms, calling of *Globigerinoides trilobus* cf. *fistulosus,* are correlated with the latest Pliocene. In the Ceara Rise, the HO of *G. fistulosus* has an estimated age of 1.88 Ma (Chaisson and Pearson, 1997), and later Lourens et al. (2004) provided two astronomical ages for this event, around 1.77 Ma for the ODP Site 677 (Shipboard Scientific Party, 1988; Shackleton et al, 1990) and 1.88 Ma for Site 925 (Chaisson and Pearson, 1997). However, Wade et al. (2011) suggested the age of 1.88 Ma from Ceara Rise, ounces the Site 677 present a widely spaced core catcher samples. In the Brazilian Equatorial Margin, the estimated age is closer to the Ceara Rise records (ODP Site 925; Chaisson and Pearson, 1997; Lourens et al., 2004).

Globorotalia menardii complex Disappearance Event D5 (G. menardii D5):

The first disappearance of *G. menardii* complex (*G. menardii* D5; Figures 4b) has been recorded at 3092 cm (0.5%) and marks the base of EW68 Zone Q (Subzone Q2). We present the first record of this event for the Brazilian Equatorial Atlantic, however, it was recorded in the Northwest Gulf of Mexico (ODP 625B), Caribbean Sea (DSDP 502B), and Tropical Atlantic (core V16-205) close to the HO *Discoater brouweri* and above the LO *G. truncatulinoides*, with an estimated age of ~1.80 Ma (Martin et al., 1990, 1993). This event occurs in our records above the LO *G. truncatulinoides* and HO *G. fistulosus* (Figures 4b), within MIS 64 and a median age of 1.79 Ma (1.78-1.79 Ma; Table 2). The presence of the *G. menardii* complex in high abundance recorded in the interval between the base of the core and the *G. menardii* D5 event suggests that the interval is represented by the EW68 Zone P (Martin et al. 1990). Martin et al. (1993) used the Zone P to the placement of Olduvai Subchron in core V16-205 (Tropical Atlantic) and associated this Subchron to the top of the Zone in Site 502B at the Caribbean

Highest Occurrence of Globigerinoides extremus (T G. extremus)

The HO of *G. extremus* (T *G. extremus*; Figure 4b) is close to the base of core (1% at 3070 cm), with a median age estimated of 1.77 Ma (1.77-1.78 Ma; MIS 63; Table 2). The records of this event ranging from ~2.88 Ma in the SW Pacific to ~1.80 Ma in the Indian Ocean (Berggren et al., 1985b), and later considered to be diachronous (Berggren et al., 1995b). Srinivasan and Sinha (1992) suggested that the HO of *G. extremus* is synchronous at the top of the Olduvai Subcron (C2n), however, Chaproniere et al. (1994) suggested a younger age than previously recorded, from the top of the Olduvai Subchron to the base of the Brunhes Chron at Site 838.

In the Caribbean area, the extinction level of *G. extremus* was recorded around 2.74 Ma for Site 999 (ODP Leg 165; Chaisson and D´Hondt, 2000), and in the same extinction level of *Globigerinoides trilobus fistulosus* for Sites 29, 31 (Leg 4) and 154 (Leg 15; Bolli and Premoli-Silva, 1973). However, the presence of the species overlying the *Globorotalia exilis* Subzone at Site 148 (Leg 15; Bolli and Premoli-Silva, 1973). In the Ceara Rise, the HO of *G. extremus* occurs in the lower part of the Zone N22, with an estimated age of ~1.98 Ma (Chaisson and Pearson, 1997; Lourens et al., 2004), while in the Benguela Current (ODP Leg 108) this bioevent ranging from ~1.94-1.20 Ma in the Holes 662A and 664D, and between ~2.56-1.10 Ma in the Holes 667A and 665A, respectively (Weaver and Raymo, 1989). At the Lau Basin (ODP Leg 135, Sites 834, 835, 837, and 839) and Tongan Platform (Sites 840 and 841), the event had an estimated age of ~1.80 Ma (Chaproniere et al., 1994). All these results demonstrated a considerably diachronism between the different basins. For Bolli and Sauders (1985), these differences could be the result of morphologic-taxonomic problems with recognition of the species itself. The authors considered *G. extremus* a variant of *G. obliquus*, who present a gradual transition between the forms, and your corrected recognition cannot be easy.

In Pará-Maranhão Basin (core CDH-79), the HO of *G. extremus* was recorded above the HO of *G. fistulosus,* during the EW68 Zone Q (Subzone Q2), characterized by the absence of the *G. menardii* complex, closer to the age of 1.77 Ma suggested by Berggren et al. (1995a, 1995b) and Chaproniere et al. (1994), then to the age of ~1.99 Ma presented by Wade et al. (2011).

Globorotalia menardii complex Reappearance Event R5 (G. menardii R5)

The first reappearance event of the *G. menardii* complex (R5) has been recorded at 2890 cm (~12.8%; Figure 4b) and marks the base of EW68 Zone R (Subzone R3). Observed for the first time in a Brazilian basin, this event had been recorded in the North (core V16-205), South (cores V16-39, V22-163, and V12-18) and Equatorial Atlantic (core V19-297) by Ericson and Wollin (1968), and associated to the Mutuyama Chron (C1r.2r.2r Subchron) slightly above

of Olduvai Subchron boundary. In the northeast of Gulf of Mexico (cores 625B and E67-135), Columbian Basin (core 502B) and North Atlantic (core V16-205), Martin et al (1993) recorded this event above the Olduvai Subchron as well and estimated age around 1.50-1.40 Ma for the zonal boundary Q/R (subzone boundary Q1/R3) based on HO of *Calcidiscus macintyrei* (~1.45 Ma; Backman et al., 1983; Berggren et al., 1985b). However, the revision of the calcareous nannofossil datum presented by Raffi et al. (2006) including astronomical calibration (ATNTS2004; Lourens et al., 2004), shows an age around 1.60 Ma for this event, which suggests a slightly older age for zonal boundary Q/R. In our records, this event occurs with MIS 59 and estimated age between 1.67-1.68 Ma (median age 1.68 Ma; Table 2), closer to the HO of *C. macintyrei* presented for Raffi et al. (2006).

Highest Occurrence of Globoturborotalia obliquus (T G. obliquus):

The HO of *G. obliquus* has been recorded at 2610 cm (0.25%; Figure 4b), with the lowest values of MIS 49, and an estimated median age of 1.48 Ma (1.47-1.48 Ma; Table 2). At Ceara Rise (Site 925), this event had an estimated age of ~1.30 Ma (Chaisson and Pearson, 1997; Lourens et al., 2004). The same age was observed at Canary Current in the eastern tropical Atlantic (Hole 658A Leg 108) by Weaver and Raymo (1989), and in the Site 999 at the western Caribbean Sea as well (Chaisson and D´Hondt, 2000). Those Pleistocene ages are younger than the Pliocene age suggestion by Kennett and Srinivasan (1983) and Bolli and Saunders (1985) and recorded for Chaisson and Leckie (1993) at the western Equatorial Pacific (Ontong Java Plateau, Site 806), showing a diachronism between the basins.

Highest Occurrence of Globorotalia tosaensis (T G. tosaensis):

The HO of *G. tosaensis* has been recorded at 2050 cm (0.26%; Figure 4b), within MIS 31 and a median age of 1.07Ma (1.06-1.07 Ma; Table 2). This event presented a variable chronostratigraphic position. In the Equatorial Pacific Thompson and Sciarrillo (1978) recording this event ranging from the upper Matuyama Chron (above the Jaramillo Subchron) to the lower Brunhes Chron (~0.60 Ma), while a set of DSDP cores evaluated by Hills and Theirstein (1989) show its position spanning from the upper Matuyama Chron to within the Brunhes Chron. The authors have estimated a mean age for the HO of *G. tosaensis* around 0.89 Ma, slightly above the Jaramillo Subchron. The HO of *G. tosaensis* usually has been found above the HO of *G. crassaformis hessi* (e.g. Berggren et al. 1995a, b; Wade et al., 2011), however, Chaproniere et al. (1994), recorded an inverse sequence at Lau Basin (Site 834). The authors record this event spanning from within the Jaramillo Subchron (Sites 834, 838, and 839) to a

level between the Jaramillo Subchron and below the Brunhes Chron (Site 837). At Sites 835 and 836, this event occurs within Brunhes Chron but was considered reworked by the authors.

In the southeastern Brazilian Continental Margin, the HO of *G. tosaensis* has not been observed in the records of the last ~0.62 and 0.77 Ma presented by Ferreira et al. (2012) and Toledo et al. (2016), respectively. However, Toledo et al. (2016) recorded the HO of *G. crassaformis hessi* witch estimated age around 0.77 Ma, suggesting that the HO of *G. tosaensis* can occur below this event in the Santos Basin, as observed at Lau Basin Site 834 by Chaproniere et al. (1994). In our record (Pará-Maranhão Basin), this event has been recorded below the HO of *G. crassaformis hessi* as well, an age that permits correlate with the lower Jaramillo Subchron (~1.07 Ma, Table 2).

Globorotalia menardii complex Disappearance Event D4 (G. menardii D4)

The second disappearance event of *G. menardii* complex (*G. menardii* D4), have been recorded for the first time in a Brazilian basin at 2032 cm (0%). This event occurs during the MIS 30 and marks the base of EW68 Zone S (Subzone S2; Figure 4b). The *G. menardii* D4 event had been recorded during the Matuyama Event in North (core V16-205), South (cores V16-39, V22-163, and V12-18) and Equatorial Atlantic (core V19-297) by Ericson and Wollin (1968), and in the Caribbean Sea (core 502B) and northeast of Gulf of Mexico by Martin et al. (1990, 1993) as well. Ericson and Wollin (1968) suggested an age around 1.40 Ma for the base of Zone S, however, Martin et al. (1993) based on HO *Helicosphaera selll* (~1.30; Berggren et al., 1985; Raffi et al., 2006) suggested an age ~1.20 Ma for this boundary. In our records, this event had an estimated median age of 1.05 Ma (1.04-1.06 Ma; MIS 30; Table 2), a younger age (~0.25 Ma) that presented in the previous work.

Globorotalia menardii complex Reappearance Event R4 (G. menardii R4)

The second reappearance event of *G. menardii* complex (*G. menardii* R4), had been recorded for the first time in a Brazilian basin at 1912 cm (1.84%) and marks the base of EW68 Zone T (Subzone T4; Figure 4b). This event had been recorded close to the base of Jaramillo Subchron (Subchron C1R.1N) in the North (core V16-205) and South Atlantic (cores V12-18, V16-39, and V22-163) by Ericson and Wollin (1968). Martin et al. (1990) record this boundary at MIS 24/25 boundary in the northeast Gulf of Mexico (core 625B), and MIS 25/26 boundary in the Columbia Basin (core 502B) and tropical Atlantic (core V16-205). According to Martin et al. (1993), the S/T (S1/T4) boundary occur within MIS 24-25 (~0.94 Ma), however, in the western Atlantic Ocean (ODP Leg 164, Hole 997A; Nishi et al., 2000) this boundary has been recorded close to the top of Jaramillo Subchron (~0.99 Ma; MIS 27/28; Berggren et al., 1995a).

In our records, the event *G. menardii* R4 occurs within MIS 26, slightly below the MIS 25/26 boundary, with an estimated median age of 0.96 Ma (0.96-0.97 Ma; Table 2).

Lowest Occurrence of Globorotalia crassaformis (B G. crassaformis hessi):

The LO of *G. crassaformis hessi* has been recorded at 1692 cm (0.81%), during the EW68 Zone T (Subzone T3), with an estimated age of 0.77-0.78 Ma (median age 0.78 Ma; MIS 19; Figure 4b) for our records. The LO of *G. crassaformis hessi* was first described by Bolli and Premoli Silva (1973) in the Cariaco Basin (ODP Leg 15 - Site 147) and used for the authors as a Caribbean index for the base of Lower Pleistocene Subzone *G. crassaformis hessi*. This Subzone extends from the HO of the zonal marker to the HO of *Globigerina calida calida* (Upper Pleistocene). The LO of *G. crassaformis hessi* event had been used for zonal subdivision in the Indian Ocean (DSDP Leg 27 – Site 262; Rögl, 1974), the North (DSPD Leg 48; Krasheninnikov, 1979) and South Atlantic (DSDP Leg 74; Pflaumann, 1988) as well. In the eastern Coral Sea of Australia, Chaproniere (1991) recorded the LO of *G. crassaformis hessi* during the MIS 17, below the last occurrence of *G. tosaensis* and in the lower part of the Brunhes Chron. While in the Lau Basin sites (Leg 135; Chaproniere et al., 1994) this bioevent was considered variable, where the oldest occurrence had been recorded just below the Cobb Moutain Subchron (Sites 838 and 839), and within the Matuyama Chron immediately above the Jaramillo Subchron (Sites 835 and 837).

In the revision presented by Berggren et al. (1995a), the authors suggested a corresponding age ~0.75 Ma for this event. Bylinskaya (2005) revised the stratigraphic ranges of *G. crassaformis* subspecies from Equatorial to Subarctic region (DSDP Site 25 - 0° 31’ S, 39° 31’ W to DSPD Site 408 - 63° N), and reported ages spanning from upper lower Pliocene (~4.5 Ma; Site 397 - 26° 50´ N) to Lower Pleistocene (age, DSDP Sites 403 and 406 - 55° - 56° N). Based on those observations the author suggested that the first occurrence of this subspecies is a strongly diachronous event in different climatic realms, and the Quaternary *G. crassaformis hessi* Subzone (Bolli and Premoli Silva, 1973) represent an acme zone in tropical/subtropical areas. However, the last revision of the Cenozoic tropical planktonic foraminiferal biostratigraphy presented by Wade et al. (2011) supported the age around 0.75 Ma suggested by Chaproniere et al. (1994) and Berggren et al. (1995a, 1995b). This event had been recorded in the Santos Basin, southeastern Brazilian Continental Margin, with an estimated age of ~0.77 Ma (MIS 19; Toledo et al., 2016). In our records the lowest occurrence of *G. crassaformis hessi* had been recorded around 0.78 Ma, closer to the ages suggested by Chaproniere (1991); Chaproniere et al. (1994), Berggren et al. (1995a, 1995b), Wade et al. (2011), and Toledo et al. (2016).

Globorotalia menardii complex Disappearance Event D3 (G. menardii D3):

The third disappearance event of *G. menardii* complex (*G. menardii*D3), has been recorded at 1370 cm (0.82%) and marks the base of EW68 Zone U (Figure 4a). In the Northeastern Gulf of Mexico this event had been recorded in the Lagniappe Delta with an estimated age of ~0.61 Ma (Kohl et al., 2004), and in the lower part of Brunhes Chron (C1N) at Caribbean Sea (core 502B), the Northeast Gulf of Mexico (cores 625B and E67-135), and the Tropical Atlantic (core V16-205) as recorded by Martin et al. (1990; 1993). These authors reported further a stratigraphic anomaly (high sedimentation rate) for this interval, assuming ages between 0.62-0.52 Ma for the zonal boundary T/U. In southeastern Brazilian Continental Margin, this event had been recorded in the Santos Basin cores BS-C (Ferreira et al., 2012) and GL-854 (Toledo et al., 2016), where the last authors estimated the age of ~0.63 Ma (MIS 16) for this event. At CDH-79 the disappearance event of *G. menardii* complex had been recorded close to an increase in $\delta^{18}O$ values, during the MIS 15 (Figure 4b), with an estimated median age of 0.59 Ma (0.58-0.59; Table 2).

Globorotalia menardii complex Reappearance Event R3 (G. menardii R3)

The third reappearance event of *G. menardii* complex (*G. menardii*R3), has been recorded at 1312 cm (9.52%) and marks the base of EW68 Zone V (Subzone V3; Figure 4a). The reappearance of *G. menardii* complex was observed closer to the HO of *Pseudoemiliania lacunosa*, during the Brunhes Chron, in the Northeast Gulf of Mexico (core 625B), the Caribbean Sea (core 502B) and the Tropical Atlantic (core V16-205) by Martin et al. (1993). This event had an estimated age of ~0.48 Ma for the Northeastern Gulf of Mexico (Kohl et al., 2004) and observed in the western Caribbean Sea during the MIS 13 (ODP Site 999A; Martinez et al., 2007). In southeastern Brazilian Continental Margin, this event had been recognized in the Santos Basin cores BS-C and BS-D by Ferreira et al. (2012) and core GL-854 by Toledo et al. (2016), who estimated the age around 0.49 Ma (MIS 13). In Brazilian Equatorial Margin (core CDH-79), the event is recorded in the MIS 13/14 boundary, within the Termination VI (MIS 14, 0.53 Ma), and had an estimated median age of 0.54 Ma (0.53-0.54 Ma; Table 2).

Highest Occurrence of Globorotalia crassaformis hessi (T G. crassaformis hessi):

The HO of *G. crassaformis hessi* has been recorded at 920 cm (0.32%; Figure 4a), within MIS 9/10 boundary and median age 0.33 Ma (0.32-0.33 Ma; Subzone V2; Table 2). This event had been recorded by Bylinskaya (2005) near to the top of Bolli and Saunders (1985) Zone *G. calida calida* witch age range between 0.20-0.10 Ma for the tropical Atlantic. However, in the

southeastern Brazilian Continental Margin, this event had been recognized in the Santos Basin with a mean age of ~0.058 Ma (MIS 4; Toledo et al., 2016). This age difference suggests a wide range for this event, and a possible HO of *G. crassaformis hessi* in the Equatorial Atlantic, followed by a latter occurrence in the North and South Atlantic.

Globorotalia menardii complex Disappearance Event D2 (G. menardii D2)

The fourth disappearance event of *G. menardii* complex (*G. menardii*D2), has been recorded at 352 cm (0%) and marks the base of EW68 Zone W (Subzone W2; Figure 4a). The disappearance of *G. menardii* complex had been recorded in the Gulf of Mexico with an age between 0.20–0.18 Ma (MIS 7) for Martin et al. (1990; 1993) and Kohl et al. (2004) respectively. In the Caribbean Sea, this bioevent had registered at the MIS 7/6 boundary by Martin et al. (1990), and along with the MIS 6 by Martinez et al. (2007). For the southeastern Brazilian Continental Margin, this event had recorded at ~0.142 Ma (MIS 6b; Toledo et al., 2016), while in our records occur around 0.16 Ma (0.15-0.16 Ma; MIS 6). This diachronism suggests that the disappearance of the complex initially occurred in the northern hemisphere, later in the Equatorial Atlantic, and extended in the southeastern Brazilian Continental Margin.

Lowest Occurrence of Globigerinella calida calida (B G. calida calida):

The LO of *G. calida calida* has been recorded at 320 cm (0.43%), during the EW68 Zone W (Subzone W1) with the estimated median age of 0.14 Ma (0.14-0.15 Ma; MIS 6; Figure 4a). The LO of this species was first recorded in the upper part of the early Pliocene Zone N19 (~4.70 Ma) by Kennett and Srinivasan (1983). But Bolli and Premoli Silva (1973) had been recorded and used this bioevent as a Caribbean marker for the top of *G. crassaformis hessi* Subzone, with an age estimated ~0.14 Ma (Table 2). Later Chaproniere et al. (1994) and Berggren et al. (1995a, 1995b) suggested an age around 0.220 Ma, which was confirmed by Wade et al. (2011). In southeastern Brazilian Continental Margin, this event had been recorded between ~0.137-0.133 Ma (cores GL-854 and GL-852; Toledo et al., 2016; Table 2), at the beginning of MIS 6a and during de EW68 Zone W.

Globorotalia menardii complex Reappearance Event R2 (G. menardii R2)

The fourth reappearance event of *G. menardii* complex (*G. menardii* R2; Figure 4a), has been recorded at 290 cm (1.62%). This bioevent marks the base of EW68 Zone X (Subzone X3) and appears to be synchronous bioevent from the Caribbean Sea to the southeastern Brazilian Continental Margin, with ages around 0.130-0.129 Ma (Kohl et al., 2004; Martinez et al., 2007; Ferreira et al., 2012; Toledo et al., 2016). In our material, this bioevent had been recorded

within the MIS 5/6 boundary together with the Termination VII, estimated median age of 0.13 Ma (0.13-0.14 Ma; Table 2).

Highest Occurrence of Globorotalia flexuosa (T G. flexuosa) and Globorotalia menardii complex Disappearance Event D1 (G. menardii D1)

The HO of *G. flexuosa* and the fifth disappearance event *of G. menardii* complex (*G. menardii* D1) have been recorded at 70 cm (4.46%) and 60 cm (0%), respectively. The HO of *G. flexuosa* had been recorded at the west Florida continental slope (ODP Leg 100 – Hole 625B) with an estimated age of ~0.068 Ma by Joyce et al. (1990). This age was revised to around 0.070 Ma by Berggren et al. (1995a, 1995b) and Wade et al. (2011). In the southeastern Brazilian Continental Margin, this event had been recorded in Campos (e.g. Portilho-Ramos et al., 2014) and Santos Basin (e.g. Ferreira et al., 2012), where Toledo et al., (2016) suggested an age around 0.088 Ma. In our records, the HO of *G. flexuosa* occurs within an estimated median age of 0.085 Ma (0.080-0.085 Ma; Table 2) at the top of EW68 Zone X (Subzone X1), during MIS 5 (Figure 4a), and occurring below the *G. menardii* D1 event.

The *G. menardii*D1event marks the base of EW68 Zone Y and has an estimated age range between 0.090–0.084 Ma in the Gulf of Mexico (e.g. Martin et al., 1990, 1993; Kohl et al., 2004) and southeastern Brazilian Continental Margin (e.g. Vicalvi, 1997; Portilho-Ramos et al., 2006; Ferreira et al., 2012; Toledo et al., 2016). The occurrence of the *G. menardii* complex observed in the interval 60-62 cm (8.92%) had an estimated age between 0.069-0.0083 Ma (median age 0.077 Ma).

Text S2. Ericson and Wollin (1968) Zones and Subzones of the Western Equatorial Atlantic

The presence of the *G. menardii* complex between the base of core CDH-79 (3212 cm; MIS 73; 1.90-1.93 Ma) and the *G. menardii* D5 event (3092 cm; MIS 63/64; 1.78-1.79 Ma) suggests that this interval is represented by the EW68 Zone P (Table 3; Martin et al. 1990, 1993). Martin et al. (1990) associate the top of Zone P to the base of Olduvai Subchron and recorded the first disappearance of the *G. menardii* complex (*G. menardii*D5 – top of Zone P) during the Olduvai event. This further correlates to the LO of *G. truncatulinoides* (~1.93 Ma; Wade et al., 2011) and the HO of *Discoaster brouweri* (~1.95 – 1.92 Ma – Zone NN18-NN19; Raffi et al., 2006) in the Gulf of Mexico as well. In our records, the Zone P presents an accumulation rate of ~0.94 cm/kyr and recorded the LO of *G. truncatulinoides* (~3200 cm - 1.89-1.91 Ma; Table 2; Figure 4b).

The first disappearance of *G. menardii* complex marked by *G. menardii* D5 event followed by the first reappearance *G. menardii* R5event (2892 cm; MIS 60; 1.67-1.68 Ma; Table 2) is associated to the base and top of EW68 Zone Q, respectively (Figure 4b). This Zone is characterized by the near absence of the *G. menardii* complex (Ericson and Wollin, 1968). Following Martin et al. (1990, 1993), our records had been divided into two subzones; Subzone Q2 (estimated median age 1.80-1.74 Ma; Table 3) is characterized by the lower abundance of the *Pulleniatina* complex, varying between 3-18% (mean 10.19%), and *G. truncatulinoides* and *G. inflata* (mean 1.96% and 0.03% respectively; Figure 4b), showing an accumulation rate ~1.67 cm/kyr. While the Subzone Q1 is marked by higher *Pulleniatina* complex values (7-20%, mean 13.86%), and *G. truncatulinoides* and *G. inflata* (mean 4.96% and 1.30%, respectively), and accumulation rate 1.67 cm/kyr (Table 3). The boundary Q2/Q1 (3002 cm, 1.73-1.74 Ma) occurs within MIS 61/62 and is marked by the increase in abundance of *Pulleniatina* complex, following by *G. truncatulinoides* and *G. inflata* (Figure 4b). The abrupt reappearance marked by the *G. menardii* R5 event (Table 2) marks the Zonal boundary Q/R.

The presence of *G. menardii* complex between the *G. menardii*R5 event and the disappearance event marked by *G. menardii* D4 (2032 cm; MIS 30; 1.04-1.06 Ma) were associated with the base and top of EW68 Zone R, respectively (Figure 4b). This Zone is characterized by the presence of *G. menardii* complex (Ericson and Wollin, 1968), and can be divided into three subzones following Martin et al. (1990, 1993). The Subzone R3 had an accumulation rate of ~2.41 cm/kyr (Table 3) and is marked by the high abundance of the *G. menardii* complex (mean 12.42%), while *Pulleniatina* complex and *G. truncatulinoides* presented intermediate abundance (10.70% and 1.05%, respectively). The species *G. inflata* undergoes a sharp fall after the boundary Q1/R3 (*G. menardii* R5 event; Figure 4b) as observed by Martin et al. (1990). The boundary R3/R2 (1.65-1.66 Ma, Table 3) is marked by a sharp fall in the abundance of *G. menardii* complex followed by the increase in *G. truncatulinoides*, occurring above to the MIS 58/59 boundary (Figure 4b). Subzone R2 is marked by the highest abundance of the *Pulleniatina* complex and *G. truncatulinoides*, ranging from ~3.70-30.23% and zero to 14.43% respectively, while the *G. menardii* complex presents it lowest abundances recorded along with Zone R (mean 0.38%) as observed by Martin et al. (1990). The Subzone has been recorded between the MIS 58-41, presented an accumulation rate of ~1.13 cm/kyr (Table 3) and the HO of *G. obliquus* (T *G. obliquus*; Table 2). The boundary R2/R1 (1.32-1.31 Ma; Table 3) occurs within MIS 41, and marked by the increase in the abundance of the *G. menardii* complex, while the *Pulleniatina* complex shows a small fall followed by the increase in its abundance, while *G. truncatulinoides* shows a marked increase followed by a sudden drop in its abundance (Figure 4b). The Subzone R1 is marked by the return of a high abundance

of *G. menardii* and *Pulleniatina* complex (mean 12.18% and 9.02%), while *G. truncatulinoides* shows an abundance decrease (mean 0.91 %). With an accumulation rate of ~1.60 cm/kyr (Table 3), the HO of *G. tosaensis* (T *G. tosaensis*, MIS 31, 1.06-1.07 Ma; Table 2) was recorded in the upper part of this Subzone. The abrupt disappearance marked by the *G. menardii* D4 event (Table 2) marks the Zonal boundary R/S (Subzones R1/S2).

The second disappearance event of the *G. menardii* complex (*G menardii*D4) and second reappearance event of the complex (*G. menardii* R4; 0.96-0.97 Ma; MIS 26) marks the base and top of the EW68 Zone S (Table 2).In addition to the absence of the *G. menardii* complex, this Zone is marked by the presence of *G. inflata*, which reappears after the *G menardii* D4 event. This species strongly declines about the *G. menardii*R4 event, helping the recognition of the zonal boundary S/T (R1/S2 boundary). The Zone S can be divided into two subzones, where Subzone S2 spanning from MIS 30-28 and presented an accumulation rate of ~1.18 cm/kyr (Table 3). This Subzone is marked by the highest abundance of the *Pulleniatina* complex (between 5.36-14.73%; mean 8.96%), while *G. truncatulinoides* presents intermediate values ranging from 1.83-9.28% (mean 4.05%), and *G. inflata* has its highest abundance peaks along the Subzone (Figure 4b). The boundary S2/S1 (1962 cm, MIS 28; 0.99-1.00 Ma, Table 3) is marked by *G. truncatulinoides* increase, followed by a sharp fall of the *Pulleniatina* complex. The downward tendency presented by the *Pulleniatina* complex at the S2/S1 boundary and its virtual disappearance characterizes Subzone S1, where the complex varied between the total absence and 0.23% (average 0.16%). Also, this Subzone shows the highest abundance of *G. truncatulinoides* (between 6.19-9.41%, mean 8.47%) and a stable presence of *G. inflata* (between 1.03-1.77%, mean 1.35%). This subzone spans from MIS 28-26/27 boundary and presents an accumulation rate of ~1.92 cm/kyr (Table 3). The abrupt reappearance marked by the *G. menardii* R4 event marks the zonal boundary S/T (Subzones S1/T4).

This is followed by the second reappearance event of *G. menardii* complex (*G. menardii* R4) and the third disappearance event (*G. menardii*D3; MIS 15; 0.58-0.59Ma) outlining the base and top of the EW68 Zone T, respectively (Table 1). This Zone is characterized by the constant presence of the *G. menardii* complex, except for Subzone T2. This Zone can be divided into four Subzones following Martin et al. (1990, 1993). The Subzone T4 had an accumulation rate of ~1.41 cm/kyr, and spanning from MIS 26-22 (Table 3; Figure 4b). This Subzone is marked by the high abundance of the *Pulleniatina* complex (between 0.29-15.14%; mean 7.84%), while the *G. menardii* complex shows values between 1.84-22.59% (mean 14.35%), and *G. truncatulinoides* range from absence to 1.57% (mean 0.58%).The boundary T4/T3 (1802 cm, MIS 22; 0.88-0.89Ma, Table 3) is defined by the sharp drop in *Pulleniatina* complex abundance followed by a slight increase in *G. truncatulinoides* values. In

the northeast of Golf of Mexico, Martin et al. (1993) suggested an age around 0.9-0.7 Ma for this boundary based on the position of the base of Brunhes Chron (core 625B) and the near to the top of the Jaramillo reversal in the Caribbean Sea and tropical Atlantic (cores 502B and V16-205). Just above the T4/T3 boundary, an abundance peak of *G. inflata* is recorded and repeated along with the subzone T3.The subzone T3 is marked by the upward decrease in the *G. menardii* complex abundance, followed by the low abundance of *Pulleniatina* complex (between 0- 0.38%, mean 0.22%) and intermediate values of *G. truncatulinoides.* This subzone presents an accumulation rate of ~ 1.27 cm/kyr spanning from MIS 22-17.In our records, the LO of *G. crassaformis hessi* occurs in this subzone (Table 2). The boundary T3/T2 (1562 cm, MIS 17; 0.69-0.71Ma, Table 3) is marked by a complete disappearance of the *G. menardii* complex followed by the increase in the *Pulleniatina* complex and *G. truncatulinoides.*

Subzone T2 is marked by the absence of the *G. menardii* complex, while the *Pulleniatina* complex presents the highest abundances (23-17.84%; mean 8.12%).Is also recorded the highest values of *G. truncatulinoides* (4.04-11.14%, mean 6.25%), and an abundance peak of *G. inflata* in the base of the Subzone (2.29%, 1560 cm), and an accumulation rate ~2.19 cm/kyr (Table 3). The boundary T2/T1 (1500 cm, MIS 16; 0.67-0.68 Ma, Table 3) is characterized by the return of the *G. menardii* complex followed by the decrease of the *Pulleniatina* complex as well as *G. truncatulinoides*. The Subzone T1presented an accumulation rate of ~1.85 cm/kyr, spanning from slightly above MIS 16 to the base of MIS 15. This Subzone is marked by the presence of the *G. menardii* complex (4.49-29.59%; mean 18.13%), while the *Pulleniatina* complex (0-1.20%, mean 0.14%) and *G. truncatulinoides* (0-4.73%, mean 0.87%) are rare, and *G. inflata* is absent. The abrupt disappearance labeled as *G. menardii* D3 event (Table 2) marks the zonal boundary T/U (Subzones T1/U).

The third disappearance event of *G. menardii* complex (*G. menardii*D3) and the third reappearance event of the complex (*G. menardii* R3; MIS 13/14; 0.53-0.54 Ma) correspond to the base and top of the EW68 Zone U (Table 2). This Zone had an accumulation rate of ~1.06 cm/kyr, spanning from MIS 15-14. Martin et al. (1990) recorded this Zone at the same interval (between MIS 15-14) in the northeast of the Gulf of Mexico (core 625B), and in the Caribbean Sea and Tropical Atlantic (cores 502B and V16-205), as well as the southeastern Brazilian Continental Margin (core GL-854; Toledo et al., 2016). The Zone U is marked by a high abundance of *G. truncatulinoides* (4.52-8.06%, mean 6.71%), extremely low levels of the *Pulleniatina* complex (0-0.23%, mean 0.05%) and the absence of *G. inflata*. During the Zone, the abundance of the *Pulleniatina* complex varied (Figure 4b). This Zone was not subdivided into subzone and the abrupt reappearance marked by *G. menardii*R3 (Table 2) represents the zonal boundary U/V (Subzones U/V3).

The third reappearance event of *G. menardii* complex (*G. menardii* R3) and the fourth disappearance event of the complex (*G. menardii*D2; MIS 6; 0.15-0.16 Ma) mark the base and top of the EW68 Zone V (Table 3). This Zone can be divided into three following Martin et al. (1990, 1993), where Subzone V3 has an accumulation rate of~1.60 cm/kyr, spanning from MIS 13/14 boundary to MIS 9. During this subzone, the highest abundance of the *G. menardii* complex occurred (6.78-24.18%, mean 13.50%) next to a stable abundance of *G. truncatulinoides* (0-7.47%, mean 3.79%), whereas the *Pulleniatina* complex showed a set of disappearance and reappearance events with the lowest values for the entire Zone V (0-8.17%; 0.33%). In this Subzone, the presence of *G. inflata* (between zero and 0.28%, average 0.02%) is extremely rare. The *Pulleniatina* complex's disappearance and reappearance events had been previously recorded in the Subzone V3 by Ferreira et al. (2012) in the southeastern Brazilian Continental Margin (Santos Basin; core BS-C and BS-D; Table 4).In the Santos Basin, those events were labeled for a local correlation between cores as V*P*.1*,* V*P*.3, V*P*.5*,* andV*P*.7 each representing the disappearance of the complex, and V*P*.2*,* V*P*.4, V*P*.6*, and* V*P*.8 representing the reappearance events (Table 4). However, the estimated ages suggested for these events in Santos Basin are slightly older than observed in our records, except for the V*P*.1 bioevent which is first recorded in core CDH-79. The V3/V2 boundary (982 cm, MIS 10, ~0.34 Ma; Table 3) is marked by the drop in the abundance of the *G. menardii* complex and *G. truncatulinoides*, while the *Pulleniatina* complex reappears in the record (V*P*.8; Ferreira et al., 2012). Martin et al. (1990) recorded this subzones boundary within the MIS 10/11, suggesting an age around ~0.40 Ma, and thus slightly older than recorded in core CDH-79.

The Subzone V2 presented an accumulation rate of ~3.75 cm/kyr and has been recorded within MIS 9-8. Throughout this Subzone a gradual increase in the abundance of the *G. menardii* and the *Pulleniatina* complex co-occur, ranging from 0.23-23.53% (mean 13.36%) and 0.46-10.60% (mean 5.11%) respectively. The constant presence of the *Pulleniatina* complex opposed by intermediate mean values distinguishes between subzones V3 and V2.Throughout Subzone V2 an abundance increase of *G. truncatulinoides* can be observed, reaching the highest values close to MIS 8/9 boundary. The HO of *G. crassaformis hessi* (T *G. crassaformis hessi*; Table 1) was also recorded during this Subzone. The boundary V2/V1 (0.26 Ma; Table 3) is marked by the dropped of *G. menardii* complex and *G. truncatulinoides* abundances, while the *Pulleniatina* complex shows a small increase (Figure 4a). The subzone V1 spans from MIS 8-6, with an accumulation rate of ~3.34 cm/kyr. This Subzone shows the lowest abundances of the *G. menardii* complex (between 0-21.39%; mean 9.69%) and *G. truncatulinoides* (between 0-6.30%; mean 2.22%) in the Zone V, while the *Pulleniatina* complex

presents the highest mean (5.94%). The abrupt disappearance marked by *G. menardii*D2 (Table 2) marks the zonal boundary V/W (Subzones V1/W2; Figure 4a).

The fourth disappearance event of *G. menardii* complex (*G. menardii*D2) and the fourth reappearance event of the complex (*G. menardii* R2; MIS 5/6; 0.13-0.14 Ma) mark the base and top of the EW68 Zone W (Table 2). This Zone can be divided into two and occurs at the top of MIS 6 (Figure 4a). The Subzone W2 was characterized by the highest abundances of *G. truncatulinoides* (5.54-10.90%, mean 7.68%), *G. crassaformis* complex (0.41-0.64%, mean 0.51%) and *G. inflata* (0-0.85%, mean 0.56%) with an accumulation rate of ~2.12 cm/kyr. The boundary W2/W1 (0.14-0.15 Ma, Table 3) is marked by the sharp fall in the abundance of *G. truncatulinoides,* followed by the *G. crassaformis* complex and *G. inflata.* Ferreira et al. (2012) suggested an age between 0.16-0.14 Ma for this subzone boundary following the zonal boundary V/W of Kohl et al. (2014) (~0.18 Ma; *G. menardii* D2) to estimate the W2/W1 boundary in the cores BS-C and BS-D (Santos Basin). The Subzone W1 is characterized by the lower abundances of *G. truncatulinoides* (2.36-2.81%, mean 2.58%), followed by the *G. crassaformis* complex (0-0.21%, mean 0.11%), and the absence of *G. inflata*. This Subzone had an accumulation rate of 2.87 cm/kyr. The abrupt reappearance of the *G. menardii* complex, *G. menardii* R2 event (Table 2) marks the zonal boundary W/X (Subzones W1/X3).

The fourth reappearance event of *G. menardii* complex (*G. menardii*R2) and the fifth disappearance event of the complex (*G. menardii* D1; MIS 5; 0.07-0.08 Ma) mark the base and top of the EW68 Zone X (Table 2). This Zone occurs within MIS 5, and the oscillation of *G. menardii*, *Pulleniatina,* and *G. crassaformis* complexes allow the division of the Zone into three parts. The Subzone X3 is characterized by the highest abundances of the *G. menardii*(1.62-19.23%; mean 10.53%) and *G. crassaformis* complex (0.51-2.31%, mean 1.04%), and *G. flexuosa* (0.17-5.59%, mean 3.02%), while *G. truncatulinoides* occurs with the lowest values (0.28-6.06%, mean 3.82%). This Subzone had an accumulation rate of ~4.11 cm/kyr, and the most negative values of $\delta^{18}O$ are observed along the MIS 5 (Figure 4a).The X3/X2 boundary (222 cm; ~0.11-0.12 Ma, Table 3) shows a sharp drop in the abundance of the *G. menardii* and *G. crassaformis* complex, while *G. truncatulinoides* increase. An age between 0.118-0.115 Ma was estimated for the Santos Basin by Ferreira et al. (2012), showing a good correlation with our records. Within accumulation rate ~4.66 cm/kyr, the Subzone X2 is characterized by the lowest abundances of the *G. menardii* complex (0-0.51%, mean 0.12%) and *G. crassaformis*(0-0.85%, mean 0.38%), followed by a sharp drop in *G. flexuosa* (0-0.26%, mean 0.05%), while *G. truncatulinoides* occurs with the highest abundances (3.67-12.61%, mean: 8.91%).Near the top of the Subzone, a sharp fall in the abundance of the *Pulleniatina* complex is followed by an increase in the *G. menardii* complex and the lowest values of *G. truncatulinoides*. These events

characterize the X2/X1 boundary (92 cm, 0.087-0.089 Ma; Table 3). Ages suggested previously for this boundary in the Santos Basin (~0.099-0.093 Ma) by Ferreira et al. (2012) is slightly older than our records.

The Subzone X1 is characterized by the return of the *G. menardii* complex (0.72-10.26%, mean 7.10%), while the *Pulleniatina* complex (1.91-18.91%, mean 7.31%) exhibits high abundance peak followed by a sharp fall and later disappearing from the record at the top of Zone X (top of Subzone X1). *G. truncatulinoides* occurs with intermediate values (1.21-8.11%, mean 5.01%). The Subzone had an accumulation rate of ~3.28 cm/kyr. Near the top of the Subzone have been recorded the HO of *G. flexuosa* (T *G. flexuosa*; Table 2). The abrupt disappearance marked by the *G. menardii* D1 event (Table 2) mark the Zonal boundary X/Y (Subzones X1/Y).

The fifth disappearance event of the *G. menardii* complex (*G. menardii* D1; ~0.069-0.083 Ma) marks the base of EW68 Zone Y (Table 2). This zone is marked by the virtual absence of the *G. menardii* complex (Figure 4a), and by the fall of *G. crassaformis* complex abundance, while *G. truncatulinoides* increase during this Zone. The absence of the *G. menardii* and the *Pulleniatina* complex suggests that the top of our record correlates with the Subzone Y1B (Ferreira et al., 2012). The ages obtained by AMS ^{14}C for the intervals 50 to 10 cm (~0.030-0.016 Ma; Table 1) supporting the suggestion of the presence of the EW68 Zone Y, represented by the Subzone Y1B.

References

Berger, W.H., Bickert, T., Schmidt, H., Wefer, G., 1993. Quaternary oxygen isotope record of pelagic foraminifers: Site 806, Ontong Java Plateau. In: Berger, W.H., Kroenke, L.W., Mayer, L.A., et al., Proc. ODP, Sci.Results, 130: College Station, TX (Ocean Drilling Program), 381–395.

Berggren, W. A., Kent, D. V., van Couvering, J. A., 1985a. Neogene geochronology and chronostratigraphy. In: Snelling, N. J., (Ed.), The chronology of the geological record. Geological Society of London Memoir, 10, 211–250.

Berggren, W. A., Kent, D. V., Flynn, J. J., van Couvering, J. A., 1985b. Cenozoic geochronology. Geological Society of America Bulletin, 96, 1407–1418.

Berggren, W.A. 1977. Late Neogene planktonic foraminiferal biostratigraphy of DSDP Site 357 (Rio Grande Rise). Initial Reports of the Deep Sea Drilling Project, 29, 591-614.

Berggren, W.A., 1973. The Pliocene time scale: calibration of planktonic foraminifera and calcareous nannoplankton zones. Nature, 243, 391-397.

Berggren, W.A., Hilgen, F.J., Langereis, C.G., Kent, D.V., Obradovich, J.D., Raffi, I., Raymo, M.E., Shackleton, N.J., 1995a. Late Neogene chronology: new perspectives in high-resolution stratigraphy. Geological Society of America Bulletin, 107, 1272-1287.

Berggren, W.A., Kent, D.V., van Couvering, J. A., 1995b. Neogene geochronology and chronostratigraphy. Geological Society Memoirs, 10, 211-260. DOI: 10.1144/GSL.MEM.1985. 010. 01.18.

Blow, W.H., 1969. Late middle Eocene to Recent planktonic foraminiferal biostratigraphy. In: P. Bronnimann, H.H. Renz (Eds.), Proceedings of the First International Conference on Planktonic Microfossils, Geneva, pp. 199-422.

Bolli, H.M., Premoli Silva, I., 1973. Oligocene to Recent Planktonic Foraminífera and Stratigraphy of Leg 15 sites in the Caribean Sea. Initial Reports of the Deep Sea Drilling Project, 15, 475-497.

Bolli, H.M., Saunders, J.B., 1985. Oligocene to Holocene low latitude planktic foraminifera. In: Bolli, H.M., Saunders, J.B., Perch-Nielsen, K. (Eds.), Plankton Stratigraphy. Cambridge University Press, New York, pp. 156-262.

Bylinskaya, M.E., 2005. Range and stratigraphic significance of the *Globorotalia crassaformis* plexus. Journal of Iberian Geology, 31(1), 51–63.

Chaisson, W.P., D´Hondt, S.L., 2000. Neogene planktonic foraminífera biostratigraphy at Site 999, Western Caribbean Sea. In: Leckie, R.M., Sigurdsson, H., Acton, G.D., and Draper, G., (Eds.), Proceedings of the Ocean Drilling Program, Scientific Results, 165, 19-56.

Chaisson, W.P., Leckie, R.M., 1993. High-resolution Neogene planktonic foraminifer biostratigraphy of Site 806, Ontong Java Plateau (western equatorial Pacific). In: Berger, W.H., Kroenke, L.W., Mayer, L.A., et al., (Eds.), Proceedings of the Ocean Drilling Program: Scientific Results, 130, 137–178.

Chaisson, W.P., Pearson, P.N. 1997. Planktonic foraminifer Biostratigraphy at Site 925: Middle Miocene-Pleistocene. In: Shackleton, N.J., Curry, W.B., Richter, C., Bralower, T.J. (Eds.) Proceedings of the Ocean Drilling Program, Scientific Results, 154, 3-31.

Channell, J.E.T., Hodell, D.A., Curtis, J.H., 2016. Relative paleointensity (RPI) and oxygen isotope stratigraphy at IODP Site U1308: North Atlantic RPI stack for 1.2-2.2 Ma (NARPI-2200) and age of the Olduvai Subchron. Quaternary Science Reviews, 131, 1-19. doi.org/10.1016/j.quascirev.2015.10.011.

Chaproniere, G.C.H., Styzen, M.J., Sager, W.W., Nishi, H., Quinterno, P.J., Abrahamsen, N., 1994. Late Neogene biostratigraphic and magnetostratigraphic synthesis, Leg 135. In: Hawkins, J; Parson, L; Allan, J; et al. (Eds.), Proceedings of the Ocean Drilling Program,

Scientific Results, College Station, TX (Ocean Drilling Program), 135, 857-877, https://doi.org/10.2973/odp.proc.sr.135.116.1994.

Chaproniere, G.C.H., 1991. Pleistocene to Holocene planktic foraminiferal biostratigraphy of the Coral Sea, offshore Queensland. Australia.Journal of Australian Geology & Geophysics, 12(3), 195-221.

de Garidel-Thoron, T., Rosenthal, Y., Bassinot, F., Beaufort, L., 2005. Stable sea surface temperatures in the western Pacific warm pool over the past 1.75million years. Nature, 433(7023), 294-298.

Ericson, D.B., Wollin, G., 1968. Pleistocene climates and chronology in deep-sea sediments. Science, 162, 1227-1243.

Ferreira, F., Frontalini, F., Leão, C.J., Leipnitz, I.I., 2014. Changes in the water column structure and paleoproductivity in the western South Atlantic Ocean since the middle Pleistocene: Evidence from benthic and planktonic foraminífera. Quaternary International, 352, 111-123.

Ferreira, F., Leipnitz, I.I., Vicalvi, M.A., Sanjinés, A.E.S., 2012. Zoneamento Paleoclimático do Quaternário da Bacia de Santos com base em foraminíferos planctônicos. Revista Brasileira de Paleontologia, 15 (2), 173–188.

Hayward, B.W., Le Coze, F., Vachard, D., Gross, O., 2019. World Foraminifera Database. Accessed at http://www.marinespecies.org/foraminifera on 2019-12-14. DOI:10.14284/305

Hills, S.J., and Thierstein, H.R., 1989. Plio-Pleistocene calcareous plankton biochronology. Marine Micropaleontology, 14, 67-96.

Joyce, J.E., Tjalsma, L.R., Prutzman, J.M., 1990. High-resolution planktonic isotope record and spectral analysis for the last 5.35 Ma: Ocean Drilling Program Site 625 – Northeast Gulf of Mexico. Paleoceanography, 5(4), 507-529.

Keigwin Jr., L.D., 1982. Neogene planktonic foraminifers from Deep Sea Drilling Project Sites 502 and 503. Initial Reports of the Deep Sea Drilling Project. Government Printing Office, Washington, D.C., US, pp. 269–288.

Kennett, J.P., Srinivasan, M.S., 1983. Neogene planktonic foraminifera. Stroudsburg: Hutchinson Ross Publishing Company, 265 pp.

Kennett, J.P., Huddlestun, P., 1972. Late Pleistocene paleoclimatology, foraminiferal biostratigraphy, and tephrochronology, Western Gulf of Mexico. Quaternary Research, 2, 38-69.

Kohl, B., Fillon, R.H., Roberts, H.H., 2004. Foraminiferal biostratigraphy and paleoenvironments of the Pleistocene Lagniappe Delta and related section, Northeastern Gulf of Mexico. In:

Anderson, B., Fillon, R.H., (Eds), Late Quaternary Stratigraphic Evolution of the Northern Gulf of Mexico Margin. Society for Sedimentary Geology, 79, 190-216.

Krasheninnikov, V.A., 1979. Stratigraphy and planktonic foraminifers of Cenozoic deposits of the Bay of Biscay and Rockall Plateau, DSDP Leg 48. In: Montadert, L., Roberts, D.G., (Eds.), Initial Reports of the Deep Sea Drilling Project, 48, 431-450.

Le, J., Shackleton, N.J., 1992. Carbonate dissolution fluctuations in the western equatorial Pacific during the late Quaternary. Paleoceanography, 7(1), 21–42.

Locarnini, R. A., Mishonov, A.V., Baranova, O.K., Boyer, T.P., Zweng, M.M., Garcia, H.E., Reagan, J.R., Seidov, D., Weathers, K., Paver, C.R., Smolyar, I., 2018. World Ocean Atlas 2018, Volume 1: Temperature. A. Mishonov Technical Ed.; NOAA Atlas NESDIS 81, 52 pp.

Lourens, L.J., Hilgen, F.J., Shacketon, N.J., Laskar, J., Wilson, D., 2004. The Neogene Period. In: Gradstein, F.M., Ogg, J.G., Smith, A.G., (Eds.), Geological Time Scale 2004. Cambridge University Press, pp. 409-440.

Martin, R.E., Johnson, G.W., Neff, E.D., Krantz, D.E., 1990. Quaternary planktonic foraminiferal assemblage zones of the northeast Gulf of México, Colombia basin (Caribbean Sea), and the tropical Atlantic Ocean: Graphic correlation of microfossil and oxygen isotope datums. Paleoceanography, 5(4), 531-555.

Martin, R.E., Neff, E.D., Johnson, G.W., Krantz, D.E., 1993. Biostratigraphic Expression of Pleistocene Sequence Boundaries, Gulf of Mexico. Palaios, 8: 155-171.

Martinez, J.I., Mora, G., Barrows, T.T., 2007. Paleoceanographic conditions in the Western Caribbean Sea for the last 560 kyr as inferred from planktonic foraminifera. Marine Micropaleontology, 64, 177-188.

Nishi, H., Norris, R.D., Okada, H., 2000. Paleoceanographic changes in the dynamics of subtropical surface conditions at Hole 997A. In: Paull, C.K., Matsumoto, R., Wallace, P.J., and Dillon, W.P. (Eds.), Proceedings of the Ocean Drilling Program, Scientific Results, 164, 343-363.

Pflaumann, U., 1988. Stratigraphy and paleoecology of the Quaternary in the eastern South Atlantic. The record by planktonic Foraminifera from sediments of the central Walvis Ridge, DSDP Leg 74. Meyniana, 40, 71-117.

Portilho-Ramos, R.C., Barbosa, C.F., Rios-Netto, A.M., 2014. Planktonic foraminiferal variations in the southwestern Atlantic since the last glacial-interglacial cycle. Palaios, 29, 38–44. http://dx.doi.org/10.2110/palo.2012.104.

Portilho-Ramos, R.C., Rios-Netto, A.M., Barbosa, C.F., 2006. Caracterização bioestratigráfica do Neógeno superior da Bacia de Santos com base em foraminíferos planctônicos. Revista Brasileira de Paleontologia, 9, 349–354.

Prell, W.L., Damuth, J.E., 1978. The climate-related diachronous disappearance of *Pulleniatinaobliquiloculata* in Late Quaternary sediments of the Atlantic and Caribbean. Marine Micropaleontology, 3, 267-277.

Shackleton, N.J., Berger, A., Peltier, W.R., 1990. An alternative astronomical calibration of the lower Pleistocene timescale based on ODP Site 677. Philosophical Transactions of the Royal Society of Edinburgh, Earth Sciences 81, 251–261.

Shipboard Scientific Party, 1988. Sites 677 and 678. In: Becker, K., Sakai, H., et al. (Eds.), Proceedings of the Ocean Drilling Program, Initial Reports 111, 253–346.

Sinha, D.K., Singh, A.K., 2008. Late Neogene planktonic foraminiferal biochronology of the ODP Site 763, Exmouth Plateau, Southeast Indian Ocean. Journal of Foraminiferal Research, 38(3), 251–270.

Spencer-Cervato, C., Thierstein, H.R., 1997. First appearance of *Globorotalia truncatulinoides*: cladogenesis and immigration. Marine Micropaleontology, 30, 267-291.

Spencer-Cervato, C., Thierstein, H.R., Lazarus, D.B., and Beckmann, J.-P., 1994. How synchronous are Neogene marine plankton events. Paleoceanography, 9, 739-763

Srinivasan, M. S., Kennett, J. P., 1981. Neogene planktonic foraminiferal biostratigraphy and evolution: equatorial to subantarctic, south Pacific. Marine Micropaleontology. 6, 499-533.

Srinivasan, M.S., Sinha, D.K., 1992. Late Neogene planktonic foraminiferal events of the southwest Pacific and Indian Ocean: A comparison, In: Tsuchi, R., and Ingle, J. C., Jr., (Eds.), Pacific Neogene environment, evolution, and events: Tokyo, University of Tokyo Press, p. 203–220.

Thompson, P.R., Sciarrillo, J.R., 1978. Planktonic foraminiferal biostratigraphy in the equatorial Pacific. Nature, 276, 29-33.

Thunell, R.C., 1984. Pleistocene planktonic foraminiferal biostratigraphy and paleoclimatology of the Gulf of México. In: Healy-Williams, N., (Ed.), Principles of Pleistocene Stratigraphy Applied to the Gulf of Mexico. Boston, International Human Resources Development Corporation, p. 25-64.

Toledo, F.A.L., Quadros, J.P.,Camilo Jr., E., Santarosa, A.C.A., Flores, J.A., Costa, K.B. 2016.Plankton biochronology for the last 772,000 years from the western South Atlantic Ocean. Marine Micropaleontology, 127, 50–62. http://dx.doi.org/10.1016/j.marmicro. 2016.07.002

Vicalvi, M.A., 1997. Zoneamento bioestratigráfico e paleoclimático dos sedimentos do Quaternário superior do talude da Bacia de Campos, RJ, Brasil. Boletim de Geociências da Petrobrás, 11(1), 132-165.

Weaver, P.P.E., Raymo, M.E., 1989. Late Miocene to Holocene planktonic foraminifers from the equatorial Atlantic, Leg 108. In: Ruddiman, W., Sarnthein, M., et al., Proceedings of the Ocean Drilling Program, Scientific Results, 108, 71–91.

Wilkens, R.H., Westerhold, T., Drury, A.J., Lyle, M., Gorgas, T., Tian, J., 2017, Revisiting the Ceara Rise, equatorial Atlantic Ocean: isotope stratigraphy of ODP Leg 154 from 0 to 5 Ma: Climate of the Past, 13, 779–793. DOI: https://doi.org/10.5194/cp-13-779-2017.

Williams, D.F., Healy-Williams, N., Leschak, P., 1985. Dissolution and water-mass patterns in the Southeast Indian Ocean. Part I. Evidence from Recent to late Holocene foraminiferal assemblages. Geological Society of America Bulletin, 96(2), 176–189.

4.2. Chapter 2: Paleoceanographic reconstructions of western equatorial Atlantic for the last ~1.93 Ma

Paleoceanographic reconstructions of western equatorial Atlantic for the last ~1.93 Ma

Fabricio Ferreira[1,2]; Gary Dwyer[3]; Allan Sandes Oliveira[2]; Cristiano M. Chiessi[4]; Cleverson Guisan Silva[2]; Paul A. Baker[3], Andrea K. Kern[4]; Catherine A. Rigsby[5]

[1]Postgraduate Program in Ocean and Earth Dynamics, Institute of Geosciences, Federal Fluminense University, Niterói, Av. Gal. Milton Tavares de Souza s/n, CEP: 24.210-346 Rio de Janeiro RJ, Brazil – *ferreira_paleo@hotmail.com*

[2]Marine Geology Laboratory (LAGEMAR), Institute of Geosciences, Federal Fluminense University, Niterói, Av. Gal. Milton Tavares de Souza s/n, CEP: 24.210-346 Rio de Janeiro RJ, Brazil

[3]Division of Earth and Ocean Sciences, Duke University, Durham, NC 27708, USA

[4]School of Arts, Sciences and Humanities, University of São Paulo, São Paulo, Av. Av. Arlindo Bettio 1000, CEP: 03828-000 São Paulo SP, Brazil

[5]Department of Geological Sciences, East Carolina University, Greenville, NC 27858-4353, USA.

Abstract

We present the integration of planktonic foraminifera proxies, as census-based, stable oxygen isotopic records ($\delta^{18}O$, $\delta^{18}O_{ssw}$), and Mg/Ca-SST analysis applied for the Pleistocene (~1.93-0.01 Ma) paleoceanographic reconstructions of the western Equatorial Atlantic, an area considered the main route for cross-equatorial transport of heat and salinity to the North Atlantic, and a key component of the climate system. Over the Mid-Pleistocene Transition (~0.88 Ma and ~0.63 Ma), two large scale events with negative anomalies on $\delta^{18}O_{IVC\text{-}SW}$ were recorded for the first time. During these events, the superficial water column is characterized by a cold and low-salinity layer (>50 m), results in the coupling between large freshwater influx (large river influx and heavy precipitation) and strongest NBCR system. Our results also provide the first record of salty and warm accumulation events (~1.26-1.12 Ma and ~0.33 Ma), here related to the coupling between North Atlantic stadial events and increased Agulhas leakage. In the last ~1.4 Ma, the near-synchronous and drastic abundance changes (disappearance and reappearance events) of *Globorotalia menardii* complex presents close relation with the records of the Agulhas leakage strength oscillations, presented by Caley et al. (2012). The *G. menardii* complex reappearance/increase abundance events are related to the increase in the heat and salty waters transported from the southern hemisphere to the Equator (due southward migration/position of the subtropical front - STF), in especial the events R4 (~0.96 Ma; MIS 26; boundary T/S); R3 (~0.54 Ma; MIS 12/14; boundary U/V) and R2 (~0.13 Ma; MIS

5/6; boundary W/X) and the subzonal boundaries R2/R1 (~1.31 Ma; MIS 41) and T2/T1 (~0.68; MIS 16). While the disappearance events of the taxon are related to synchronous action of decrease or interruption of the Agulhas leakage (due to North Atlantic stadial events). Those results provides a complete reconstruction of the long-term paleoceanographic changes for the longest continuous record in the Brazilian equatorial margin, addressing the influence of NBCR strength system as an important inter-hemisphere heat and salt transport regulator, and the impact of the millennial-scale current oscillations in the global and local climate.

Key Words:

Paleotemperature reconstruction; Planktonic foraminifera; Mg/Ca-SST; Sea surface salinity; Tropical Atlantic; Pará-Maranhão Basin.

1. Introduction

The western equatorial Atlantic margin is an ideal region to study the variability in ocean currents and atmospheric dynamics of tropical South America. The sediments deposited in this area provide the complete record of past changes of the North Brazil Current (NBC) system, that associated with the Atlantic Meridional Overturning Circulation (AMOC), promote the main pathway for the cross-equatorial transport of warm and salty surface waters into high latitudes of the North Atlantic (e.g. Nace et al., 2014; Zhang et al., 2015), and one of the most important components of the thermohaline circulation and Earth's climate (eg. Arz et al., 1998; Zhang et al., 2017; Crivellari et al., 2018).

The variation of the AMOC presents a positive correlation with the transport variability of NBC (Zhang et al., 2011; Zhang et al., 2015), and can lead to local and global changes in the distribution of sea surface temperature (SST) and salinity (SSS) (e.g., Huisman et al., 2010; Garzoli and Matano, 2011; Castellanos et al., 2019). The AMOC slow down events (e.g. due to North Atlantic cold events) promote changes in the positions of the NBC, moving the current away from the coast, and feeding in the superficial (Silva et al., 2005) and subsuperficial layers (Silva et al., 2009) the North Equatorial Countercurrent (NECC), in a process known as NBC retroflection (NBCR) (Fonseca et al., 2004). Modeling studies suggested that the freshwater input into the high latitudes of North Atlantic were able to trigger a reversal of the NBC under both present-day (Chang et al., 2008) and Last Glacial Maximum (LGM, 23-19 kyr) conditions (Schmidt et al., 2012; Nace et al., 2014). That variability is also observed on the millennial-scale, where the NBC presented a marked decrease in the strength during AMOC slowdown events of the last deglaciation, such as the Younger Dryas (i.e. YD, 13–11.5ka) and Heinrich Stadial 1 (i.e. H1, 18–15ka) (Arz et al., 1999; Wilson et al., 2011).

Those millennial-scale oscillations in the temperature gradient between the North and South Atlantic Ocean due to abrupt changes in the AMOC strength also promote the shift in the position of the Intertropical Convergence Zone (ITCZ), influenced the South American Monsoon System (SAMS) by producing climatic oscillation in northeastern Brazil (central and west Amazon area) and dry conditions and northern South America (e.g. Arz et al., 1998; Peterson and Haug, 2006; Zhang et al., 2017; Crivellari et al., 2018). In the coastland and the northwest of the NEB, the strong precipitation related to the ITCZ also led to low sea surface salinity (SSS), which could have an important role in ocean circulation due to buoyancy and stratification of the water column (Da-Allada et al., 2013), impacting the NADW formation (e.g. Wilson et al., 2011). It is also suggested that a freshwater influence from the equatorial Atlantic leads to a weakening of the AMOC, which results in surface air temperatures over the North Atlantic cool, and temperatures over the South Atlantic warm (Broecker, 1998; Barker et al., 2009). However, paleoclimatic studies of the Tropical area are limited for both, short period instrumental record as well as paleo records, in comparison to higher latitudes, despite the central role of the low latitudes in the global climate system (e.g. Baker and Fritz 2015).

To investigate the main mechanisms evolved in the changes of the NBC system, and its relation with local and global climate records, we applied planktonic foraminifera multiproxy analysis (key species, transfer function, oxygen isotopic records - $\delta^{18}O$ and $\delta^{18}O_{sw}$, trace elements - Mg/Ca-SST). The integration of this multiproxy analysis provides a complete reconstruction of the long-term paleoceanographic changes (e.g. water column structure, SST, and SSS) of the western equatorial Atlantic over the Gelasian to late Pleistocene (1.93-0.016 Ma; MIS 73-2), addressing the influence of NBCR strength system as an important inter-hemisphere heat and salt transport regulator, and the impact of the millennial-scale current oscillations in the global and local climate.

2. Study Area

2.1. Ocean circulation

The modern surface ocean circulation in the western equatorial Atlantic is controlled by the North Brazil Current (NBC) and the North Equatorial Countercurrent (NECC). The NBC results from the bifurcation of the South Equatorial Current (SEC) at 10-15°S and flows northwestwards along the continental margin of northeastern Brazil (Figure 1; Peterson and Stramma, 1991; Schott et al., 1995; Stramma et al., 1995). NBC extends from the surface to intermediate water depths (approximately 800 m water depth) where it merges with northward advected Antarctic Intermediate Water (Talley et al., 2011), being the main pathway for the cross-equatorial transport of warm and salty surface waters that balances the

southward export of North Atlantic Deep Water (Johns et al., 1998; Goni and Johns, 2001; Haarsma et al., 2011). In the region of our record (core CDH-79; Figure 1), long-term annual mean sea surface temperature is 27.5°C (between 27.3°C and 28.2°C) (Locarnini et al., 2018), while sea surface salinity is 35.7 (between 28.2 and 36.2) (Zweng et al., 2018).

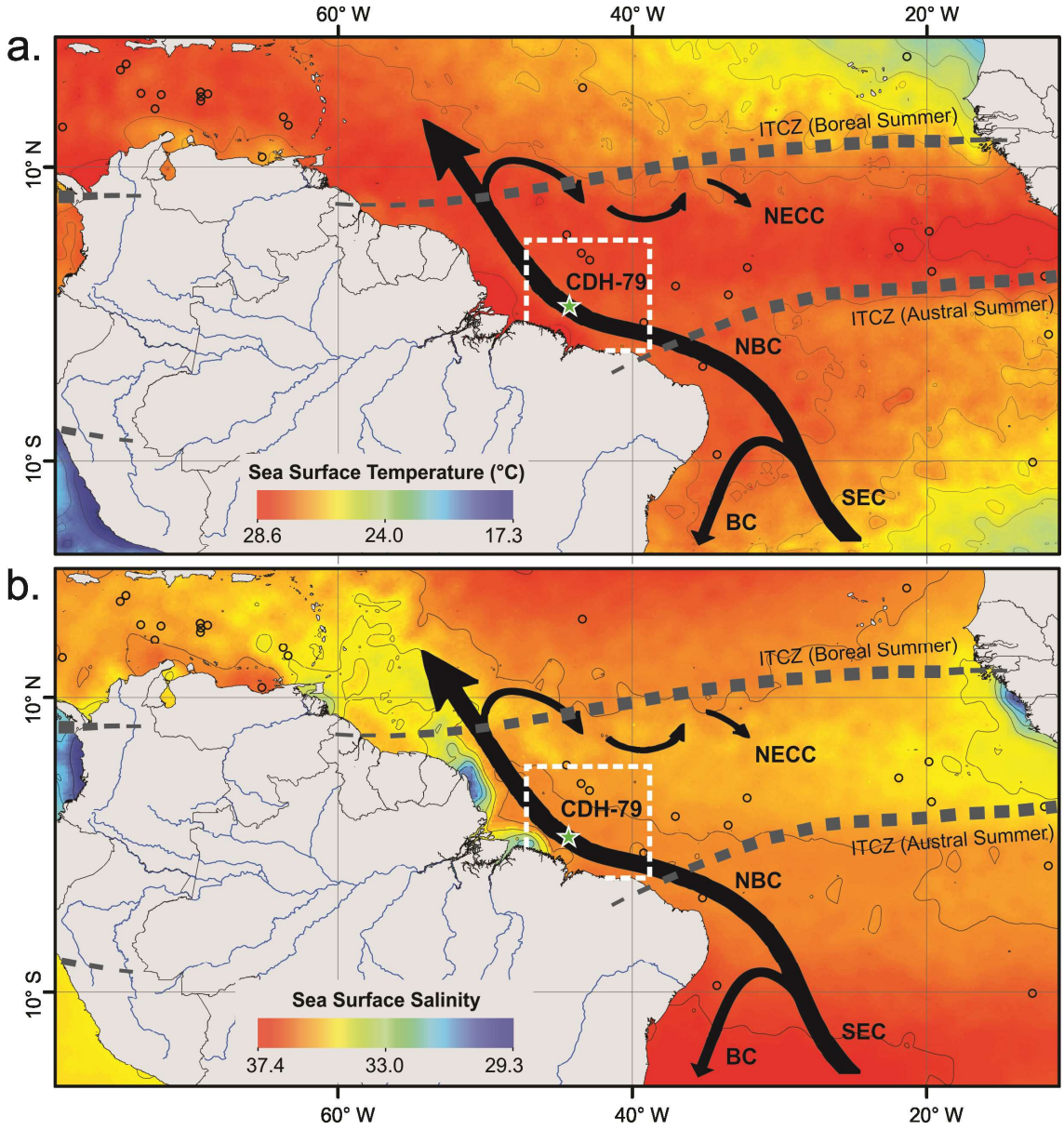

Figure 1. Location of marine sediment core CDH-79 (green star) with (a.) long-term mean annual sea surface temperature (color scale) (Locarnini et al., 2018) and (b) long-term mean annual sea surface salinity (color scale) (Zweng et al., 2018), and the surface ocean currents of interest for this study (black arrows). The white dashed rectangle indicates the area used to estimate the long-term mean sea surface temperature and salinity for the study area. BC - Brazil Current; NBC-North Brazil Current; NECC- North Equatorial Countercurrent; SEC - South Equatorial Current (Peterson and Stramma, 1991).

The seasonal variability in the heat and salinity northward transport is highly variable, with maximum and minimum measured transport of approximately 36 Sv during the austral winter and 13 Sv during the austral fall, and seasonal retroflection into the NECC at 6–8°N from June to January (Johns et al., 1998). Those variabilities are also responsible for change the position of the current, where between July and February the superficial layer separates from the coast at approximately 8°N, mixing with the NECC in a process known as NBC retroflection (NBCR) (Fonseca et al., 2004). Between March and June, NBC flow northwestward along the continental slope of South America, eventually entering the Caribbean Sea and feeding the Gulf Stream (Johns et al., 1998; Lux et al., 2001). A weakening or even reversal NECC is coincident with increased NBC transport, due to wind stress variation resulting in a greater flux of heat and salinity to the northern hemisphere (e.g. Johns et al., 1998).

2.2. Climate

The Northeast Region of Brazil (NEB) covers an area of 1,588,196 km^2, between 1°N-18°S and 34.5°W-48.5°W, can be divided into subregions with different climatic characteristics, such as coastal area, semiarid regions, and Amazon forest (Alvares et al. 2013). The annual rainfall can fluctuate from less than 500 mm in the semiarid areas to more than 1500 mm in the coastland and the northwest of the NEB (Oliveira et al., 2016), due to the action of different atmospheric systems, like the ITCZ (Uvo and Nobre, 1989), the upper-tropospheric cyclonic vortex (Kousky and Gan 1981), the easterly waves disturbances (Riehl 1945), the squall lines (Kousky 1980), Front Systems (Kousky 1979), and the South Atlantic convergence zone (Kodama 1992).

The ITCZ can be identified as a tropical belt of deep convective clouds (Waliser and Gautier, 1993), or as the maximum in time-mean precipitation (e.g. Hastenrath and Heller 1977; Philander et al., 1996), associated with the expansion and contraction of subtropical anticyclones over the North and South Atlantic Ocean (Hastenrath and Heller 1977). The Atlantic ITCZ is a branch of the Hadley cell, which marks a dynamic boundary between the southeast and northeast Atlantic trade winds, that migrates from a further north position about 14°N in August-September to the further south position at about 4°S during March-April (Schneider et al, 2014). The seasonal ITCZ migration plays a major role in controlling the patterns of rainfall over the northern area of the NEB and the adjacent continent, imposing distinctive wet and dry season across northern South America (Hastenrath and Heller 1977). Convection and wind direction patterns, controlled largely by insolation changes, are associated with the equatorial low-pressure trough and the South American Monsoon System

(SAMS), which also influences the timing of the onset of the wet season across South America (central and west Amazon area) (Wilson et al., 2011).

Two modes of ocean-atmosphere variability present a significant effect in the regional climate of the NEB (e.g. Servain et al., 1998). The first mode is similar to the El-Niño Southern Oscillation and is characterized by warm and cold phases near the equator (Chang et al., 1997). The second mode is characterized by a north-south inter-hemispheric SST gradient (e.g. the Atlantic dipole; Chang et al., 1997; Utida et al., 2019). According to Hastenrath (2006), the inter-annual variability of rainfall in the NEB is associated with variations of SST patterns over the tropical oceans, affecting the position and intensity of the ITCZ. Cruz et al. (2009) suggested that the fluctuations in rainfall over Northeast Brazil follow the precession cycle, occurring in a coordinated stage with paleoclimatic records in the northern hemisphere and reverse with the records of South speleothems and southeastern Brazil (Cruz et al. 2005, Cruz et al. 2006). However, the magnitudes of Amazon and Northeast precipitation and ecosystems changes in the orbital time scale are almost totally unknown, by the limited paleoclimatic record (Baker and Fritz, 2015).

Millennial time scale changes in the ITCZ position were recorded in Cariaco Basin (Caribbean Sea; Petterson et al., 2000), suggesting that the southern ITCZ position occurs with glacial and stadials stages. During glacial stages, an increased latitudinal thermal gradient is thought to have led to reduced penetration of the ITCZ into the northern hemisphere, which greatly alters the dynamics of regional climate causing a decrease in the cross-equatorial transport of heat and salinity by upper-level ocean currents (Berger and Wefer, 1996; Maslin et al., 1997; Vink et al., 2002), changing the vegetation, continental runoff and river outflow patterns in the Amazon Basin (Wilson et al., 2011).

3. Material and Methods

We investigated core CDH-79 (00° 39.6853' N, 44° 20.7723' W; 32.12 m core length; 2345 m water depth; Figure 1), retrieved during RV Knorr cruise KNR 197-4 in February 2010. The coring site is located on the top of a sea mountain in the western equatorial Atlantic (Pará-Maranhão Basin), 320 km from the modern coastline of northeastern Brazil. Core CDH-79 was sectioned and split onboard. All sections were continuously refrigerated while shipped to Woods Hole Oceanographic Institution for storing at 4^{o}C. Subsequently, the working halves were visually described and sampled (10 cm^{3}) every 10 cm.

3.1. Planktonic foraminifera - preparation and analysis

The unlithified sediment samples were washed through a sieve of 62 µm mesh size (keeping the retained material) and dried at 50°C (Leipnitz et al., 2005). Dry residues were weighed and stored in glass vials. Planktonic foraminifera were dry picked from the >150 µm fraction in subsample splits (if necessary) containing 300–600 specimens. This results in a 95% level of confidence for species with at least 1% of abundance (Patterson and Fishbein, 1989). The subsamples were stored in micropaleontological slides and all specimens were identified and counted. The specimen preservation was qualitatively estimated and the Le and Shackleton (1992) fragmentation index (FRAG) was calculated for each sample. The taxonomic concepts for Neogene taxa were adopted from Stainforth et al. (1975), Kennett and Srinivasan (1983), and Bolli and Saunders (1985) and revised based on Hayward et al. (2019). The used taxonomic terms are available in Table S1.

For each sample, species richness (S), Shannon-Weaver diversity (H´), and equitability (J) were calculated (Buzas and Gibson, 1969). Species richness is the number of species in each sample, whereas the Shannon-Weaver index describes diversity, taking into account the relative population of each species within a sample ($H = -\Sigma Pi \ lnPi$; where Pi is the proportion of each species). Equitability is a measure of the evenness of the species distribution within a sample (E=H/S). Equitability equals one if all species are present in the same population and approaches zero when one species dominates the fauna. The planktonic foraminifera diversity is controlled by the structure of the upper water column (e.g., Rutherford et al., 1999), presenting a diversity decreases from the central gyres of the ocean towards continental margins and/or eutrophic regions (e.g. Martinez et al., 2007). The lower diversity values also were related to a deep thermocline in the Caribbean Sea (Martinez et al., 2007).

For paleoceanographic reconstruction and interpretations, we considered only the abundance of significant species for the paleoceanographic and paleoclimatic reconstructions of the Quaternary (e.g. Nishi et al., 2000; Caley et al., 2012; Portilho-Ramos et al., 2017). The species *G. ruber* and *Globigerinoides sacculifer* were applied as indicators of the oligotrophic conditions with stable deep-mixed layers (e.g. Nishi et al., 2000; Martinez et al., 2007). While the opportunistic species as *Globigerinita glutinata*, *Globigerina bulloides,* and *Neogloboquadrina dutertrei* are applied as indicators of eutrophic conditions and used to track the past variability and intensity of surface euthofization (Schiebel et al. 2004; Kucera et al., 2005; Mohtadi et al., 2005; Lessa et al., 2014). The dwelling species as *Globorotalia truncatulinoides* e *Globoconella inflata* are used in the recognization of the water column conditions stratification conditions. The specie *G. inflata* are used as indicators of cold subtropical water (Kipp, 1976), and related to low SST (~15-20°C), reduced salinity seasonality,

and well-oxygenated waters, that characterizing times when the surface-water stratification decreased (e.g. Nishi et al., 2000).

We also apply the abundance events of *Globorotalia menardii* complex (disappearance events *G. menardii* D5, D4, D3, D2 and D1; and reappearance events *G. menardii* R5, R4, R3, R2; Ferreira et al., A) as a track the past inter-ocean exchange from Indian to the Atlantic Ocean (eg. Peter et al., 2004; Caley et al., 2011). We assume that the Quaternary taxon reseeding of the Atlantic Ocean was related to an increase in the Agulhas leakage (Caley et al., 2012) as discussed below, on item 5.1. In this study, *G. menardii* refers to the complex assemblage who combines *G. menardii spp.* and *Globorotalia tumida* without distinction of the different morphotypes or subspecies.

As a proxy for the mixed layer depth, we applied the *Neogloboquadrina* sp./*G. glutinata* ratio (RN/Gg ratio) from Portilho-Ramos et al. (2017). This proxy considers the opposite abundance patters of *Neogloboquadrina* species (*N. dutertrei* and *Neogloboquadrina imcopta*) and *G. glutinata* in the equatorial Atlantic Ocean as a proxy to track significant changes in the hydrographic and trophic structure of the upper ocean associated with the shallowest mixed layer related to the ITCZ (Portilho-Ramos et al., 2017).

RN/Gg = %Neogloboquadrina/(%Neogloboquadrina + %G. glutinata) ***(1)***

3.2. Modern Analogue Technique (MAT)

Mean sea surface temperature was estimated from planktonic foraminifera assemblage data (>150µm size fraction) using the Modern Analog Technique (MAT) performed on the software Past3.25 (Hammer et al., 2001). The planktonic foraminiferal calibration data set used here composed of a compilation of 430 surface samples from the Atlantic Ocean (predominantly South Atlantic), between 10°N and 30°S from the MARGO Project (Kucera et al., 2005a) that is available at PANGAEA DATABASE (http://epic.awi.de/30068/). For the MAT transfer function, the squared chord distance was applied as a similarity measure. Additionally, when reconstruction results were evaluated, the weighted mean of the best ten modern analogs was used (Kucera et al., 2005b). We estimate the annual mean SST and the temperature of the warmest and coolest months. The SST reconstruction presented a correlation (P>95%; Figure S2) and an average standard deviation of R^2= 0.992 and 0.26°C for the annual mean temperature, and R^2=0.984 and 0.17°C for warmest (summer) and R^2=0.980 and 0.32°C for the coolest months (winter).

3.3. Age Model

The age model for core CDH-79 is based on five calibrated AMS ^{14}C ages (Table 1) and 114 $\delta^{18}O$ tie-points (for more details see Ferreira et al., A). The age model and associated uncertainties were calculated by using the BACON algorithm version 2.2 (Blaauw and Christen, 2011) within the PaleoDataView software version 0.9.2 (Langner and Mulitza, 2019). A total of 10000 age-depth realizations have been used to calculate the median age and the 2σ uncertainty at 1 cm resolution for the interval 10-50 cm core depth (Figure 2b), and 5 cm resolution for the interval 60-3212 cm (Figure 2a). We assume the presence of a depositional unconformity (hiatus) between 50-60 cm (Ferreira et al., A).

Table 1. *Raw ^{14}C AMS data and calibrated ages for core CDH-79.*

Depth (cm)	Lab ID	Radiocarbon age (yr BP)	Age error (yr)	Reservoir age (yr)	Reservoir age error (yr)	Calibrated age mean [95%] (cal a BP)	Calibrated age min [95%] (cal a BP)	Calibrated age max [95%] (cal a BP)
10	OS122410	13900	290	559	55	16054	15225	16942
20	OS122411	17950	510	675	46	20930	19738	22202
30	OS122412	22800	940	781	62	26347	24438	28115
40	OS122413	22900	960	793	63	26437	24506	28272
50	OS122414	25700	1400	740	92	29355	26973	32361

The biochronostatrigraphic model built indicates an average accumulation rate of 3.35 cm/kyr, showing a good correlation with the LR04 stack (Lisiecki and Raymo, 2005) and the revised isotopic stratigraphies of ODP Leg 154 (Ceara Rise - Sites 925, 926, and benthic smooth; Wilkens et al, 2017), and ODP Site 806b (equatorial Pacific; de Garidel-Thoron et al., 2005) (Figure S1). CDH-79 reaches an estimated age of 1.93 Ma at the base (i.e., 32.12 m core depth) of the core and records marine isotopes stages (MIS) 1-73, thus covering most of the Quaternary (Figure S1).

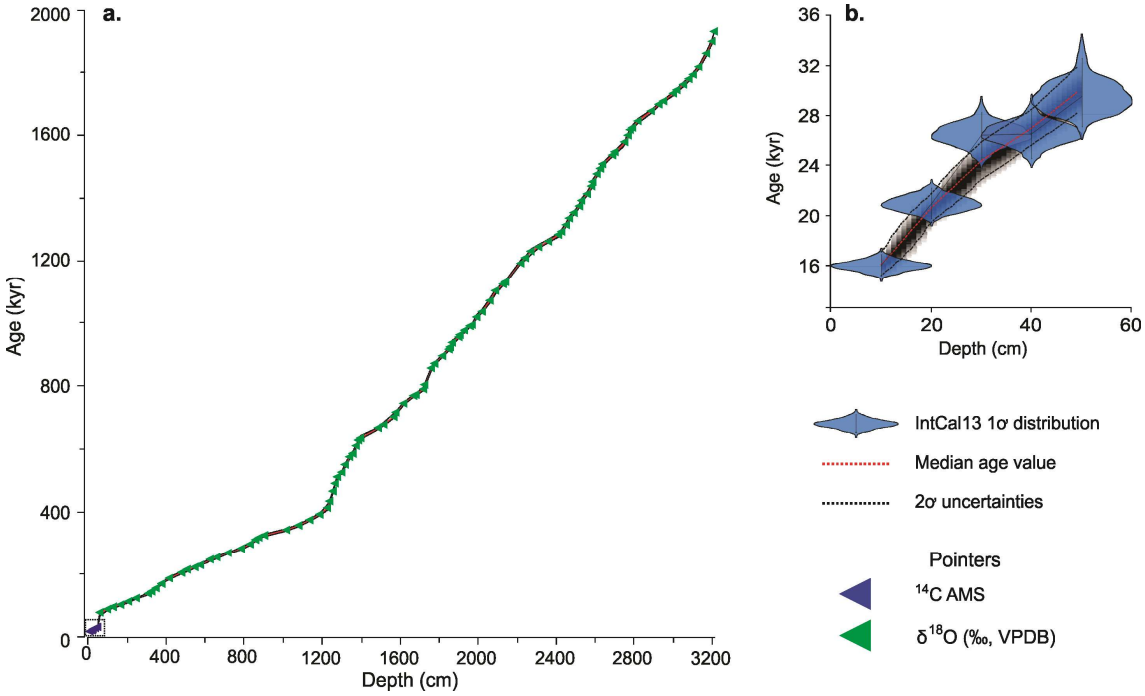

Figure 2. Age model of core CDH-79 based on calibrated AMS ^{14}C ages (blue triangles) and tie-points (green triangles) based on the alignment of our stable oxygen isotopic ($\delta^{18}O$) records to the reference $\delta^{18}O$ stack LR04 (Lisiecki and Raymo, 2005). Black dotted lines indicate the uncertainty of the median age (solid red line) at (a.) 5 cm, and (b.) 1 cm resolution. Note that between 50 -60 cm core depth, there is a hiatus.

3.4. Stable oxygen isotopic records, Mg/Ca ratio, and derived temperature estimation

Five specimens of the planktonic foraminifer *Globigerinoides ruber* (white) were hand-picked (size fraction 250-350 µm) for the stable oxygen isotopic analyses (310 samples; Ferreira et al., A). While typically around 40-50 specimens of *G. ruber* (white) (250-350 µm) were selected for the magnesium (Mg) and calcium (Ca) analysis (233 samples). The specie *G. ruber* is ideally suited for this study because a) it is cosmopolitan nature, high abundance, and continuously abundant throughout the core; b) the specie is the most widely applied proxy for tropical and sub-tropical SST (Gray et al., 2018). The highest Mg/Ca ratio observed in *G. ruber* white indicates that it inhabits the shallowest habitat, calcifying at or close to the sea surface in warm temperatures (Dekens et al. 2002), living and representing mixed layer temperature (Bé, 1977; Fairbanks et al., 1982). Measured calcification temperature for this specie is in good agreement with predicted $\delta^{18}O$ at 25–50 m water depth (Anand et al. 2003). Its restricted migration through the water column makes *G. ruber* white thought to be the most accurate recorder of SST (Dekens et al., 2002; Lea et al., 2000).

For sample preparation, the samples were gently crushed using glass plates, to open chambers, homogenized, and then were chemically cleaned following modified Barker et al. (2003), with adding a reductive step to remove oxide contamination prior to analysis. The samples were analyzed by a direct current plasma atomic emission spectrometer Spectraspan 7, in the Earth and Ocean Sciences Division of the Duke University. Analytical precision on internal standards throughout this study was <0.75%. A total of ten whole sample replicates for each size fraction were performed and yielded a mean of Mg/Ca concentration with relative standard deviation (RSD) of 2.17% from size fraction 250-350 μm, suggesting that digenetic alternation and detrital contamination are minimal.

For Mg/Ca derived temperature calibrations we applied the Dekens et al. (2002) equation for specie G. ruber, based on core-tops samples from the Ceara Rise:

$$Mg/Ca=0.38\ exp(0.09*T) \qquad (2)$$

Where T is in °C and Mg/Ca is a mole ratio. The SST reconstruction presented a correlation (P>95%; Figure S2) of R2= 0.997, and a standard error of the estimate is 1.2°C, 95% confidence interval for the preexponential constant is ±0.05, and 95% confidence interval for the exponential constant is ±0.015 (Dekens et al., 2002). Other equatorial Atlantic calibrations for G. ruber (white) presented similar pre-exponential and exponential constants (e.g. Kısakürek et al., 2008; Regenberg et al., 2009). For Mg/Ca derived temperature calibrations we applied the Dekens et al. (2002) equation for specie G. ruber, based on core-tops samples from the Ceara Rise:

3.5. Seawater oxygen isotopic record ($\delta^{18}O_{SW}$) and ice volume correction

To reconstruct the patterns of freshwater discharge over the area, we applied the Mg/Ca derived temperature (°C) to estimate the ancient seawater $\delta^{18}O$ ($\delta^{18}O_{SW}$), using the temperature and $\delta^{18}O$ relation from Bemis et al. (1998), which applied to *G. ruber* (Thunell et al., 1999):

$$SST=14.9-4.8(\delta^{18}O_{Ca}-\delta^{18}O_{SW}) \qquad (3)$$

Where SST is at °C and $\delta^{18}O_{Ca}$ is $\delta^{18}O$ of the *G. ruber* white. The $\delta^{18}O_{SW}$ is reported in per mil relative to the Vienna Standard Mean Ocean Water (VSMOW) by adding 0.27‰ from the calculated $\delta^{18}O_{SW}$ (Bemis et al., 1998). We correct the ice-volume using the sea level estimates of Elderfield et al. (2012), and a linear conversion from the relative sea-level of

0.012‰/m sea-level fall, by assuming linear sequestration of $\delta^{16}O$ by continental ice sheets through the time (Shackleton, 1987).

$$\delta^{18}O_{IVC-SW} = \delta^{18}O_{SW} - (ESL * 0.012) \quad (4)$$

Where $\delta^{18}O_{IVC-SW}$ is the seawater oxygen isotopic values corrected for ice volume changes and ESL is the estimated sea level difference in meters. The $\delta^{18}O_{IVC-SW}$ is a first-order approximation of SSS. . For the reconstruction of the SSS, we applied the relationship presented by Weldeab et al. (2006). The estimated uncertainty of $\delta^{18}O_{IVC-SW}$ values was calculated taking into account the (i) standard error of the Mg/Ca-SST calibration (±1.2°C that corresponds to ~0.2‰; Dekens et al., 2002), and (ii) analytical error in the oxygen isotope (~0.07‰) analyses, resulting in cumulative error estimation of $\delta^{18}O_{SW}$ of ±0.27‰. This is close to the error estimation of $\delta^{18}O_{SW}$ (±0.22‰) reported by Schimidt et al. (2004), and ±0.25‰ reported by Weldeab et al. (2006). The uncertainties typically result in a 1σ error of about 0.3 - 0.4 ‰ for $\delta^{18}O_{IVC-SW}$ (Schmidt, 1999; Mohtadi et al., 2014).

4. Results

4.1. Planktonic foraminifera - fauna and proxies

A total of 111,749 foraminifera (planktonic and benthic forms) were recovered from the sediments of core CDH-79, where planktonic forms represented 99.24% (110,913 specimens). The integration of biostratigraphy, radiocarbon dating (AMS ^{14}C), and isotopic stratigraphy (MIS) support a spanning time from the Lower to Upper Pleistocene, with estimated ages between ~1.93-0.016 Ma (MIS 73-2), recording the paleoceanographic and paleoclimatic events of almost Pleistocene of the western Equatorial Atlantic (Pará-Maranhão basin). The recovery foraminifera presented an excellent state of preservation, which allowed the classification of planktonic forms at the species level, and the performance of the trace elements analysis as well.

The abundance of selected species, proxies and ecological index shows long and short-term trends changes during the last ~1.80 Ma (Figure 3, 4). In general, the *G. menardii* complex abundance closely following the long-term changes (average 9.7% for the last 1.80 Ma), varying from the high abundance (average >12%) during the intervals recognized as Ericson and Wollin (1968) Zones P, R, T, V and X, and the absence (<1%) at the Zones Q, S V, W, and Y. The *Pulleniatina* complex presents a high abundance through lower-middle Pleistocene (average 10.6% between ~1.80-0.90 Ma) and in the last ~0.35 Ma (average 4.5%), while during the Mid-Pleistocene, the complex presets the lower mean (0.8%). While *G. inflata* presented

three intervals of occurrence, with relatively low abundance (between 1-3%), decreasing the abundance average towards the Early Pleistocene. *G. truncatulinoides* presented a low-amplitude, and-frequency fluctuations whit relative low abundance between ~1.80-0.20 Ma, increasing towards the last ~0.20 Ma. The superficial dwelling species as *G. ruber* and *G. sacculifer* show high-amplitude, high-frequency fluctuations whit relatively high abundances, showing an average of 21% and 7%, respectively. The abundance oscillation of these species, usually follow the glacial-interglacial cycle, decreasing during the glacial and increase during the interglacial periods and also towards the Early Pleistocene.

The species as *G. glutinata* (average 10.6%) and *G. bulloides* (average 1.9%) usually presented an opposite abundance trend, when the increase of *G. glutinata* is closely following by a decrease in *G. bulloides.* While *N. dutertrei* presents high-frequency fluctuations whit relative high abundances (average 6.9%), closely following the glacial-interglacial cycles, and usually increasing abundance close to glacial/interglacial boundaries (Figure 3). *N. pachyderma* (average 1.6%) shows low-frequency fluctuations between ~1.80 -1.05 Ma, increasing the relative abundance at the beginning of the Mid-Pleistocene to Early Pleistocene (Figure 3).

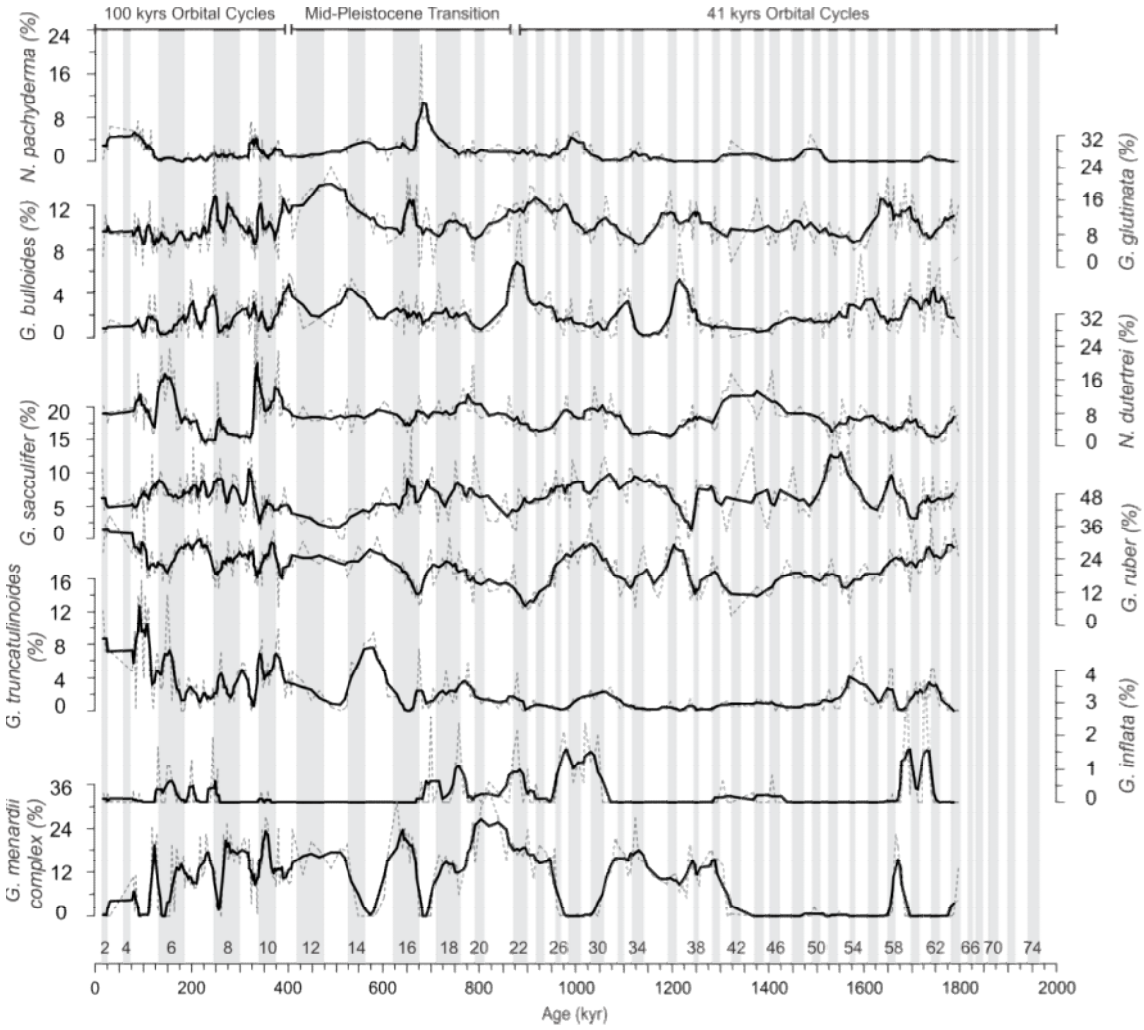

Figure 3. The relative abundance of main species of planktonic foraminifera in the core CDH-79. The dashed line shows the relative abundance and the full line is the 5 points mean. The grey boxes indicate glacial marine isotopic stages (MIS).

The ecological index as specie richness (S), and the Shannon Diversity (H´) showing long-term trends, decreasing between ~1.80-1.30 Ma (MIS 64-41) and presented the lower values between ~1.30-1.07 Ma (MIS 40-30) with higher fragmentation index (MIS 33), increasing to the higher values between ~1.07-0.68 Ma (MIS 29-17). Planktonic foraminifera fragmentation index (FRAG), just exceeds 5% in discrete intervals during glacial stages MIS 62, 40, 32, 16, and 10, and in the interglacial stages MIS 51, 15, and 9 showing a slight decrease (~0.68-0.4 Ma; MIS 16-11) following by high values during the last 0.4 Ma (MIS 10–2). However, in the intervals MIS 46, 35, 33, and 22 the FRAG index exceeds 10%.

The proxy *Neogloboquadrina* sp./*G. glutinata* ratio ($R_{N/Gg}$; Figure 4) show values bigger than ~0.3 during almost records and the higher values were recorded between ~1.45-1.30 (MIS

42-48; average 0.72), 0.79-0.67 Ma (MIS 16-20; average 0.66) and from 0.36-0.34 Ma (MIS 10-11) and 0.22-0.016 Ma (MIS 2-6) which average ~0.64. The proxy *G. bulloides/G. ruber* ratio showing lower values during almost records (average 0.11), an exception was recorded during ~0.97 – 0.87 Ma (MIS 26 – 21; average 0.42), 1.09-1.12 Ma (MIS 32-34; average 0.21), and 1.20-1.25 Ma (MIS 35/36-37/38; average 0.21).

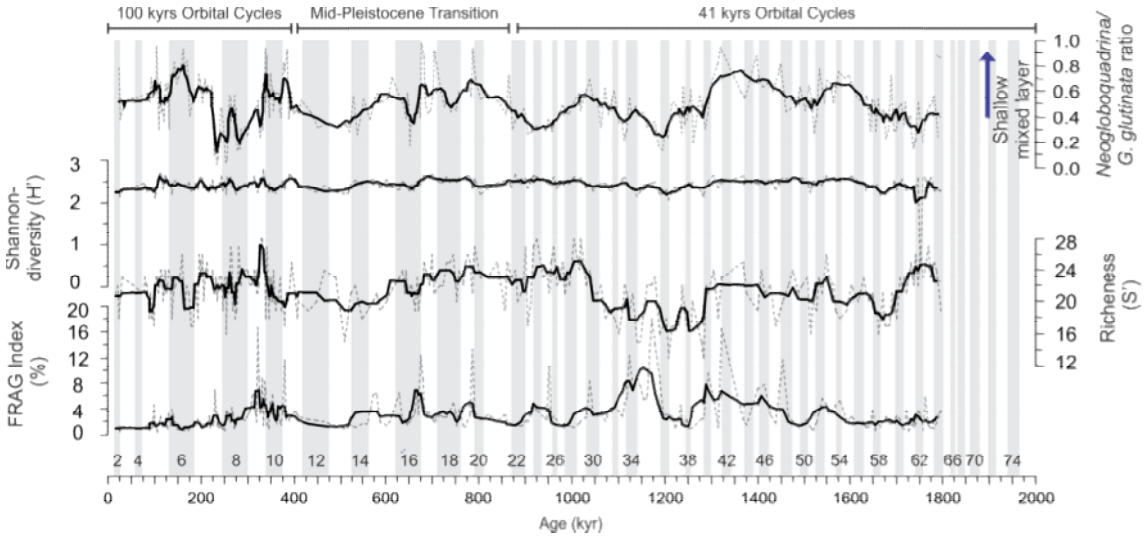

Figure 4. Planktonic foraminifera faunal proxy and ecological index. The dashed line shows the relative abundance and the full line is the 5 points mean. The grey boxes indicate glacial marine isotopic stages (MIS).

4.2. Stable oxygen isotopes

The planktonic foraminiferal oxygen isotopes records oscillated from -1.64 to 0.38‰ with a maximum amplitude ~2.02‰ (1.93-0.016 Ma; 73-2 MIS; Figure 3). On the base of core (1.93-1.25 Ma; MIS73-38), occur the lower amplitude in our records ~1.17‰, with values oscillating from -1.63 to -0.46‰ and average~-1.03‰. The highest value for this interval was recorded at ~1.75 Ma (MIS 62), while the lowest value was recorded at ~1.44 Ma (MIS 47). Around ~1.25 (MIS 38) was recorded a high amplitude change ~1.35‰. Above this interval, from ~1.25-0.42 Ma (MIS 37/38 - 11/12), we recorded the lowest average values ~-0.63‰ (-1.41 to 0.38‰), with amplitude oscillation ~1.79‰. During this depth interval, the lower value was recorded at ~0.71 Ma (MIS 17/18) and 0.96 Ma (MIS 25/26) showing values -1.41‰ and -1.25‰ respectively. The interval 0.43-0.41 Ma (MIS 11/12) showed the highest amplitude in our records, ~2 ‰ (from 0.38 to -1.62‰). For interval 0.41-0.016 Ma (MIS 11-2), our records oscillating from -1.64 - 0.02‰ with amplitude ~1.66‰ and average values close to -0.74‰.

During this depth, the interval was recorded the lower values were recorded at 0.32 Ma (-1.67‰; MIS 9), 0.22 Ma (-1.62‰; MIS 7), and at 0.13 Ma (-1.57‰; MIS 5).

4.3. SST Reconstructions - MAT and Mg/Ca derived paleotemperature

The sea surface temperatures reconstructed (MAT and Mg/Ca derived SSTs), presented long and short-trends change, with the Mg/Ca derived SSTs closely following the $\delta^{18}O$ records (Figure 5). The MAT-SSTs reconstructions cover the last ~1.8 Ma (Figure 5), varying from ~24.1-28.4°C (average ~27.2°C; RSD 2.25%) for summer, and 20.4-27.0°C (average ~24.4°C; RSD 4.36%) for winter, while the annual mean varies from 22.6-27.6°C (average 26.1°C; RSD 3.78%). The seasonal thermal amplitude, the difference between summer and winter MAT-SSTs (MAT-ΔSST; Figure 5) had an average of ~2.8°C (ranges between ~4.4-0.5°C). The recorded average MAT-SSTs for interglacial periods ranges from ~23.3-27.3°C for annual mean, and between ~25.5-27.8°C (average of 27.1°C) and ~21.3-25.8°C (average ~24.2°C) for summer and winter MAT-SSTs respectively. While, the glacial periods showing a MAT-SSTs ranging between 23.8-27.2°C for annual mean, and from ~25.9-27.7°C (average 27.1°C) and ~22.1-25.8°C (average24.3°C) for summer and winter, respectively. The seasonal thermal amplitude average ranges from ~2.9°C (between 1.5-4.3°C) and ~2.8°C (between 1.6-4.4°C) for the interglacial and glacial intervals, respectively.

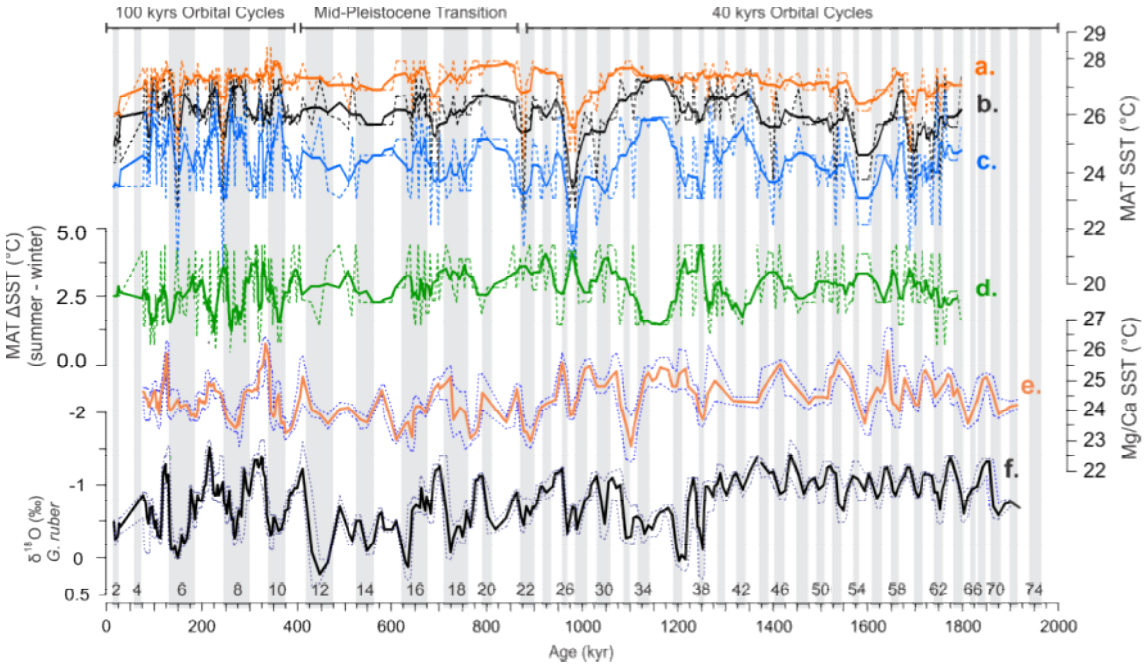

Figure 5. Sea surface temperature reconstruction based on the Modern Analogue Technique MAT-SST based on planktonic foraminifera fauna .and trace elements (Mg/Ca ratio) for the last

1.93 Ma of western Equatorial Atlantic (core CDH-79) (a.) Summer MAT-SST (°C); (b.) Annual MAT-SST (°C); (c.) Winter MAT-SST (°C); (d.) Seasonal thermal amplitude (the difference between summer and winter SST; ΔSST in °C); (e.) Mg/Ca-SST and, (f.) $\delta^{18}O$ from *G. ruber* white (250-350 µm size fraction). The dashed line shows the temperature reconstructed and full line smooth (5 points mean); (f.) $\delta^{18}O$ of *G. ruber* (‰; VPDB); blue dashed line indicates the analytical uncertainty of the median Mg/Ca-SST (e.) and $\delta^{18}O$ (*black line*) and the 2σ uncertainty at 5 cm resolution calculated by down core Monte Carlo. The grey box indicates glacial Marine Isotopic Stages (MIS).

The Mg/Ca-SST were reconstructed for the last 1.92 Ma (Figure 5), and present values between ~20.8-24.7°C (average 22.6°C; RSD 3.06%).The recorded average Mg/Ca-SSTs for interglacial periods ranges from ~23.5-25.4°C (average ~24.6°C), where high SST values were recorded during the MIS 57 (~1.63 Ma; 26.8°C), 31 (~1.06 Ma; 25.9°C), 25 (~0.96 Ma; 25.9°C), 9 (~0.33 Ma; 26.4°C), and 5 (~0.13 Ma; 26.3°C). While, the glacial Mg/Ca-SST varies between 23.3-25.9°C (average 24.4°C), where low SST values were recorded during the MIS 55 (~1.59 Ma; 23.2°C), 38 (~1.25 Ma; 23.6°C), 32 (~1.09 Ma; 22.4°C), 22 (~0.89 Ma; 23.2°C), and 18 (~0.76 Ma; 22.8°C). The interglacial-glacial thermal amplitude demonstrated a slightly high glacial mean values for the MAT-SSTs (annual mean ~0.04°C; summer ~0.09°C; winter 0.11°C), while Mg/Ca-SSTs presents a high interglacial mean value (~0.21°C).

4.4. Seawater oxygen stable isotope record ($\delta^{18}O_{SW}$) and paleosalinity estimation (SSS)

The $\delta^{18}O_{sw}$ (Figure 6) was reconstructed based on the Mg/Ca derived temperature and shows values from 0.34-2.20‰ (average ~1.14‰), while paleosalinity estimation (SSS) shows an average of 35.7 (between 32.8-38.2). The high values of $\delta^{18}O_{sw}$ and SSS were both recorded during MIS 36 (~1.20 Ma; 2.06‰ and 38.2), however, the lower SSS (Figure 6) was recorded during the glacials MIS 22 (~0.89 Ma; 33.2), 20 (~0.79 Ma; 33.3) and 16 (~0.64 Ma; 33.8), while the lower value of $\delta^{18}O_{sw}$ was recorded during the MIS 11/12 boundary. These records are in agreement with the values of the open ocean surface waters, measured during the Amasseds cruises, in the Amazon shelf ($\delta^{18}O_{sw}$ ~-1 - +2‰; Karr and Showers, 2002).

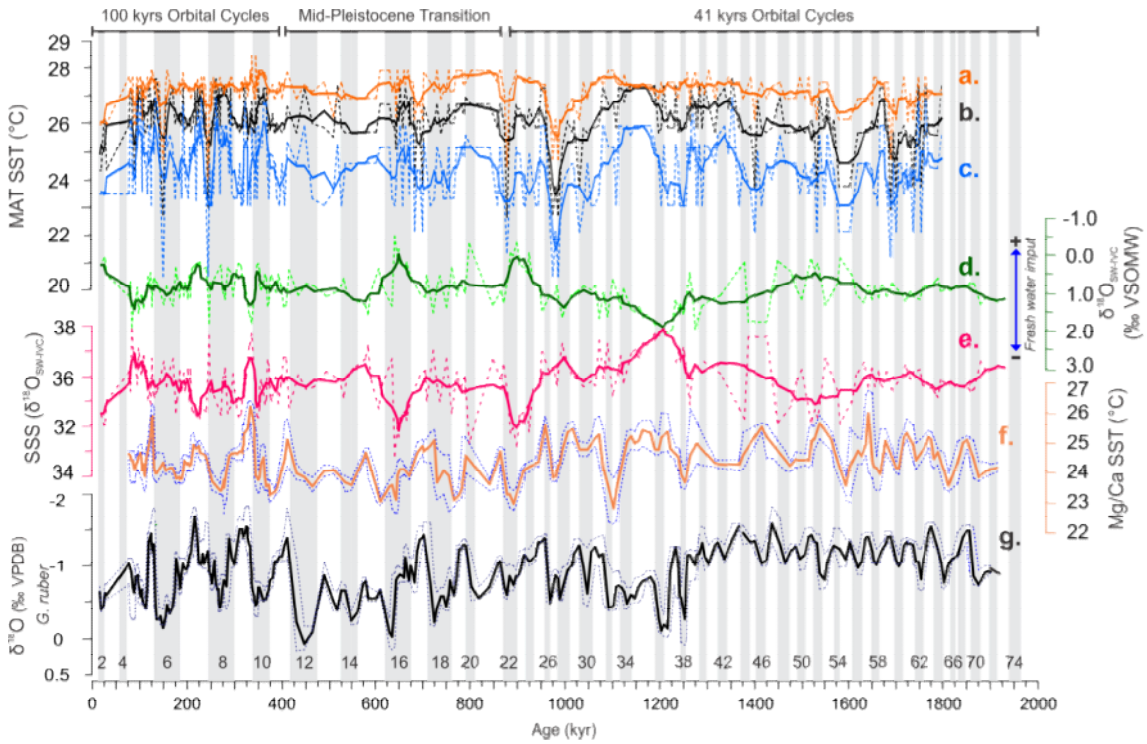

Figure 6. Sea surface temperature reconstruction based on the Modern Analogue Technique MAT-SST based on planktonic foraminifera fauna .and trace elements (Mg/Ca ratio) for the last 1.93 Ma of western Equatorial Atlantic (core CDH-79) (a.) Summer MAT-SST (°C); (b.) Annual MAT-SST (°C); (c.) Winter MAT-SST (°C); (d.) seawater oxygen stable isotope ice volume corrected ($\delta^{18}O_{SW}$); (e.) paleo sea surface salinity estimation (SSS); (f.) Mg/Ca-SST reconstruction, blue dashed line indicates the analytical uncertainty of the median Mg/Ca-SST; and (g.) $\delta^{18}O$ of *G. ruber* white (‰; VPDB) and the 2σ uncertainty at 5 cm resolution calculated by down core Monte Carlo. The grey box indicates glacial marine isotopic stages (MIS).

5. Discussion

The integrations of multi-proxies analysis performed on core CDH-79, combined planktonic foraminifera faunal and proxies analysis (Figure 3, 4), MAT and Mg/Ca derived SSTs (Figure 5); carbonate $\delta^{18}O$ (*G. ruber* white) and the reconstructed $\delta^{18}O$ of seawater ($\delta^{18}Osw$) and the sea surface salinity (SSS) (Figure 6) evidenced the main superficial paleoceanographic changes of the western Equatorial Atlantic through the lower to upper Pleistocene (last 1.93 Ma). These major scenarios are marked by changes in the oceanographic conditions as the water column structure, SST and SSS, and $\delta^{18}Osw$.

5.1. G. menardii complex abundance as a proxy for AMOC strength in the western Equatorial Atlantic

The near-synchronous and drastic abundance changes (disappearance and reappearance events) of *G. menardii* complex in the Quaternary records of the Atlantic Ocean are extensively used in biostratigraphic, paleoceanographic, and paleoclimatic studies of the tropical (Ericson and Wollin, 1968; Martin et al., 1993; Ferreira et al., A) and subtropical Atlantic Ocean realms (Portilho-Ramos et al., 2014; Toledo et al., 2016). However, the taxon presents a continuous record in the Indian and the Pacific Ocean throughout this same time interval (e.g. Caley et al., 2012). It has been suggested that the difference in the taxon occurrence over the Quaternary time scale and its abundance events can be used to track the past inter-ocean exchange of surface waters from Indian to the Atlantic Ocean, via the Agulhas leakage (Peeters et al., 2004; Caley et al., 2011, 2012). The Agulhas leakage is considered a major influence on our study area and the global climate as well. The warm and salty waters from the Indian Ocean help drive the upper Atlantic circulation towards the subpolar northern Atlantic (e.g. Santos et al., 2014). Recently, Caley et al. (2012) demonstrated that the Atlantic Ocean taxon reseeding mechanism over the last 1.35 Ma is associated with the southward migration of the subtropical front (STF) and extreme leakage events (strong Agulhas current). These events are expressed by *G. menardii* concentrations peaks at the Benguela region (ODP Site 1087). While, periods of reduced inter-ocean exchange (weak Agulhas current), are associated with the northward migration of STF and marked by minimum or absence of the taxon. Modeling studies have suggested that the Agulhas leakage dynamic affect AMOC in different time scales (e.g. Caley et al., 2011), and the signals originating in the Agulhas leakage region contribute to decadal- to millennial-time scale AMOC variability on the same order of magnitude as the often invoked northern source (e.g. Biastoch et al., 2008). Zhang et al. (2011) demonstrated a positive correlation between NBC transport and AMOC strength. Also, paleoceanographic records suggest the occurrence of disrupted cross-equatorial heat transport over millennial-scale events characterized by the slowdowns of the AMOC (McManus et al., 2004; Lippold et al., 2009).

The millennia–scale changes in the AMOC strength are also related to stadials intervals from the North Atlantic as recorded during the Heinrich events (i.e. H1, H2, H4, and H5) (e.g. Bond et al., 1992, 1999; Rashid et al., 2003; Hemming, 2004), and Hudson Strait Heinrich events (i.e. H3 and H6) (e.g. Hemming et al, 1998; Hemming, 2004). Instability of Northern Hemisphere ice sheets promotes massive fluxes of icebergs and meltwater into the North Atlantic (i.e., Heinrich events, H; Jaescheke et al., 2007; Hoddel et al., 2008), influencing the North Atlantic deep-water formation (Weijer et al., 2001, 2002). The meltwater produced from these abundant icebergs decreases sea surface salinity and increases surface water stratification. This process acts as a positive feedback to cooling by both increasing sea ice

formation (thereby increasing albedo) and diminishing rates of the thermohaline circulation (i.e. AMOC) (Hodell et al., 2008). In North Atlantic, the diagnostic feature for the reorganization of Heinrich events in the sediment records in the presence of detrital carbonate (limestone and dolomite) derived from lower Paleozoic basins of northern Canada (Broecker et al., 1992; Bond et al., 1999; Hemming, 2004). Additionally, Heinrich events are also marked by high lithic-to-foraminifer ratio and increased relative abundance of the polar planktonic foraminifer *Neogloboquadrina pachyderma* sinistral (Heinrich, 1988). However, HS Heinrich events display a lower flux of ice-rafted detritus (IRD) in the central and eastern North Atlantic (McManus et al., 1998; Hemming, 2004) and possibly contain significant amounts of detrital silicate derived from European and/or Greenland sources (e.g. Gwiazda et al., 1996; Snoeckx et al., 1999).

Hodell et al. (2008) used the XRF analysis to track the sedimentary diagnostic feature of the Heinrich events (Figure 7) for the last 1.4 Ma of North Atlantic climatic history. The authors showed that the elemental ratio Si/Sr provides a millennial time scale proxy for IRD layers that are rich in detrital silicate minerals and poor in biogenic carbonate, which can reflect the source origin and the related glaciological processes as well. The coupling of benthic $\delta^{13}C$ and Si/Sr (Site U1308) supports previous findings of a strong link between iceberg discharge (freshwater fluxes), lowered salinity, and weakening of thermohaline circulation (Hodell et al., 2008). While the elemental ratio Ca/Sr is used as an indicator of IRD layers that are rich in detrital carbonate (i.e., Heinrich layers). The IRD events that are poor in detrital carbonate and rich in silicate minerals are identified by peaks in Si/Sr, low Ca/Sr, and decreases in bulk $\delta^{18}O$ reaching about ~2%.

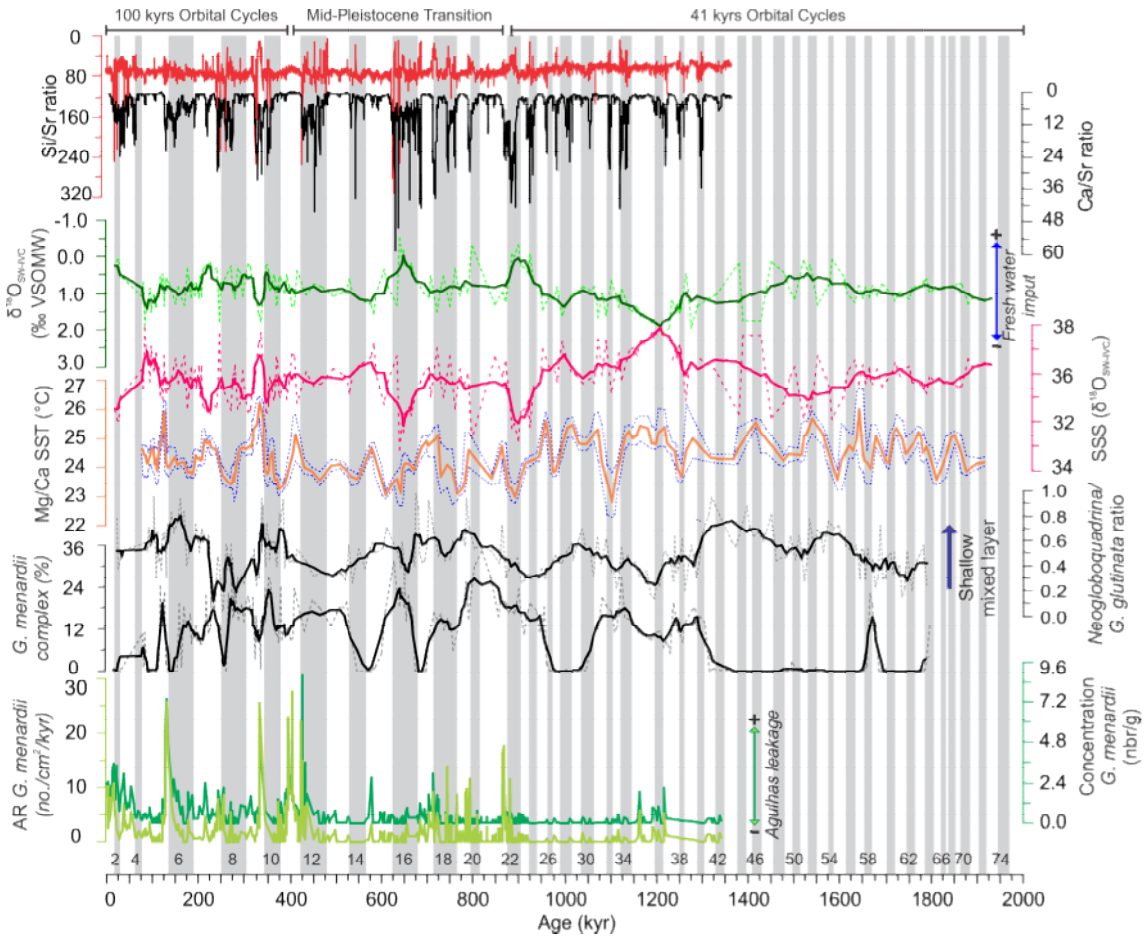

Figure 7. North Atlantic Site U1308 XRF elemental ratio Si/Sr (red line) and Ca/Sr (black line); western equatorial Atlantic core CDH-79 and reconstructed seawater oxygen stable isotope ice volume corrected ($\delta^{18}O_{SW}$; green line); sea surface salinity (SSS; pink line); and Mg/Ca-SST reconstruction (orange line), blue dashed line indicate the analytical uncertainty of the median Mg/Ca-SST; and planktonic foraminifera proxy *Neogloboquadrina* sp./*G. glutinata* ratio ($R_{N/Gg}$) and abundance of the *G. menardii* complex. From the south Atlantic ODP Site 1087, the concentration of *G. menardii* and accumulation rate of *G. menardii* (Caley et al., 2012).

Our record from the western Equatorial Atlantic show the long-term abundance changes of *G. menardii* complex (average ~9.7% for the last 1.80 Ma), where high abundance (average >12%) are related to the Ericson and Wollin (1968) Zones P, R, T, V and X, and low abundance or absence of the taxon (<1%) are related to Zones Q, S V, W and Y (Ferreira et al. A). The biostratigraphic *G. menardii* complex reappearance events (R events; Ferreira et al. A) shows a near synchronism with the increase in the concentration and accumulation rate of *G. menardii* in the southern Benguela region (Site 1083; Caley et al., 2012), while in the North Atlantic (Site U1308) the elemental IRD proxy (Si/Sr ratio; Hodell et al., 2008) show low values

(Figure 7). These features suggest a close relation witch the increasing of the AMOC strength and the reseeding of the taxon to the western Atlantic Ocean, especially during the *G. menardii* events R4 (~0.96 Ma; MIS 26; boundary T/S); R3 (~0.54 Ma; MIS 12/14; boundary U/V) and R2 (~0.13 Ma; MIS 5/6; boundary W/X). This mechanism appears to works during the subzonal boundaries R2/R1 (~1.31 Ma; MIS 41) and T2/T1 (~0.68; MIS 16) as well. The suggested increase in the AMOC strength can also be supported by the increase in the SST records (Mg/Ca-SST; Figure 7) in our site (core CDH-79).

However, the biostratigraphic *G. menardii* complex disappearance events (D events; Ferreira et al. A) are associated with an increase in the IRD proxy in the North Atlantic and decrease/low values of concentration and accumulation rate of *G. menardii* in the southern Benguela region, as *G. menardii* D4 (~1.05 Ma; MIS 30; boundary R/S), D3 (~0.59 Ma; MIS 15; boundary T/U), D2 (~0.16 Ma; MIS 8; boundary V/W), and D1 (~0.07 Ma; MIS 5; boundary X/Y) (Figure 7). Associate to these events our records shows a decrease in the reconstructed SST (Mg/Ca-SST; Figure 7), supporting the suggestions of reduced and/or disrupted Agulhas leakage due to northward STF migration, followed by the slowdown AMOC (e.g. Hodell et al., 2008; Carley et al., 2012).

Although the Agulhas leakage and AMOC changes have been well studied for the last 1.40 Ma (e.g. Hodell et al., 2008; Caley et al., 2011, 2012), less is known about their changes prior to this interval. Appling the proposed taxon reseeding mechanism (Caley et al., 2012), associated to the IRD proxy (Hodell et al., 2008) and comparing with *G. menardii* complex abundance records of the tropical Atlantic, we suggest a proxy to track the influence of the AMOC strength over ~1.92-1.30 Ma (MIS 73-40/41). Our record supports the interpretation of continuous migration and a northward mean position of the STF over ~1.92-1.78 Ma (MIS 73-64), expressed by the upward decrease of *G. menardii* complex (Zone Q; Ferreira et al., A). This time interval (~175 kyr) represents a decrease of AMOC strength, lowering the heat and salt inter-ocean and inter-hemisphere exchange. The disappearance of the taxon (*G. menardii* D5; ~1.78 Ma, MIS 64; Ferreira et al., A) and its absence in the western equatorial Atlantic records until ~1.68 Ma (MIS 59 boundary) suggest a continuous decrease or a complete interruption of the Agulhas leakage (northward STF position). This slowdown AMOC scenario is also supported by a decreasing trend in MAT-SST records between ~1.80-1.68 Ma (MIS 64-59; Figure 5).

The reappearance event *G. menardii* R5 (~1.68 Ma; MIS 59; boundary Q/R) mark the onset of the followed ~20 kyr time interval (~1.68-1.65 Ma; MIS 59-58; Subzone R3; Ferreira et al., A) characterized by high abundance of the taxon (average 13.18%). These features suggest the resumption of the AMOC strength by the southward migration of the STF. During this interval, the reconstructed average SST showed high values (Mg/Ca-SST 24.6°C; MAT-SST

annual mean 26.7°C). The higher abundance of the taxon (22.44%) was associated with elevated reconstructed SST (Mg/Ca-SST 25.5°C; MAT-SST annual mean 27.3°C) supporting a southern position of the STF over ~1.66 Ma. The following interval (~1.65-1.30 Ma; MIS 58-40/41) are marked by the low abundance of the *G. menardii* complex (between absences to 2.52%) and a decreasing trend in the MAT-SSTs (Figure 5) probably associated with the northward migration of the SFT and reduced overturning strength (e.g. Caley et al., 2012).

5.2. Pleistocene planktonic foraminifera as tracers for water column changes

5.2.1. Gelasian - Calabrian - ~1.93 – 1.30 Ma (MIS 73-40/41)

Over ~1.93-1.30 Ma (MIS 73–40/41), the western equatorial Atlantic show a slight increase in the mean SST, ranging from 23.2-26.8°C (Mg/Ca-SST average 24.7°C; Figure 5) and 22.9-27.4°C (MAT-SST annual mean average 25.7°C; Figure 5). Our record is in agreement with estimated SST (MAT average 25.6°C) for the last 0.56 Ma of the Caribbean Sea (ODP Site 999; Martinez et al., 2007). However, they are lower than reported for the Amazon Fan (28.8°C) and Ceara Rise (28.9°C) SST for last ~0.30 Ma (Wilson et al., 2011), and from modern data range (average 27.5°C; between 27.3-28.2°C; Locarnini et al., 2018; Figure 1a). The glacial mean SST (Mg/Ca-SST 24.7°C; MAT-SST: annual 25.8°C, summer 27.1°C, and winter 24.1°C) are close or higher than the average SST recorded during the interglacial interval (Mg/Ca-SST 24.7°C; MAT-SST: annual 25.6°C, summer 26.9°C, and winter 24.2°C), showing a warm glacials with low thermal amplitude in the glacial-interglacial cycles. The reconstructed SSS (average 35.7; Figure 6) was in agreement with the modern data range ~35.6 (Zweng et al., 2018; Figure 1b), with the glacial intervals presenting the higher mean SSS (average 35.9) than interglacial (average 35.6).

The abundance changes of *G. menardii* complex (discussion on item 5.1) suggest a continuous slowdown in the AMOC through MIS 74-60 (~1.93-1.69 Ma), followed by NBC, the decreasing trend in the SST, and low thermal amplitude between glacial-interglacial cycles (Figure 5). A decrease in the thermal amplitude between both reconstructed SST (~2.6°C), suggesting the shoaling of the mixed layer. Following this change in the thermal amplitude an opposite trend with the mixed layers species (decrease of *G. ruber*, *G. glutinata,* and *G. sacculifer*; Figure 3) and the $R_{N/Gg}$ proxy (increase; Figure 4), support the continuous shoaling of the mixed layer. The abundance of *G. ruber* and *G. sacculifer* are related to oligotrophic and seasonal conditions with stable deep-mixed layers that characterize the central subtropical gyre of the Sargasso Sea, the southern Caribbean Sea, and equatorial Atlantic (Nishi et al., 2000). The shoaling of the mixed layer can promote the presence of cold and nutrient-rich thermocline waters in the photic zone, boosting regional primary productivity (Longhurst,

1993; Portilho-Ramos et al., 2017). These changes in the water column structure allowed the increase in the abundance of opportunistic species as recorded on core CDH-79 by *G. bulloides* and *N. dutertrei* (Figure 3). Both species positively related to eutrophic conditions, and used to track the past variability and intensity of surface upwelling systems (Schiebel et al. 2004; Kucera et al., 2005; Mohtadi et al., 2005; Lessa et al., 2014).

The behavior recorded by dweller specie, decreasing in *G. truncatulinoides* (average 1.90% over ~1.80-1.69 Ma) followed by abundance peaks of *G. inflata* (3.3% at ~1.73 and 1.69 Ma), also support the suggestion of the breakdown of surface-water stratification (Martinez, 1997; Nishi et al., 2000; Schiebel and Hemleben, 2017) by the shoaling of the mixed layer and thermocline. *G. truncatulinoides* is a mid-latitude specie that prefers a deep and permanent thermocline (Martinez, 1997) and free of any pycnocline barrier, as a deep chlorophyll maximum (Lohmann and Schweitzer, 1990; de Vargas et al., 2001; Renaud and Schmidt, 2003). Moreover, *G. inflata* is only abundant in the transition zone between the subpolar and subtropical provinces (Kipp, 1976), and low SST (~15-20°C), reduced salinity seasonality and well-oxygenated waters, characterizing times when the surface-water stratification decreased (e.g. Nishi et al., 2000). The recorded abundance peaks of the dwellers' species *G. truncatulinoides* and *G. inflata* was also observed in the Sargasso Sea (Site 977a) between 1.6-1.9 Ma (Nishi et al., 2000), supporting the suggestion of colder and low stratified water column for both areas, probably by weakening in the AMOC strength.

The drop in the abundance of *G. inflata* occurs ~1.69 Ma (MIS 59/60 boundary), followed by *G. menardii* R5 event (boundary zones Q/R), suggesting the resumption of the AMOC strength for a short time interval (~20 kyr), as supported by *G. menardii* complex abundance peak. This short and warm interval represented by MIS 59 (Subzone R3), recorded a high MAT-SST annual mean (average 25.9°C) and thermal amplitude between superficial water column layers of ~1.7°C. Besides, a high abundance of oligotrophic mixed layer species (*G. ruber* and *G. sacculifer*; Figure 3) and lower abundance of opportunistic species as *G. bulloides*, and *N. dutertrei* (Figure 3) and values of an ecological index (i.e. richness – R and diversity - H´; Figure 4) characterized this period as well. The geographic distribution of the planktonic foraminifera group present diversity decreases from the central gyres of the ocean towards continental margins and/or eutrophic regions (e.g. Martinez et al., 2007), while lower diversity values also were related to a deep thermocline in the Caribbean Sea (Martinez et al., 2007) and by the presence of *G. truncatulinoides* (e.g. Nishi et al., 2000; de Vargas et al., 2001; Renaud and Schmidt, 2003). Following the warm interval recorded at MIS 59, through ~1.67-1.60 Ma (MIS 58-55) an abrupt decrease in *G. menardii* complex, and in the SST and the thermal amplitude (average ~0.3°C at ~1.62 Ma; MIS 56) was recorded and associated to a

decrease in the AMOC strength (reduced overturning strength). *G. truncatulinoides* presents intermediate abundance (~2.62%) suggesting a continuous deep thermocline between ~1.69-1.60 Ma (Figure 3).

Over ~1.60-1.30 Ma (MIS 55-40/41) an increase in the superficial water column temperatures was recorded for both, MAT-SST (~2.6°C; from 24.0-26.6°C) and Mg/Ca-SST (~1.5°C; from 23.2-24.7°C), as well as observed in the thermal gradient, from ~0.3°C to ~1.8°C (Figure 6). Our faunal record, suggests a continuous shoaling of the mixed layer (increasing $R_{N/Gg}$ proxy and *N. dutertrei;* decrease in mixed layers species; Figure 3, Figure 4) and the slowdown of the AMOC and NBC (lower abundance of *G. menardii* complex; average ~0.55%). Also, a decreasing trend until the lower abundance of *G. truncatulinoides* and *G. bulloides* was recorded. At the regional and seasonal scale, the quantity and quality of food are predominantly important for the distribution of shallow- and subsurface dwelling plankton foraminifers (e.g. Fairbanks et al., 1980; Schiebel and Hemleben, 2017). The enrichment of nutrients caused by shoaling of the mixed layer can induce the thermocline shoals in the photic zone, promoting the nutrients enrichment of the water column and a new phytoplankton production (e.g., diatoms), and the planktonic forms that prefer 'fresh' prey (e.g. *N. dutertrei*) proliferate (Schiebel et al. 2001, 2004). The lower abundance of *G. truncatulinoides* also supported the presence of the thermocline in the photic zone (e.g. Nishi et al., 2000; de Vargas et al., 2001; Martinez et al., 2007).

An alternative hypothesis involves the input of nutrients by the freshwater influx. The freshwater and nutrients supply can also promote the increase of species as *N. dutertrei*, as recorded in the eastern and western Caribbean (Orinoco and Magdalena rivers; Schmuker and Schiebel, 2002; Martinez et al., 2007), and the Brazilian Equatorial Margin (Amazon river; Schmuker and Schiebel, 2002). *N. dutertrei* is a tropical to subtropical thermocline dwelling species (Bé, 1977), that in the modern ocean is common in the eastern tropical regions and along eastern boundary currents (Bé, 1977) as of the subtropical gyre (Nishi et al., 2000). This specie is also abundant in active current systems along the continental margin and upwelling regions (Kipp, 1976), associated with the chlorophyll maximum (Fairbanks et al., 1982). At Ceara Rise (Site 925), tropical neogloboquadrinids are associated with the most thermal stratification of the euphotic zone (Chaisson and Ravelo, 1997). The reconstructed $\delta^{18}O_{sw}$ shows the lower average 0.85‰ (between 0.06-1.75‰) during MIS 55-40/41, within the increasing of *N. dutertrei*. Detrital riverine input reduces the salinity and supply nutrients (e.g. nitrate, silica, and ammonia) to the oceans basins, increasing the biomass (diatoms) and shoaling the chlorophyll-α maximum (Corredor and Morell, 2001). In the western Caribbean, Martinez et al. (2007) recorded a high abundance of *N. dutertrei* during events of disruption of

the mixed layer and related to the freshwater influx. The reduction on salinity and establishment of chlorophyll-α maximum in the photic zone can explain the behavior of *N. dutertrei* and *G. truncatulinoides*, once, the last specie is considered an indicator of the high salinity (e.g. Shmuker and Schiebel, 2002), wich preferences of pycnocline barrier in the water column (e.g., de Vargas et al., 2001; Renaud and Schmidt, 2003). The more eutrophic conditions and lower mixing of surface waters by the shoaling of the mixed layer (i.e. $R_{N/Gg}$ proxy) also can explain the continuous decrease in the oligotrophic species as *G. ruber* and *G. sacculifer* (Figure 4).

Associated to the base of Olduvai Subchron (~1.93-1.69 Ma; MIS 73-59/60) the changes in the faunal records of western equatorial Atlantic (core CDH-79) supported a transition from the warm, stratified, and oligotrophic water column to more eutrophic, and colder waters, which lower thermal stratification on the euphotic zone, associated to a slowdown in the AMOC strength. Following this interval, over the early Matuyama (~1.69-1.30 Ma; MIS 59/60-40/41), we record slight warming in the superficial waters with a continuous increase in the salinity and stratification of the water column due to the mixed layer and thermocline shoaling. These features support a slight increase in the AMOC strength, followed by increased freshwater inflow (lower values of $\delta^{18}O_{sw}$).

5.2.2. Calabrian to Middle Pleistocene - ~1.30 – 0.89 Ma (MIS 40/41 – 12)

Around 1.30 Ma (MIS 40/41), an abrupt change in the paleoceanographic conditions are evidenced by our faunal and geochemical records. The onset changes in the western equatorial Atlantic appears to be near synchronous with IRD proxy peak (Figure 7) in the North Atlantic (Site U1308; Hodell et al., 2008), and with a slight increase in the concentration of *G. menardii* at the Benguela region, recorded over 1.35 to 1.30 Ma at Site 1087 (Caley et al., 2012). In the western equatorial Atlantic (CDH-79) the subzonal boundary R2/R1 (~1.31 Ma; MIS 41; Ferreira et al., A) marked by the return of high abundance of *G. menardii* complex (average 13.17%), is followed by the highest SSS recorded (from 35.0 to 38.2; average 37.0) and by high SST values (MAT-SST annual mean and Mg/Ca-SST averages 26.5°C and 24.8°C). The increased thermal amplitude between the water column layers (average 1.6°C) is also recorded over ~1.30-1.12 Ma (MIS 40/41-33/34).

Studies using modern instrumental observations coupled to ocean-atmosphere climate simulations (e.g. Zhang et al., 2011), and the sedimentary records (e.g. Nace et al., 2014) suggest a correlation with the NBC transport and North Atlantic SST in both, centennial and millennial timescales. The authors also suggest an increase in the western equatorial Atlantic SST and precipitation on the adjacent continent due to the decrease northward cross-

equatorial heat transport during massive fluxes of icebergs and meltwater into the North Atlantic (i.e., IRD proxy peak; Figure 7) (Hodell et al., 2008; Zhang et al., 2011; Nace et al., 2014). However, some studies suggest that the signals originated in the Agulhas leakage region contribute to decadal- to millennial-time scale AMOC variability on the same order of magnitude as the often invoked northern source (e.g. Biastoch et al., 2008; Caley et al., 2011).

This saltiest event recorded in the western equatorial Atlantic, and centered over ~1.26-1.12 (MIS 33/34-38/39), can be a result of the coupling of both mechanisms, the decrease in the NBC transport by AMOC slowdown due to the cold event in North Atlantic (IRD proxy peak; Figure 7), as support for the weak upper NADW ventilation recorded at Blake Ridge (ODP Leg 164 Site 997A; mid-latitude western Atlantic; Nishi et al., 2000), after ~1.2 Ma (Becquey and Gersonde, 2002; Diekmann and Kuhn, 2002). Whilst in the southern hemisphere, increased strength at Agulhas leakage (peak of *G. menardii* concentration; Figure 7) by the southward migration of the STF (Site 1087; Caley et al., 2012), promote a continuous transport of the salty and warm waters from the south hemisphere to the Equator.

The slowdown of AMOC (due to North Atlantic cold events) promotes changes in the position of the NBC, moving the current away from the coast, and feeding in the superficial (Silva et al., 2005) and subsuperficial layers (Silva et al., 2009) the NECC, in a process known as NBC retroflection (NBCR) (Fonseca et al., 2004). Besides, modeling studies suggested that the freshwater input into the high latitudes of North Atlantic were able to trigger a reversal of the NBC under both present-day (Chang et al., 2008) and Last Glacial Maximum (LGM, 23-19 kyr) conditions (Schmidt et al., 2012; Nace et al., 2014).

As recorded by modern instrumental observations at the area (3°S-7°N; 40°-52°W), high sanity concentrations (>36.8) occurs near 100 m depth, and are associated with the subsurface maximum salinity waters formed in the region of the subtropical gyres in the North of Equator (Silva et al., 2005. 2009). The rings formation at the north Equator (4-5° N) are linked to the increase in the NBC/NBCR (and the subsurface North Brazilian Under Current) system (Pailler et al., 1999; Stramma et al., 2005) that can act as a physical barrier for the cross-equatorial heat and salinity transport (e.g. Johns et al., 1990, 2003), and possible transport some of those rings over the study area (Silva et al., 2005; 2009). That tropical accumulation of salt and warmth that would result from a reduction in northward NBC transport ultimately impacts the density of high latitude surface waters and thus has important implications for the formation and production of NADW (e.g. Wilson et al., 2011)

This saltiest event is also characterized by lower richness and diversity (Figure 4), and increasing in the abundance of oligotrophic mixed layer species (Figure 3), those features characterized the central subtropical gyre of the Sargasso Sea (Nishi et al., 2000), and suggest

the establishment of a warm and salty ring in the area by the action of the BL. A strong NBCR can also redistribute the sediments southeastward (Silva et al., 2005; 2009), promoting the redistribution of the fresh nutrients in the superficial waters, the establishment of an intermediate to deep mixed layer, and thermocline shifts to depth (e.g. Schiebel and Hemleben, 2017). This scenario is also supported by the increase in the *G. bulloides*, while the shifts in the thermocline position can explain the *N. dutertrei* decrease (Figure 3).

From ~1.11 (MIS 33/34) to 0.97 Ma (MIS 26/27), a continuous decrease in the MAT-SSTs (annual average 25.4°C; summer average26.8°C; winter average 23.5°C), is followed by an opposite trend between SSS (decrease) and $\delta^{18}O_{sw}$ (increase). Additionally, a high amplitude changes in the abundance of the mixed layer, and dwelling species (Figure 3), suggesting the changes from a salty, warm, and more stratified water column (intermediate to deep mixed layer and thermocline) to a continuous less salty and colder waters which shallow mixed layer and thermocline (over MIS 30/31-33). The salty and warm decrease is probably related to a weak AMOC, marked in our study area by the absence of *G. menardii* complex between the events D4 (~1.05 Ma) and R4 (~0.96 Ma), and low concentration on the Benguela area (Figure 7) (Caley et al., 2012). Following the absence of *G. menardii* complex, abundance peaks of *G. inflata* (average ~1.46%; MIS 30-26) characterizing times when the surface-water stratification decreased (e.g. Nishi et al., 2000). Our records also show a sharp decrease trend in the MAT-SST, who began soon after (MIS 30), showing the lowest values over ~0.98-0.97 Ma (MIS 27; average ~23.2°C), as recorded for Mg/Ca-SST (average ~24.1°C) as well. The faunal records suggested colder (superficial waters colder than mixed layer) waters with a low surface-water stratification and a decrease in productivity, probably by a change to the deep thermocline position. Those interpretations were supported by the opposite trend between *G. menardii* complex and *G. infalta* as well.

The boundary MIS 25/26 (~ 0.96 Ma; *G. menardii* R4 event) mark the increase in the AMOC strength, and the return of warm waters to the area, where MAT-SST increased ~1.7°C while Mg/Ca-SST decrease ~0.3°C, which thermal amplitude between superficial layers ~1°C. The return of *G. menardii* complex (R4 event; MIS 25/26) was followed by the low abundance of *G. inflata*, while oligotrophic species from the mixed layer shows an opposite abundance trend with *G. bulloides*. The lower abundance of *N. dutertrei* suggested a deep thermocline.

5.2.3. Middle Pleistocene - ~0.89– 0.41 Ma (MIS 22-11)

Slightly before and during the early half of the Middle Pleistocene, important changes in western equatorial Atlantic surface water dynamics (currents and water column structure) were addressed by both faunal and geochemistry records. Spanning over ~0.97-0.86 (MIS 26-

21) the first abrupt change that marks the onset of the Middle Pleistocene appears in our records (core CDH-79). This event is featured by an abrupt decrease on the SSTs of 2-3.8°C centered at ~0.88 Ma, where the lower values are recorded (Mg/Ca-SST 22.9°C; MAT-SSTs: annual mean 22.6°C, summer 24.4°C, winter 21.3°C). Before this cold event, a rapid increase of 1.1-4.4°C (Mg/Ca-SST 1.1°C; MAT-SSTs: annual mean 3.8°C, summer 2.9°C, winter 4.4°C) are recorded over ~0.97-0.94 Ma (MIS 26-25) and also followed by close among the increase of 1.9- 4°C (Mg/Ca-SST 1.9°C; MAT-SSTs: annual mean 4°C, summer 2.3°C, winter 3.8°C) over ~0.88-0.86 (MIS 21-22). These oscillations observed in SSTs are followed by SSS and $\delta^{18}O_{sw}$, which the lowest values recorded at 0.89-0.88 Ma (SSS 33. 2; $\delta^{18}O_{sw}$ -0.37‰) as well. These large changes in SSTs, $\delta^{18}O_{sw}$ and SSS (~1.1-4.4°C, 1.82‰ and 3.8, respectively) support a high among of freshwater influx, affecting the superficial oceanography of the area (e.g. Schmidt et al., 2004; Weldeab et al., 2006; Wilson et al., 2011; Nace et al; 2014).

The large increase in freshwater offshore was interpreted as the product of massive fluvial input from the adjacent continent (e.g. Arz et al., 1998; Jennerjahn et al., 2004; Dupont et al., 2010; Zhang et al. 2015). The nearest and main source of freshwater and terrigenous sediments to the site location is the Parnaíba river, with a modern drainage basin area of about 333,056 km^2 (3.9% of Brazil) (ANA, 2015) which annual average discharge rate of 1272 m^3/s (e.g. Marques et al., 2004), and considered the second most important drainage basin of northeast Brazil (ANA, 2015). In addition, the northeast of the site is located the Amazon river basin, with an annual average discharge rate of $2\times10^6 m^3/s$ (Lentz, 1995; Allison et al., 2000). Based on the river-ocean model of Karr and Showers (2002), that suggests a linear mixing pattern between isotopically negative fresh river water and the saline ocean, where the modifications by atmospheric processes are negligible, we assume that more isotopically negative ice-volume corrected oxygen isotope values ($\delta^{18}O_{sw}$) indicate a greater riverine influx (e.g. Wilson, et al., 2011). Some studies demonstrated that a freshwater influence from the equatorial Atlantic leads to a weakening of the AMOC (e.g. Goelzer et al., 2006). The increase in the NBCR due to NBC reduction (AMOC decrease) promotes changes in the position of the NBC, feeding in the superficial (Silva et al., 2005) and subsuperficial layers (Silva et al., 2009) the NBC retroflection (Fonseca et al., 2004). Some studies demonstrate that modern seasonal NBC retroflection feeds the NECC with freshwater and sediment from the Maranhão coast (Bourles et al. 1999, Silva et al. 2005), and also suggest that during strongest NBCR (Aug–Oct), almost 70% of the Amazon freshwater plume is transported eastwards towards the NECC (Rühlemann et al., 2001). Modern instrumental observations indicated that freshwater from the Amazon could induce a marked pycnocline (3-30 m depth range), creating a thick barrier layer (>40m) here a large portion of the solar radiation might be trapped and could extend

over a large portion of the equatorial Atlantic basin (Pailler et al., 1999; Masson and Delecluse, 2001).

An additional mechanism that possible might have influenced the surface freshening in our site are related to the millennial-scale events of disrupted cross-equatorial heat transport by massive fluxes of icebergs and meltwater into the North Atlantic (i.e., Heinrich Stadials, HS) (Hodell et al., 2008; Kageyama et al., 2013); promoting the slowdowns of the AMOC (MaManus et al., 2004; Lippold et al., 2009). Our record from MIS 22 event (Figure 7) are synchronous with low values of *G. menardii* concentration in the Benguela region (Site 1087; Caley at al., 2012) and which high values of IRD proxy (Si/Sr ratio average ~29.33 over 0.89-0.88 Ma) at North Atlantic (Site U1308, Hodell et al., 2008), supporting previous findings of a strong link between iceberg discharge, lowered salinity, and weakening of thermohaline circulation that characterize the events recorded during the last glacial cycle as the Heinrich events (e.g. Hemming, 2004; Alley, 2007; Zhang et al., 2011). These events promote a cool air temperature surface in the North Atlantic, while temperatures over the South Atlantic warm (Barker et al., 2009) in the process known as thermal bipolar seesaw (Broecker, 1998). As a result, ITCZ adjusted its position by the migration towards the warmer hemisphere (Kageyama et al., 2013), in this case to the southern hemisphere. The position of the ITCZ at the tropical Atlantic Ocean can be tracked by the low-salinity belt and by prominent changes in water column structure due to the excess of freshwater flux (e.g. Portilho et al. 2017). The freshwater flux creates a thin low salinity surface layer that hampers efficient wind-driven vertical mixing (Montégut et al., 2007; Mignot et al., 2007) changing the density of the upper water column (e.g. Portilho-Ramos et al., 2017). In the western Pacific Ocean, some studies demonstrated that heavy precipitation is the main mechanism for barrier layer formation (e.g. Sprintall and Tomczak, 1992; Ando and McPhaden, 1997).

The actuation of both mechanism simultaneously (precipitation over the ocean due to southern position of the ITCZ and increased river influx) can promote a deep extension of cold and freshening conditions in the water column, probably until the 50 m depth (or deeper) of the water column (e.g. Pailler et al., 1999; Masson and Delecluse, 2001). Different from HS events of the last glacial, a weak AMOC can promote a southward migration of the positive/negative boundary of the SST anomaly, leaving the core site in the negative domain. This suggestion is also supported for the restricted vertical migration of the specie *G. ruber* (between 25-50 m; Anand et al., 2003), and the lowest derived SST (Mg/Ca-SST 22.9°C) and SSS (33.2; $\delta^{18}O_{sw}$ -0.37‰) values, all these proxies based on the $\delta^{18}O$ of the specie. The abundance peaks of *G. inflata* (average 1%) and low abundance of *G. truncatulinoides* (average 1.34%) also support the breakdown of the water column stratification (e.g. Martinez, 1997; Nishi et

al., 2000; de Vargas et al., 2001; Renaud and Schmidt, 2003; Schiebel and Hemleben, 2017). While high values of *G. bulloides* (10.40%) and *G. glutinata* (14.11%) also support the fertilization of the water column (e.g. Schiebel et al. 2004; Kucera et al., 2005; Mohtadi et al., 2005; Lessa et al., 2014) by the increased detrital supply (e.g. nitrate, silica, and ammonia) due riverine input to the oceans basins (Corredor and Morell, 2001).

Our record supports the occurrence of a colder and freshening event centered on MIS 22 (0.89-0.88 Ma) that marks the onset of new paleoceanographic conditions in the western equatorial Atlantic. This event is associated with changes in the dominant periodicity of the glacial-interglacial cycles from symmetrical low-amplitude, high-frequency ice volume variations (41 kyr) to high-amplitude, low-frequency asymmetrical ice volume variations (100 kyr) that indicate gradual ice build-up terminated by rapid deglaciation events (e.g. Maslin et al., 2001; Ruddiman, 2003). These changes in the periodicity of the cycle seem to be the trigger for abrupt climate changes and atmospheric reorganization that characterize the Middle Pleistocene Transition (MPT; Mudelsee and Schulz, 1997). Our records (faunal and geochemistry proxies) also support the coupling between the massive flows of icebergs and melted water in the North Atlantic (Hodell et al., 2008) and the strongest NBCR in the western equatorial Atlantic (our record), both mechanisms related to slowdown of the AMOC (e.g. Zhang et al., 2011; Crivellari et al., 2018), that promote a high latitudinal thermal gradient, reducing the ITCZ penetration in the northern hemisphere, and maintaining a mainly southern position (probably over the continent area) during ~0.94-0.86 Ma (MIS 21-25). This longer-term migration in the mean position of the ITCZ can promote longest wet seasons (e.g. Maslin and Burns, 2000; Dahl et al., 2005), and greatly alters the dynamics of regional climate causing a decrease in the cross-equatorial transport of heat and salinity by upper-level ocean currents (Berger and Wefer, 1996; Maslin et al., 1997; Vink et al., 2002) and increase the sedimentation yield from the river drains. The onset event age in our records is in agreement whit suggested by others works (e.g. Mix et al. 1993), and for the closed record at the Ceara Rise, with the estimated age of 0.93 Ma (Site 927; Bassinot et al., 1997).

Over the middle MPT (~0.73-0.61 Ma; MIS 15-17), other important changes in the paleoceanographic conditions similarly to MIS 22 event, supporting the occurrence of a second cold and freshening event during the MPT at the western equatorial Atlantic. As recorded on the previous event, the MIS 16 event (centered at ~0.63 Ma) is characterized by the lowest SSTs (MAT-SSTs: annual mean 26.2°C, summer 27.1°C, winter 23.3°C; Mg/Ca-SST 22.7°C), associated with the lowest values of SSS (32.8), and $\delta^{18}O_{sw}$ (-0.55‰). In addition, a short interval prior to MIS 16 event (over ~0.73-0.68 Ma), is marked by the increase in the SSTs of around 1.9-2.9°C (Mg/Ca-SST 1.9°C; MAT-SSTs: annual mean 2.9°C, summer 1.8°C, winter

0.4°C), and also followed by the increase of 1.1-2°C (Mg/Ca-SST 1.1°C; MAT-SSTs: annual mean 1.6°C, summer 1.8°C, winter 2°C) over ~0.64-0. 61 (MIS 15-16). The pattern presented for the SSTs is also followed by the SSS and $\delta^{18}O_{sw}$, supporting an increase in the freshwater input as discussed above. The MIS 16 event is also synchronous with the low concentration of *G. menardii* in the Benguela region (Site 1087; Caley et al., 2012), and with high values of IRD proxy (Si/Sr ratio average ~11.06 over 0.67-0.63 Ma) in the North Atlantic (Site U1308; Hodell et al., 2008). The MIS 16 differs from the previous event by the low occurrence of *G. bulloides*, while the abundance peak of *N. pachyderma* marks the onset of this event (~20% at 0.67 Ma).

Coupling the features observed in our surface water proxies (faunal and geochemistry proxies) with the high values of the IRD proxy in the North Atlantic (Hodell et al.,2008) and low *G. menardii* concentration, we suggest the occurrence of the two oldest Heinrich event recorded at the western equatorial Atlantic. The first one centered over ~0.89-0.88 Ma (MIS 22), and the second one over ~0.63 Ma (MIS 16), supporting the proposal of Hoddel et al. (2008) for MIS 16 event. These events presented a similar pattern between then, as a short increase in the SSTs and SSS, followed by close among decrease until the apex of the event, and later a sharp increase at the end of the event. While $\delta^{18}O_{sw,}$.present an opposite pattern than SSTs. Additionally, both events are characterized by a deep extension of cold and freshening conditions in the water column, probably until the 50 m depth (or deeper) of the water column, as supported by the *G. ruber* $\delta^{18}O$ proxies. The main difference is that over MIS 16 higher values of the Ca/Sr ratio (average 208.8 around 0.64 Ma) in the North Atlantic (Hodell et al., 2008) and the highest abundance of *N. dutertrei* in the western equatorial Atlantic. Those millennial-scale events observed in the tropical Atlantic are associated with a marked slowdown of the AMOC, and with the rearrangement in the poleward heat transport (Dahl et al, 2005). They also change the position of the thermal equator, affecting the mean position of the ITCZ and the location of the tropical rain belt, increased precipitation in tropical South America and the Altiplano (e.g. Baker et al. 2001, Cruz et al., 2005; Cruz et al., 2009), increased runoff in the Northeast Brazil (e.g. Arz et al., 1998; Dupont et al., 2010; Zhang et al., 2015) and also recorded during the younger Heinrich event (HS1) (Crivellari et al., 2018).

Between those "Heinrich event" (MIS 22 and 16), the superficial proxies support a time interval characterized by the shoaling of the mixed layer ($R_{N/Gg}$ proxy and decrease of mixed layer species; Figures 3 and 5; Nishi et al., 2000; de Vargas et al., 2001; Martinez et al., 2007). The increase in the AMOC strength (high values of *G. menardii* complex) are also suggested for the interval MIS 19/20-21 and followed by a decrease in the current strength over MIS 16-19/20. A decrease in the freshwater input ($\delta^{18}O_{sw}$ average 0.85‰) promotes the increase in the SSS (average 35.7) is also supported and suggests an abrupt decrease in the river input

associated to change in the ITCZ position. The low values of the IRD proxy recorded at the North Atlantic (Figure 7) support a slightly northward main position by North Atlantic warming (Hodell et al., 2008) due to the increase in the AMOC and Agulhas leakage (an increase of *G. menardii* concentration; Caley et al., 2012) (Figure 7).

After the MIS 16 event, over the early Middle Pleistocene (~0.63-0.41 Ma; MIS 15/16-11/12), a new scenario has been established. The reconstructed SST (25.1-26.9°C; average 25.9°C) and mixed layer temperature (23.3-25.7°C; average 24.2°C) showing the highest thermal amplitude between the surface layers (average 1.8°C), however lower frequency and amplitude changes along with this interval, probably resulting for the weak AMOC strength (Figure 7; Hodell et al., 2008; Caley et al., 2012) as suggested by the low/absence of *G. menardii* complex. This warm and stable period, shows high values of $\delta^{18}O_{sw}$ (average 0.94; Figure 5), presenting intermediate and almost constant values of the mixed layer and opportunistic species, suggesting a well mixed and thermal stratification in the surface waters (deep of the mixed layer). However, during a short interval between the MIS 15-14 (Zone U, absence of *G. menardii*), an abundance peak of *G. truncatulinoides* was recorded, followed by *G. bulloides,* suggesting a short interval with deep thermocline or the breakdown of surface-water stratification.

5.2.4.Middle - Early Pleistocene - ~0.41– 0.014 Ma (MIS 11-2)

Following the MPT, the Earth´s climate system had lower mean global temperatures, increased global ice volume, lower mean sea-surface temperatures, and increasingly severe glacial temperatures (Shackleton et al., 1990). Those features marked the Mid-Brunhes Event (MBE) onset. The MBE represents a major climatic decoupling of climate conditions in different latitudes with glacial-interglacial contrasts up to 8°C (Kunz et al., 2002; Holden et al., 2011). It is also marked by the strong increase in the accumulation of carbonate in the oceans that might have been caused by the proliferation of phytoplankton (Flores et al., 2003, Barker et al., 2006). Significant changes in the thermohaline circulation took place during this climate transition causing a reduction of NADW input to the Antarctic Circumpolar Current, a weakening of the surface waters from the Indian Ocean to the South Atlantic via the Agulhas Current, and an increase in biological activity was documented during glacial stages of the last ~0.6 Ma (Schimieder et al., 2000; Kuhn and Diekmann, 2002).

In the western equatorial Atlantic, the last 0.41 Ma (0.41 – 0.016 Ma; MIS 11-2) was characterized by the highest frequency and amplitude oscillations in the MAT-SST (averages annual mean 26.3°C; summer 27.2°C; winter 24.7°C), and Mg/Ca-SST with an average of 24.3°C (22.6-26.37°C), high values between ~0.34-0.33 (MIS 9; 26.2-26.4°C), and low values ~20.63

Ma (MIS 2; 22.6°C). The SST reconstructions indicate the highest thermal amplitude between the surface layers (average ~1.6°C) and the highest temperature amplitude and frequency changes along with this interval. On the western Caribbean, the recoded SST for this interval oscillates from 25.5 to 27.5°C (ODP Site 999; Martinez et al., 2007). The high abundance of *G. menardii* complex (average ~11%) is recorded during almost interval and support a continuous taxon transport by Agulhas leakage, suggesting a southern mean position of the STF in the Benguela region (Figure 7; Caley et al., 2012). Whereas at North Atlantic, the IRD proxy support the occurrence of cold periods (Hodel et al., 2008), usually associated with a decrease in the Mg/Ca-SST of western equatorial Atlantic (core CDH-79).

Over ~0.33Ma (MIS 9) an event characterized by high average on SST (Mg/Ca-SST 26.3°C; MAT-SST annual mean 25.9°C, summer 27.4°C, and winter 23.8°C), SSS (37.4) and $\delta^{18}O_{sw}$ (1.65‰), suggesting the actuation of a similar mechanism recorded at Gelasian (~1.26-1.12 Ma; MIS 33/34-38/39). As recorded on the previous event, the synchronous occurrence between events in a different hemisphere, as North Atlantic cold events (Si/Sr ratio average 19.3 over ~0.34-0.33 Ma; and 18.2 over 0.33-0.32 Ma; Figure 7) and strong Agulhas leakage (*G. menardii* concentration peak; Figure 7), promote the increase in the NBCR system and the related ring formation, trapping the northward transport of heat and salty waters (Pailler et al., 1999; Stramma et al., 2005) over the area (this study). Those mechanisms promote a high stratification of the water (deepening in the mixed decrease and thermocline) as supported by the sharp decrease in the $R_{N/Gg}$ (Figure 6) proxy and *G. truncatulinoides*, while mixed layer and oligotrophic species increase (Figure 5) due to the formation of a salty barrier layer associated to the NBCR ring formation (Silva et al., 2005, 2009).

An opposite trend between SST (decrease) and SSS ($\delta^{18}O_{sw}$) are recorded over the MIS 8 (~0.27 Ma) and suggesting the continuous strong NBCR due to slowdown AMOC. The decrease in the AMOC is also supported by the recorded North Atlantic cold event (Si/Sr ratio average 15.4 over ~0.27 Ma; Hodell et al., 2008) and low concentration of *G. menardii* in the southern hemisphere (Figure 7; Caley et al., 2012) and appears to impact the western equatorial Atlantic with lower SST average (Mg/Ca-SST 24.1°C; MAT-SST annual mean 22.9°C; summer 24.0°C; winter 20.5°C) and a salty increase due to NBCR actuation. The following interval, over ~0.23-0.22 Ma (MIS 7) marks the increase in average SST (Mg/Ca-SST 24.5°C; MAT-SST annual mean 26.7°C; summer 27.0°C; winter 25.2°C) followed by SSS decrease and $\delta^{18}O_{sw}$.increase, that support a freshwater influx. This event is synchronous with the concentration peak of *G. menardii* in the Benguela region (Caley et al., 2012) and followed by low IRD proxy in the North Atlantic (Hodell et al., 2008) (Figure 7). This feeding is also supported by our faunal records (i.e. *G. menardii* complex), supporting an increase in the

precipitation ($\delta^{18}O_{sw}$ increase) by positive SST anomalies in the western equatorial Atlantic, probably due action of strong Agulhas leakage, that promote a continuous heat transport from south hemisphere to the Equator, and reduced transport from the Equator to the northern hemisphere.

After ~0.22 Ma until 0.08 Ma (MIS 7-5), especially over MIS 6 (~0.12 Ma), our records suggest a continuous strong NBCR due to slowdown AMOC (and NBC), supported by an increase in the IRD proxy at North Atlantic and Agulhas leakage, that promote the increase in the salinity associated to a decrease of freshwater influx (increase in $\delta^{18}O_{sw}$). A short interval characterized by a sharp increase in the SST (~0.13 Ma; Mg/Ca-SST 23.3°C; MAT-SST annual mean 26.6°C; summer 27.8), marked by the *G. menardii* R2 event in the area and associated with high *G. menardii* proxy peak (Caley et al., 2012), support a rapid increase in the AMOC strength.

6. Conclusion

The integration of independent proxies based on planktonic foraminifera species, geochemical (oxygen stable isotopic, $\delta^{18}O$) and trace elements (Mg/Ca ratio) analysis were applied to an ~32 m-long core CDH-79 to reconstruct the main changes in the superficial ocean circulation of the western equatorial Atlantic. Our results provide a reconstruction of the main mechanisms evolved on the oscillations of the AMOC (global scale) and NBC (local scale) systems and the characterizations of the main paleoceanographic changes for the longest continuous record of the Brazilian equatorial margin, covering the almost Pleistocene (~1.93-0.01 Ma; Gelasian to Late Pleistocene). Our superficial oceans reconstructions also support that strong NBCR event when synchronous with events on the south and/or north hemisphere can promote the accumulation and transport of salty and warm waters, as well as accumulation/transport of cold and low-salinity freshwater plumes in the site area.

Our records support the correlation between the western equatorial Atlantic biostratigraphic events of *G. menardii* complex (disappearance - D and reappearance – R events) with the oscillations at the Agulhas leakage due to STF migrations, and slowdown AMOC due north hemisphere stadial intervals. The *G. menardii* R events are related to increased Agulhas leakage due southward migrations of the STF (south tropical front) in the Benguela region, in special the events R4 (~0.96 Ma; MIS 26; boundary T/S); R3 (~0.54 Ma; MIS 12/14; boundary U/V) and R2 (~0.13 Ma; MIS 5/6; boundary W/X). This mechanism also is related to the subzonal boundaries marked by the return of the high abundance of the taxon as R2/R1 (~1.31 Ma; MIS 41) and T2/T1 (~0.68; MIS 16). While the *G. menardii* D events are associated with both mechanism, decrease or interruption of the Agulhas leakage due

northward migration of STF, and slowdown AMOC due to massive fluxes of icebergs and meltwater into the North Atlantic (stadials intervals) as recorded during the events D4 (~1.05 Ma; MIS 30; boundary R/S), D3 (~0.59 Ma; MIS 15; boundary T/U), D2 (~0.16 Ma; MIS 8; boundary V/W), and D1 (~0.07 Ma; MIS 5; boundary X/Y). We also suggest that the influence and residence time of the salty and warm transported by the AMOC from the southern hemisphere to the western equatorial Atlantic can be tracked by the abundance oscillations of the *G. menardii* complex.

The occurrence of two cold events in the North Atlantic and its impact on the tropical Atlantic paleoceanography and climatology are addressed and support the occurrence of the oldest Heinrich events, here for the first time recorded in the western equatorial Atlantic. The oldest large scale event occurs with the onset of the Mid-Pleistocene Transition (~0.89-0.88 Ma, MIS 22), and later, a second event occurs with the middle MPT (~0.63 Ma; MIS 16). In both, a thick cold and low-salinity layer (>50 m) dominated the superficial ocean at the site area. We suggest the synchronized large-scale river inflow (and freshwater plume) by increased (heavy) precipitation, both due to the southern mean position of the ITZC (probably over the continent), with the stadial events in the North Atlantic that promote strongest NBCR due to slowdown AMOC and weak NBC. The strongest NBCR can bring to the site area freshwater plumes from the main fluvial drainage (Parnaíba river), and possibly due southward transport in the superficial and subsuperficial layers of the retroflections system, freshwater plumes from Amazon river as well. However, the origin of the cold and low-salinity waters remains inconclusive.

We also provide the first record of millennial-time scale events of salty and warm accumulation in the Brazilian equatorial margin. Our records linked the salt and warm accumulation in the area with increased NBCR system, that can act as a physical barrier for the cross-equatorial heat and salinity transport and a possible accumulation of the salty water on the NBC rings, transported over the study area. We support the action of both mechanism, decrease in the NBC transport by AMOC slowdown (due stadial North Atlantic event), and increased strength of Agulhas leakage due to southward migration of the STF. The simultaneous occurrence between south and north hemisphere events promotes a continuous transport of the salty and warm waters from the southern hemisphere to the Equator, followed by weak transport or a temporary interruption on the Equator to north hemisphere transport. The coupling of these mechanisms can also impact the density of high latitude surface waters and thus has important implications for the formation and production of NADW. These events are recorded over the late (~1.26-1.12 Ma; MIS 33/34-38/39) and early (~0.33 Ma; MIS 9) Pleistocene

The main contribution of this manuscript is addressed the application of the abundance events of *G. menardii* complex recorded in the tropical Atlantic, as a proxy for the heat and salty waters transport from the southern hemisphere to the Equatorial region due to Agulhas leakage. We also addressed the influence of the NBCR strength system as an important inter-hemisphere heat and salt transport regulator, and the impact of the millennial-scale current oscillations in the global and local climate.

Acknowledgments

Fabricio Ferreira has the support of the Brazilian agency CAPES [grant numbers 99999.000623/2016-04, 88882.151083/2017-01, 88881.185132/2018-01], which allowed the development of this study.

References

Alley, R. B. 2007. Wally was right: Predictive ability of the North Atlantic ‘‘conveyor belt’’ hypothesis for abrupt climate change, Annu. Rev. Earth Planet. Sci.. 35:241-272. 10.1146/annurev.earth.35.081006.131524.

Allison, M.A., Lee, M.T., Ogston, A.S., Aller, R.C., 2000. Origin of Amazon mudbanks along the northeastern coast of South America. Mar. Geol., 163 (1-4):241–256.

Alvares, C.A., Stape, J.L., Sentelhas, P.C., de Moraes Gonçalves, J.L., Sparovek, G. 2013. Köppen’s climate classification map for Brazil. Meteorologische Zeitschrif, 22:711–728. DOI 10.1127/0941-2948/2013/0507.

ANA, A. N. d. á., 2015. Drainage basin of Parnaiba river features. Retrieved 22/07/2018 from http://www2.ana.gov.br/Paginas/portais/bacias/Parnaiba.aspx.

Ando, K., McPhaden, M. J. 1997. Variability of surface layer hydrography in the tropical Pacific Ocean. J. geophys. Res., 102:23063-23078.

Ando, K., McPhaden, M. J. 1997. Variability of surface layer hydrography in the tropical Pacific Ocean. J. geophys. Res., 102:23063-23078.

Arz, H. W., Pätzold, J., Wefer, G. 1998. Correlated millennial-scale changes in surface hydrography and terrigenous sediment yield inferred from last-glacial marine deposits off northeastern Brazil. *Quaternary Research*, 50(2):157-166.

Baker, P. A., Rigsby, C.A. Seltzer, G.O. Fritz, S.C. T., Lowenstein, K. N., Bacher, P., Veliz, C. 2001. Tropical climate changes at millennial and orbital timescales on the Bolivian Altiplano. Nature, 409: 698-701.

Bard E., Rickaby, E.M. 2009. Migration of the subtropical front as a modulator of glacial climate. Nature, 460:380–383.

Barker, S., Diz, P., Vautravers, M.J., Pike, J., Knorr, G., Hall, I.R., Broecker, W.S., 2009. Interhemispheric Atlantic seesaw response during the last deglaciation. Nature 457 (7233), 1097–1102. http://dx.doi.org/10.1038/nature07770.

Barker, S., Greaves, M., Elderfield, H., 2003. A study of cleaning procedures used for foraminiferal Mg/Ca paleothermometry. Geochem. Geophys. Geosyst. 4, 8407. http://dx.doi.org/10.1029/2003GC000559.

Bassinot, F.C., Beaufort, L., Vincent, E., Labeyrie, L., 1997. Changes in the dynamics of western equatorial Atlantic surface currents and biogenic productivity at the mid-Pleistocene revolution (930 ka). In: Shackleton, N.J., Curry, W.B., Richter, C., Bralower, T.J. (Eds.), Proceedings of the Ocean Drilling Program, Scienti"c Results, vol. 154. Ocean Drilling Program, College Station, TX, U.S.A, pp. 269–284.

Bé, A.W.H. 1977. An ecological, zoogeographic and taxonomic review of Recent planktonic foraminifera. In Ramsay, A.T.S. (Ed.), Oceanic Micropaleontology (Vol. 1): London (Acad. Press), 1–100.

Becquey, S., Gersonde, R. 2002. Past hydrographic and climatic changes in the Subantartic Zone of the South Altantic - The Pleistocene record form ODP Site 1090. Palaeogeography, Palaeoclimatology, Palaeoecology, 182:221-239.

Bemis, B.E., Spero, H.J., Bijma, J., Lea, D.W., 1998. Reevaluation of the oxygen isotopic composition of planktonic foraminifera: Experimental results and revised paleotemperature equations. Paleoceanography 13, 150–160.

Berger, W.H., Wefer, G., 1996. Central themes of South Atlantic circulation. In: Wefer, G., Berger, W.H., Siedler, G., Webb, D.J. (Eds.), The South Atlantic: Present and Past Circulation. Springer-Verlag, Heidelberg, Germany, pp. 1–11.

Biastoch, A., Boning, C.W., Lutjeharms, J.R.E. 2008. Agulhas leakage dynamics affect decadal variability in Atlantic overturning circulation. Nature, 456:489–492.

Blaauw, M., Christen, J.A., 2011. Flexible paleoclimate age-depth models using an autoregressive gamma process. Bayesian Anal, 6(3):457-474.

Bolli, H.M., Saunders, J.B., 1985. Oligocene to Holocene low latitude planktic foraminifera. In: Bolli, H.M., Saunders, J.B., Perch-Nielsen, K. (Eds.), Plankton Stratigraphy. Cambridge University Press, New York, pp. 156-262.

Bond, G. C., Showers, W., Elliot, M., Evans, M., Lotti, R., Hajdas, I., Bonani, G., Johnson, S. 1999. The North Atlantic's 1–2 kyr climate rhythm: Relation to Heinrich events, Dansgaard/ Oeschger cycles and the Little Ice Age, in Mechanisms of Global Climate Change at Millennial Time Scales, Geophys. Monogr. Ser., vol. 112, edited by P. U. Clark, R. S. Webb, and L. D. Keigwin, pp. 35–58, AGU, Washington, D. C. Broecker, W. S., G. Bond, M. Klas, E. Clark, and J. McManus (1992), Origin of the northern Atlantic's Heinrich events, Clim. Dyn., 6: 265–273. doi:10.1007/BF00193540.

Bond, G. C., Showers, W., Elliot, M., Evans, M., Lotti, R., Hajdas, I., Bonani, G., Johnson, S. 1999. The North Atlantic's 1 – 2 kyr climate rhythm: Relation to Heinrich events, Dansgaard/ Oeschger cycles and the Little Ice Age, in Mechanisms of Global Climate Change at Millennial Time Scales, Geophys. Monogr. Ser., vol. 112, edited by P. U. Clark, R. S. Webb, and L. D. Keigwin, pp. 35–58, AGU, Washington, D. C.

Bond, G., et al. (1992), Evidence for massive discharges of icebergs into the North Atlantic Ocean during the last glacial period, Nature, 360, 245– 249, doi:10.1038/360245a0.

Bourles, B., Molinari, R., Johns, E., Wilson, Leaman, W. 1999. Upper layer currents in the western tropical North Atlantic. Journal of Geophys. Res., 104: 1361-1375.

Broecker, W. S., Bond, G., Klas, M., Clark, E., McManus, J. 1992. Origin of the northern Atlantic's Heinrich events, Clim. Dyn., 6: 265-273. doi:10.1007/BF00193540.

Broecker,W.S., 1998. Paleocean circulation during the last deglaciation: a bipolar seesaw? Paleoceanography 13 (2), 119–121.

Butzin, M., P. Köhler, and G. Lohmann (2017), Marine radiocarbon reservoir age simulations for the past 50,000 years, Geophys. Res. Lett., 44, 8473 – 8480, doi:10.1002/2017GL074688

Buzas, M.A., Gibson, T.G. 1969. Species diversity: benthonic foraminifera in the western North Atlantic. Science, 163:72-75.

Caley, T., Giraudeau, J., Malaizé, B., Rossignol, L., Pierre, C. 2012. Agulhas leakage as a key process in the modes of Quaternary climate changes. Proceedings of the National Academy of Sciences, 109 (18) 6835-6839; DOI: 10.1073/pnas.1115545109.

Caley, T., Kim, J.-H., Malaizé, B., Giraudeau, J., Laepple, T., Caillon, N., Charlier, K., Rebaubier, H. , Rossignol, L., Castañeda, I. S., Schouten, S., Sinninghe Damst, J.S. 2011. High-latitude obliquity as a dominant forcing in the Agulhas current system. Climate of the Past, 7:1285-1296.

Castellanos, P., Olmedo, E., Pelegrí, J.L., Turiel, A., Campos, E.J.D. 2019. Seasonal Variability of Retroflection Structures and Transports in the Atlantic Ocean as Inferred from Satellite-Derived Salinity Maps. Remote Sensing, 11:802. doi:10.3390/rs11070802.

Chaisson, W.P., Pearson, P.N. 1997. Planktonic foraminifer Biostratigraphy at Site 925: Middle Miocene-Pleistocene. *In*: Shackleton, N.J., Curry, W.B., Richter, C., and Bralower, T.J. (Eds.) Proceedings of the Ocean Drilling Program, Scientific Results, Vol. 154

Chang, P., Ji, L., Li, H., 1997. A decadal climate variation in the tropical Atlantic Ocean from thermodynamic air–sea interactions. Nature, 385:516–518.

Chang, P., Zhang, R., Hazeleger, W., Wen, C., Wan, X., Ji, L., Haarsma, R.J., Breugem, W., Seidel, H., 2008. Oceanic link between abrupt changes in the North Atlantic Ocean and the African monsoon. Nat. Geosci., 1:444–448.

Cohen, K.M. and Gibbard, P.L. 2019. Global chronostratigraphical correlation table for the last 2.7 milion years, version 2019 QI-500. Quaternary International, 500:20-31.

Corredor, J. E., Morell, J. M. 2001. Seasonal variation of physical andbiogeochemical features is eastern Caribbean Surface Water, J. Geo-phys. Res., 106, 4517–4525.

Crivellari, S., Chiessi, C.M., Kuhnert, H., Haggi, C., Portilho-Ramos, R.C., Zeng, J.Y., Zhang, Y., Schefub, E., Mollenhauer, G., Hefterm J., Alexandre, F., Sampaio, G., Mulitza, S. 2018.

Increased Amazon freshwater discharge during late Heinrich Stadial 1. Quaternary Science Reviws, 181:144-155.

Cruz, F. W., Burns, S.J., Karmann, I., Sharp, W.D., Vuille, M., Cardoso, A.O., Ferrari, J.A., Silva Dias, P.L., Viana, O. 2005. Insolation-driven changes in atmospheric circulation over the past 116,000 years in subtropical Brazil. Nature, 434(7029): 63-66.

Cruz, F. W., Vuille, M., Burns, S. J., Wang , X. F., Cheng, H., Werner, M., Edwards, R. L., Karmann, I., Auler, A.S., Nguyen, H. 2009. Orbitally driven east-west antiphasing of South American precipitation. Nature Geoscience, 2(3): 210-214.

Cruz, F. W., Vuille, M., Burns, S.J., Wang, X.F., Cheng, H., Werner, M., Edwards, R.L., Karmann, I., Auler, A.S., Nguyen, H. 2009. Orbitally driven east-west antiphasing of South American precipitation. Nature Geoscience, 2(3):210-214.

Dahl, K.A., Broccoli, A.J., Stouffer, R.J., 2005. Assessing the role of North Atlantic freshwater forcing in millennial scale climate variability: a tropical Atlantic perspective. Clim. Dyn. 24 (4), 325e346. https://doi.org/10.1007/s00382-004- 0499-5.

De Vargas, C., Renaud, S., Hillbrecht, H., Pawlowski, J. 2001. Pleistocene adaptive radiation in *Globorotalia truncatulinoides*: genetic, morphologic, and environmental evidence. Paleobiology, 27(1):104.

Dekens, P.S., Lea, D.W., Pak, D.K., Spero, H.J., 2002. Core top calibration of Mg/Ca in tropical foraminifera: re"ning paleotemperature estimation. Geochemistry, Geophysics, Geosystems 3 doi:10.1029/2001GC000200.

Diekmann, B., Kuhn, G., 2002. Sedimentary record of the Mid-Pleistocene climate transition in the Southeastern Atlantic Ocean (ODP, Site 1090). Palaeogeography, Palaeoclimatology, Palaeoecology, S0031-0182(01)00498-9.

Dupont, L.M., Schlütz, F., Teboh Ewah, C., Jennerjahn, T.C., Paul, A., Behling, H., 2010. Two-step vegetation response to enhanced precipitation in Northeast Brazil dur-ing Heinrich event 1. Glob. Change Biol., 16:1647–1660.

Elderfield, H.; Ferretti, P., Greaves, M., Crowhurst, S.J.; McCave, I Nick; Hodell, D., A; Piotrowski, A.M. 2012. Evolution of ocean temperature and ice volume through the Mid-Pleistocene Climate Transition. Science, 337(6095): 704-709. doi.org/10.1126/science.1221294

Ericson, D.B., Wollin, G. 1968. Pleistocene climates and chronology in deep-sea sediments. *Science*, **162**:1227-1243.

Fairbanks, R., Sverdlove, M., Free, R., Wiebe, P., Bé, A. 1982. Vertical distribution and isotopic fractionation of living planktonic foraminifera from the Panama Basin. Nature, 298:841-844. 10.1038/298841a0.

Fairbanks, R.G., Wiebe, P.H., and Bé, A.W.H., 1980. Vertical distribution and isotopic composition of living planktonic foraminifera in the western North Atlantic. Science, 207:61–63.

Fonseca, C.A., Goni, G.J., Johns,W.E., Campos, E.J.D., 2004. Investigation of the North Brazil Current retroflection and North Equatorial Countercurrent variability. Geophys. Res. Lett. 31 (21), 1–5. http://dx.doi.org/10.1029/2004GL020054.

Garzoli, S.L., Matano, R. 2011. The South Atlantic and the Atlantic Meridional Overturning Circulation. Deep Sea Research Part II, 58:1837–1847.

Gibbard, P.L., Head, M.J. 2010 The newly-ratified definition of the Quaternary System/Period and redefinition of the Pleistocene Series/Epoch, and comparison of proposals advanced prior to formal ratification. Episodes 33, 152-158.

Gibbard, P.L; Head, M.J.; Walker, M.J.C., The Subcomission on Quaternary Stratigraphy. 2010. Formal ratification of the Quaternary System/Period and the Pleistocene Series/Epoch with a base at 2.58 Ma. *Journal of Quaternary Science*, **25**:96-102.

Goelzer, H., Mignot, J., Levermann, A., Rahmstorf, S., 2006. Tropical versus high latitude freshwater influence on the Atlantic circulation. Clim. Dyn., 27(7–8):715–725. http://dx.doi.org/10.1007/s00382-006-0161-5.

Goni, G.J., Johns,W.E., 2001. A census of North Brazil Current Rings observed from TOPEX/POSEIDON altimetry: 1992–1998. Geophys. Res. Lett. 28 (1), 1–4.

Gray, W.R., Weldeab, S., Lea, David W., Rosenthal, Y., Gruber, N., Donner, B., Fischer, G. 2018. The effects of temperature, salinity, and the carbonate system on Mg/Ca in Globigerinoides ruber (white): A global sediment trap calibration. Earth and Planetary Science Letters, 482:607-620. doi.org/10.1016/j.epsl.2017.11.026

Gwiazda, R. H., Hemming, S. R., Broecker, W. S. 1996. Provenance of icebergs during Heinrich event 3 and the contrast to their sources during other Heinrich episodes, Paleoceanography, 11:371 – 378, doi:10.1029/96PA01022.

Haarsma, R.J., Campos, E.J.D., Drijfhout, S., Hazeleger, W., Severijns, C., 2011. Impacts of interruption of the Agulhas leakage on the tropical Atlantic in coupled ocean–atmosphere simulations. Clim. Dyn. 36 (5–6), 989–1003.

Hammer, O., Harper, D.A.T., Rayan, P.D. 2001. PAST: Paleontological Statistics software package for education and data analysis. Paleontologia Electronica, 4(1):9 pp.

Harris, P. P., Huntingford, C., Cox, P.M. 2008. Amazon Basin climate under global warming: the role of the sea surface temperature. P*hilosophical Transactions of the Royal Society of London B:* Biological Sciences, 363(1498): 1753-1759.

Hastenrath, S. 2006. "Circulation and teleconnection mechanisms of Northeast Brazil droughts." Progress in Oceanography70(2): 407-415.

Hastenrath, S., Heller, L. 1977. "Dynamics of climatic hazards in northeast Brazil." Quarterly Journal of the Royal Meteorological Society103(435): 77-92.

Hayward, B.W.; Le Coze, F.; Vachard, D.; Gross, O. (2019). World Foraminifera Database. Accessed at http://www.marinespecies.org/foraminifera on 2019-12-14. doi:10.14284/305

Heinrich, H. 1988. Origin and consequences of cyclic ice rafting in the northeast Atlantic Ocean during the past 130,000 years. Quaternary Res., 29:142-152. doi:10.1016/0033-5894(88)90057-9

Hemming, S. R. 2004. Heinrich events: Massive late Pleistocene detritus layers of the North Atlantic and their global climate imprint. Rev. Geophys., 42:RG1005. doi:10.1029/ 2003RG000128.

Hemming, S. R., Broecker, W. S., Sharp, W. D., Bond, G. C., Gwiazda, R. H., McManus, J. F., Klas, M. Hajdas, I. 1998. Provenance of the Heinrich layers in core V28-82, northeaster Atlantic: 40Ar-39Ar ages of ice-rafted hornblende, Pb isotopes in feldspar grains, and Nd-Sr-Pb isotopes in the fine sediment fraction, Earth Planet. Sci. Lett., 164:317-333. doi:10.1016/S0012-821X(98)00224-6.

Hodell, D.A., Channell, J.E.T., Curtis, J.H., Romero, O.E., Rohl, U. 2008. Onset of "Hudson Strait" Heinrich events in the eastern North Atlantic at the end of the middle Pleistocene transition (~640 ka)?. Paleoceanography, 23:PA4218. doi:10.1029/2008PA001591

Huisman, S.E., Toom, M., Dijkstra, H.A., Drijfhout, S. 2010. An indicator of the multiple equilibria regime of the Atlantic Meridional Overturning Circulation. Journal of Physical Oceanography, 40:551–567.

Jaeschke, A., Rühlemann, C., Arz, H., Heil, G., Lohmann, G., 2007. Coupling of millennial-scale changes in sea surface temperature and precipitation off north-eastern Brazil with high-latitude climate shifts during the last glacial period. Paleoceanography, 22(4). http://dx.doi.org/10.1029/2006PA001391.

Jennerjahn, T. C., Ittekkot, V., Arz, H.W., Behling, H., Pätzold, J., Wefer G. 2004. Asynchronous Terrestrial and Marine Signals of Climate Change During Heinrich Events. Science, 306(5705):2236-2239.

Johns, W. E., Lee, T. N., Schott, F. A., Zantopp, R. J., Evans, R. H. 1990. The North Brazil Current retroflection: seasonal structure and eddy variability, J. Geophys. Res., 95(C12):22103–22120.

Johns, W., Lee, T., Beardsley, R.C., Candela, J., Limeburner, R., Castro, B., 1998. Annual cycle and variability of the North Brazil Current. J. Phys. Oceanogr. 103–128. http://dx.doi.org/10.1175/15200485(1998)028%3C0103:ACAVAC%3E2.0.CO%3B2.

Johns,W. E., Zantopp, R. J., and Goni, G. J. 2003. Cross-gyre water mass transport by North Brazil Current Rings, in: Interhemispheric Water Exchanger in the Atlantic Ocean, edited by: Goni, G. J., Malanotte-Rizzoli, P. Elsevier Oceanographic Series, 68:411–441, ISBN 0-444-51267-5.

Kageyama, M. et al. Climatic impacts of fresh water hosing under Last Glacial Maximum conditions: a multi-model study. Climate of the Past 9, 935–953, doi:10.5194/cp-9-935-2013 (2013).

Karr, J.D., Showers, W.J., 2002. Stable oxygen and hydrogen isotopic tracers in Amazon shelf waters during AMASSEDS. Oceanological Acta, 25:71–78.

Kennett, J.P., Huddlestun, P. 1972. Late Pleistocene paleoclimatology, foraminiferal biostratigraphy and tephrochronology, Western Gulf od Mexico. Quaternary Research, 2:38-69.

Kipp, N.G., 1976. New transfer function for estimating past sea-surface conditions from sea-bed distribution of planktonic foraminiferal assemblages in the north Atlantic. In Cline, R.M., and Hays, J.D. (Eds.), Investigation of Late Quaternary Paleoceanography and Paleoclimatology. Mem.- Geol. Soc. Am., 145:3–41.

Kısakürek, B., Eisenhauer, A., Böhm, F., Garbe-Schönberg, D., Erez, J. 2008. Controls on shell Mg/Ca and Sr/Ca in cultured planktonic foraminiferan, *Globigerinoides ruber* (white). Earth and Planetary Science Letters, 273:3-4.

Kodama, Y. 1992. Large-scale common features of subtropical precipitation zones (the Baiu frontal zone, the SPCZ and the SACZ), part I:characteristics of subtropical frontal zones. Journal of the Meteorological Society of Japan, 70:813–836.

Kousky, V.E. 1979. Frontal influences on Northeast Brazil. Monthly Weather Review, 107:1140–1153.

Kousky, V.E. 1980. Diurnal rainfall variation in Northeast Brazil. Monthly Weather Review, 108:488–498.

Kousky, V.E., Gan, M.A. 1981. Upper tropospheric cyclonic vortices in the tropical South Atlantic. Tellus 33:538–551.

Kucera, M., Rosell-Melé, A., Schneider, R., Waelbroeck, C., Weinelt, M., 2005a. Multiproxy approach for the reconstruction of the glacial ocean surface (MARGO). Quat. Sci. Rev. 24, 813–819. http://dx.doi.org/10.1016/j.quascirev.2004.07.017.

Kucera, M., Weinelt, M.M., Kiefer, T., Pflaumann, U., Hayes, A., Chen, M.-T., Mix, A.C., Barrows, T.T., Cortijo, E., Duprat, J., Juggins, S., Waelbroeck, C., 2005b. Reconstruction of sea-surface temperatures from assemblages of planktonic foraminifera: multitechnique approach based on geographically constrained calibration data sets and its application to glacial Atlantic and Pacific Oceans. Quat. Sci. Rev. 24, 951–998. http://dx.doi.org/10.1016/j.quascirev.2004.07.014.

Langner, M. and Mulitza, S. 2019. Technical Note: PaleoDataView – A software toolbox for the collection, homogenization and visualization of marine proxy data, Climate of the Past, 15:2067–2072. doi.org/10.5194/cp-15-2067-2019.

Le, J., Shackleton, N.J., 1992. Carbonate dissolution fluctuations in the western equatorial Pacific during the late Quaternary. Paleoceanography, 7(1):21–42.

Leipnitz, I.I., Silva, J.L.L., Leipnitz, B., Aguiar, E.S., Leão, C.J., Giovanoni, L., Ferreira, F. 2005. Métodos para o trabalho com microfósseis e formas atuais. In Timm, L.L. & Cademartoti, C.V., eds, Cadernos La Salle XI - Métodos de Estudo em Biologia, ISSN: 1678-2003, vol. 2, n. 1, pp. 49-58.

Lentz, S.J., 1995. Seasonal variations in the horizontal structure of the Amazon Plume inferred from historical hydrographic data. J. Geophys. Res., Oceans, 100:2391–2400.

Lessa, D.V.O., Portilho-Ramos, R.C., Barbosa, C.F., da Silva, A.R., Belem, A.L., Turcq, B.J., Albuquerque, A.L.S. 2014. Planktonic foraminifera from sediment core CF10-01B (Cabo Frio - Brazil). Marine Micropaleontology, 106, 55-68, https://doi.org/10.1016/j.marmicro.2013.12.003

Lippold, J. et al. Does sedimentary 231Pa/230Th from the Bermuda Rise monitor past Atlantic Meridional Overturning Circulation? Geophysical Research Letters 36, 1–6, doi:10.1029/2009GL038068 (2009).

Lisiecki, L., Raymo, M.E. 2005. A Pliocene-Pleistocene stack of 57 globally distributed benthic δ18O records. Paleoceanography, 20, PA1003, doi:10.1029/2004PA001071.

Lohmann, G.P., Schweitzer, P.N. 1990. *Globorotalia truncatulinoides*' growth and chemistry as probes of the past thermocline: 1. shell size. Paleoceanography, 5:55-75.

Longhurst, A. 1993. Seasonal cooling and blooming in tropical oceans. *Deep Sea Research Part I: Oceanographic Research Papers* **40**, 2145–2165, doi:10.1016/0967-0637(93)90095-K.

Lux, M., Mercier, H., Arhan, M., 2001. Interhemispheric exchanges ofmass and heat in the Atlantic Ocean in January–March 1993. Deep-Sea Res. I 48, 605–638.

Marchito, T.M., Curry, W.B., Lynch-Stieglitz, J., Bryan, S.P., Cobb, K.M., Lund, D.C. 2014. Improved oxygen isotope temperature calibrations for cosmopolitan benthic foraminifera. Geochimica et Cosmochimica Acta, 130: 1-11.

Martin, R.E.; Neff, E.D.; Johnson, G.W., Krantz, D.E. 1993. Biostratigraphic Expression of Pleistocene Sequence Boundaries, Gulf of Mexico. *Palaios*, **8**:155-171.

Martinez, J.I; Mora, G. & Barrows, T.T. 2007. Paleoceanographic conditions in the Western Caribbean Sea for the last 560 kyr as inferred from planktonic foraminifera. *Marine Micropaleontology,* **64**:177-188.

Maslin, M.A., Burns, S.J., 2000. Reconstruction of the Amazon Basin effective moistureavailability over the past 14, 000 years. Science, 290:2285–2287.

Maslin, M.A., Burns, S.J., Erlenkeuser, H., Hohnemann, C., 1997. Stable isotope records from sites 932 and 933. In: Flood, R.D., Piper, D.J.W., Klaus, A., Peterson, L.C. (Eds.), Proceedings of the Ocean Drilling Program, Scienti"c Results, vol. 155. Ocean Drilling Program, College Station, TX, U.S.A., pp. 305–318.

Masson, S., Delecluse, P. 2001. Influence of the Amazon River runoff on the tropical Atlantic. Phys. Chem. Earth. B, 26:137-142.

McManus, J. F., Anderson, R. F., Broecker, W. S., Fleisher, M. Q., Higgins, S. M. Higgins. 1998. Radiometrically determined sedimentary fluxes in the sub-polar North Atlantic during the last 140,000 years, Earth Planet. Sci. Lett., 1 5 5, 2 9 – 4 3, d o i : 1 0 . 1 0 1 6 / S 0 0 1 2 - 821X(97)00201-X.

McManus, J. F., Francois, R., Gherardi, J.-M., Keigwin, L. D. & Brown-Leger, S. 2004. Collapse and rapid resumption of Atlantic meridional circulation linked to deglacial climate changes. Nature, 428: 834–7. doi:10.1038/nature02494

Mignot, J., de B Montégut, C., Lazar, A. & Cravatte, S. Control of salinity on the mixed layer depth in the world ocean: 2. Tropical areas. Journal of Geophysical Research: Oceans 112, 1–12 (2007).

Mix, A.C., Morey, A.E., Pisias, N.G., Hostetler, S.W., 1999. Foraminiferal faunal estimates of palaeotemperature: circumventing the no-analog problem yields cool ice age tropics. Paleoceanography 14, 350–359.

Mohtadi, M. Hebbeln, D., Marchant, M. 2005. Upwelling and productivity along the Peru-Chile current derived from faunal and isotopic compositions of planktic foraminifera in surface sediments. Marine Geology, 216(3):107-126. https://doi.org/10.1016/j.margeo.2005.01.008

Montégut, C. B., Mignot, J., Lazar, A. & Cravatte, S. Control of salinity on the mixed layer depth in the world ocean: 1. General description. Journal of Geophysical Research 112, C06011 (2007).

Mudelsee, M., Schulz, M. 1997. The Mid-Pleistocene climate transition: onset of 100 ka cycle lags ice volume build-up by 280 ka. Earth and Planetary Science Letters, 151:117-123. 10.1016/S0012-821X(97)00114-3.

Nace, T. E., P. A. Baker, G. S. Dwyer, C. G. Silva, C. A. Rigsby, S. J. Burns, L. Giosan, B. Otto-Bliesner, Z. Liu and J. Zhu. 2014. The role of North Brazil Current transport in the paleoclimate of the Brazilian Nordeste margin and paleoceanography of the western tropical Atlantic during the late Quaternary. Palaeogeography, Palaeoclimatology, Palaeoecology, 415(0): 3-13.

Nishi, H., Norris, R.D., Okada, H. 2000. Paleoceanographic changes in the dynamics of subtropical surface conditions at Hole 997A. *In:* Paull, C.K., Matsumoto, R., Wallace, P.J., and Dillon, W.P. (Eds.), Proceedings of the Ocean Drilling Program, Scientific Results, Vol. 164.

Oliveira, P.T., Santos e Silva, C.M., Lima, K.C. 2016. Climatology and trend analysis of extreme precipitation in subregions of Northeast Brazil. Theoretical and Applied Climatology, DOI 10.1007/s00704-016-1865-z.

Pailler, K.; Bourlès, B. & Gouriou, Y. 1999. The barrier layer in the western Atlantic Ocean. Geophys. Res. Lettes., 26:2069-2072.

Pailler, K.; Bourlès, B. & Gouriou, Y. 1999. The barrier layer in the western Atlantic Ocean. Geophys. Res. Lettes., 26:2069-2072.

Patterson, R.T., Fishbein, E. 1989. Re-Examination of the statistical methods used to determine the number of point counts needed for micropaleontological quantitative research. Journal of Paleontology, 63:245-248.

Peeters, F.J., Acheson, R., Brummer, G.-J.A., Rujiter, W.P.M., Schneider, R.R., Ganssen, G.M., Ufker, E., Kroon, Dick. 2004. Vigorous exchange between the Indian and Atlantic oceans at the end of the past five glacial periods. Nature, 430:661-665.

Peterson, R.G., Stramma, L. 1991. Upper-Level circulation in the South Atlantic Ocean. Prog. Oceanog., 26:1-73.

Philander, S., Gu, D., Lambert, G. & Li, T. 1996. Why the ITCZ is mostly north of the equator. Journal of Climate, 9:2958–2972, https://doi.org/10.1175/1520-0442(1996)009<2958:WTIIMN>2.0.CO;2 (1996).

Portilho-Ramos, R.C., Barbosa, C.F., Rios-Netto, A.M., 2014. Planktonic foraminiferal variations in the southwestern Atlantic since the last glacial–interglacial cycle. PALAIOS 29, 38–44. http://dx.doi.org/10.2110/palo.2012.104.

Portilho-Ramos, R.C., Chiessi, C.M., Zang, Y., Mulitza, S., Kucera, M., Siccha, M., Prange, M., Paul, A. 2017. Coupling of equatorial Atlantic surface stratification to glacial shifts in the tropical rainbelt. Nature Scientific Reposts, 7:1561. DOI:10.1038/s41598-017-01629-z

Rashid, H., Hesse, R., Piper, D. J. W. 2003. Evidence for an additional Heinrich event between H5 and H6 in the Labrador Sea. Paleoceanography, 18(4):1077, doi:10.1029/ 2003PA000913.

Regenberg, Steph, Silke; Marcus; Tiedemann, Ralf; Mulitza, Stefan; Nürnberg, Dirk. 2009. Stable isotopes of planktonic foraminifera from tropical Atlantic/Caribbean core-tops: Implications for reconstructing upper ocean stratification. Marine Micropaleontology, 71(1-2): 1-19. doi.org/10.1016/j.marmicro.2008.12.004

Reimer, P. J., Bard, E., Bayliss, A., Beck, J.W., Blackwell, P.G., Ramsey, C.B., Buck, C.E., Edwards, R.L., Friedrich, M., Grootes, P.M., Guilderson, T.P., Haflidason, H., Hajdas, I., Hatté, C., Heaton, T.J., Hoffmann, D.L., Hogg, A.G., Hughen, K.A., Kaiser, K.F., Kromer, B., Manning, S.W. , Niu, M., Reimer, R.W., Richards, D.A., Scott, E.M., Southon, J.R., Staff, R.A., Turney, C.S.M., van der Plicht, J. 2013. INTCAL13 and MARINE13 Radiocarbon Age Calibration Curves 0–50,000 Years Cal BP. Radiocarbon, 55(4):1869–1887.

Renaud, S., Schmidt, D.N. 2003. Habitat tracking as response of the planktonic foraminifer *Globorotalia truncatulinoides* to environmental fluctuations during the last 140 kyr. Marine Micropaleontolgy, 49(1-2):97-122.

Richardson, P.L., Hufford, G.E., Limeburner, R., Brown, W.S., 1994. North Brazil Current retroflection eddies. J. Geophys. Res., 99: 5081–5093.

Riehl, H. 1945. Waves in the easterlies and the polar front in the tropics. Chicago University, Department of Meteorology, 79 p.

Rühlemann, C., Diekmann, B., Mulitza, S., Frank, M., 2001. Late Quaternary changes of western equatorial Atlantic surface circulation and Amazon lowland climate recorded in Ceara Rise deep-sea sediments. Paleoceanography, 16:293–305.

Rutherford, S. D'Hondt, S., Prell, W. 1999. Rutherford S, D'Hondt S, Prell W.. Environmental controls on the geographic distribution of zooplankton diversity. Nature 400: 749-753. Nature. 400. 749-753. 10.1038/23449.

Santos, T.P., Belem, A.L., Barbosa, C,.F., Dokken, T., Albuquerque, A.L.S. 2014. Paleoceanographic reconstruction of the western equatorial Atlantic during the last 40 kyr. Palaeogeography, Palaeoclimatology, Palaeoecology, 415:14-20.

Schiebel, R., Hemleben, C. 2017. Planktic Foraminifers in the Modern Ocean. 10.1007/978-3-662-50297-6.

Schiebel, R., Waniek, J., Bork, M., Hemleben, C. 2001. Planktic foraminiferal production stimulated by chlorophyll redistribution and entrainment of nutrients. Deep Sea Research Part I: Oceanographic Research Papers, 48(3), 721-740, https://doi.org/10.1016/S0967-0637(00)00065-0

Schiebel, R., Zeltner, A., Treppke, U.F., Waniek, J.J., Bollmann, J., Rixen, T., Hemleben, C. 2004. Distribution of diatoms, coccolithophores and planktic foraminifers along a trophic gradient during SW monsoon in the Arabian Sea. Marine Micropaleontology, 51(3-4):345-371. https://doi.org/10.1016/j.marmicro.2004.02.001

Schmidt, M.W., Chang, P., Hertzberg, J.E., Them II, T.R., Ji, L., Otto-Bliesner, B.L., 2012. Impact of abrupt deglacial climate change on tropical Atlantic subsurface temperatures. Proc. Natl. Acad. Sci. U. S. A. 109, 14348–14352.

Schmidt, M.W., Spero, H.J., Lea, D.W., 2004. Links between salinity variation in the Caribbean and North Atlantic thermohaline circulation. Nature, 428:160–163.

Schmuker, B., Schiebel, R. 2002. Planktic foraminifers and hydrography of the eastern and northern Caribbean Sea. Marine Micropaleontology, 46:387–403. doi:10.1016/S0377-8398(02)00082-8 (2002).

Schmuker, B., Schiebel, R. 2002. Planktic foraminifers and hydrography of the eastern and northern Caribbean Sea. Marine Micropaleontology, 46:387-403. 10.1016/S0377-8398(02)00082-8

Schott, F., Stramma, L., Fischer, J., 1995. The warm water inflow into the western tropical Atlantic boundary regime, spring 1994. J. Geophys. Res. 100, 24745–24760.

Servain, J., Busalacchi, A.J., Mcphaden, M.J., Moura, A.D., Reverdin, G., Vianna, M., Zebiak, S.E., 1998. A Pilot Research Moored Array in the Tropical Atlantic (PIRATA). Bulletin of the American Meteorological Society, 79(10):2019–2031.

Silva, A., Araujo, M, Medeiros, C., Silva, M., Bourles, B. 2005. Seasonal changes in the mixed and barrier layers in the western equatorial Atlantic. Brazilian Journal of Oceanography, 53(3/4):83-98.

Silva, A.C., Boules, B., Araujo, M. 2009. Circulation of the thermocline salinity maximum waters off the Northern Brazil as inferred from in situ measurements and numerical results. Annales Geophysicae, 27:1861-1873.

Snoeckx, H., Grousset, F., Revel, M., Boelaert, A. 1999. European contribution of ice-rafted sand to Heinrich layers H3 and H4, Mar. Geol., 158:197-208. do i : 1 0.1016/S0025-3227(98)00168-6.

Sprintall, J., Tomczak, M. 1992. Evidences of the barrier layer in the surface layer of the tropics. J. geophys. Res., 97:7305-7316.

Sprintall, J., Tomczak, M. 1992. Evidences of the barrier layer in the surface layer of the tropics. J. geophys. Res., 97:7305-7316.

Stainforth, R.M.; Lamb, J.L.; Luterbaqcher, H.; Beard, J.H. & Jeffords, R.M. 1975. Cenozoic planktonic foraminiferal zonation and characteristics of index forms. Paleontological Contributions, 62. Lawrence: University of Kansas Press. 425 p.

Stramma, L., Fischer, J., Reppin, J., 1995. The North Brazil undercurrent. Deep Sea Res. I 42, 773–795.

Stramma, L., Rhein, M., Brandt, P., Dengler, M., Boning, C., Walter, M.: Upper ocean circulation in the western tropical Atlantic in boreal fall 2000, Deep-Sea Res., 52, 221–240, 2005

Talley, L., Pickard, G., Emery,W., Swift, J., 2011. Descriptive physical oceanography: An introduction. Elsevier Academic.

Thunell, R., Tappa, E., Pride, C., Kincaid, E., 1999. Sea-surface temperature anomalies associated with the 1997–1998 El Nino recorded in the oxygen isotope composition of planktonic foraminifera. Geology 27, 843–846.

Toledo, F.A.L., Quadros, J.P.,Camilo Jr., E., Santarosa, A.C.A., Flores, J.A., Costa, K.B. 2016.Plankton biochronology for the last 772,000 years from the western South Atlantic Ocean. Marine Micropaleontology, 127: 50–62. http://dx.doi.org/10.1016/j.marmicro.2016.07.002

Utida, G., Cruz, F.W., Etourneau, J., Bouloubassi, I., Schefuß E., Vuille, M., Novello, V.F., Prado, L.F., Sifeddine, A., Klein, V., Zular, A., Viana, J.C.C., Turcq, B. 2019. Tropical South Atlantic influence on Northeastern Brazil precipitation and ITCZ displacement during the past 2300 years. Nature Scientific Reports. 9:1698. https://doi.org/10.1038/s41598-018-8003-6.

Vink, A., Brune, A., Holl, C., Zonneveld, K.A.F., Willems, H., 2002. On the response of calcareous dino!agellates to oligotrophy and strati"cation of the upper water column in the equatorial Atlantic Ocean. Palaeogeography, Palaeoclimatology, Palaeoecology, 178:53–66.

Waliser, D. E., Gautier, C.. 1993. A satellite-derived climatology of the ITCZ. Journal of Climate, 6:2162–2174. https://doi.org/10.1175/1520-0442(1993)006<2162:ASDCOT>2.0.CO;2 (1993).

Weijer, W., De Ruijter, W.P.M., Dijkstra, H.A. 2001. Stability of the Atlantic overturning circulation: Competition between Bering Strait freshwater flux and Agulhas heat and salt sources Journal of Physical Oceanography, 31:2385-2402.

Weijer, W., De Ruijter, W.P.M., Sterl, A., Drijfhout, S. S. 2002. Response of the Atlantic overturning circulation to South Atlantic sources of buoyancy. Global and Planetary Change, 34:293-311.

Weldeab, S., Schneider, R., Kölling, M., 2006. Deglacial sea surface temperature and salinity increase in the western tropical Atlantic in synchrony with high latitude climate instabilities. Earth and Planetary Science Letters 241, 699–706.

Wilkens, R.H., Westerhold, T., Drury, A.J., Lyle, M., Gorgas, T., and Tian, J., 2017, Revisiting the Ceara Rise, equatorial Atlantic Ocean: isotope stratigraphy of ODP Leg 154 from 0 to 5 Ma: Climate of the Past, v. 13, p. 779–793, doi: https://doi.org/10.5194/cp-13-779-2017.

Wilson, K.E., Maslin, M.A., Burns, S.J., 2011. Evidence for a prolonged retroflection of the North Brazil Current during glacial stages. Palaeogeogr. Palaeoclimatol. Palaeoecol., 301(1–4): 86–96. http://dx.doi.org/10.1016/j.palaeo.2011.01.003.

Zhang, D., Msadek, R., McPhaden, M.J., Delworth, T., 2011. Multidecadal variability of the North Brazil Current and its connection to the Atlantic meridional overturning circulation. J. Geophys. Res. 116, C04012. http://dx.doi.org/10.1029/2010JC006812.

Zhang, Y., Chiessi, C. M., Mulitza, S., Zabel, M., Trindade, R.I.F., Hollanda, M.H.B.M., Dantas, E.L., Govina, A., Tiedemann, R., Wefer, G. 2015. Origin of increased terrigenous supply to the NE SouthAmerican continental margin during Heinrich Stadial 1 and the Younger Dryas. Earth and Planetary Science Letters, 432:493-500. http://dx.doi.org/10.1016/j.epsl.2015.09.054.

Zweng, M. M., J. R. Reagan, D. Seidov, T. P. Boyer, R. A. Locarnini, H. E. Garcia, A. V. Mishonov, O. K. Baranova, K. Weathers, C. R. Paver, and I. Smolyar, 2018. World Ocean Atlas 2018, Volume 2: Salinity. A. Mishonov Technical Ed.; NOAA Atlas NESDIS 82, 50 pp.

Paleoceanographic reconstructions of western equatorial Atlantic for the last ~1.93 Ma

- SUPPLEMENTARY MATERIAL -

Fabricio Ferreira[1,2]; Gary Dwyer[3]; Allan Sandes Oliveira[2]; Cristiano M. Chiessi[4]; Cleverson Guisan Silva[2]; Paul A. Baker[3], Andrea K. Kern[4]; Catherine A. Rigsby[5]

[1]Postgraduate Program in Ocean and Earth Dynamics, Institute of Geosciences, Federal Fluminense University, Niterói, Av. Gal. Milton Tavares de Souza s/n, CEP: 24.210-346 Rio de Janeiro RJ, Brazil – *ferreira_paleo@hotmail.com*

[2]Marine Geology Laboratory (LAGEMAR), Institute of Geosciences, Federal Fluminense University, Niterói, Av. Gal. Milton Tavares de Souza s/n, CEP: 24.210-346 Rio de Janeiro RJ, Brazil

[3]Division of Earth and Ocean Sciences, Duke University, Durham, NC 27708, USA

[4]School of Arts, Sciences and Humanities, University of São Paulo, São Paulo, Av. Av. Arlindo Bettio 1000, CEP: 03828-000 São Paulo SP, Brazil

[5]Department of Geological Sciences, East Carolina University, Greenville, NC 27858-4353, USA.

Supplementary material:

It contains two supplementary figures and one supplementary table.

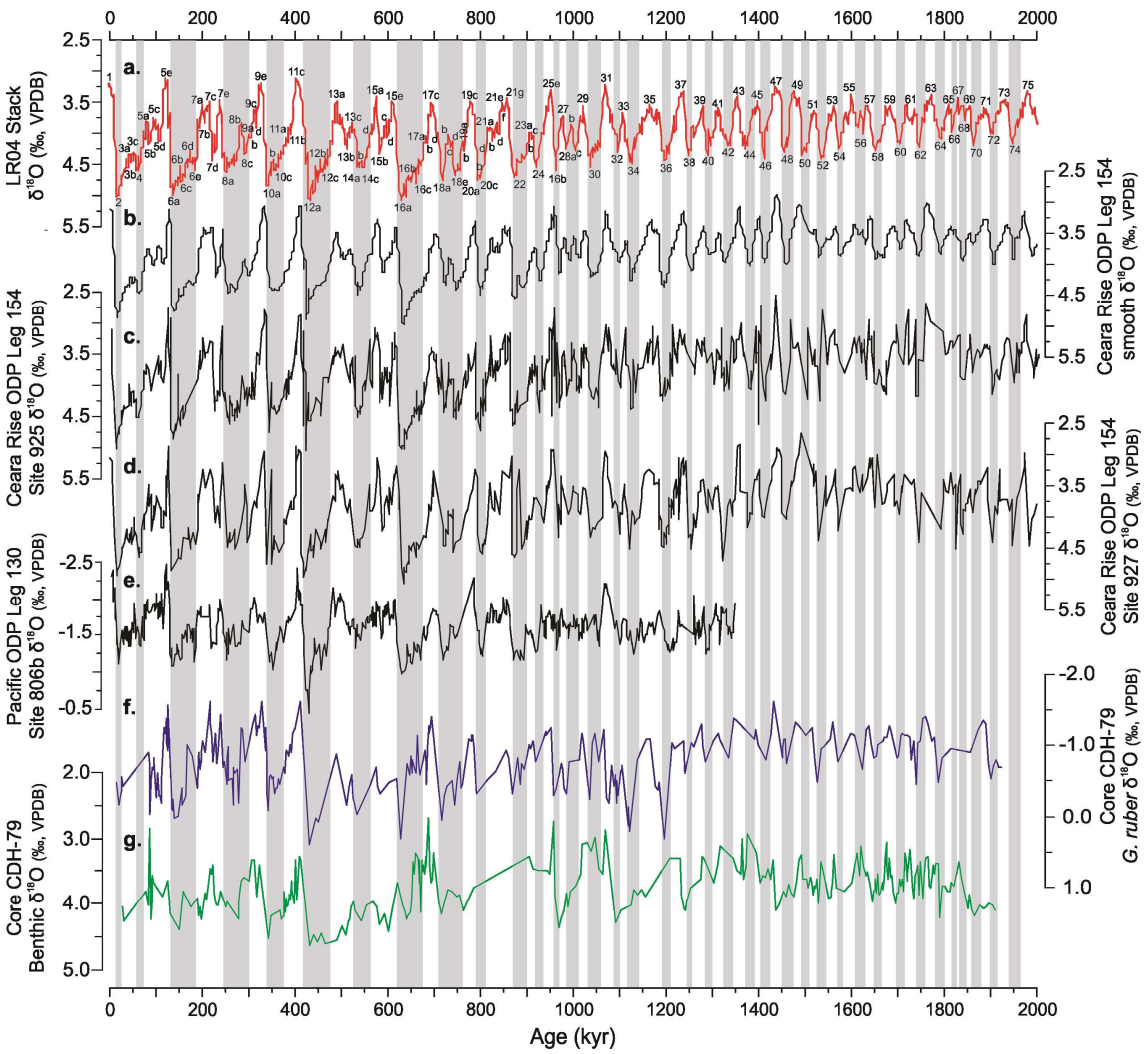

Supplementary Figure S1. Stable oxygen isotopic ($\delta^{18}O$) records from (a.) LR04 stack (Lisiecki and Raymo, 2005); revised isotope stratigraphy of Ceara Rise ODP Leg 154 (b.) smooth; (c.) Site 925; (d.) Site 927 (Wilkens et al., 2017); (e) equatorial Pacific ODP Leg 130 Site 806b (de Garidel-Thoron et al.,2005); and western equatorial Atlantic core CDH-79 (f.) *Globigerinoides ruber* (white); (g.) benthic foraminifera (this study). Marine isotopic stages according to the LR04 stack (Lisiecki and Raymo, 2005), and substages according to Railsback et al. (2015).

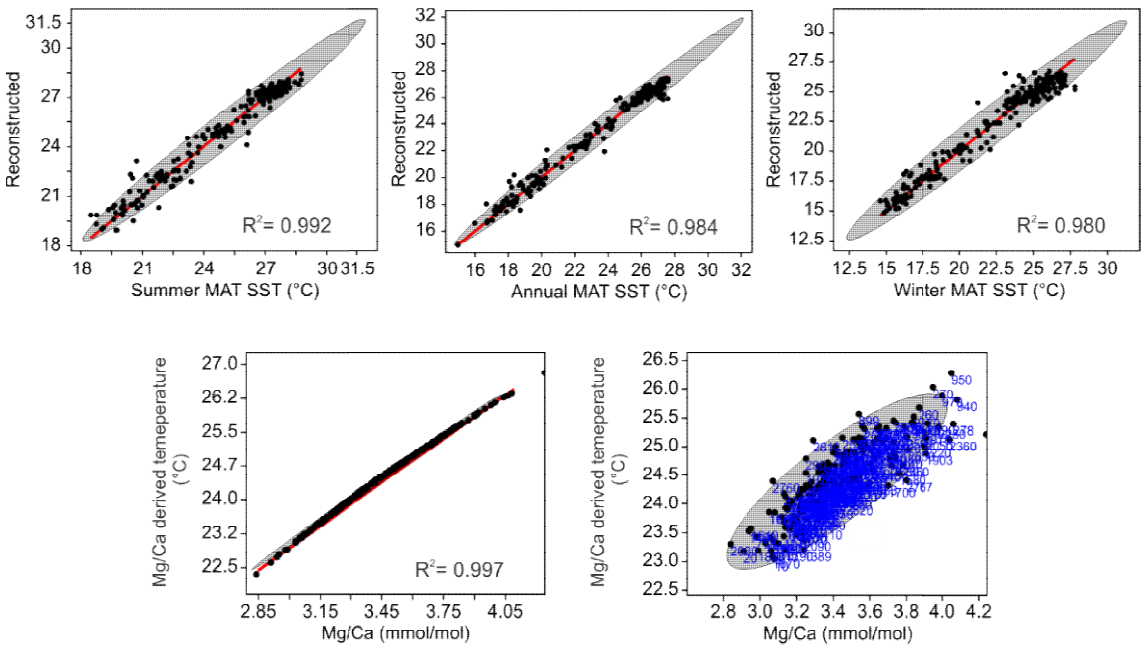

Supplementary Figure S2. Sea surface temperature reconstructions standard deviation. MAT-SST reconstruction correlation (P>95%) and average standard deviation of R^2= 0.992 and 0.26°C for the annual mean temperature, and R^2=0.984 and 0.17°C for warmest (summer) and R^2=0.980 and 0.32°C for the coolest months (winter). Mg/Ca-SST correlation (P>95%) of R^2= 0.997.

Supplementary Table S1. Taxonomic list based in World Foraminifera Database -WoRMS (Hayward et al., 2019)of all species of planktonic foraminifera recovery from the last 1.93 Ma from core CDH-79, located in the western equatorial Atlantic (Pará-Maranhão Basin).

Kingdon: Chromista
Subkingdom: Harosa
Infrakingdom: Rhizaria
Phylum: Foraminifera
Class: Globothalamea
Subclass: Rotaliana
Order: Rotaliida
Suborder: Globigerinina
Superfamily: Globigerinitoidea
Family: Globigerinitidae
Subfamily: Globigerinitinae
Genus: *Globigerinita* Brönnimann, 1951
Specie: *Globigerinita glutinata* (Egger, 1893)
Globigerinita uvula (Ehrenberg, 1861)
Superfamily: Globigerinoidea
Family: Globigerinidae
Subfamily: Globigerininae
Genus: *Beella* Banner & Blow,1960
Beella digitata (Brady, 1879)
Genus: *Globigerina* d'Orbigny, 1826
Globigerina bulloides d'Orbigny, 1826
Globigerina falconensis Blow, 1959
Genus: *Globigerinella* Cushman, 1927
Globigerinella calida (Parker, 1962)
Globigerinella siphonifera (d'Orbigny, 1839)
Genus: *Globigerinoides* Cushman, 1927
Globigerinoides conglobatus (Brady, 1879)
Globigerinoides obliquus Bolli, 1957
Globigerinoides ruber (d'Orbigny, 1839)
Globigerinoides tenellus Parker, 1958
Genus: *Globoturborotalita* Hofker, 1976
Globoturborotalita rubescens (Hofker, 1956)
Genus: *Sphaeroidinella* Cushman, 1927
Sphaeroidinella dehiscens (Parker & Jones, 1865)
Genus: *Trilobatus* Spezzaferri et al., 2015
Trilobatus sacculifer (Brady, 1877)
Trilobatus trilobus (Reuss, 1850)
Genus: *Turborotalita* Blow & Banner, 1962
Turborotalita humilis (Brady, 1884)
Turborotalita quinqueloba (Natland, 1938)
Genus: *Globorotaloides* Bolli, 1957
Globorotaloides hexagonus (Natland, 1938)
Subfamily: Orbulininae

Genus: Orbulina d'Orbigny, 1839

Orbulina universa d'Orbigny, 1839

Family: Hastigerinidae

Genus: *Hastigerina* Thomson in Murray, 1876

Hastigerina pelagica (d'Orbigny, 1839)

Superfamily: Globorotalioidea

Family: Candeinidae

Subfamily: Candeininae

Genus: *Candeina* d'Orbigny, 1839

Candeina nítida d'Orbigny, 1839

Family: Globorotaliidae

Genus: *Globorotalia* Cushman, 1927

Globorotalia crassaformis (Galloway&Wissler, 1927)

Globorotalia hessi Bolli&Premoli Silva, 1973

Globorotalia crassaformis subsp. *Imbricata* Krasheninnikov & Bylinskaya, 2002

Globorotalia ronda Blow, 1969

Globorotalia viola Blow, 1969

Globorotalia hirsuta (d'Orbigny, 1839)

Globorotalia menardii (d'Orbigny in Parker, Jones & Brady, 1865)

Globorotalia flexuosa (Koch, 1923)

Globorotalia scitula (Brady, 1882)

Globorotalia tumida (Brady, 1877)

Genus: *Globoconella* Bandy, 1975

Globoconella inflata (d'Orbigny, 1839)

Genus: *Neogloboquadrina* Bandy, Frerichs & Vincent, 1967

Neogloboquadrina dutertrei (d'Orbigny, 1839)

Neogloboquadrina incompta (Cifelli, 1961)

Neogloboquadrina pachyderma (Ehrenberg, 1861)

Family: Pulleniatinidae

Genus: *Pulleniatina* Cushman, 1927

Pulleniatina obliquiloculata (Parker & Jones, 1865)

Pulleniatina okinawaensis Natori, 1976

5. Conclusion

Based on the identification of planktonic foraminifera from the ~32 m-long core CDH-79 and the calibration of the biostratigraphic events with oxygen isotope records and radiocarbon ages, a biochronostratigraphic framework was established for the longest continuous record (~1.93-0.01 Ma) in the Brazilian equatorial margin. We present 16 calibrated biostratigraphic events and their associated uncertainties, providing the first recognition and description of the taxon appearance, such as the earliest occurrence of *G. truncatulinoides* (1.89-1.91 Ma) and taxon disappearance, as *G. fistulosus* (1.81-1.82 Ma) for the Pará-Maranhão Basin. Evolutionary events in deeper time as last occurrences of *G. fistulosus* appears to be younger in your record, while *G. obliquus* and *G. tosaensis* presented older ages than previous records. However, the reasons for these differences cannot be explained herein, demonstrating the need for more biostratigraphic studies for the lower Pleistocene, particularly in the tropical Atlantic.

Oscillations in the abundance of the *G. menardii* complex showed the oldest Pleistocene disappearance and reappearance events of the complex (*G. menardii* D5, R5, D4, and R4) in the western Atlantic and Brazilian basins in this study. These new events allowed the first determination of the biostratigraphic zones P, Q, R, and S and subzones Q2, Q1, R3, R2, R1, S2, and S1 in the Brazilian basins, improving the resolution of lower Pleistocene events for the area. Our data presented a small diachronism of *G. menardii* events compared to other sites in the North and South Atlantic, possible related to the reseeding mechanism of the taxon due to latitudinal migration of the subtropical front, which is directly connected to the strength of warm waters entering the South Atlantic from the Indian Ocean through the Agulhas leakage

The integration between the bioevents *G. menardii* R2 (reappearance) and T *G. flexuosa* (disappearance) and a radiocarbon age suggests the occurrence of an unconformity (hiatus) of approximately 50 kyr close to the top of our core (i.e., 50-62 cm core depth) between MIS 5 and MIS 2. Furthermore, the absence of *G. menardii*R1 event and *G. fimbriata* specimens, corroborated by the uppermost radiocarbon age (10 cm core depth), demonstrate the absence of sediments deposited during the Holocene. Both recognized unconformities were recognized in the upper section of our records (uppermost 60 cm) and may relate to changes in the sea level and/or a coring disturbance

This record strongly improved the resolution of the biostratigraphic events from the lower Calabrian to the upper Pleistocene, which represents an important base for paleoenvironmental reconstructions in the tropical western Atlantic.

The integration of independent proxies based on planktonic foraminifera species, geochemical (oxygen stable isotopic, $\delta^{18}O$) and trace elements (Mg/Ca ratio) analysis were applied to an ~32 m-long core CDH-79 to reconstruct the main changes in the superficial ocean circulation of the western equatorial Atlantic. Our results provide a reconstruction of the main mechanisms evolved on the oscillations of the AMOC (global scale) and NBC (local scale) systems and the characterizations of the main paleoceanographic changes for the longest continuous record of the Brazilian equatorial margin, covering the almost Pleistocene (~1.93-0.01 Ma; Gelasian to Late Pleistocene). Our superficial oceans reconstructions also support that strong NBCR event when synchronous with events on the south and/or north hemisphere can promote the accumulation and transport of salty and warm waters, as well as accumulation/transport of cold and low-salinity freshwater plumes in the site area.

Our records support the correlation between the western equatorial Atlantic biostratigraphic events of *G. menardii* complex (disappearance - D and reappearance – R events) with the oscillations at the Agulhas leakage due to STF migrations, and slowdown AMOC due north hemisphere stadial intervals. The *G. menardii* R events are related to increased Agulhas leakage due southward migrations of the STF (south tropical front) in the Benguela region, in special the events R4 (~0.96 Ma; MIS 26; boundary T/S); R3 (~0.54 Ma; MIS 12/14; boundary U/V) and R2 (~0.13 Ma; MIS 5/6; boundary W/X). This mechanism also is related to the subzonal boundaries marked by the return of the high abundance of the taxon as R2/R1 (~1.31 Ma; MIS 41) and T2/T1 (~0.68; MIS 16). While the *G. menardii* D events are associated with both mechanism, decrease or interruption of the Agulhas leakage due northward migration of STF, and slowdown AMOC due to massive fluxes of icebergs and meltwater into the North Atlantic (stadials intervals) as recorded during the events D4 (~1.05 Ma; MIS 30; boundary R/S), D3 (~0.59 Ma; MIS 15; boundary T/U), D2 (~0.16 Ma; MIS 8; boundary V/W), and D1 (~0.07 Ma; MIS 5; boundary X/Y). We also suggest that the influence and residence time of the salty and warm transported by the AMOC from the southern hemisphere to the western equatorial Atlantic can be tracked by the abundance oscillations of the *G. menardii* complex.

The occurrence of two cold events in the North Atlantic and its impact on the tropical Atlantic paleoceanography and climatology are addressed and support the occurrence of the oldest Heinrich events, here for the first time recorded in the western equatorial Atlantic. The oldest large scale event occurs with the onset of the Mid-Pleistocene Transition (~0.89-0.88 Ma, MIS 22), and later, a second event occurs with the middle MPT (~0.63 Ma; MIS 16). In both, a thick cold and low-salinity layer (>50 m) dominated the superficial ocean at the site area. We suggest the synchronized large scale river inflow (and freshwater plume) by

increased (heavy) precipitation, both due to the southern mean position of the ITZC (probably over the continent), with the stadial events in the North Atlantic that promote strongest NBCR due to slowdown AMOC and weak NBC. The strongest NBCR can bring to the site area freshwater plumes from the main fluvial drainage (Parnaíba river), and possibly due southward transport in the superficial and subsuperficial layers of the retroflections system, freshwater plumes from Amazon river as well. However, the origin of the cold and low-salinity waters remains inconclusive.

We also provide the first record of millennial-time scale events of salty and warm accumulation in the Brazilian equatorial margin. Our records linked the salt and warm accumulation in the area with increased NBCR system, that can act as a physical barrier for the cross-equatorial heat and salinity transport and a possible accumulation of the salty water on the NBC rings, transported over the study area. We support the action of both mechanism, decrease in the NBC transport by AMOC slowdown (due stadial North Atlantic event), and increased strength of Agulhas leakage due to southward migration of the STF. The simultaneous occurrence between south and north hemisphere events promotes a continuous transport of the salty and warm waters from the southern hemisphere to the Equator, followed by weak transport or a temporary interruption on the Equator to north hemisphere transport. The coupling of these mechanisms can also impact the density of high latitude surface waters and thus has important implications for the formation and production of NADW. These events are recorded over the late (~1.26-1.12 Ma; MIS 33/34-38/39) and early (~0.33 Ma; MIS 9) Pleistocene

The main contribution of this manuscript is addressed the application of the abundance events of *G. menardii* complex recorded in the tropical Atlantic, as a proxy for the heat and salty waters transport from the southern hemisphere to the Equatorial region due to Agulhas leakage. We also addressed the influence of the NBCR strength system as an important inter-hemisphere heat and salt transport regulator, and the impact of the millennial-scale current oscillations in the global and local climate.

6. References

Allison, M.A., Lee, M.T., Ogston, A.S., Aller, R.C., 2000. Origin of Amazon mudbanks along the northeastern coast of South America. Mar. Geol., 163 (1-4):241–256.

Anand, P., Elderfield, h., Conte, M.H. 2003. Calibration of Mg/Ca thermometry in planktonic foraminifera from a sediment trap time series. Paleoceanography, 18(2):1050. doi:10.1029/2002PA000846

Arz, H. W., Pätzold, J., Wefer, G. 1998. Correlated millennial-scale changes in surface hydrography and terrigenous sediment yield inferred from last-glacial marine deposits off northeastern Brazil. *Quaternary Research*, 50(2):157-166.

Arz, H.W., Patzold, J.,Wefer, G., 1999. The deglacial history of thewestern tropical Atlantic as inferred from high-resolution stable isotope records off northeastern Brazil. Earth Planet. Sci. Lett., 167:105–117.

Baker, P.A., S.C. Fritz. 2015. Nature and causes of Quaternary climate variation of tropical South America. Quaternary Science Reviews, 124:31-47.

Barker, S., Archer, D., Booth, L., Elderfield, H., Henderiks, J., Rickaby, R.E.M., 2006. Globally increased pelagic production during the Mid-Brunhes dissolution interval and the CO2 paradox of MIS 11. Quaternary Science Reviews 25, 3278-3293.

Barker, S., Diz, P., Vautravers, M.J., Pike, J., Knorr, G., Hall, I.R., Broecker, W.S., 2009. Interhemispheric Atlantic seesaw response during the last deglaciation. Nature 457 (7233), 1097–1102. http://dx.doi.org/10.1038/nature07770.

Barker, S., Greaves, M., Elderfield, H., 2003. A study of cleaning procedures used for foraminiferal Mg/Ca paleothermometry. Geochem. Geophys. Geosyst. 4, 8407. http://dx.doi.org/10.1029/2003GC000559.

Bé, A.W.H. 1977. An ecological, zoogeographic and taxonomic review of Recent planktonic foraminifera. In Ramsay, A.T.S. (Ed.), Oceanic Micropaleontology (Vol. 1): London (Acad. Press), 1–100.

Bé, A.W.H.; Damuth, J.E.; Lott, L., Free, R. 1976. Late Quaternary Climatic Record in Western Equatorial Atlantic Sediment. In: Geological Society of America. Investigations of Late Quaternary Paleoceanograph and Paleoclimatology. Geological Society of America Memoir, 145:162-200.

Becquey, S., Gersonde, R. 2002. Past hydrographic and climatic changes in the Subantartic Zone of the South Altantic - The Pleistocene record form ODP Site 1090. Palaeogeography, Palaeoclimatology, Palaeoecology, 182:221-239.

Bemis, B.E., Spero, H.J., Bijma, J., Lea, D.W., 1998. Reevaluation of the oxygen isotopic composition of planktonic foraminifera: Experimental results and revised paleotemperature equations. Paleoceanography 13, 150–160.

Berger, A., Loutre, M. F. 1991. Insolation values for the climate of the past 10 m.y.Quaternary Science Reviews 10, 297–317.

Berger, A., Loutre, M. F. 2003. Climate 400,000 years ago, a key to the future? In Droxler A. W., Poore R. Z. & Burckle L. H. (eds). Earth's Climate and Orbital Eccentricity, pp. 17–26. American Geophysical Union, Washington, DC.

Berger, W. H., Herguera, J. C., Lange, C. B., Schneider, R. 1994. Peloproductivity: flux proxies versus nutrient proxies and other problems concerning the Quaternary productivity record. In: Zahn, R. (ed) Carbon cycling in the glacial ocean: constraints on the ocena´s role in global change. Nato Asi Series, Berlin, 385-412.

Berger, W.H., Wefer, G., 1996. Central themes of South Atlantic circulation. In: Wefer, G., Berger, W.H., Siedler, G., Webb, D.J. (Eds.), The South Atlantic: Present and Past Circulation. Springer-Verlag, Heidelberg, Germany, pp. 1–11.

Berggren, W. A., Kent, D. V., and van Couvering, J. A., 1985a, Neogene geochronology and chronostratigraphy, in Snelling, N. J., ed., The chronology of the geological record: Geological Society of London Memoir 10, p. 211–250.

Berggren, W.A., Hilgen, F.J., Langereis, C.G., Kent, D.V., Obradovich, J.D., Raffi, I., Raymo, M.E., and Shackleton, N.J., 1995a. Late Neogene chronology: new perspectives in high-resolution stratigraphy. Geol. Soc. Am. Bull., 107:1272-1287.

Berggren, W.A., Kent, D.V., Swisher, C.C., III, and Aubry, M.-P., 1995b. A revised Cenozoic geochronology and chronostratigraphy. In Berggren, W.A., Kent, D.V.,

Bickert, T, Curry, W.B., Wafer, G. 1997. Deep-water circulation: inferences from benthic stable isotopes. In Shackleton, N.J., Curry, W.B., Richter, C., Bralower, T.J. (Eds.), Proceedings of the Ocean Drilling Program, Scientific Results, 154:239-254.

Blaauw, M., Christen, J.A., 2011. Flexible paleoclimate age-depth models using an autoregressive gamma process. Bayesian Anal, 6(3):457-474.

Blow, W.H. 1969. Late middle Eocene to Recent planktonic foraminiferal biostratigraphy. *In:* P. Bronnimann & H.H. Renz (eds) *Proceedings of the First International Conference on Planktonic Microfossilis,* Geneva, 1967, p. 199-422.

Bolli, H.M., Premoli Silva, I. 1973. Oligocene to Recent Planktonic Foraminífera and Stratigraphy of Leg 15 sites in the Caribean Sea. *Initial Reports of the Deep Sea Drilling Project*, **15**:475:497.

Bolli, H.M., Saunders, J.B., 1985. Oligocene to Holocene low latitude planktic foraminifera. In: Bolli, H.M., Saunders, J.B., Perch-Nielsen, K. (Eds.), Plankton Stratigraphy. Cambridge University Press, New York, pp. 156-262.

Broecker, W., Van Donk, J. 1970. Insolation changes, ice volumes, and the 18O record in deep-sea cores: Reviews of Geophysics and Space Physics, 8:169-198.

Butzin, M., P. Köhler, and G. Lohmann (2017), Marine radiocarbon reservoir age simulations for the past 50,000 years, Geophys. Res. Lett., 44, 8473 – 8480, doi:10.1002/2017GL074688

Buzas, M.A., Gibson, T.G. 1969. Species diversity: benthonic foraminifera in the western North Atlantic. Science, 163:72-75.

Caley, T., Giraudeau, J., Malaizé, B., Rossignol, L., Pierre, C. 2012. Agulhas leakage as a key process in the modes of Quaternary climate changes. Proceedings of the National Academy of Sciences, 109 (18) 6835-6839; DOI: 10.1073/pnas.1115545109.

Caley, T., Kim, J.-H., Malaizé, B., Giraudeau, J., Laepple, T., Caillon, N., Charlier, K., Rebaubier, H. , Rossignol, L., Castañeda, I. S., Schouten, S., Sinninghe Damst, J.S. 2011. High-latitude obliquity as a dominant forcing in the Agulhas current system. Climate of the Past, 7:1285-1296.

Chen, J. Farrell, J. W., Murray, D. W., Prell, W. L. 1995. Timescale and paleoceanographic implications of a 3.6 m.y. oxugen isotope record from the northeast Indian Ocean (ODP Site 758). Paleoceanography, 10:21-47.0

Cohen, K.M. and Gibbard, P.L. 2019. Global chronostratigraphical correlation table for the last 2.7 milion years, version 2019 QI-500. Quaternary International, 500:20-31.

Crivellaria, S., Chiessi, C.M., Kuhnert, H., Häggi, C., Portilho-Ramos, R.C., Zeng, J.Y., Zhang, Y., Schefuß, E., Mollenhauer, G., Hefter, J., Alexandre, F., Sampaio, G., Mulitza, S. 2017.

Increased Amazon freshwater discharge during late Heinrich Stadial 1. Quaternary Science Reviews, 181: 144-155. doi.org/10.1016/j.quascirev.2017.12.005

Cruz, F. W., Burns, S.J., Karmann, I., Sharp, W.D., Vuille, M., Cardoso, A.O., Ferrari, J.A., Silva Dias, P.L., Viana, O. 2005. Insolation-driven changes in atmospheric circulation over the past 116,000 years in subtropical Brazil. Nature, 434(7029): 63-66.

Cruz, F. W., Vuille, M., Burns, S. J., Wang , X. F., Cheng, H., Werner, M., Edwards, R. L., Karmann, I., Auler, A.S., Nguyen, H. 2009. Orbitally driven east-west antiphasing of South American precipitation. Nature Geoscience, 2(3): 210-214.

Cruz, J. F. W., Burns, S.J., Karmann, I., Sharp, W.D., Vuille, M. 2006.Reconstruction of regional atmospheric circulation features during the late Pleistocene in subtropical Brazil from oxygen isotope composition of speleothems. Earth and Planetary Science Letters, 248(1-2):495-507.

de Garidel-Thoron, T., Y. Rosenthal, F. Bassinot and L. Beaufort. 2005. Stable sea surface temperatures in the western Pacific warm pool over the past 1.75million years. Nature, 433(7023): 294-298.

Dekens, P.S., Lea, D.W., Pak, D.K., Spero, H.J., 2002. Core top calibration of Mg/Ca in tropical foraminifera: re"ning paleotemperature estimation. Geochemistry, Geophysics, Geosystems 3 doi:10.1029/2001GC000200.

Diekmann, B., Kuhn, G., 2002. Sedimentary record of the Mid-Pleistocene climate transition in the Southeastern Atlantic Ocean (ODP, Site 1090). Palaeogeography, Palaeoclimatology, Palaeoecology, S0031-0182(01)00498-9.

Dupont, L.M., Schlütz, F., Teboh Ewah, C., Jennerjahn, T.C., Paul, A., Behling, H., 2010. Two-step vegetation response to enhanced precipitation in Northeast Brazil dur-ing Heinrich event 1. Glob. Change Biol., 16:1647–1660.

Durham, E. L., Maslin, M. A., Platzman, R., Rosell-Mele, A., Marlowm J. R., Leng, M., Lowry, D., Burns, S. J., ODP Leg 175 Shipboard Scientific Party, 2001. Reconstructing the climatic history of the western coast of Africa over the past 1.5 m.y: a comparison of proxy record from the Congo Basin and the Walvis Ridge and the search for evidence of the Mid-Pleistocene Revolution. Proceedings of the Ocean Drillng Program, Scientific Results, 175:1-46.

Elderfield, H., Ferretti, P., Greaves, M., Crowhurst, S.J., McCave, I Nick, Hodell, D., A, Piotrowski, A.M. 2012. Evolution of ocean temperature and ice volume through the Mid-Pleistocene Climate Transition. Science, 337(6095): 704-709. doi.org/10.1126/science.1221294

Elderfield, H., Ganssen, G. 2000. Past temperature and d18O of surface ocean waters inferred from foraminiferal Mg/Ca ratios. Nature:405, 442–445.

Ericson, D.B., Wollin, G. 1968. Pleistocene climates and chronology in deep-sea sediments. *Science*, **162**:1227-1243.

Fairbanks, R., Sverdlove, M., Free, R., Wiebe, P., Bé, A. 1982. Vertical distribution and isotopic fractionation of living planktonic foraminifera from the Panama Basin. Nature, 298:841-844. 10.1038/298841a0.

Fairbanks, R.G., Wiebe, P.H., and Bé, A.W.H., 1980. Vertical distribution and isotopic composition of living planktonic foraminifera in the western North Atlantic. Science, 207:61–63.

Ferreira, F., Frontalini, F., Leão, C.J., Leipnitz, I.I. 2014. Changes in the water column structure and paleoproductivity in the western South Atlantic Ocean since the middle Pleistocene: Evidence from benthic and planktonic foraminífera. Quaternary International, 352: 111-123.

Ferreira, F., Leipnitz, I.I., Vicalvi, M.A., Sanjinés, A.E.S., 2012. Zoneamento Paleoclimático do Quaternário da Bacia de Santos com base em foraminíferos planctônicos. Rev. Bras. Paleontol. 15 (2), 173–188.

Flores, J.A., Marino, M., Sierro, F.J., Hodell, D.A., Charles, C.D., 2003. Calcareous plankton dissolution pattern and coccolithophore assemblages during the last 600 kyr at ODP Site 1089 (Cape Basin, South Atlantic): paleoceanographic implications. Palaeogeography, Palaeoclimatology, Palaeoecology 196, 409-426.

Gibbard, P.L., Head, M.J. 2010 The newly-ratified definition of the Quaternary System/Period and redefinition of the Pleistocene Series/Epoch, and comparison of proposals advanced prior to formal ratification. Episodes 33, 152-158.

Gibbard, P.L; Head, M.J.; Walker, M.J.C., The Subcomission on Quaternary Stratigraphy. 2010. Formal ratification of the Quaternary System/Period and the Pleistocene Series/Epoch with a base at 2.58 Ma. *Journal of Quaternary Science*, **25**:96-102.

Goni, G.J., Johns,W.E., 2001. A census of North Brazil Current Rings observed from TOPEX/POSEIDON altimetry: 1992–1998. Geophys. Res. Lett. 28 (1), 1–4.

Govin, A., Capron, E., Tzedakis, P.C., Verheyden, S., Ghaleb, B., Hillaire-Marcel, C., St-Onge, G., Stoner, J.S., Bassinot, F., Bazin, L., Blunier, T., Combourieu-Nebout, N., El Ouahabi, A., Genty, D., Gersonde, R., Jimenez-Amat, P., Landais, A., Martrat, B., Masson-Delmotte, V., Parrenin, F., Seidenkrantz, M.-S., Veres, D., Waelbroeck, C., Zahn, R. 2015. Sequence of events from the onset to the demise of the Last Interglacial: Evaluating strengths and limitations of chronologies used in climatic archives. Quaternary Science Reviews, 129: 1-36.

Gray, W.R., Weldeab, S., Lea, David W., Rosenthal, Y., Gruber, N., Donner, B., Fischer, G. 2018. The effects of temperature, salinity, and the carbonate system on Mg/Ca in Globigerinoides ruber (white): A global sediment trap calibration. Earth and Planetary Science Letters, 482:607-620. doi.org/10.1016/j.epsl.2017.11.026

Haarsma, R.J., Campos, E.J.D., Drijfhout, S., Hazeleger, W., Severijns, C., 2011. Impacts of interruption of the Agulhas leakage on the tropical Atlantic in coupled ocean–atmosphere simulations. Clim. Dyn. 36 (5–6), 989–1003.

Hammer, O., Harper, D.A.T., Rayan, P.D. 2001. PAST: Paleontological Statistics software package for education and data analysis. Paleontologia Electronica, 4(1):9 pp.

Hastenrath, S. 2006. Circulation and teleconnection mechanisms of Northeast Brazil droughts. Progress in Oceanography, 70(2):407-415.

Hastenrath, S., Heller, L. 1977. Dynamics of climatic hazards in northeast Brazil. Quarterly Journal of the Royal Meteorological Society, 103(435):77-92.

Hayward, B. W., Kawagara, S., Sabaa, A., Grenfell, H., Kerckhoven,L. V., Johnson, K., Thomas, E. 2012. The Last Global extinction (Mid-Pleistocene) of deep-sea benthic foraminifera (Chrysalogoniidae, Ellipsoidinidae, Glandulonodosariidae, Plectofrondicullariidar, Pleurostomellidae, Stilostomellidae) their late Cretaceous-Cenozoic History and taxonomy. Cushman Foundation for Foraminiferal Reseach Special Publication no. 43, 408 p.

Hayward, B.W.; Le Coze, F.; Vachard, D.; Gross, O. 2019. World Foraminifera Database. Accessed at http://www.marinespecies.org/foraminifera on 2019-12-14. doi:10.14284/305

Holden, P.B., Edwards, N.R., Wolff, E.W., Valdes, P.J., Singarayer, J.S., 2011. The Mid- Brunhes Event and West Antartic Ice Sheet stability. Journal of Quaternary Science 26(5), 474-477.

Imbrie, J., Berger, A., Boyle, E. A., Clemens, S. C., Duffy, A., Howard, W. R., Kukla, G., Kutzbach, J., Martinson, D. G., McIntyre, A., Mix, A. C., Molfino B., Morley, J. J., Peterson, L. C., Pisias, N. G., Prell, W. L., Raymo, M. E., Shackleton, N. J., Toggweile, J. R.. 1993. On the structure and origin of major glaciation cycles, 2: the 100,000 cycles. Paleoceanography, 8:699-735.

Imbrie, J., McIntyre, A., Mix, A. 1989. Oceanic response to orbital forcing in the late Quaternary: Observational and experimental strategies. Climate Geo-sci., 285:121-164.

Jansen, J. H. F., Kuijpers, A., Troelstra, S. R. 1986. A Mid-Brunhes climatic event: Long term changes in global atmosphere and ocean circulation. Science 232, 619–22.

Jennerjahn, T. C., Ittekkot, V., Arz, H.W., Behling, H., Pätzold, J., Wefer G. 2004. Asynchronous Terrestrial and Marine Signals of Climate Change During Heinrich Events. Science, 306(5705):2236-2239.

Johns, W., Lee, T., Beardsley, R.C., Candela, J., Limeburner, R., Castro, B., 1998. Annual cycle and variability of the North Brazil Current. J. Phys. Oceanogr. 103–128. doi.org/10.1175/15200485(1998)028%3C0103:ACAVAC%3E2.0.CO%3B2.

Kemp, A.E.S., Grigorov, I., Pearce, R.B., Naveira Garabato, A.C., 2010. Migration of the Antarctic Polar Front through the mid-Pleistocene transition: evidence and climatic implications. Quaternary Science Reviews 29, 1993-2009.

Kennett, J. P., Srinivasan, M. S., 1983. Neogene planktonic foraminifera. Stroudsburg: Hutchinson Ross Publishing Company, 265pp.

Kennett, J.P., Huddlestun, P. 1972. Late Pleistocene paleoclimatology, foraminiferal biostratigraphy and tephrochronology, Western Gulf od Mexico. Quaternary Research, 2:38-69.

Kipp, N.G., 1976. New transfer function for estimating past sea-surface conditions from sea-bed distribution of planktonic foraminiferal assemblages in the north Atlantic. In Cline, R.M., and Hays, J.D. (Eds.), Investigation of Late Quaternary Paleoceanography and Paleoclimatology. Mem.- Geol. Soc. Am., 145:3–41.

Kısakürek, B., Eisenhauer, A., Böhm, F., Garbe-Schönberg, D., Erez, J. 2008. Controls on shell Mg/Ca and Sr/Ca in cultured planktonic foraminiferan, *Globigerinoides ruber* (white). Earth and Planetary Science Letters, 273:3-4.

Kohl, B.; Fillon, R.H. & Roberts, H.H. 2004. Foraminiferal biostratigraphy and paleoenvironments of the Pleistocene Lagniappe Delta and related section, Northeastern Gulf of Mexico. *In:* B. Anderson & R.H. Fillon (eds) *Late Quaternary Stratigraphic Evolution of the Northern Gulf of Mexico Margin.*Society for Sedimentary Geology, p. 190-216 (Special Publication No. 79).

Kucera, M., Rosell-Melé, A., Schneider, R., Waelbroeck, C., Weinelt, M., 2005a. Multiproxy approach for the reconstruction of the glacial ocean surface (MARGO). Quat. Sci. Rev. 24, 813–819. http://dx.doi.org/10.1016/j.quascirev.2004.07.017.

Kucera, M., Weinelt, M.M., Kiefer, T., Pflaumann, U., Hayes, A., Chen, M.-T., Mix, A.C., Barrows, T.T., Cortijo, E., Duprat, J., Juggins, S., Waelbroeck, C., 2005b. Reconstruction of sea-surface temperatures from assemblages of planktonic foraminifera: multitechnique approach based on geographically constrained calibration data sets and its application to glacial

Atlantic and Pacific Oceans. Quat. Sci. Rev. 24, 951–998. http://dx.doi.org/10.1016/j.quascirev.2004.07.014.

Kuhn, G., Diekmann, B., 2002. Late Quaternary variability of ocean circulation in the southeastern South Atlantic inferred from the terrigenous sediment record of a drift deposit in the southern Cape Basin (ODP Site 1089). Palaegeography, Palaeoclimatology, Palaeoecology 182, 287-303.

Kunz-Pirrung, M., Gersonde, R., Hodell, D.A., 2002. Mid-Brunhes century-scale diatom sea surface temperature and sea ice records from the Atlantic sector of the SouthernOcean (ODP Leg 177, Sites 1093, 1094 and core PS2089-2). Palaeogeography, Palaeoclimatology, Palaeoecology 183(3-2):305-328.

Langner, M. and Mulitza, S. 2019. Technical Note: PaleoDataView – A software toolbox for the collection, homogenization and visualization of marine proxy data, Climate of the Past, 15:2067–2072. doi.org/10.5194/cp-15-2067-2019.

Le, J., Shackleton, N.J., 1992. Carbonate dissolution fluctuations in the western equatorial Pacific during the late Quaternary. Paleoceanography, 7(1):21–42.

Lea, D.W., Mashiotta, T.A., Spero, H.J. 1999. Controls on magnesium and strontium uptake in planktonic foraminifera determined by live culturing. Geochimica at Cosmochimica Acta, 63(16):2369-2379.

Lea, D.W., Pak, D.K., Spero, H.J. 2000. Climate impact of Late Quaternary equatorial Pacific sea surface temperature variations. Science, 289:1719–1724.

Leipnitz, I.I., Silva, J.L.L., Leipnitz, B., Aguiar, E.S., Leão, C.J., Giovanoni, L., Ferreira, F. 2005. Métodos para o trabalho com microfósseis e formas atuais. In Timm, L.L. & Cademartoti, C.V., eds, Cadernos La Salle XI - Métodos de Estudo em Biologia, ISSN: 1678-2003, vol. 2, n. 1, pp. 49-58.

Lentz, S.J., 1995. Seasonal variations in the horizontal structure of the Amazon Plume inferred from historical hydrographic data. J. Geophys. Res., Oceans, 100:2391–2400.

Leonhardt, A., Toledo, F.A.L., Coimbra, J.C. 2015. The Mid-Brunhes event un the southwestern Atlantic ocean coccolithophore assembleges during the MIS 11-9. Revista Brasileira de Paleontologia, 18(3):343-354.

Lessa, D.V.O., Portilho-Ramos, R.C., Barbosa, C.F., da Silva, A.R., Belem, A.L., Turcq, B.J., Albuquerque, A.L.S. 2014. Planktonic foraminifera from sediment core CF10-01B (Cabo Frio - Brazil). Marine Micropaleontology, 106, 55-68, doi.org/10.1016/j.marmicro.2013.12.003

Lisiecki, L., Raymo, M.E. 2005. A Pliocene-Pleistocene stack of 57 globally distributed benthic δ18O records. Paleoceanography, 20, PA1003, doi:10.1029/2004PA001071.

Locarnini, R. A., A. V. Mishonov, O. K. Baranova, T. P. Boyer, M. M. Zweng, H. E. Garcia, J. R. Reagan, D. Seidov, K. Weathers, C. R. Paver, and I. Smolyar, 2018. World Ocean Atlas 2018, Volume 1: Temperature. A. Mishonov Technical Ed.; NOAA Atlas NESDIS 81, 52 pp.

Marchitto, T.M., Curry, W.B., Lynch-Stieglitz, J., Bryan, S.P., Cobb, K.M., Lund, D.C. 2014. Improved oxygen isotope temperature calibrations for cosmopolitan benthic foraminifera. Geochimica et Cosmochimica Acta, 130: 1-11.

Marques, M., Costa, M.F., Mayorga, M.I.O., Pinheiro, P. 2004. The water environment: antropogenic pressures and ecosystem changes in the Atlantic drainage basin of Brazil. Ambio, 33:68-77.

Martin, R.E.; Johnson, G.W.; Neff, E.D., Krantz, D.E. 1990. Quaternary planctonic foraminiferal assemblages zones of the northest Gulf of México, Colombia basin (Caribbean Sea), and

tropical Atlantic Ocean: Graphic correlation of microfossil and oxygen isotope datums. *Paleoceanography*, **5**(4):531-555.

Martin, R.E.; Neff, E.D.; Johnson, G.W., Krantz, D.E. 1993. Biostratigraphic Expression of Pleistocene Sequence Boundaries, Gulf of Mexico. *Palaios*, **8**:155-171.

Martinez, J.I; Mora, G. & Barrows, T.T. 2007. Paleoceanographic conditions in the Western Caribbean Sea for the last 560 kyr as inferred from planktonic foraminifera. *Marine Micropaleontology,* **64**:177-188.

Mashiotta, T. A., Lea, D. W., Spero, H. J. 1999. Glacial-interglacial changes in Subantarctic sea surface temperature and d18O-water using foraminiferal Mg, Earth Planet. Sci. Lett., 170, 417–432.

Maslin, M. A., Seidov, D., Lowe, J. 2001. Synthesis of the nature and causes of sudden climate transitions during the Quaternary. In: Seidov, D., Hapt, B. J., Maslin, M. A. (eds) The Oceans and Rapid Climate Change: Past, Present and Future: American Geophysical Union, Geophysical Monograph Series, 126:9-52.

Maslin, M.A., Burns, S.J., Erlenkeuser, H., Hohnemann, C., 1997. Stable isotope records from sites 932 and 933. In: Flood, R.D., Piper, D.J.W., Klaus, A., Peterson, L.C. (Eds.), Proceedings of the Ocean Drilling Program, Scienti"c Results, vol. 155. Ocean Drilling Program, College Station, TX, U.S.A., pp. 305–318.

McConnell, M.C., Thunell, R.C. 2005. Calibration of the planktonic foraminiferal Mg/Ca paleothermometer: Sediment trap results from the Guaymas Basin, Gulf of California. Paleoceanography, 20:PA2016. doi.org/10.1029/2004PA001077

McManus, J. F., Anderson, R. F., Broecker, W. S., Fleisher, M. Q., Higgins, S. M. Higgins. 1999. Radiometrically determined sedimentary fluxes in the sub-polar North Atlantic during the last 140,000 years. Earth Planet. Sci. Lett., 155:29-4 3, doi:10.1016/S0012-821X(97)00201-X.

McManus, J. F., Oppo, D., Cullen, J.L. 1999. A 0.5-million-year record of millennial-scale climate variability in the North Atlantic. Science 283, 971–5.

Mix, A. C., Pisias, N. G., Rugh, W., Wilson, J., Morey, A., Hagelberg, T. K. 1995. Benthic foraminifera stable isotope record from Site 849 (0–5 Ma): Local and global climate changes. Proceedings of the Ocean Drilling Program, Scientific Results 138, 371–412.

Mohtadi, M. Hebbeln, D., Marchant, M. 2005. Upwelling and productivity along the Peru-Chile current derived from faunal and isotopic compositions of planktic foraminifera in surface sediments. Marine Geology, 216(3):107-126. doi.org/10.1016/j.margeo.2005.01.008

Molion, L.C.B., Bernardo, S.d.O. 2000. Dinâmica das chuvas no Nordeste Brasileiro. Congresso Brasileiro de Meteorologia, SBM

Mudelsee, M., Schulz, M. 1997. The Mid-Pleistocene climate transition: onset of 100 ka cycle lags ice volume build-up by 280 ka. Earth and Planetary Science Letters, 151:117-123. 10.1016/S0012-821X(97)00114-3.

Nace, T. E., P. A. Baker, G. S. Dwyer, C. G. Silva, C. A. Rigsby, S. J. Burns, L. Giosan, B. Otto-Bliesner, Z. Liu and J. Zhu. 2014. The role of North Brazil Current transport in the paleoclimate of the Brazilian Nordeste margin and paleoceanography of the western tropical Atlantic during the late Quaternary. Palaeogeography, Palaeoclimatology, Palaeoecology, 415(0): 3-13.

Niebler, H. S., Gersonde, R. 1998. A planktic foraminiferal transfer function for the southern South Atlantic Ocean. Marine Micropaleontology 34, 213–234. Oppo, D.W., R.G., Fairbanks,

1989. Carbon isotope composition of phosphate-free surface water of the past 22,000 years. Paleoceanography 4, 333-351.

Nishi, H., Norris, R.D., Okada, H. 2000. Paleoceanographic changes in the dynamics of subtropical surface conditions at Hole 997A. *In:* Paull, C.K., Matsumoto, R., Wallace, P.J., and Dillon, W.P. (Eds.), Proceedings of the Ocean Drilling Program, Scientific Results, Vol. 164.

Nurnberg, D., Muller, A., Schneider, R.R. 2000. Paleo-sea surface temperature calculations in the equatorial east Atlantic from Mg/Ca ratios in planktonic foraminifera: A comparison to sea surface estimates from U37k0 , oxygen isotopes, and foraminiferal transfer functions. Paleoceanography, 15:124–134.

Oliveira, A.S. 2016. Paleoclimate/paleoceanographic reconstructions of the Tropical South America. Ph.D. thesis, Programa de Pós-graduação em dinâmica dos Oceanos e da Terra da Universidade Federal Fluminense - DOT/UFF, 79 p.

Oppo, D.W., McManus, J. F., Cullen, J. L. 1998. Abrupt climate events 500,000–340,000 years ago: Evidence from subpolar North Atlantic sediments. Science 279, 1335–8. Patterson, R.T., Fishbein, E. 1989. Re-Examination of the statistical methods used to determine the number of point counts needed for micropaleontological quantitative research. Journal of Paleontology, 63:245-248.

Patterson, R.T., Fishbein, E. 1989. Re-Examination of the statistical methods used to determine the number of point counts needed for micropaleontological quantitative research. Journal of Paleontology, 63:245-248.

Peeters, F.J., Acheson, R., Brummer, G.-J.A., Rujiter, W.P.M., Schneider, R.R., Ganssen, G.M., Ufker, E., Kroon, Dick. 2004. Vigorous exchange between the Indian and Atlantic oceans at the end of the past five glacial periods. Nature, 430:661-665.

Peterson, L.C., Haug, G.H., Hughen, K.A., Röhl, U. 2000. Rapid Changes in the Hydrologic Cycle of the Tropical Atlantic During the Last Glacial. Science, 290(5498):1947-1951.

Peterson, R.G., Stramma, L. 1991. Upper-Level circulation in the South Atlantic Ocean. Prog. Oceanog., 26:1-73.

Portilho-Ramos, R.C., Barbosa, C.F., Rios-Netto, A.M., 2014. Planktonic foraminiferal variations in the southwestern Atlantic since the last glacial–interglacial cycle. PALAIOS 29, 38–44. http://dx.doi.org/10.2110/palo.2012.104.

Portilho-Ramos, R.C., Chiessi, C.M., Zang, Y., Mulitza, S., Kucera, M., Siccha, M., Prange, M., Paul, A. 2017. Coupling of equatorial Atlantic surface stratification to glacial shifts in the tropical rainbelt. Nature Scientific Reposts, 7:1561. DOI:10.1038/s41598-017-01629-z

Railsback, L.B., Gibbard, P.L., Head, M.J., Voaristsoa, N.R.G., Toucanne, S. 2015. Na optimized scheme of lettered marine isotopic stages for the last 1.0 million years, and the climatostratigraphic nature of isotope stage and substages. Quaternary Science Reviews, 111:94-106.

Regenberg, M., Regenberg, A., Garbe-Schönberg, D., Lea, D. W. 2014. Global dissolution effects on planktonic foraminiferal Mg/Ca ratios controlled by the calcite-saturation state of bottom waters. Paleoceanography, 29:127–142. https://doi.org/10.1002/2013PA002492

Regenberg, Steph, Silke; Marcus; Tiedemann, Ralf; Mulitza, Stefan; Nürnberg, Dirk. 2009. Stable isotopes of planktonic foraminifera from tropical Atlantic/Caribbean core-tops: Implications for reconstructing upper ocean stratification. Marine Micropaleontology, 71(1-2): 1-19. doi.org/10.1016/j.marmicro.2008.12.004

Reimer, P. J., Bard, E., Bayliss, A., Beck, J.W., Blackwell, P.G., Ramsey, C.B., Buck, C.E., Edwards, R.L., Friedrich, M., Grootes, P.M., Guilderson, T.P., Haflidason, H., Hajdas, I., Hatté, C., Heaton, T.J., Hoffmann, D.L., Hogg, A.G., Hughen, K.A., Kaiser, K.F., Kromer, B., Manning, S.W. , Niu, M., Reimer, R.W., Richards, D.A., Scott, E.M., Southon, J.R., Staff, R.A., Turney, C.S.M., van der Plicht, J. 2013. INTCAL13 and MARINE13 Radiocarbon Age Calibration Curves 0–50,000 Years Cal BP. Radiocarbon, 55(4):1869–1887.

Rongstad, B.L., Marchitto, T.M., Herguera, J.C. 2017. Understanding the Effects of Dissolution on the Mg/Ca Paleothermometer in Planktic Foraminifera: Evidence From a Novel Individual Foraminifera Method. Paleoceanography and Paleoclimatology. Paleoceanography, 32:1386-1402. https://doi.org/10.1002/2017PA003179

Rosenthal, Y., Boyle, E.A., Slowey, N. 1997. Temperature control on the incorporation of magnesium, strontium, fluorine, and cadmium into benthic foraminiferal shells from Little Bahama Bank: Prospects for thermocline paleoceanography. Geochem. Cosmochim. Acta, 61:3633–3643.

Rosenthal, Y., Lohmann, G.P. 2002. Accurate estimation of sea surface temperature using dissolution corrected calibrations for Mg/Ca paleothermometry. Paleoceanography, 17(3):1044. doi:10.1029/2001PA000749.

Rosenthal, Y., Lohmann, G.P., Lohmann, K.C., Sherrell, R.M. 2000. Incorporation and preservation of Mg in Globigerinoides sacculifer: Implications for reconstructing the temperature and 18O/16O of seawater. Paleoceanography, 15:135–145.

Ruddiman, W.F., 2003. Orbital insolation, ice volume, and greenhouse gases. Quaternary Science Reviews 22, 1597-1623.

Ruddiman, W.F., Raymo, M. E., Martinson, D. G., Clement, B. M., Backman, J. 1989. Pleistocene evolution of Northern Hemisphere climate: Paleoceanography, 4:353-412.

Rutherford, S. D'Hondt, S., Prell, W. 1999. Rutherford S, D'Hondt S, Prell W.. Environmental controls on the geographic distribution of zooplankton diversity. Nature 400: 749-753. Nature. 400. 749-753. 10.1038/23449.

Rutherford, S., D´Hondt, S. 2000. Early onset and tropical forcing of 100,000 – year Pleistocene glacial cycles. Nature, 408:72-75.

Sarnthein, M., Winn, K., 1990. Reconstruction of low and middle latitude export productivity, 30,000 years to Present: Implications for global carbon reservoirs. In: Schlesinger, M.E. (Ed.), Climate-Ocean Interaction. Kluwer, Dordrecht, pp. 319-342.

Schiebel, R., Hemleben, C. 2017. Planktic Foraminifers in the Modern Ocean. 10.1007/978-3-662-50297-6.

Schiebel, R., Zeltner, A., Treppke, U.F., Waniek, J.J., Bollmann, J., Rixen, T., Hemleben, C. 2004. Distribution of diatoms, coccolithophores and planktic foraminifers along a trophic gradient during SW monsoon in the Arabian Sea. Marine Micropaleontology, 51(3-4):345-371. https://doi.org/10.1016/j.marmicro.2004.02.001

Schmieder, F., Dobeneck, T. von, Bleil, U., 2000. The Mid-Pleistocene climate transition as documented in the deep South Atlantic Ocean: initiation, interim state and terminal event. Earth and Planetary Science Letters 179, 539–549.

Schneider, T., Bischoff, T., Haug, G.H. 2014. Migrations and dynamics of the intertropical convergence zone. Nature, 513(7516):45-53.

Schott, F., Stramma, L., Fischer, J., 1995. The warm water inflow into the western tropical Atlantic boundary regime, spring 1994. J. Geophys. Res. 100, 24745–24760.

Sexton, P.F., Barker, S. 2012. Onset of 'Pacific-style' deep-sea sedimentary carbonate cycles at the mid-Pleistocene transition. Earth and Planetary Science Letters, 321-322:81-94.

Shackleton, N.J. 1987. Oxygen isotopes, ice volume and sea level. Quaternary Science Reviews, 6(3): 183-190.

Shackleton, N.J., Berger, A., Peltier, W.R., 1990. An alternative astronomical calibration ofthe lower Pleistocene timescale basedon ODP Site 677. Transactions ofthe Royal Society ofEdinburgh. Earth Sciences 81:251–261.

Sigman, D.M., Boyle, E.A., 2000. Glacial/interglacial variations in atmospheric carbon dioxide. Nature 407, 859–869.

Silva, A., Araujo, M, Medeiros, C., Silva, M., Bourles, B. 2005. Seasonal changes in the mixed and barrier layers in the western equatorial Atlantic. Brazilian Journal of Oceanography, 53(3/4):83-98.

Stainforth, R.M.; Lamb, J.L.; Luterbaqcher, H.; Beard, J.H. & Jeffords, R.M. 1975. Cenozoic planktonic foraminiferal zonation and characteristics of index forms. Paleontological Contributions, 62. Lawrence: University of Kansas Press. 425 p.

Stramma, L., Fischer, J., Reppin, J., 1995. The North Brazil undercurrent. Deep Sea Res. I 42, 773–795.

Talley, L., Pickard, G., Emery,W., Swift, J., 2011. Descriptive physical oceanography: An introduction. Elsevier Academic.

Thunell, R., Tappa, E., Pride, C., Kincaid, E., 1999. Sea-surface temperature anomalies associated with the 1997–1998 El Nino recorded in the oxygen isotope composition of planktonic foraminifera. Geology 27, 843–846.

Thunnell, R.C. 1984. Pleistocene planktonic foraminiferal biostratigraphy and paleoclimatology of the Gulf of México. In: N. Healy-Williams (ed.) Principles of Pleistocene Stratigraphy Applied to the Gulf of Mexico. Boston, International Human Resources Development Corporation, p. 25-64.

Toledo, F.A.L., Quadros, J.P.,Camilo Jr., E., Santarosa, A.C.A., Flores, J.A., Costa, K.B. 2016.Plankton biochronology for the last 772,000 years from the western South Atlantic Ocean. Marine Micropaleontology, 127: 50–62. doi.org/10.1016/j.marmicro.2016.07.002

Tzedakis, P. C., McManus, J. F., Hooghiemstra, H., Oppo D. W., Wijmstra, T. A. 2003. Comparison of changes in vegetation in northeast Greece with records of climate variability on orbital and suborbital frequencies over the last 450,000 years. Earth and Planetary Science Letters 212, 197–212.

Vicalvi, M.A. 1997. Zoneamento bioestratigráfico e paleoclimático dos sedimentos do Quaternário superior do talude da Bacia de Campos, RJ, Brasil. *Boletim de Geociências da Petrobrás*, **11**(1):132-165.

Vink, A., Brune, A., Holl, C., Zonneveld, K.A.F., Willems, H., 2002. On the response of calcareous dino!agellates to oligotrophy and strati"cation of the upper water column in the equatorial Atlantic Ocean. Palaeogeography, Palaeoclimatology, Palaeoecology, 178:53–66.

Wade, B. S., Pearson, P.N., Berggren, W.A., Pälike, H. 2011. Review and revision of Cenozoic tropical planktonic foraminífera biostratigraphy and calibration to the geomagnetic polarity and astronomical time scale. Earth-Science Reviews, 104: 111-142.

Wang, X., Auler, A.S., Edwards, R.L., Cheng, H., Cristalli, P.S., Smart, P.L., Richards, D.A., Shen, C.-C. 2004. Wet periods in northeastern Brazil over the past 210 kyr linked to distant climate anomalies. Nature, 432(7018):740-743.

Weldeab, S., Schneider, R., Kölling, M., 2006. Deglacial sea surface temperature and salinity increase in the western tropical Atlantic in synchrony with high latitude climate instabilities. Earth and Planetary Science Letters 241, 699–706.

Wilkens, R.H., Westerhold, T., Drury, A.J., Lyle, M., Gorgas, T., and Tian, J., 2017, Revisiting the Ceara Rise, equatorial Atlantic Ocean: isotope stratigraphy of ODP Leg 154 from 0 to 5 Ma: Climate of the Past, v. 13, p. 779–793, doi: https://doi.org/10.5194/cp-13-779-2017.

Wilson, K.E., Maslin, M.A., Burns, S.J., 2011. Evidence for a prolonged retroflection of the North Brazil Current during glacial stages. Palaeogeogr. Palaeoclimatol. Palaeoecol., 301(1–4): 86–96. http://dx.doi.org/10.1016/j.palaeo.2011.01.003.

Zhang, D., Msadek, R., McPhaden, M.J., Delworth, T., 2011. Multidecadal variability of the North Brazil Current and its connection to the Atlantic meridional overturning circulation. J. Geophys. Res. 116, C04012. http://dx.doi.org/10.1029/2010JC006812.

Zhang, Y., Chiessi, C. M., Mulitza, S., Sawakuchic, A.O., Häggi, C.,.Zabel, M., Portilho-Ramos, R.C., Schefuß, E., Crivellari, S., Wefer, G. 2017. Different precipitation patterns across tropical South America during Heinrich and Dansgaard-Oeschger stadials. Quaternary Science Reviews, 177: 1-9. doi.org/10.1016/j.quascirev.2017.10.012

Zhang, Y., Chiessi, C. M., Mulitza, S., Zabel, M., Trindade, R.I.F., Hollanda, M.H.B.M., Dantas, E.L., Govina, A., Tiedemann, R., Wefer, G. 2015. Origin of increased terrigenous supply to the NE SouthAmerican continental margin during Heinrich Stadial 1 and the Younger Dryas. Earth and Planetary Science Letters, 432:493-500. doi.org/10.1016/j.epsl.2015.09.054.

Zweng, M. M., J. R. Reagan, D. Seidov, T. P. Boyer, R. A. Locarnini, H. E. Garcia, A. V. Mishonov, O. K. Baranova, K. Weathers, C. R. Paver, and I. Smolyar, 2018. World Ocean Atlas 2018, Volume 2: Salinity. A. Mishonov Technical Ed.; NOAA Atlas NESDIS 82, 50 pp.